

Hydrodynamic and ecological performance of a new modular unit for living breakwaters

Wave flume experiments and results

E.R.I. van den Brekel





Hydrodynamic and ecological performance of a new modular unit for living breakwaters

Wave flume experiments and results

by

E.R.I. van den Brekel

to obtain the degree of Master of Science in Civil Engineering at the Delft University of Technology

Student number:	4383001	
Thesis Committee	Prof. dr. ir. Marcel van Gent (Chair)	TU Delft
	Assoc. Prof. dr. ir. Bas Hofland	TU Delft
	Ass. Prof. dr. ir. Alessandro Antonini	TU Delft
Reefy:	Ir. Jaime Ascencio	Reefy

This thesis is confidential and cannot be made public until October 17, 2023.

An electronic version of this thesis is available at <http://repository.tudelft.nl/>.
October 2021



ABSTRACT

Living breakwaters are designed to protect the coast against flooding and erosion, whilst at the same time they enhance the local ecological system by incorporating natural reef components. This study investigates the design of a modular artificial reef developed by the company called Reefy. Reefy breakwaters will consist of interlocking blocks with holes inside and rounded corners. For the configuration of the breakwater no proper design guidelines exist yet which incorporate both the hydrodynamic and ecological functionalities, as both this field of engineering and this reef system are relatively new. Therefore, this study aims to provide insight and develop preliminary design guidance on how to design a hybrid living breakwater from Reefy blocks under wave loading.

To this end, an experimental study was performed in the Eastern Scheldt wave flume of Deltares investigating the impact of different design variables on both the 2D hydrodynamic and ecological performance under wave loading, in shallow water conditions. Both irregular and regular wave conditions are tested. This thesis focuses on submerged structures and therefore the freeboard is defined to be positive for submerged structures. In total, 15 different designs are tested amongst which 7 are 2D configurations and the other 8 are complex 3D configurations. Single as well as double 3D structures are tested and the space between a double structure is referred to as "channel". The dimensionless design variables which are investigated are the relative structure height ($\frac{h_c}{d_f}$), - freeboard ($\frac{R_c}{H_{m0,i}}$), - crest width ($\frac{B}{L_0 \text{ or } H_{m0,i}}$), - channel length ($\frac{L_{channel}}{L_0}$), the surf similarity parameter ($\frac{\tan(\alpha_{front})}{\sqrt{s_{0,m-1,0}}}$) and the porosity of a structure (ϕ). Furthermore, the influence of the slope orientation (zigzag vs. straight), canopy density and block permeability on the hydraulic- and ecological performance are also investigated.

For the hydrodynamic performance, the impact of each design variable on the transmission coefficient (K_t) and reflection (K_r) is quantified. In this study, K_t is defined as the transmitted waveheight behind the structure divided by the incoming waveheight at the same location without a structure. These coefficients are based on the incident wave signals. As most of these tests had shallow water conditions, with large Ursell numbers, the usual methods to determine the incoming wave did not work. Therefore, to obtain the incoming wave signal, a new method was used, based on a combination of the existing techniques. Lastly, from the irregular waves the transmitted- and reflected energy density spectra are investigated and compared to the results from the regular waves.

The existing formulae for the K_t and K_r are compared to results of the hydrodynamic performance as measured. The one with the best correlation is optimized using a non linear regression analysis. The correlation coefficient of the optimized equation for K_r is lower than for K_t . For K_t two empirical equations are defined, each applicable to another range of the surf similarity parameter. For conditions in which $\zeta_{0,m-1,0} \geq 3$, the K_t can be predicted from the relative freeboard and crest width, whereas the exact value of $\zeta_{0,m-1,0}$ has no influence on the outcome of K_t . For conditions in which $\zeta_{0,m-1,0} < 3$, the K_t can be predicted from the relative freeboard, - structure height and $\zeta_{0,m-1,0}$, whereas the energy dissipation occurring over the width of the crest is less significant here. For $K(r)$, the optimized equation with the

best performance included the relative freeboard, porosity, fictitious wave steepness and front slope. The results suggest that the fictitious wave steepness $s_{0,m-1,0}$ has more impact on K_r than the slope steepness. An increase in channel length increased the reflection significantly and a zigzag orientation decreased the reflection.

For the ecological performance, the stream-wise peak velocities $u_{x,peak}$ are investigated in the wake behind the structure and in the channel. The performance is investigated based on a tranquility index Tr . Tr increases if the flow is more tranquil and is related to the percentile values of $|u_{x,peak}|$ with and without a structure. Furthermore, the 95th percentile value of $|u_{x,peak}|$ in the wake is compared to the maximum flow velocity in which a branching coral type named *Acropora intermedia* can survive.

The outcomes of Tr showed that in general, Tr increases for an increase in the design variables that were inversely proportional related to K_t . Furthermore, the zigzag orientation decreased the tranquility and the results suggest the porosity of the structure has a more significant impact on Tr than on K_t . However, a higher Tr should not be associated with a better ecological performance by definition. As such, for nutrient circulation considerations a more complex structure is preferred even though this decreases the tranquility.

The results of this study reveal that for the same number of blocks, a more complex structure can be built without making a compromise in the hydrodynamic performance parameters. The 95% confidence intervals from K_d for a complex Reefy structure with a relative freeboard between $0.2 < R_c/H_{m0,i} < 0.5$ are [0.73 0.78]. Thus, the predicted dissipation of the incoming wave energy lies around 75% in the case of a shallow submerged structure. As tidal differences and wave conditions vary enormously throughout the world, the design and height of the structure has to be adapted accordingly. Further exploring of the stability and the expected sediment patterns behind the structure will contribute to the design optimization process of a Reefy structure. In conclusion, the performed tests and analysis provide insight into relevant physical processes and design parameters for artificial reefs, and therefore assists the designer of artificial reefs.

ACKNOWLEDGEMENTS

This master thesis is written to complete my studies at the Delft University of Technology. Of course, it was only possible to finish it with the help of a lot of people and I would like to express my gratitude to those who have supported me throughout this process.

In September 2020, I initially started with another topic, about the Jamuna-Brahmaputra river. After two months of hard work, my supervisors from the TU Delft and I decided that the research could not be continued, due to corona related circumstances. I am very thankful for the caring role of Astrid Blom at that time. Soon after, on November 9th 2020, I was added to a WhatsApp-group in which the preparations for the physical experiments of this thesis were already up and running. I am extremely honoured that I was allowed to perform and prepare these experiments together with the Reefy-team. Above that, I felt very lucky at that time to be able to escape my room despite the COVID outbreak!

First of all, I would like to thank my committee members. Bas Hofland, thank you for your willingness to regularly meet with me during a very crucial period of my research. I am very thankful for the many ideas you've shared and your enthusiasm. I am also impressed by your knowledge and your capability of transferring this. Jaime Ascencio, I am thankful for your non-stop interest in the results and your active engagement from the start. It has always felt as if my research mattered to you and that has motivated me a lot. Alessandro Antonini, thank you for your helpfulness, especially a few times when you've guided me through Matlab. After these sessions I was able to continue more confidently with my research. Marcel van Gent, I want to thank you for being the chair of my committee and for the extensive feedback you gave me on my green light version.

Second of all, I want to thank Daan Houtzagers, who was part of the team during the experiments. I am also thankful for the helpfulness of Menno de Ridder, Wesly Stet and all the other people who were working in the laboratory of Deltares at that time. Additionally, I want to thank Daniel Dacomba and Leon Haines for bringing a lot of good vibes to the VriMiBo's with Reefy.

Thirdly, I want to thank all my friends. The laughs and side activities definitely contributed more to this project than I am aware of. I want to thank Pauline Janssen and Esther Heineke for our strong hydraulic bond. They've listened to my presentations a few times, even if they had to put their alarm at 7:00 AM during their own holidays. Moreover, Floris, thank you for asking me almost every day of a year: "Hoe ging het vandaag met je afstudeer project?" :)

And last but definitely not least, I want to express my gratitude to my family for their unconditional support and their wisdom. And above all, for raising me in a safe environment, which gave me the opportunity to develop myself and obtain this degree in the first place. I hope in my future career I can give something back to them and the rest of the world!

I wish Jaime and the rest of the Reefy team a lot of success with the further developments of their company.

Yours sincerely, Evelien van den Brekel.
Delft, October 2021

CONTENTS

1	INTRODUCTION	4
1.1	Context	4
1.2	Scope	6
1.2.1	Research objective	7
1.2.2	Research questions	7
1.2.3	Methodology and outline	7
2	LITERATURE STUDY	9
2.1	Hydrodynamic performance	9
2.1.1	Wave transmission	10
2.1.3	Wave reflection	17
2.2	Ecological performance	19
2.2.1	Environmental enhancement	19
2.2.2	Impact mitigation	25
3	PHYSICAL MODEL	27
3.1	Scaling	27
3.2	Experimental set-up	28
3.3	Wave conditions	33
3.4	Design configurations	35
4	DATA PROCESSING HYDRODYNAMIC PERFORMANCE	39
4.1	Definition wave height	39
4.2	Definition transmission coefficient	40
4.3	Definition wave reflection coefficient	42
4.4	Decomposition incoming and reflected waves	42
5	RESULTS HYDRODYNAMIC PERFORMANCE	57
5.1	Structure height	57
5.2	Crest width	66
5.3	Blocked holes	73
5.4	Slope steepness	75
5.5	Porosity of the structure	80
5.6	Channel length	82
5.7	Surface roughness	89
5.8	New empirical formulae	92
5.8.1	Transmission	92
5.8.2	Reflection	95
5.8.3	Applicability new formulae for irregular wave conditions	98
6	DATA PROCESSING ECOLOGICAL PERFORMANCE	101
6.1	Performance parameters	101
6.1.1	Tranquility index	102
6.1.2	Safety score	103
6.2	Data processing electromagnetic liquid velocity meter	103
7	RESULTS ECOLOGICAL PERFORMANCE	107
7.1	Tranquility index	108
7.1.1	Structure height	108
7.1.2	Crest width	109

7.1.3	Blocked holes	110
7.1.4	Slope steepness	111
7.1.5	Channel length	112
7.1.6	Channel vs. back	113
7.1.7	Outer surface roughness	114
7.2	Safety score	116
7.2.1	Branching corals	116
7.3	Ink injection	117
8	DISCUSSION, CONCLUSION AND RECOMMENDATIONS	119
8.1	Discussion	119
8.2	Conclusions	127
8.2.1	Hydrodynamic performance	127
8.2.2	Ecological performance	129
8.3	Recommendations	130
8.3.1	Future research	130
8.3.2	Design of a Reefy structure	134
A	PHYSICAL MODEL	143
A.1	Design configurations pictures and 3D sketches	143
A.2	Deep water depth	149
A.3	Overview wave conditions + performed tests	150
B	LITERATURE STUDY	153
B.1	Hydrodynamic performance	153
B.1.1	Related physical processes	153
B.1.2	Empirical equations erosion mitigation	154
B.1.3	Data bases DELOS	157
B.1.4	Double submerged breakwaters with "Channel"	158
B.2	Ecological performance	160
B.2.1	Related physical processes	160
B.2.2	Limiting conditions aquatic organisms	160
B.2.3	Modelling tool DELOS	162
B.3	Water waves	163
C	DATA PROCESSING	169
C.1	Hydrodynamic performance	169
C.1.1	Wave decomposition methods	169
C.1.2	Spectral analysis	169
C.1.3	Foreshore effect based on energy balance	170
C.1.4	Relative MSE Zelt and Skjelbreia	171
C.1.5	Relative spacing wave gauges	173
C.2	Ecological performance	175
D	RESULTS HYDRODYNAMIC PERFORMANCE RESULTS	180
D.1	Crest width	180
D.1.1	Crest-width relative to incoming waveheight	180
D.2	Surface roughness	180
D.3	Type of waves	181
D.3.1	Type of waves and transmission	181
D.3.2	Type of waves and reflection	183

ABBREVIATIONS

2DV	Two dimensional vertical	MAE	Mean Average Error
3D	Three dimensional	MSE	Mean squared error
AR	Artificial Reef, a man-made structure which is submerged in a natural environment	PVC	Pipes from polyvinyl chloride, if it is mentioned behind a structure number it refers to a structure with 4cm tall PVC pipes out of the holes on top of the blocks
BH	Blocked holes, if it is mentioned behind a structure number it refers to a structure with PVC pipes vertically inserted in the holes of the blocks	R	Regular wave test
DELOS	Research project about the environmental design of low crested coastal defence structures	REF	Reference test (without a structure)
EVM	Electromagnetic liquid velocity meter	RMSE	Relative Mean Square Error
G&S	Wave separation method from [Goda and Suzuki, 1977]	RtMSE	Root Mean Square Error
I	Irregular wave test	Struc	Structure (#), referring to one of the tested configurations
LB	Living Breakwater, submerged breakwaters which are designed to protect the coast and to enhance the ecosystem by incorporating natural habitat components of various aquatic species	WG	Wave gauge
M&F	Wave separation method from [Mansard and Funke, 1980]	WG123	Wave gauges 1 , 2 and 3 in the deep area of the wave flume
		WG456	Wave gauges 4 , 5 and 6 in front of the structure above the foreshore
		WG789	Wave gauges 7 , 8 and 8 behind the structure above the foreshore
		Z&S	Wave separation method from [Zelt and Skjelbreia, 1993]

SYMBOLS

(f)	Indication that the value in front (e.g. waveheight) is obtained from a reference test and therefore is the result of the foreshore only	g	Gravitational acceleration
(f, s)	Indication that the value in front (e.g. waveheight) is obtained from a test with a structure and therefore is the result of the foreshore and the structure	$H_{1/3}$	Significant wave height as the average of $1/3^{th}$ of the highest waves measured based on a zero up-/down crossing analysis of a time signal
(s)	Indication that the value in front (e.g. transmission coefficient) is the result of the structure only and the impact of the foreshore is eliminated	h_c	Height of a structure from toe to crest
α_{front}	The seaward slope steepness of a structure	h_f	Height of the foreshore
ω	Angular frequency	H_i	Incoming wave height measured at a set of three wave gauges
Φ	Porosity of a structure: $\frac{V_{tot} - V_{material}}{V_{tot}}$	H_{m0}	Significant wave-height as: $4 * \sqrt{m_0}$
ζ	Surf similarity number: $\frac{\tan(\alpha_{front})}{\sqrt{s_0}}$	H_r	Reflected wave height measured at a set of three wave gauges
$\zeta_{0,m-1,0}$	Surf similarity number with $s_{0,m-1,0}$	H_s	Generic symbol of the significant wave height
$\zeta_{0,p}$	Surf similarity number with $s_{0,p}$	H_{tot}	Total wave height measured at a set of three wave gauges
A_{tot}	Total surface area based on the total silhouette of the cross-section of a structure	k	Wave number
B	Crest width of a structure	K_d	Dissipation coefficient
d_0	Deep water depth in the wave flume	K_r	Reflection coefficient
d_f	Water depth at the toe of a structure	K_t	Transmission coefficient
E_d	Dissipated wave energy	L	Wavelength, calculated with the dispersion relation
E_i	Incoming wave energy	L_0	Deep-water wavelength of the incoming wave: $\frac{g * T_{m-1,0, WG456}^2}{2\pi}$
E_r	Reflected wave energy	L_{ch}	Length of the channel, defined as the stream-wise length of empty space between a front- and back part of a structure
E_t	Transmitted wave energy	m_0	Total variance of a frequency wave spectrum
f	Wave frequency	m_n	n^{th} moment of a wavespectrum, defined as $\int_0^\infty f^n S(f) df$, in which $S(f)$ is the non directional wave spectral density function
f_p	Wave frequency at spectral peak		

n_l	The length scale factor of the experiments	$Tr_{30\%}$	Tranquility index of a wake based on the 30 th percentile value of $ u_{x,peak} $
R^2	Coefficient of determination	$Tr_{50\%}$	Tranquility index of a wake region based on the 50 th percentile value of $ u_{x,peak} $
R_c	Freeboard , defined as the distance between the crest to the water surface. <i>Note: positive for submerged configurations and negative for (partly) emerged configurations</i>	$Tr_{95\%}$	Tranquility index of a wake region based on the 95 th percentile value of $ u_{x,peak} $
$s_{0,m-1,0}$	Fictitious wave steepness with $T_{m-1,0,WG456}$	$Tr_{x\%}$	Collective reference for $Tr_{30\%}$, $Tr_{50\%}$ and $Tr_{95\%}$
$s_{0,p}$	Fictitious wave steepness with $T_{p,WG456}$	U	Ursell parameter
s_0	Fictitious wave steepness: $\frac{2*\pi*H_{m0,i,WG456}}{g*T_{WG456}^2}$	u_x	x-velocity, measured with the EVM 75 cm above the foreshore (1:1 scale)
S_{ch}	Spacing of the channel, defined as the stream-wise length between the front- and back crest	$V_{material}$	The total volume of material of a structure
T	Wave period	V_{tot}	The total volume of voids plus material of a structure
$T_{m-1,0}$	Mean (spectral) energy wave period	$ u_{x,peak} $	Absolute values of the peaks and troughs measured in the x-velocity signal
$T_{m_{x1,x2}}$	Spectral wave period where $T_{m_{x1,x2}} = \frac{m_{x1}}{m_{x2}}$	$\Delta Tr_{x\%}$	The difference between the outcome of $Tr_{30\%}$ from the investigated structures, - of $Tr_{50\%}$ from the investigated structures, or - of $Tr_{95\%}$ from two structures
T_p	Wave period at spectral peak		
Tr	Tranquility index of a wake		
$Tr_{30\%}$	Tranquility index of a wake based on the 30 th percentile value of $ u_{x,peak} $		

This thesis is written in collaboration with the Delft University of Technology and a start-up company called Reefy. This company strives to design stable coastal protection structures which enhance the ecosystems in place. This research investigates the effectiveness of different design configurations from a hydrodynamic- and ecological perspective, based on experiments conducted in the Eastern Scheldt Flume of Deltares.

1.1 CONTEXT

Conventional, solid installations such as emerged breakwaters have been widely applied in defying beach erosion and protect coasts against floodings. Despite their defensive efficiency against erosion, it has been observed that they have an environmental impact. They have an adverse impact on the aesthetics of the beach and especially when non permeable, on the water quality as well [Diplarakos, 2017].

Submerged breakwaters ease water circulation near the surface and have less impact on the aesthetics of the beach. Therefore they are often chosen as an alternative, confining side effects of emerged breakwaters [Metallinos et al., 2016] [Hashish et al.]. The “rubble mound” breakwater is a very well-known type of submerged breakwater. Its environmental impact has been investigated as a part of the DELOS project (Environmental Design of Low Crested Coastal Defence Structures). It was concluded these structures can be considered as a poor surrogate of natural rocky shores [Moschella et al., 2005].

Nowadays engineers aim to design multipurpose submerged breakwaters, such that they do not only minimize wave action, but also enhance the marine life conditions in the nearshore. The Living Breakwater (LB) is one of the most investigated type of submerged breakwaters for that purpose [Mendoza et al., 2019]¹. A LB can mimic both the functions and the form of natural reefs² [Bleck, 2006].

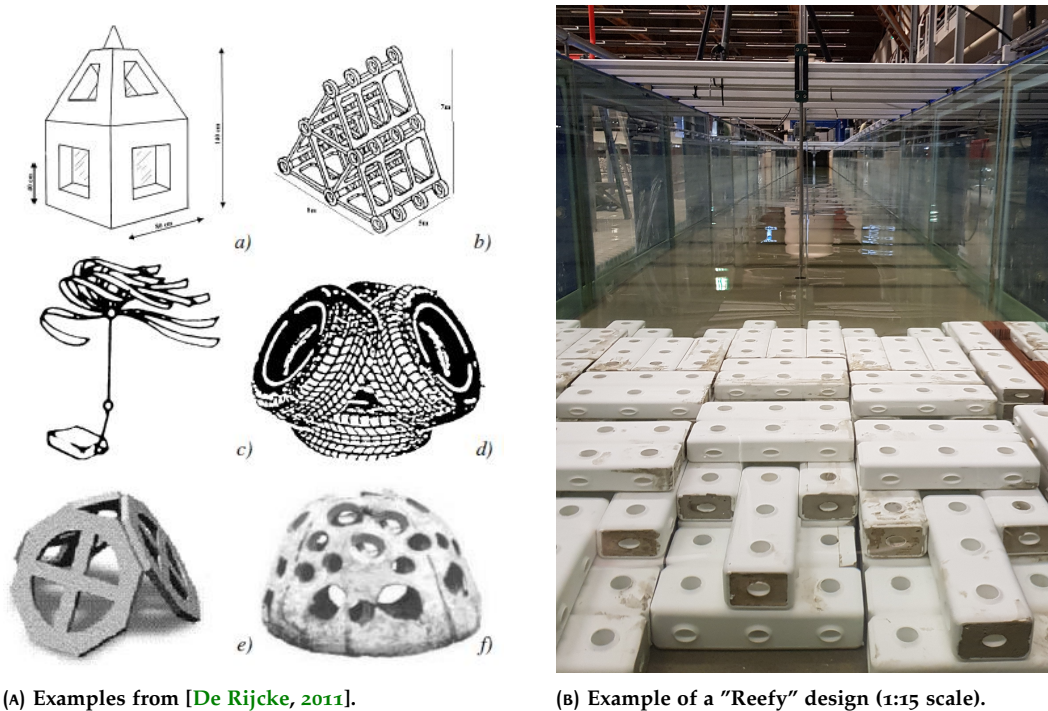
The function of coral reefs to attract and enhance marine life has been mimicked for ages. For example, the use of drowned wooden frames to create a sheltered area was already reported by Japanese fisherman in the 18th century [Bleck, 2006]. Multiple Artificial Reef (AR) designs for solely this function have been brought to the market already. Some of the existing reef units are presented in Figure 1.1. Above that, the function of a coral reef systems as a very effective, naturally occurring, coastal protection in some regions of the world, has been proven in 2004. It became clear during a tsunami in South-East Asia that the areas protected by coral reefs appeared to have less damage [Bleck, 2006]. In Figure 1.2 the value of coral reefs for flood

¹ In literature, a living breakwater is sometimes also referred to as an artificial reef (AR). Nevertheless, not all artificial reefs are living breakwaters, as an AR can be any solid man-made structure, submerged in the natural environment [Bohnsack, 1989]

² Natural reefs which are referred to with the word reef are sand bars, cliffs and the coral reefs [Bleck, 2006]

protection per coastal area in the world is visualized on a map, emphasizing the importance on a global scale.

This study focuses on how to design a LB that consists of specific interlocking blocks from a company called Reefy. The aim of this study is to provide insight and guidelines for the optimisation process of a Reefy breakwater design, integrating both the hydrodynamic- and ecological performance considerations.



(A) Examples from [De Rijcke, 2011].

(B) Example of a "Reefy" design (1:15 scale).

FIGURE 1.1: Different examples of artificial reef unit designs. Names of structures in Figure 1.1a: a) Simple hollow concrete module; b) Japanese reef module "JUMBO"; c) Plastic Kelp; d) American tyre reef modules; e) Tecnoreef module; f) Reef ball.

Reefy design

The Reefy company designed a hydrodynamic block as the core component to built their AR from. The design of the block is focused on the hydrodynamic performance as it has holes inside and rounded corners to reduce the drag. In some of the tested configurations of blocks, spaces in between the blocks are left empty to create sheltered areas for fish. A high porosity and complexity also allows nutrients to circulate within the structure. Furthermore, it reduces the water level set-up at the lee side of the structure because of the possibility for a return current to flow through the structure. See Figure 1.3 for an example of a tested Reefy structure design.

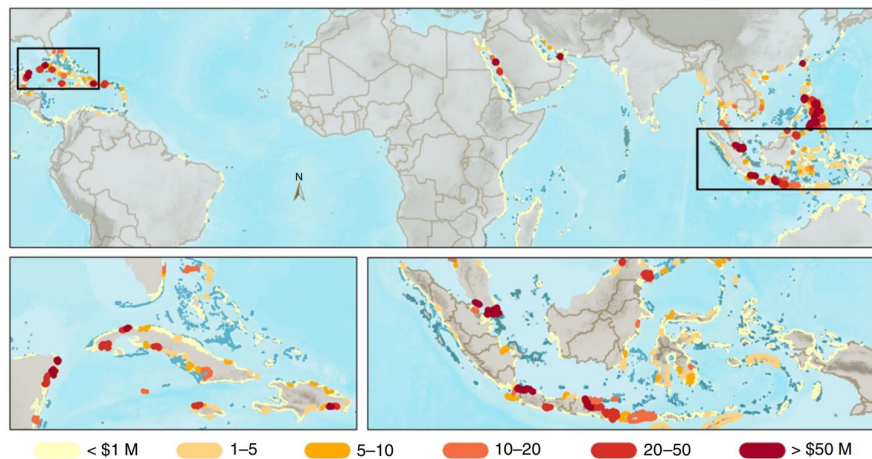


FIGURE 1.2: Circles represent the annual expected benefit from coral reefs for flood protection (\$US millions). The values are the difference in annual expected damages with and without of reefs for the 20 km coastal study units. The scenarios without reefs assume a decrease of only 1 m in the height and roughness of coral reefs Beck et al. [2018].

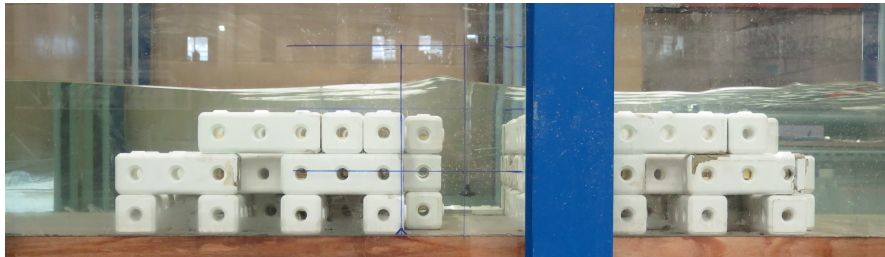


FIGURE 1.3: Close-up of one of the Reefy design configurations tested during the experiments for this thesis. Scale is 1:15. Waves come from the left side of the picture.

1.2 SCOPE

In order to be able to use Reefy structures as a hybrid artificial living breakwater, preliminary design guidance is required. This research focuses both on the hydrodynamic- and ecological performance. Other important aspects such as costs, construction phase, material choice, stability and failure mechanisms are not considered in this research.

Furthermore, as a part of this research experiments have been conducted in a 2D wave flume and therefore this research does not include 3D effect such as the impact of a long-shore current on the transmission. Nevertheless, for the completeness of this research, some 3D processes which play a role in the morphological response mode of the coast (erosion or accretion) are explained in Appendix B.1.2.

1.2.1 Research objective

The research objective is formulated as: *To provide insight and develop design guidelines for hydrodynamic and ecologic functionalities of Reefy design configurations under wave loading based on experimental data.*

1.2.2 Research questions

To further clarify the research objective, the following research questions are defined:

- **1. Literature:** What are the main physical processes related to the hydrodynamic and ecological performance in shallow water conditions and which parameters can be used to evaluate the performance?
- **2. Hydrodynamic performance:** What is the impact of each structural design variable on the physical processes assessing the hydrodynamic performance in shallow water conditions, namely the wave transmission and wave reflection?
- **3. Ecological enhancement:** What is the impact of the structural design variables on the physical processes determining the ecological enhancement performance in shallow water conditions, based on the tranquility index in the wake-zones of a structure?

1.2.3 Methodology and outline

As a part of this research, physical experiments have been conducted for two weeks in the Eastern Scheldt flume of Deltares. From conducting physical experiments on a new type of structure - such as a Reefy LB - useful knowledge about the wave-structure interaction can be obtained, which later can be used for the input of numerical models. Furthermore, from these experiments the impact of different configurations can be tested for many wave conditions. During these experiments, several configurations have been exposed to varying wave conditions, generated by a wave paddle. By investigating the interaction of the structure and the waves, more insight was gained in the performance of each design configuration.

The report is subdivided into 8 chapters, to answer the research questions and reach the research objective (Figure 1.4).

In Chapter 1, an introduction of the topic is given and the research objective and structure of the report are presented. Chapter 2 gives an overview of the relevant studies and projects found in literature. In this chapter, the first research question is answered. Published research on the hydraulic performance and structural ecological performance of submerged breakwaters is analysed and discussed. Chapter 3 gives an overview of the conducted physical experiments at Deltares. The scaling parameters, flume layout, wave conditions and design configurations are written down here. In Chapter 4, the processing methods are explained to convert the raw data of the wave gauges into parameters for the hydrodynamic performance. In Chapter 5, the impact of the tested design variables on the wave transmission, reflection and set-up is analyzed. This chapter is related to the second research question. For each design variable,

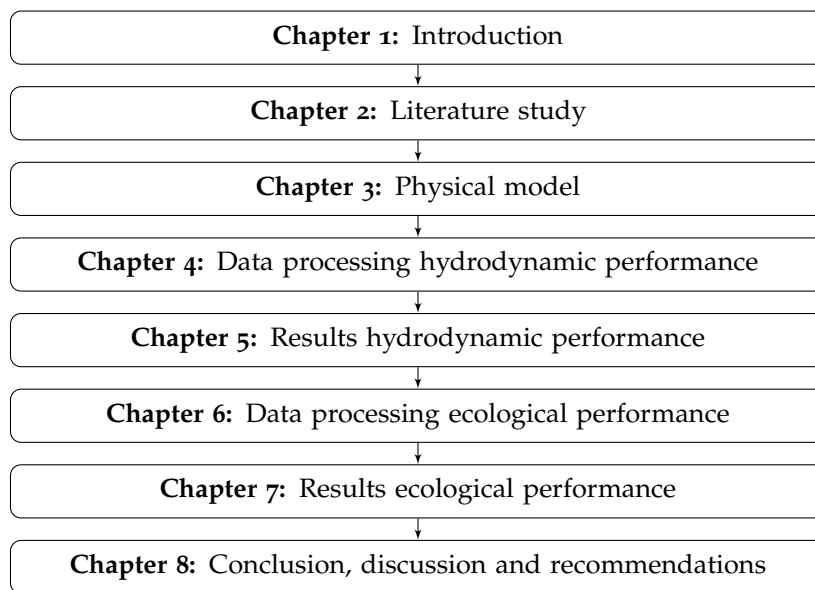


FIGURE 1.4: Structure of the report

the results of the regular- and irregular wave tests are discussed separately. In Chapter 6, the data processing method is explained for irregular waves on how to convert the raw data of an electromagnetic velocity meter into the parameters for the ecological performance. In Chapter 7 the results of the impact of the design variables on the tranquility as a measure of the ecological performance is discussed. Furthermore, in this chapter a safety factor is calculated for some wave conditions to predict whether breakage of branching corals is expected. This chapter answers research question number 3. In Chapter 8, the strengths and weaknesses of the research are discussed and the final conclusion with regards to the research objective and -questions are given. Furthermore, at the end recommendations are made for the Reefy design and for future research topics.

2 | LITERATURE STUDY

In this literature search, design aspects for a Reefy breakwater are investigated with regard to the hydrodynamic performance and the ecological enhancement. Section 2.1, gives a summary of main aspects important for the hydrodynamic performance. With respect to the hydrodynamic performance, sections 2.1.1 and 2.1.3 give an overview of the existing published research for the determination of the transmission - and reflection coefficients by submerged breakwaters. Section 2.2 describes the literature found on the ecological function of a living breakwater. In Section 2.2.1, several aspects about the ecological enhancement potential of a submerged breakwater are explained. In Section 2.2.2, measures which are known to mitigate the environmental impact of a coastal defence structure on a broader scale are described.

2.1 HYDRODYNAMIC PERFORMANCE

The hydrodynamic function of a Reefy structure is both to prevent floods and mitigate the erosion problems.

FLOOD PROTECTION For flooding it is important to understand the energy transformation processes over the structure. The two-dimensional local hydrodynamic processes were identified by [Armono, 2004] and are visualized in Figure 2.1. At a submerged Reefy breakwater, a part of the energy is transmitted above the crest of the structure and through the structure, another part is dissipated by the structure and the last part is reflected seaward.

Furthermore, the non-linearity of the waves increases as they travel over the structure. Non-linearity's occur if waves travel over the front slope from shoaling and if waves travel over the crest from interactions between different wave phases. These phenomena result in the generation of shorter- and smaller waves, which are phase-locked with the primary wave and can be released during the breaking phase. In a wave spectrum these effects induce an energy transfer from the peak frequency to the higher harmonics [Losada et al., 2003].

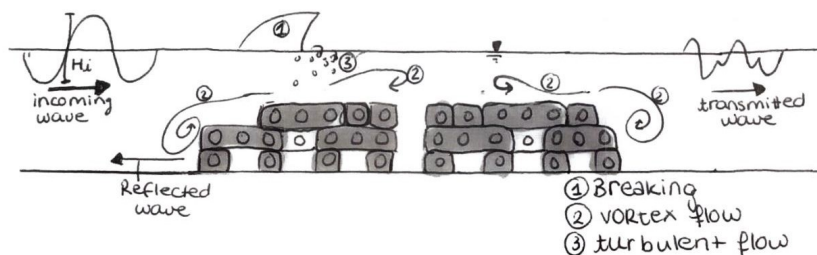


FIGURE 2.1: Sketch of possible wave dissipation processes on Artificial Reef(y) structure

Different processes are related to the wave dissipation from the interaction with an artificial reef structure. First of all, from friction with the inner- and outer surface area of the structure wave

energy gets dissipated [Losada et al., 2003]. Another part is dissipated from turbulence which is formed when waves travel through the reef and along the corners of the structure [Kontaxi and Memos, 2005]. For waves near the critical wave height, the reduction in the local water depth above the crest causes the waves to break earlier [Gallerano et al., 2019]. For non-breaking waves, the fact that the structure forces a flow resistance upon the incoming waves accounts for the largest part in the dissipation process [Losada et al., 2003].¹

According to the energy conservation law, the incoming energy is equal to the sum of the transmitted-, reflected- and dissipated energy ($E_{in} = E_t + E_r + E_d$) [Mendoza et al., 2019]. For the prevention of floods it is important to know to what extent a structure is able to dissipate the incoming wave energy under certain weather conditions. As can be derived from the energy conservation equation, the dissipation performance of a structure can be assessed based on the transmission- and reflection coefficient. Therefore, these parameters are investigated for the hydrodynamic performance.

EROSION MITIGATION A submerged breakwater creates a local variation of the mean water level at the lee-side of the breakwater [Cáceres et al., 2005]. This variation induces modifications in the nearshore current patterns in which sediments are transported, which ultimately influence the morphological response mode of the coast. In short, accretion can be obtained if the set-up behind the structure is lower than the one at the side/in between the gaps of multiple structures. The subsequent current pattern are converging towards the breakwater. If the set-up at the lee-side is greater than on the sides, diverging currents are formed and these are associated with coastline erosion.

For the prediction of the shoreline response to a detached low-crested breakwater, the wave transmission k_t is also a leading parameter [Wamsley and Ahrens, 2004]. Therefore, it is critical to be able to express a reliable k_t for different designs and wave conditions.

Furthermore, several empirical formulas are used to predict the shoreline response mode to single- or multiple detached submerged breakwaters. An overview of these formulas and a summary of the other physical processes related to the morphological development of the coast can be found in Appendix B.1.2. These are not included in this Chapter, because they are not further investigated in this thesis.

In sections 2.1.1 and 2.1.3, a summary is given of the existing empirical equations for the prediction of respectively the wave transmission and -reflection by submerged breakwaters.

2.1.1 Wave transmission

For flood protection, the maximum allowable wave transmission is commonly the most important design criterion. [Armono, 2004]. K_t shows how effective the height of the incoming waves is reduced on the lee side of the structure. The transmission is influenced by both the two-dimensional processes through- and over the structure, and by wave propagation around

¹ A more comprehensive explanation on the dissipation processes for breaking- and non-breaking waves is explained in appendix B.2.1. Together with the unique breaking types of waves passing over artificial reefs in a 2DV wave flume, due to the presence of a return current.

the structure (refraction and diffraction) [Blacka et al., 2013]. The latter is a 3D process and therefore not investigated for this research.

Existing empirical formula

Several studies have been performed in the past to derive empirical equations for the wave transmission over submerged- and/or low crested breakwaters in a 2DV wave setting. An overview of all the formulae and their applicability range is given in Table 2.1. A short description of each study is given in the paragraphs below. The ranges of parameters involved in the experiments from literature and from this thesis are compared in Table 2.2². Lastly, a summary of the key takeaways from the research on the wave transmission can be found in Section 2.1.2.

[VAN DER MEER AND PILARCZYK, 1990] The first empirical prediction formula for the wave transmission has been formulated in 1990. This formula was based on tests from several experiments conducted by Seelig (1980), Powell and Allsop (1985), Daemrich and Kahle (1985), Ahrens (1987) and van der Meer (1988) [Daemen, 1991]. The relative submergence $R_c/H_{s,i}$ is the only variable for this empirical prediction of K_t .

[VAN DER MEER AND DAEMEN, 1994] In 1994, van der Meer and Daemen re-analyzed the same data, but now the tests with a high steepness, $s_{0,p} \geq 0.6$ and breaking waves $H_{s,i}/d_f \geq 0.54$ had been removed from the data base. Furthermore, the data from Ahrens on reef type structures were not included anymore, because of the complexity of the Ahrens' so called reef-type structures. Namely, these structures could heavily deform during the experiments, which made it hard to define for example the crest width of the structure. Moreover, the hydraulic response to deforming structures differed from conventional rubble mound submerged breakwaters.

The data base from van der Meer and Daemen (1994) is often referred to as the "Old Database" in literature. Therefore, this abbreviation is also used during this study and in Table 2.2. The "Old Database" includes rubble mound rock structures as well as Tetrapod and Accropode armour layers.

The formulae of van der Meer and Daemen in 1994 used the nominal diameter D_{n50} to formulate a non-dimensional crest height R_c/D_{n50} . This enabled to make a difference between rubble mound - and more impermeable breakwaters. Intercept b represents the k_t for structures when $R_c = 0$. This intercept includes the effects of the offshore wave steepness ($s_{0,p}$) and the crest width [Van der Meer et al., 2005].

[VAN DER MEER ET AL., 1996] In 1996, the authors came up with additional empirical formulae. The formulae of this study directly relate the crest freeboard to the incident wave height and distinguish between smooth impermeable- and rubble mound breakwaters. A breakwater is considered smooth if the armour layer is covered with for example asphalt or armoured with a block revetment. Smooth structures are less permeable and due to construction

² Note: All equations are written in a form where the freeboard R_c is positive for submerged structures.

reasons often have gentler slopes than rubble mound breakwaters. The formulae were derived based on the Old Database as well.

[SEABROOK AND HALL, 1999] The experiments discussed above had been on both emerged and submerged breakwaters. The study of Hall and Seabrook on the other hand was based on submerged rubble mound breakwaters only. This study concluded the smallest wave transmission was found for larger widths and smaller relative submergences. The effect of the seaward slope was found to be relatively unimportant.

[BLECK AND OUMERACI, 2002] In 2002, Bleck and Oumeraci investigated wave transmission over a submerged sill with rectangular cross section [Mahmoudi et al., 2017] and came up with a new empirical formula, only based on the freeboard relative to the incoming waveheight.

TABLE 2.1: Summary of relevant literature formulae regarding wave transmission

Author	Formulae	Applicability
Vd Meer & J.W. & Pilarczyk (1990)	$K_t = 0.46 + 0.3 * \frac{R_c}{H_{s,i}}$ $K_t = 0.8$ $K_t = 0.1$	$-1.2 < R_c/H_{s,i} < 1.13$ $1.13 < R_c/H_{s,i} < 2.0$ $-1.2 < R_c/H_{s,i} < -2.0$
Vd Meer & Daemen (1994)	$K_t = a * \frac{R_c}{D_{n50}} + b$ $a = 0.031 \frac{H_{s,i}}{D_{n50}} - 0.24$ $b = -5.42s_{0,p} + 0.0323 \frac{H_{s,i}}{D_{n50}} - 0.0017 * \left(\frac{B}{D_{n50}}\right)^{1.84} + 0.51$	$1 < \frac{H_{s,i}}{D_{n50}} < 6$ $0.01 < s_{0,p} < 0.05$ $0.075 < K_t < 0.75$
Vd Meer & D'Angremond & Gerding (1996)	<p><u>Rubble mound structures</u></p> $K_t = 0.4 \frac{R_c}{H_{s,i}} + 0.64 * \left(\frac{B}{H_{s,i}}\right)^{-0.31} (1 - e^{-0.5\zeta})$ <p><u>Smooth impermeable structures</u></p> $K_t = 0.4 \frac{R_c}{H_{s,i}} + 0.80 * \left(\frac{B}{H_{s,i}}\right)^{-0.31} (1 - e^{-0.5\zeta})$	$-2.5 < \frac{R_c}{H_i} < 2.5$ $0.075 < K_t < 0.8$
Seabrook & Hall (1999)	$K_t = 1 - \left[e^{-0.65 \frac{R_c}{H_{s,i}} - 1.09 \frac{H_{s,i}}{B}} + 0.047 \frac{BR_c}{LD_{n50}} - 0.067 \frac{R_c H_{s,i}}{BD_{n50}} \right]$	$5 < B/H_{s,i} < 74.47$ $0 < BR_c/LD_{n50} \leq 7.08$ $0 < R_c H_{s,i}/BD_{n50} \leq 2.14$
Bleck & Oumeraci (2002)	$K_t = 1 - 0.83 * e^{-0.72 * R_c/H_{s,i}}$	-
Vd Meer & Briganti & Zanuttigh & Wang (2005)	<p><u>Rubble mound structures</u></p> $K_t = 0.35 \frac{R_c}{H_{s,i}} + 0.51 * \left(\frac{B}{H_{s,i}}\right)^{-0.65} (1 - e^{-0.41\zeta})$ $K_{t,min} = 0.05$ $K_{t,max} = 0.006 * \frac{B}{H_{s,i}} + 0.93$	$B/H_{s,i} > 12$

Author	Formulae	Applicability
	$K_t = 0.4 \frac{R_c}{H_{s,i}} + 0.64 * \left(\frac{B}{H_{s,i}}\right)^{-0.31} (1 - e^{-0.5\zeta})$ <p style="text-align: center;"><i>Interpolation</i></p> <p style="text-align: center;"><u>Smooth impermeable structures</u></p> $K_t = 0.3 \frac{R_c}{H_{s,i}} + 0.75 * (1 - e^{-0.5\zeta})$ $K_t = 0.3 \frac{R_c}{H_{s,i}} + 0.75 * \left(\frac{B}{H_{s,i}}\right)^{-0.31} (1 - e^{-0.5\zeta})$	$B/H_{s,i} < 8$ $8 < B/H_{s,i} < 12$ $0.075 \leq K_t \leq 0.8$ $\zeta < 3$ $\zeta \geq 3$
Buccino & Calabrese (2007)	$K_t = \frac{1}{1.18 \left(\frac{H_{s,i}}{R_c}\right)^{0.12} + 0.33 \left(\frac{H_{s,i}}{R_c}\right)^{1.5} * \frac{B}{\sqrt{H_{s,i}L_0}}}$ $K_t = \left[\min(0.74; 0.62\zeta_{op}^{0.17}) - 0.25 * \min(2.2; \frac{B}{\sqrt{H_{s,i}L_0}}) \right]^2$	$1/0.5 < R_c/H_{s,i} < 1/1.2$ $1/1.2 < R_c/H_{s,i} < 0$ <p style="text-align: center;">Both:</p> $0.3 \leq B/\sqrt{H_{s,i}L_0} \leq 10.5$ $1 \leq \zeta_{op} \leq 8$ $s_{0,p} > 0.01$

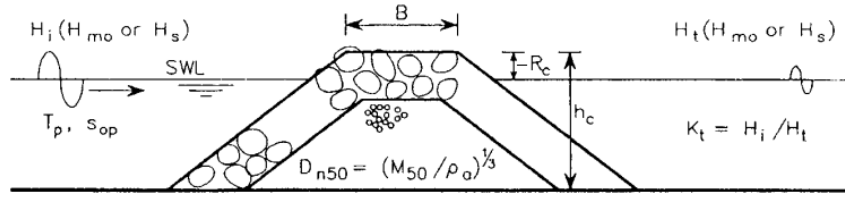
[VAN DER MEER ET AL., 2005] A large EU funded project, called DELOS (Environmental Design of Low Crested Coastal Defence Structures), investigated more than 2300 physical tests on wave transmission over low-crested structures [Blacka et al., 2013] [Van Oosten and Peixo Marco, 2005]³. The wave k_t versus relative freeboard for the DELOS sub-datasets are shown in Figure 2.3. The experimental set-up and main variables included in experiments for rubble mound structures during the DELOS experiments are presented in Figure 2.2.

The DELOS data set consists of work from [Van der Meer and Pilarczyk, 1990], [Van der Meer and Daemen, 1994], and [Van der Meer et al., 1996] on conventional rubble mound breakwaters as a starting point. Also the work of [Seabrook and Hall, 1999] on only submerged conventional rubble mound breakwaters is included as the work from Hirose et al. (2000) on a Aquareef structures, made from concrete armour units. Furthermore, several additional flume tests are performed within the project, a description of the newly added databases is given in appendix B.1.3. The ranges of the different experiments included in the DELOS data base are summarized in Table 2.2⁴ [Van Oosten and Peixo Marco, 2005].

The extensive DELOS database was studied by [Van der Meer et al., 2005]. The authors concluded that wave transmission over smooth low-crested structures is completely different from rubble mound structures. Therefore, they analyzed those structures separately.

³ Low-crested structures investigated by DELOS are defined as detached rubble-mound breakwaters, with the crown elevation near the still water level.

⁴ The newly added databases are referred to as UCA, UPC, GWK, M&M in Table 2.2



H_i = incident significant wave height, preferably H_{m0i} , at the toe of the structure

H_t = transmitted significant wave height, preferably H_{m0t}

T_p = peak period

s_{op} = wave steepness, $s_{op} = 2\pi H_i / (g T_p^2)$

R_c = crest freeboard

h_c = structure height

K_t = transmission coefficient H_t/H_i

ξ_{op} = breaker parameter $\xi_{op} = \tan\alpha / (s_{op})^{0.5}$; α = slope angle of structure

FIGURE 2.2: Governing variables for investigation K_t by DELOS project [Blacka et al., 2013]

The difference lies first of all in the energy dissipation by friction and porosity, which causes the wave transmission to be larger for smooth structures for the same crest height. Furthermore, the crest width has less effect on transmission as there is almost no energy dissipation on the crest. On the other hand, the gentle smooth slopes can - under some conditions - cause waves breaking, where steep rubble mound slopes do not. [Van der Meer et al., 2005] also investigated the difference in 3D effects for impermeable - and permeable breakwaters. The reader is referred to their open-source paper as this is out of the scope of this research.

All in all, [Van der Meer et al., 2005] concluded the formulae of [Van der Meer et al., 1996] was still applicable for narrow crested, rubble mound structures. However, they came up with a new formulation for the wave transmission of wide crested ($B/H_{m0} > 12$) rubble mound breakwaters. And with two new formulas for smooth impermeable structures, both applicable to a different range of ζ . All can be found in Table 2.1.

[BUCCINO AND CALABRESE, 2007] In 2007 Buccino and Calabrese came up with two conceptual design formulae for wave transmission over submerged breakwaters. The formulae are derived from the theoretical physical processes that govern wave transmission, namely the wave breaking, overtopping and seepage through the barriers. The parameters which are included in the equations are the relative crest width, the relative freeboard of the structure and the Iribarren parameter which determines the type of wave breaking on the structure. Furthermore, according to these results, for relatively long waves $s < 0.01$, the k_t is expected to decrease.

TABLE 2.2: Summary of the ranges of parameters involved in 2D wave transmission tests at low crested structures [Van der Meer et al., 2005] [Tajziehchi and Cox, 2008].

Database	R_c/H_i	B/H_i	$B/L_{0,p}$	$\zeta_{0,p}$	H_i/d_f	$s_{0,p}$
Old Database	min: -4.0 max: 8.7	min: 0.37 max: 43.48	min: 0.009 max: 0.51	min: 0.7 max: 8.26	min: 0.03 max: 0.62	min: 0.0002 max: 0.06
Seabrook & Hall	min: 0 max: 3.9	min: 1.38 max: 74.47	min: 0.04 max: 1.66	min: 0.8 max: 8.32	min: 0.11 max: 0.58	min: 0.01 max: 0.06

Database	R_c/H_i	B/H_i	$B/L_{0,p}$	$\xi_{0,p}$	H_i/d_f	$s_{0,p}$
Bleck & Oumeraci	-	min: 2.5 max: 12.5	-	-	min: 0.11 max: 0.29	min: 0.0014 max: 0.1
UCA	min: -1.53 max: 1.5	min: 2.67 max: 30.66	min: 0.04 max: 0.4	min: 3.97 max: 12.98	min: 0.1 max: 0.37	min: 0.002 max: 0.02
UPC	min: -0.88 max: 0.37	min: 2.66 max: 8.38	min: 0.07- 0.24	min: 2.69 max: 3.56	min: 0.17 max: 0.33	min: 0.02 max: 0.034
GWK	min: -0.66 max: 0.76	min: 1.05 max: 8.13	min: 0.02 max: 0.21	min: 3 max: 5.21	min: 0.31 max: 0.61	min: 0.01 max: 0.03
M&M	min: -8.9 max: 8.2	min: 1.02 max: 7.21	min: 0.02 max: 0.13	min: 2.87 max: 6.29	min: 0.05 max: 0.5	min: 0.01 max: 0.054
Aquareef	min: 0.09 max: 4.77	min: 1.24 max: 102.12	min: 0.02 max: 2.1	min: 1.78 max: 5.8	min: 0.1 max: 0.87	min: 0.01 max: 0.08
My Thesis Regulars	min: -0.57 max: 3.87	min: 0.93 max: 35.59	min: 0.022 max: 0.80	min: 1.49 max: 12.04	min: 0.086 max: 0.72	min: 0.016 max: 0.058
My Thesis Irregular	min: -0.78 max: 2.31	min: 1.74 max: 42.29	min: 0.049 max: 0.72	min: 1.95 max: 18.49	min: 0.072 max: 0.40	min: 0.017 max: 0.036

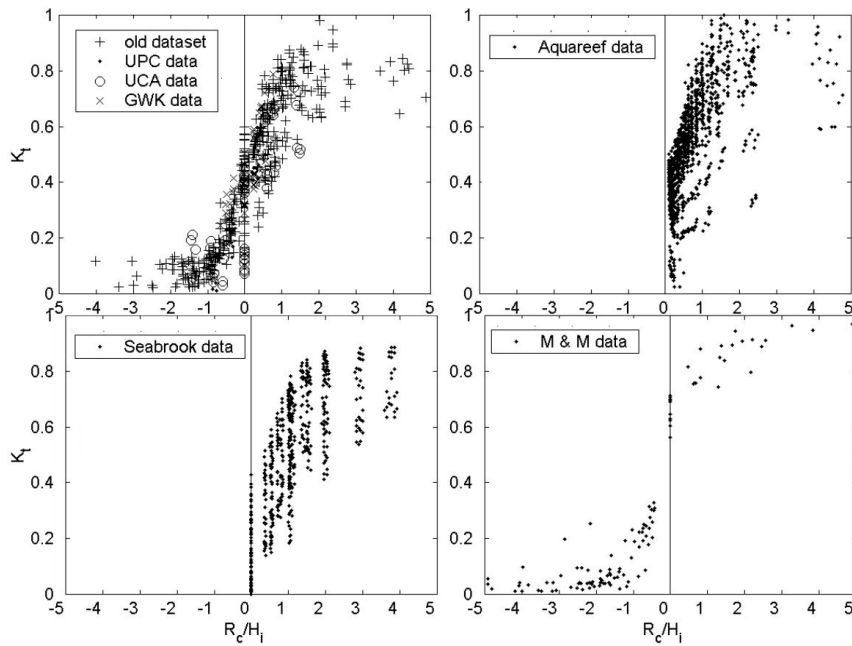


FIGURE 2.3: Wave k_t versus relative freeboard for the four sub-datasets used for the DELOS project by [Van der Meer et al., 2005].

Additional design variables

Next to the design variables which can be found in the empirical equations of Table 2.1, the impact of some other design variables is investigated during the physical experiments. Below, a short summary is given for each of these variables and the expected results based on other studies are discussed.

PERMEABILITY First, the effect of the permeability of a Reefy structure is investigated. According to [Shin et al., 2019], the k_t increases when the permeability of a structure increases. Also some equations from Table 2.1 distinguish between structures with an impermeable- and permeable outer layer. These equations expect less dissipation over the crest of impermeable structures, and therefore less impact of the crest width on K_t . For the Reefy design it is crucial to investigate the hydrodynamic effect of the permeability and come up with a design to achieve minimum wave transmission, without losing the ecological- and morphological benefits of the permeability.

DOUBLE STRUCTURE Second, the impact of a double shore-parallel breakwater on the hydrodynamic performance is investigated for different distances between two structures. In literature, two numerical studies are found which investigated a similar situation. Both studies simulated two impermeable, trapezoidal, submerged breakwaters and regular waves. More information about the wave conditions and set-ups of these studies can be found in Appendix B.1.4. Below, both results are shortly described.

The study from [Liang et al., 2015] found an optimal distance relative to the incoming deep-water wavelength, resulting in a minimum transmission. The optimal distance was found to be 0.44⁵, which gave maximum reduction in k_t of 0.25 compared to a relative spacing of e.g. 0.33 and 0.12. From the results of [Rambabu and Mani, 2005] the optimal distance relative to the incoming deep-water wave length can not be derived.

[Rambabu and Mani, 2005] investigated the distance relative to the total width of both crests. An optimum has been found around 1.00. However, the impact of the relative distance on k_t was found to be much smaller compared to the study of [Liang et al., 2015], namely around 0.05. Furthermore, according to the results of [Liang et al., 2015] the optimum of the distance relative to the total crest width lies around 1.37. Both studies are based on different wave steepness's, - slope steepness's and - width to depth ratios. Therefore, no firm conclusion can be drawn about the reason for the different outcomes.

RELATIVE STRUCTURE HEIGHT Third, the impact of the structure height relative to the local water depth is investigated. Most studies calculate the impact of crest-height as $R_c/H_{m0,i}$, as can be seen in Table 2.1. However some authors suggest h_c/d is a better estimator for the $k_t(s)$ and therefore both are investigated. Examples of such studies come from [Armono, 2004] [Srisuwan and Rattanamane, 2015], which are both based on a similar design of five shore-parallel rows

⁵ [Liang et al., 2015] calculated the relative spacing S as the length between the center of both crests as can be seen in Figure B.5a. The optimum spacing S/L_0 has been found as 1.11. Since the result is based on one wavelength $L_0 = 6.25m$ and one breakwater design, this means the optimum empty space between the structures was equal to 2.73m. Thereby, the optimum relative distance is 0.44.

of hemispherical artificial Reefs on a supporting layer. [Armono, 2004] investigated structure height to depth ratios between $0.7 < h_c/d_f < 1.0$ and [Srisuwan and Rattanamane, 2015] of $0.77 < h_c/d_f < 1.11$. Therefore, the relative structure height is quite high. These studies do include the impact of the incoming wave-height in their empirical formulas of k_t , namely in the form of $\frac{H_i}{g*T^2}$.

RELATIVE CREST WIDTH Last, the impact of the width is investigated relative to the deep-water wavelength. According to the studies from [Armono, 2004], [Vijay et al., 2021], [Shin et al., 2019], [Srisuwan and Rattanamane, 2015], [Ahmed and Anwar, 2011], [Lokesha et al., 2019], this parameter is related to the transmission of submerged artificial reefs. In many of the empirical equations from Table 2.1, the width relative to the incoming waveheight is used. Therefore, both are investigated.

2.1.2 Summary transmission

Based on the empirical equations from other researches summarized in Table 2.1, the main design variables of submerged breakwaters with an impact on the k_t are: the structure height h_c , freeboard R_c , crest width B , front slope α and the nominal diameter of the stones D_{n50} (for rubble mound type of breakwaters). In general, the k_t is expected to decrease with an increase in crest height, -width, incoming wave height, -steepness and nominal diameter. And it is expected to increase for an increase in slope and water depth. Furthermore, some studies discussed in Table 2.1 distinguish between permeable- and impermeable structures. It is expected that an increased permeability increases the transmission through the structure until a certain extent, nevertheless it is also expected to increase the dissipation of waves over the crest. Therefore an increased crest-width is expected to have a bigger impact on the transmission for more permeable structures.

Lastly, no consensus has been found in literature on the impact of the distance between a double shore-parallel breakwater of a trapezoidal shape. However, two numerical studies suggest the distance can be optimized. [Liang et al., 2015] defines an optimal distance relative to the incoming deep-water wavelength, whereas [Rambabu and Mani, 2005] defines an optimal distance relative to the total crest width. Furthermore, [Liang et al., 2015] measured a much bigger impact of the distance on k_t than [Rambabu and Mani, 2005] did.

2.1.3 Wave reflection

Wave reflection can be described using the reflection coefficient, which is calculated as the ratio of the reflected wave height to the incoming wave height [CIRIA, 2007]. Reflection is an important characteristic of an AR which is built with relatively steep slopes. The interference between the reflected- and incoming waves create standing wave patterns, which affect the near-field flow of water and is therefore also import for stability considerations.

Existing empirical formula

A summary of the empirical equations from previous studies for the reflection of waves at submerged breakwaters can be found in Table 2.3. A short description of each study is given in the paragraphs below.

TABLE 2.3: Summary of relevant literature formulae regarding wave reflection .

Author	Formulae	Applicability
Rock Manual A Rock Manual B	$K_r = f_r * 0.14 * \zeta_{0,p}^{0.73}$	$\zeta_{0,p} < 10$
Van der Meer & Briganti & Zanuttigh & Wang (2005)	$K_r = f_r * 0.071 * P^{-0.82} \cot(\alpha)^{-0.62} * s_{0,p}^{-0.46}$ $f_r = -0.2 * \frac{R_c}{H_{s,i}} + 0.9$ $f_r = 1$	$R_c/H_{s,i} > -0.5$ $R_c/H_{s,i} \leq -0.5$
Zanuttigh & van der Meer (2008)	$K_r = \tanh(a * \zeta_{0,m-1,0}^b) * (0.67 - 0.37 * \frac{R_c}{H_{s,i}})$ $a = 0.167(1 - \exp(-3.2 * \gamma_f))$ $b = 1.49(\gamma_f - 0.38)^2 + 0.86$	$-0.5 < \frac{R_c}{H_i} < 1$

[VAN DER MEER ET AL., 2005] In the Rock Manual, the wave reflection for non-overtopped structures has been described. As a part of the DELOS project, a reduction factor f_r has been formulated which can be applied to these empirical formulas for low-crested structures.

The most simple formula found in the Rock Manual is $K_r = a * \zeta^b$. Coefficients a and b vary for smooth and rough slopes. The values used in Table 2.3 are based on rough permeable slopes. This formula is referred to as *Rock Manual A* in Table 2.3.

Rock Manual B shows an alternative formula, treating the slope angle and wave steepness separately. Compared to the breaker parameter used in Rock Manual A, here the slope angle has more influence than the incoming wave steepness. The influence of the slope angle reduces if the structure gets more submerged. Furthermore a notional permeability factor P for the structure is included, which is often close to 0.4 - 0.6 in the case of overtopped structures.

[ZANUTTIGH AND VAN DER MEER, 2008] As a part of the European research program CLASH, Zanuttigh and van der Meer came up with a new formula, including the roughness parameter γ_f . This roughness value is determined by the material of the seaward slope. Namely, due to energy dissipation during interaction with a structure, rough structures reflect significantly less energy than smooth structures. Furthermore, Zanuttigh and van der Meer used the spectral wave period $T_{m-1,0}$ at the toe of the structure as an input for the breaker parameter:

$$\zeta_{0,m-1,0} = \frac{\tan \alpha}{\sqrt{\frac{2 * \pi * H_{m0,i}}{g * T_{m-1,0}}}} \quad (2.1)$$

Additional design variables

Next to the design variables from Table 2.3, the impact of the distance between two Reefy structures is investigated from the experiments. [Liang et al., 2015] concluded the stream-wise distance between two shore-parallel breakwaters has no correlation with the k_r . Nevertheless, as this conclusion is made for impermeable structures it is uncertain whether these results are applicable to the Reefy configurations as well.

Furthermore, all the dimensionless design variables discussed in the section on wave transmission are evaluated for the wave reflection as well. For example, an analysis on the impact of the crest-width on K_r is also included.

2.1.4 Summary transmission

Based on the empirical equations from other researches, the main design variables with an impact on the k_r are the crest height h_c , freeboard R_c , front slope α , permeability P and roughness γ_f . Based on previous literature, reflection is expected to decrease if the front slope and/or permeability decreases. And K_r is expected to increase if the crest height and/or roughness increases.

2.2 ECOLOGICAL PERFORMANCE

In recent years there has been an increased attention for the environmental impact of coastal defence structures and how to mitigate these; as well as on how to design artificial reefs that enhance and improve natural levels of productivity of the given ecological system. Both aspects are discussed in this chapter.

In Section 2.2.1, the aspects about the environmental enhancement function are described. For this purpose, first the importance of the flow- and wave velocities around a structure are explained. Next, the maximum orbital velocities in which some inhabitants of natural reefs are able to survive are summarized and discussed. Thereafter, two performance indicators which can be used to assess the ecological enhancement of a structure are introduced. At the end, the design features that are known to enhance the attraction of biomass to a structure are summarized.

In Section 2.2.2, the measures which can be taken to mitigate the ecological impact on a broader scale are explained.

2.2.1 Environmental enhancement

Flow field around artificial reefs

In advance to discussing the design features which can be used to enhance the ecological performance of artificial reefs, it is important to describe why marine life is attracted to artificial

reefs in the first place. Fish tend to aggregate around artificial reefs, for reasons such as presence of food, the light penetration and protected shelter. However, flow patterns within and around artificial reefs can influence the livability for marine species.

The wake region is the zone downstream of a structure. Due to the difference of flow velocities within the water column here, the flow is disturbed and recirculating [Armono, 1999]. Due to the low flow velocities, this zone reduces the energy demand of marine species and can be utilized as for example energy saving zone or spawning ground. Furthermore, a slow flow region facilitates the attachments of marine epibiota and their growth [Armono et al., 2001] as well as enhancing the settlement of sediments containing food organisms such as larvae [Armono et al., 2001].

Also the flow within the structure is an important factor which can attract fish to the reef. A moderate flow can attract high amount of plankton to the reef⁶, which serves as a food source for other marine life [Anonymous, 2003]. Furthermore, planktonic larvae need to be able to attach to the structure (settle) and thereafter metamorphose into a juvenile. In order to maintain the plankton within the structure and increase the chances for larvae to settle, the flow should recirculate through the structure [Hata et al., 2017]. If the flow within a structure is too high, the nutrients are washed out of the structure. If the velocities are too low (5 to 10 times lower than their physical limits), marine life can die due to hypoxia [Siddon and Witman, 2003] [Anonymous, 2003] or settlement of fine marine sediments can lead to siltation and closure of the reef [Kontaxi and Memos, 2005].

Lastly, the local maximum velocities to which an artificial reef is exposed are one of the most important factors determining the abundance of species [Hammond and Griffiths, 2004]. If the forces exceed the natural limits for epibiota, damage or complete dislodgement can occur. Moreover, the benthic⁷ communities as a whole can also be at risk for colony dislodgement caused by severe hydrodynamic forces. The size, shape and distribution of many species in a marine ecosystem depend on the wave-generated forces [Kontaxi and Memos, 2005]. In general, an increase in velocities is associated with a decrease in body size and increase in attachment strength.

All in all, acquiring information on the hydrodynamic field around the structure is important in order to assess the ecological potential and risks. However, it should be realized that all changes in coastal structures, such as artificial reefs, have an impact on ecology and might enhance the chances of some plants and animals, whilst impairing the chances for other organisms. According to the DELOS project the use of hydrodynamic parameters like the mean flow, seepage velocity, and the maximum- and minimum mean velocities are sufficient for the ecological issues and the evaluation of turbulent velocities is not critical at this point [Anonymous, 2003]. This can be explained from the fact that an optimal turbulence intensity for the growth in benthic suspension feeders is different per species [Kontaxi and Memos, 2005]. The studies on the mean flow fields are good to estimate for example the settlement of larvae and nutrient circulation in periods of critical low flow regimes [Losada et al., 2003]. On the other hand, the orbital velocities and forces due to waves are the most important mechanisms

⁶ Plankton is an organism which floats in the water and is carried by tides and currents

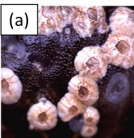
⁷ Benthic means it lives in the benthic zone, which is the lowest ecological zone in a water body. Suspension feeder means it feeds itself from material suspended in the water, such as plankton.

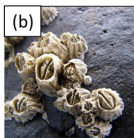
in determining the abundance, distribution and mortality of shore organisms in artificial reef systems [Kontaxi and Memos, 2005].

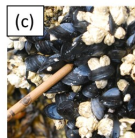
Limiting velocity conditions per species

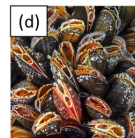
In Figure 2.4, the the maximum orbital velocities in which some organisms which naturally occur on reefs are able to survive/feed/grow, are summarized. A detailed literature study on these species, together with background information about the studies from which the limiting conditions are obtained, can be found in Appendix B.2.2. Here, only corals are discussed, because this information is used later on in the study. Different types of damage from increased

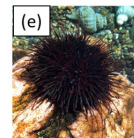
Organism type	Name	Streamwise velocity U_x limits [m/s]		Based on waves/flow
Barnacle	Balanus cretanis (a)	Growth optimum/limit	0.08 m/s	Flow
		Deflection cirri start	>0.25 m/s	
Barnacle	Balanus glandula (b)	Feeding limit	>2-4 m/s	Waves
Mussels (10-25 mm shell length)	Mytilus trossulus (c) & Mytilus edulis (d)	Dislodgement (starts from..)	>7 m/s	Waves
Sea urchin	Strongylocentrotus nudus (e)	Feeding limit	>0.40 m/s	Waves
		Movement limit	>0.80	
Sea urchins (1-4 m depth)	Strongylocentrotus droebachiensis (f) & Seastar: Asterias forbesi (g)	Dislodgement (95%)	7.5-9.9	Waves
Marine snail	Astraea undosa (h)	Dislodgement (50%)	4 m/s	Flow
		Dislodgement (100%)	>8 m/s	Flow
Branching coral	Acropora intermedia (i)	Breaking	0.5-1 m/s	Flow

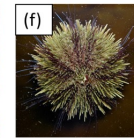


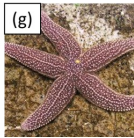


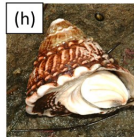












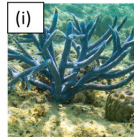


FIGURE 2.4: Summary of the limiting water velocities in which certain species can withstand based on the literature discussed in this chapter. The type of damage which is expected to occur at this limit value is shown in the figure. If the study is based on an environment exposed to waves of flow is also shown. The pictures below correspond to the discussed organisms and are linked with a letter between a and i.

flow velocities can be found in Figure 2.4. Dislodgement and size- and shape distribution is discussed in the previous paragraph. Additionally, for some organisms, the ability to feed or move ceases if the flow velocities exceed a certain limit. Appendix B.2.2 discusses the results

from Figure 2.4 for each organism separately and a paragraph on coral larvae is added there as well.

CORALS Corals live in marine environments and are sessile organisms (except during the larval stage). Some corals subtract calcium carbonate from the water to form a hard substrate of it and to built the framework of a reef. These type of corals are referred to as reef-forming corals and are often found in shallow water.

[Baldock et al., 2014] concluded that the impact of hydrodynamic forces on the expected damage of corals is different for branching- and massive corals, see Figure 2.5. Namely, massive corals are not expected to break from wave forces, whereas branching corals are. Breakage of a branching coral does not necessarily mean the coral dies. Namely, it can lead to reproduction as well, if the broken part can re-attach itself to another substratum and the other part recovers. Nevertheless, the amount of branching corals is often reduced after severe wave conditions, because the re-attachments does not always succeed.

[Baldock et al., 2014] investigated the breaking limit of a branching coral type named *Acropora intermedia*, which is one of the fastest growing coral types. The failure stress differs per location in a branching coral, see Figure 2.5⁸. The authors recommend to use section B and C for the breaking analysis, as section A in the model has a smaller cross-section and stiffness than is expected in real life conditions. For section B breaking is expected to occur for a flow velocity of 0.5 m/s and at section C for a flow velocity of 1 m/s.

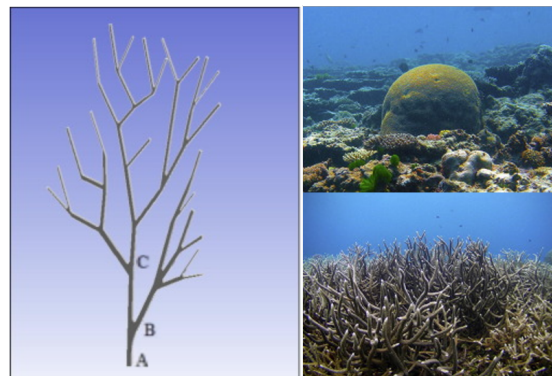


FIGURE 2.5: Picture from a typical branching corals (*Acropora* spp.), at the right bottom, left, and from a massive coral (*Favia* sp.), at the right top. Left is the geometry of branching coral as is used in the study from [Baldock et al., 2014]. The sections are labelled 'A', 'B' and 'C'.

[Rodgers et al., 2003] investigated the tensile- and compressive strength of coral species which are dominant in Hawaii. The outcomes suggest that the strength of a coral is adaptive to the hydrodynamic forces which are present in the area they inhabit.

⁸ [Baldock et al., 2014] used 10 MPa as the failure stress.

Performance parameters

As can be understood from section above, no general rule exist about the optimum turbulence or velocity levels in- and around a structure. Nevertheless, two studies are found in literature which came up with some performance parameters for the flow field around the structure with respect to the ecological enhancement. These are the tranquility index and the safety factor.

TRANQUILITY INDEX The numerical study of [Kim et al., 2016] defined three indexes to evaluate the performance of a wake region. Two of the three indexes are based on the volume of the wake. The third index is based on the flow velocities and is called the the tranquility index (Tr). The equation for this index is given in equation 2.2. A high Tr in this study means the mean velocities in the wake are much smaller than in the front.

$$Tr = \frac{u_{x,ref}}{u_{x,wake}} \quad (2.2)$$

SAFETY FACTOR The study of [Baldock et al., 2014] defined a factor of safety to determine whether a branching coral type is expected to break at a specific location. This factor is calculated from the velocity at which breakage is expected to occur divided by the root mean squared flow velocity at this location ⁹. For this, a model is used which calculated the safety factor for many locations within- and around the structure.

Design features

There exist multiple studies on how to design a reef structure, such that it produces new biomass of marine life ¹⁰ and increases biodiversity. In this section, the conclusion of the studies on ecological design characteristics are summarized.

COMPLEXITY Increased habitat complexity enhances the diversity and abundance of species proportionally by introducing the physical phenomena of turbulence and upwelling, circulating oxygen and larvae within the structure [Kostylev et al., 2005] [Charbonnel et al., 2002]. These phenomena transform the structure into a feeding area and increases the aggregation of fish [Sladonja, 2011]. Furthermore, the increase of complexity and holes on top allows solar radiation to penetrate into the structure as well as it creates protected areas for fish to hide from wave forces and predators. According to [Anonymous, 2003], complexity (holes, blocks and crevices) should be added on horizontal surface to increase in the diversity of epibiota ¹¹.

[Schoonees et al., 2019] discusses methods to increase the complexity. For example, holes inside an AR can be implemented for this purpose. The shape of holes (circular, squared or polygons)

⁹ For more information about the root mean squared orbital velocity of a monochromatic wave, the reader is referred to the paper from [Soulsby, 1987].

¹⁰ Attention should be drawn to the production versus attraction debate amongst scientists. The purpose of an AR is to increase the abundance of fish in the whole coastal area (production) and not to only attract fish from other reefs (attraction). However, both phenomena are not mutually exclusive [Degraer et al., 2020].

¹¹ Epibiota are organisms who live on the surface of another living organism, in this case on the "living breakwater".

has almost no effect on the upwelling velocity, but the diameter of the holes is closely related to current vortices [Jiang et al., 2020]. According to [Anonymous, 2003], the diameter should be larger than 50 cm to keep pores free of excessive marine growth.

SIZE/HEIGHT Every species prefers a different velocity climate and a different depth in the water column, therefore an increase of structure height increases the biodiversity [Borsje et al., 2011]. Furthermore, the attachment of species onto the surface is increased by increasing the surface area and the height of the structure [Jiang et al., 2020][Anonymous, 2003]. Also [Kostylev et al., 2005] concluded that the total abundance of animals is dependent on the available surface area, even more than on the complexity of the structure.

[Takeuchi, 1991] conducted an early study on the effect of the height and suggests the length of the wake-zone increases if the structure height increases. However, the velocities in the wake are not related to the length of the wake according to [Kim et al., 2016].

LOCATION It is expected that the diversity increases if the structure is built further offshore. As a higher number of species can survive environmental conditions lower on the shore. However, both [Anonymous, 2003] and [Moschella et al., 2005] discuss the fact that species existing in different types of tidal regimes are differently affected by the location. For example, there are exceptions to this rule such as mussels and barnacles, which actually thrive in conditions with more waves.

POROSITY There is a no consensus found in literature about the effect of porosity on the length of the wake-region behind the structure. For example, [Takeuchi, 1991] suggests the wake length of an impermeable structure is longer compared to the wake length of a permeable structure. On the other hand, [Chan et al., 2007] stated the wake gets elongated for an increased permeability of the structure, but the turbulence intensity reduces in the wake. The wake length is important for determining the space needed between multiple breakwaters.

Secondly, as explained the next section (2.2.2, an increased porosity is good for the water quality at the lee-side of the structure.

MATERIAL For the attachment of benthic species, the diversity tends to be less on smooth concrete structure compared limestone [Anonymous, 2003]. However, compared to some other factor such as the complexity, the material of the structure is probably less essential for the growth of epibiota.

A promising new development in the materials used for artificial reefs is based on the mineral accretion technology (MAT), also referred to as Bioreck [Miller, 2020]. A low voltage electricity is applied through the metal of reinforcing steel bars. The electrolysis reaction in seawater on the one hand prevent corrosion, but more importantly causes dissolved mineral to accrete on the steel, creating a better environment for the growth and survival of corals and other calcium carbonate secreting marine organisms. This even makes the coral more resistant to temperature changes.

2.2.2 Impact mitigation

With respect to the mitigation of the impact of coastal defence structures on the environment, the DELOS project investigated how to mitigate the impact to existing ecosystems. All in all, the project concluded that a site-specific environmental management plan needs to be created. In this section, the advice on measures which can mitigate the ecological impact are summarized and references are made to other relevant studies on these aspects.

BIO-GEOGRAPHIC CONTEXT A coastal defence structure can change the functioning of a coastal ecosystem on a local scale (e.g. new artificial hard-bottom habitats) and on a regional scale (e.g. spread of non-native species). Therefore, the whole coast should be treated and investigated as an integrated unit. While some consequences are applicable to each project (e.g. construction), most effects are site specific [Airoldi et al., 2005]. Environmental regional context and predominant habitat characteristics need to be investigated and monitored beforehand.¹² Moreover, long-term monitoring of the performance of the reef from an regional ecological point of view are needed to comprehend the performance of a structure.

AMOUNT OF STRUCTURES Hardening of the whole coastal area can lead to long-term and large-scale effects. Therefore it is advised to avoid large scale proliferation of breakwaters [Airoldi et al., 2005].

SPATIAL ARRANGEMENT The distance of a structure with respect to other natural reefs or structures is an important factor in determining the dispersal and interaction of species. Including non indigenous species. It should be the aim to preserve the native species as non indigenous invasive species have an adverse ecological impact and poses a threat to the marine biodiversity. For example, they can ease the spread of diseases [Dafforn et al., 2015]. According to [Schoonees et al., 2019], the colonisation of non-native species can be avoided by seeding the structure with native species or adding a coating or smoothing the construction material. [Sheehy and Vik, 2010] introduces general approaches for anticipating, assessing, and controlling non-invasive species based on a case study in Mexico.

[Jordan et al., 2005] investigated the impact of small-scale spacing between artificial reefs on the total fish abundance and the species richness. In general, both increased with increasing isolation distance. The isolation distance between structures varied between 5, 15 and 25 meters. However, species-specific and size class differences in response to isolation distance are observed.

DISTURBANCE Disturbances as scour and sedimentation can lead to changes in the diversity and mortality of marine species. These can be avoided by building a stable structure with scour protection. Also human disturbances from maintenance work have a negative impact, because these hamper the development of stable, mature assemblages [Airoldi et al., 2005]. According to

¹² An example of a modelling tool to predict the ecological response developed by [Hawkins et al., 2010], based on the outcomes of the DELOS project, is shortly described in Appendix B.1.3. Above that, more reports on ecological modelling tools can be found on the official DELOS website

[Moschella et al., 2005], there is little use in optimizing the design to enhance diversity, unless maintenance is reduced.

POROSITY/HEIGHT Increased porosity of a structure allows for better circulation and renewal of the coastal waters, enhancing thus the nearshore water quality and mitigating changes to existing environments [Airoidi et al., 2005]. The same holds for a reduction in the height of the structure compared to the water depth.

3

PHYSICAL MODEL

In this chapter a summary of the physical experiments which are conducted for this research is given. The purpose of this chapter is to create an understanding of the experiments for the reader.

First, the set-up during the experiments is explained, including the layout of the wave flume, Reefy blocks and the used data collection methods. Next, the wave conditions are treated. Lastly, the different design configurations are elaborated on and it is explained which design variables are investigated from these structures.

3.1 SCALING

"A Physical Model is a physical system reproduced (usually at a reduced size) so that the major dominant forces acting on the system are represented in the model in correct proportion to the actual physical system (Hughes, 1993)"

There are three criteria for a physical model to achieve similarity with a real system, which is believed to be achieved when all the major factors related to fluid action are in proportion between model and real system. These criteria are geometric-, kinematic- and dynamic similarity. For the perfect dynamic similarity, the Froude number ($\sqrt{\frac{\text{Inertial force}}{\text{gravitational force}}}$), Reynolds number ($\frac{\text{Inertial force}}{\text{Viscous force}}$) and Weber number ($\frac{\text{Inertial force}}{\text{Surface tension}}$) must be similar for real system and model [Chanson and Gonzalez \[2005\]](#). This is not completely possible for the Reynolds - and Weber number. If water is used as a fluid they will become inevitably lower, because the material properties do not change but the wavelength and velocities do. Nevertheless, it is widely accepted to assume the gravitation and inertia are the dominating processes in the model and the viscosity and surface tension of water do not play an important role [Frostick et al. \[2019\]](#). Then only the Froude scaling laws need to be applied, keeping the Froude number constant, see equation 3.1.

$$Fr = \frac{u}{\sqrt{gd}} \quad (3.1)$$

From applying the Froude scaling laws, the conversion ratios expressed in terms of the model length scale factor n_l , are obtained. The length scale factor of the experiments is $n_l = 15$. This simply means the lengths in model are 15 times smaller than in real system.

WAVE MAKER On the left side of the flume, at location ($x = 0m$), a piston-type (translatory) wave generator was operating with a remote-control system. The reflection compensation function has been activated for all experiments. Also the option in the settings of the wave-maker to create second-order waves had been activated for all tests. The max-frequency was set to 5Hz and the minimum frequency to 0.02 Hz.

DEEPEST WATER AREA The water depth in the area between the foreshore and the wave maker is referred to with d_0 . There was a pumping system in place, which enabled it to vary the water level. The maximum pumping capacity is $0.6m^3/s$ and the different d_0 values which have been tested are $0.61m$, $0.68m$ and $0.75m$. Three wave gauges (1, 2 and 3) are placed in this part of the flume.

ABOVE THE FORESHORE A foreshore (flat bottom) was built with a height of $44cm$. The slope at the incoming wave-side has an angle of 1:10 and was built to create more non-linear waves because these are present in real life. The Reefy structures were placed on the foreshore, in between wave gauges 6 and 9, with the front of the structure approximately at $25.10m$. However, this precise location was not consistent during the experiment and changed around 10 centimeters.

WAVE DAMPER On the right side of the flume, at location ($x = 55m$), a parabolic wave damper was installed, absorbing the waves and minimizing reflection. The top of the wave damper was approximately 10 cm below the top of the wave flume, see Figure 3.3f.

WAVE GAUGE Wave gauges were used during the experiments to derive wave characteristics at specific locations in the flume. A wave gauge (WG) consists of a pair of parallel stainless steel bars, operating as electrodes. From these electrodes the resistance of water between the rods is measured in Volts. This is an analogue signal that can be converted to the free surface elevation of the water with a conversion coefficient. The sample frequency of the wave gauges is $40Hz$. Each WG had been calibrated by Deltares prior to the experiments.

ELECTROMAGNETIC LIQUID VELOCITY METER The electromagnetic liquid velocity meter measures the water velocity by creating a magnetic field beneath the probe. This magnetic field is induced from an electrical current inside the body of the probe and should not be disturbed. It measures the water velocity in two perpendicular directions (x and z). Two electrodes inside the probe measure the voltages produced by the flow past the probe, which are proportional to the liquid velocity parallel to the plane of the electrodes. For the experiments the E30 probe of Deltares is used, which is very suitable for laboratory experiments due to its smaller probe size compared to E40. Prior to the experiments, the EVM had been calibrated by Deltares as well.

3.2.2 Data collection methods

Table 3.2 gives an overview of the abbreviation and location of each type of equipment, which has been used during the experiments to collect data. For every test one to three observation forms are filled in, depending on the task division amongst the three Reefy members present at

the experiments. On these forms, the significant observations are written down together with the start- and end time of the test. Furthermore, a camera had been installed on top and on the side of the flume, to record a video of each test.

An extra wave gauge, WG₁₀, was added behind the structure for set-up measurements during the last day of testing for Structure 4, 5, 6 and 7.

The different locations of the EVM with respect to the structure and bottom of the foreshore can be seen in Figure 3.2 for a 1:15 scale. The real life scale distances are summarized in the caption. During heavy wave conditions the EMS was placed far away from the structure, to avoid damage from loose blocks. For the milder conditions the EVM changed locations between the back and the channel of the structure.

Ink injections are used as a passive scalar source during some irregular wave conditions, to investigate the propagation of water flow. This is an indication of how the nutrients will be distributed through the structure and investigate the turbulence in- and around the structure. The transport and mixing process of this passive scalar source are documented on camera.

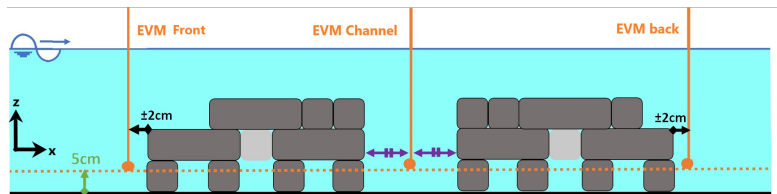


FIGURE 3.2: Sketch of the distance of the EVM locations with respect to the bottom (from the foreshore) and the structure. The scale is 1:15. Thus the EVM measurements are taken 75 cm above the bed for real life conditions. The measurements at the back are taken from approximately 30 cm behind the back of the structure (1:1). In the channel the measurements are taken at half of the channel length.

TABLE 3.2: Overview of instrumentation and measurement equipment in- and around the flume.

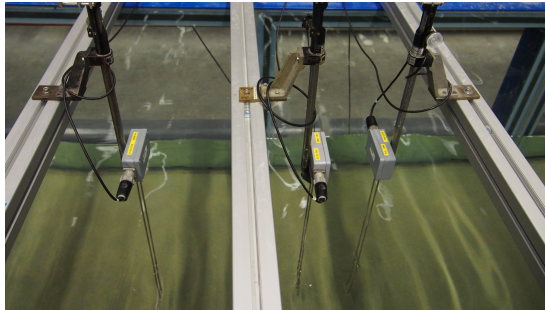
Measurement equipment	Abbreviation	Fixed/Free	x-position
Wave gauge 1	WG1	Fixed	11.97m
Wave gauge 2	WG2	Fixed	12.96m
Wave gauge 3	WG3	Fixed	13.13m
Wave gauge 4	WG4	Fixed	22.40m
Wave gauge 5	WG5	Fixed	22.79m
Wave gauge 6	WG6	Fixed	22.98m
Wave gauge 7	WG7	Fixed	27.46m
Wave gauge 8	WG8	Fixed	27.86m
Wave gauge 9	WG9	Fixed	28.05m
Wave gauge 10	WG8	Free	26.93/26.16m
Electromagnetic velocity meter	EVM	Free	Figure 3.2
Ink injector	N/A	Free	Multiple
Camera top view	N/A	Fixed	12.96m
Camera side view	N/A	Fixed	±25.22m
Camera free	N/A	Free	Multiple
Observation form	N/A	Free	N/A



(A) EVM behind the structure



(B) Set-up around the flume (top camera+observation form)



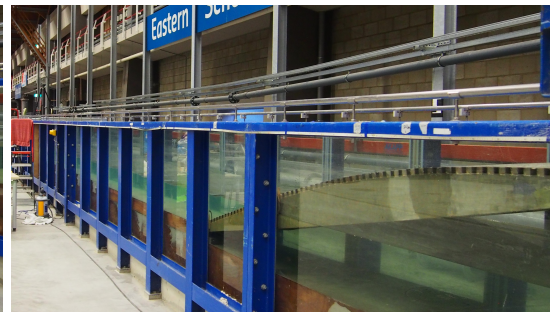
(C) Top view three wave gauges



(D) Wave maker installation



(E) The foreshore



(F) The parabolic wave damper

FIGURE 3.3: Pictures taken during the wave flume experiments.

3.2.3 Reefy block

The blocks which are used to build the Reefy structure during the physical experiments are 3D printed from biodegradable PLA and filled with a cement mixture. The block design has holes inside, these are amongst others to create shelter areas for marine life. Other benefits of the high permeability are the improved water quality, the room for the return flow through

the structure and thereby mitigate erosive patterns and the reduction of scour. A sketch of the blocks is given in Figure 3.4, together with the dimensions of a real system-block. It is not visible in the sketch, but every hole had a male or female outer part, creating an interlocking system between the blocks for extra stability. The edges of the blocks are smooth, for reduction of the drag-coefficient. Furthermore, it also creates small crevices for marine life. See Figure 3.5.

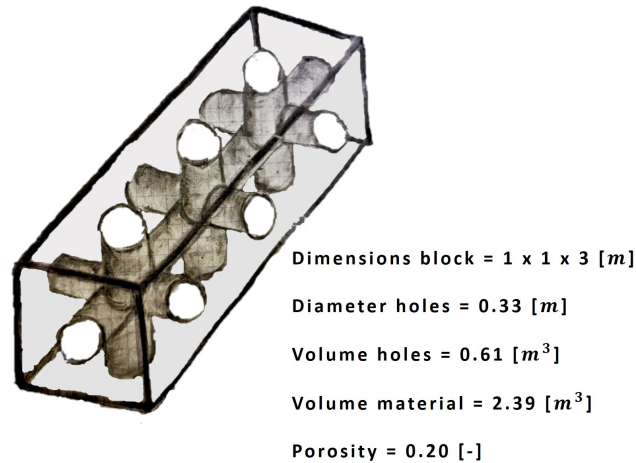


FIGURE 3.4: Sketch of block and holes inside. Dimensions given are for a 1:1 scale.

TABLE 3.3: Reefy block characteristics from the model + these characteristics converted to a real system based on Froude scaling laws

Dimension	Model 1 : 15	real system 1 : 1
width x height x length	0.067 x 0.067 x 0.20 m	1 x 1 x 3 m
Volume holes	$0.18 \times 10^{-3} \text{ m}^3$	0.61 m^3
Volume material	$0.71 \times 10^{-3} \text{ m}^3$	2.39 m^3
Mean dry weight	1329 g/block	4485 kg/block
Mean dry density	1.88 g/cm^3	1.88 g/cm^3
Mean saturated weight	1378 g/block	4651 kg/block
Mean salt water saturated weight	1379 g/block	4655 kg/block
Mean salt water saturated density	1.95 g/cm^3	1.95 g/cm^3
D_{50}	8.9 cm	1.3m

The main differences between the block design in the model and in real life are the density and the surface roughness. The density of the blocks slightly below the density of concrete of 2.4 g/cm^3 , see table 3.3¹. The final material of the Reefy block is still under considerations, but is likely to become a concrete-type of material. Furthermore, the outer part during the

¹ The weight of the block is measured before and after the experiments. The density of the blocks is calculated based on the saturated weight for salt water.

experiments consists of a smooth material, whereas in real life it will probably be made of a concrete type with a rougher surface. Both differences have an impact on the structural stability, but not on the hydrodynamic performance.



FIGURE 3.5: Close-ups of one of the Reefy design configurations tested during the experiments for this thesis. The 3D-corals are added to investigate the effect of increased surface roughness once reef-building species colonize or are pre-seeded on the structure.

3.3 WAVE CONDITIONS

During the experiments, the deep water depth d_0 varied between 0.75, 0.68 and 0.61 meters. These values are based on a potential pilot project of Reefy (location confidential). More details on how these values are obtained can be found in Appendix A.2.

Both irregular and regular wave conditions have been used. For every regular wave test, the target steepness $s[-]$, wave height $H[m]$ and period $T[s]$ had to be defined to create a wave file and upload this to the wave generator. For the irregular wave file, the target steepness $s[-]$, significant wave height $H_s[m]$ and peak period $T_p[s]$ were needed. A JONSWAP spectrum wave field was generated around these values and a peak enhancement factor γ of 3.30 was used for each condition.

It was decided to vary s between 0.02 and 0.04. Measuring both the performance in long and short waves. During the experiments for every d_0 and s , the H was increased until a limit was reached in which wave breaking occurred before the structure. Namely, regular waves that break before the structure are not interesting for the present study. Thus, for each d_0 , daily- and stormy wave conditions are tested. The T for each wave condition was calculated from the dispersion relation.

3.3.1 Documentation method

in Table 3.4, the wave conditions are given a number. For every wave conditions, a test without a structure has been performed to eliminate the effect of the foreshore on the wave dissipation

processes, as is explained in Chapter 4.2. This type of test is referred to in the text as “Reference test”.

For each test the output of the EVM- and WG-measurements were saved with an unique code. An example of such a code is given in Figure 3.6. For the tests without a structure, the letters REF^2 are added behind the code.



FIGURE 3.6: Explanation of abbreviations used in the test codes

TABLE 3.4: Overview wave conditions for input arguments of the wave files (model scale). For irregular wave tests the H stands for H_{m0} and T for T_p of a JONSWAP spectrum.

Wave condition number	d_0 [m]	T_{target} [s]	H_{target} [m]	s [-]	Regular (R) / Irregular (I)
1	0,61	1,47	0,06	0,02	R
2	0,61	1,16	0,04	0,02	R
3	0,61	0,8	0,02	0,02	R
4	0,61	0,98	0,06	0,04	R
5	0,61	1,16	0,04	0,02	I
6	0,68	2,51	0,12	0,02	R
7	0,68	2,15	0,10	0,02	R
8	0,68	1,80	0,08	0,02	R
9	0,68	1,47	0,06	0,02	R
10	0,68	1,15	0,04	0,02	R
11	0,68	0,80	0,02	0,02	R
12	0,68	1,47	0,12	0,04	R
13	0,68	1,31	0,10	0,04	R
14	0,68	1,15	0,08	0,04	R
15	0,68	0,98	0,06	0,04	R
16	0,68	1,47	0,06	0,02	I
17	0,68	0,80	0,02	0,02	I
18	0,68	1,31	0,10	0,04	I
19	0,68	1,15	0,08	0,04	I
20	0,68	0,98	0,06	0,04	I
21	0,75	3,11	0,16	0,02	R
22	0,75	2,76	0,14	0,02	R

² REF stands for “Reference”

Wave condition number	$d_0[m]$	$T_{target}[s]$	$H_{target}[m]$	$s[-]$	Regular(R)/Irregular(I)
23	0,75	2,42	0,12	0,02	R
24	0,75	2,09	0,10	0,02	R
25	0,75	1,92	0,18	0,04	R
26	0,75	1,76	0,16	0,04	R
27	0,75	1,60	0,16	0,04	R
28	0,75	1,60	0,14	0,04	R
29	0,75	1,45	0,12	0,04	R
30	0,75	1,29	0,10	0,04	R
31	0,75	1,14	0,08	0,04	R
32	0,75	0,98	0,06	0,04	R
33	0,75	0,80	0,04	0,04	R
34	0,75	0,40	0,01	0,04	R
35	0,75	1,60	0,14	0,04	I
36	0,75	1,45	0,12	0,04	I

3.4 DESIGN CONFIGURATIONS

During the experiments different structures are tested. The side-view of each structure is shown in Figure 3.7. Pictures and 3D sketches of all structures can be found in Appendix A, together with an overview of which structures have been tested in each wave condition in Table A.1. The following abbreviations are used for the dimensions of a structure:

- h_c = crest height [m]
- B = crest width [m]
- α = front slope [$^\circ$]
- L_{ch} = Channel length [m]
- S_{ch} = Spacing between middle of front- and back crest width [m]
- A_{tot} = Total surface area of the contour from the cross-section [m^2]
- Φ = Porosity [$-$], calculated as $\frac{V_{total}-V_{material}}{V_{total}}$

The values assigned to each structure are summarized in Table 3.5.

2DV STRUCTURES Structures 1 to 6 are the 2DV structures, these do not change over the width of the flume. Structure 7 is similar to structure 2, but has a different orientation in which it has a shark tooth/zig-zag shape when viewed from the top. A picture taken from the top sea-side of each 2DV structure is shown in Appendix A, Figure A.1.

3D STRUCTURES The 3D structures are numbered 8 to 15, see Figure A.2 in Appendix A for 3D sketch of each structure. It can be seen that a structure is defined as an element which is repeated over the width of the flume, each structure has a lateral width of 3 meters. Furthermore, on one side of the structure some brown wooden parts can be observed in the pictures. These are so called dummy blocks, which mimic the structure. They have a smaller lateral width, because the width of the flume was too small for a the fifth structure.

The block-void composition changes over the lateral width of a 3D structure. The location of the fronts of adjacent structures alternates with 1 meter difference (real life scale), resulting in a zig-zag pattern.

Structure 8, 9, 10, 11 and 12 have an empty space between the front- and back of the structure. This distance is referred to as "channel". By default the channel length is 1 meter. For structure 8, 11 and 12 the distance varied. If the distance is 3 meters, the corresponding structure is referred to as structure # - III, 5 meters is # - V etc.

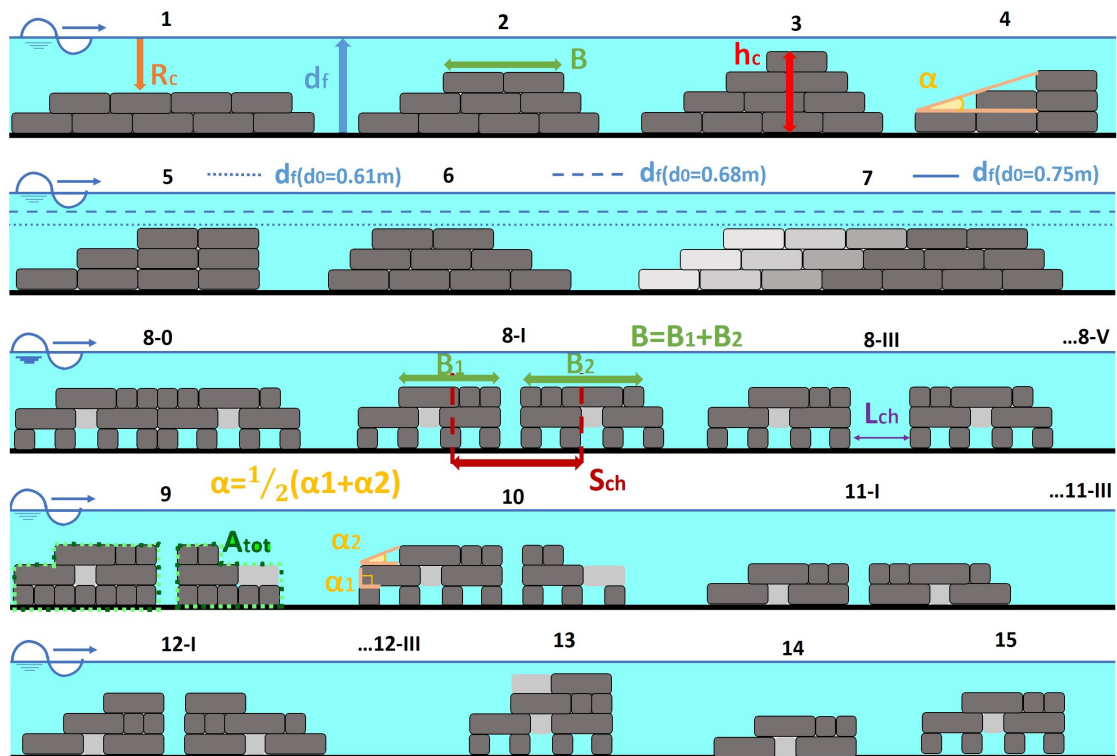


FIGURE 3.7: Sketch of the side-view from all designs. Corresponding structure-number is given above each configuration. Note that the holes inside the blocks are not shown.

Design variables

The details about the structural dimensions are summarized in Table 3.5. For each design variable, a selection is made from the structures which differ in a specific dimension and are similar in most of the other dimensions. If these structures are tested for the same wave

conditions, a comparison can be made to examine the impact of the particular variable on the performance of a structure.

The porosity in Table 3.5 is calculated as V_{voids}/V_{total} . In which V_{total} is based on $A_{total} * 3$ and V_{voids} takes into account the holes inside the blocks and the empty places $(V_{total}) - (V_{material})$.

TABLE 3.5: Details per structure based on a 1:1 scale. # of blocks is per 3 meter flume width.

Structure #	h_c [m]	B_c [m]	α [°]	Φ [-]	L_{ch} [m]	# of blocks
Structure 1	2	12	26.6	0.20	N/A	27
Structure 2	3	6	26.6	0.20	N/A	27
Structure 3	4	3	26.6	0.20	N/A	30
Structure 4	3	3	18.4	0.20	N/A	18
Structure 5	3	6	18.4	0.20	N/A	27
Structure 6	3	6	45	0.20	N/A	27
Structure 7	3	6	26.6	0.20	N/A	27
Structure 8-0	3	11	58.3	0.45	0	27
Structure 8-I	3	11	58.3	0.45	1	27
Structure 8-III	3	11	58.3	0.45	3	27
Structure 8-V	3	11	58.3	0.45	5	27
Structure 9	3	7	58.3	0.31	1	27
Structure 10	3	7	58.3	0.46	1	21
Structure 11-I	2	11	26.6	0.39	1	19
Structure 11-III	2	11	26.6	0.39	3	19
Structure 12-I	3	6	26.6	0.39	1	23
Structure 12-III	3	6	26.6	0.39	3	23
Structure 13	4	5	68.9	0.44	N/A	17
Structure 14	2	5	26.6	0.40	N/A	9
Structure 15	3	5	58.3	0.46	N/A	13

Next to the dimensional aspects of the structures, some additional features are tested. The effect of coral growth on the surface is examined by adding two type of corals on structure 8-I. The first type are 3D-printed corals as is shown in Figure 3.5 and the second are 4 cm tall PVC pipes. Both are pinned into the holes on top of the structure, referred to as Structure 8-I-3D and 8-I-PVC. Furthermore, the effect of the block permeability from the holes inside the block is investigated by blocking the holes from structure 2 vertically with PVC pipes. This mimics a the long-term scenario in which vegetation has grown in the holes of the structure. The structure is referred to as structure 2-BH.

in Table 3.6 an overview is given of the design variables which are investigated during the experiments. The table shows the structure numbers that are compared in the analysis of each variable and in if the experiments are conducted with irregular- and/or regular waves.

TABLE 3.6: Overview of tests per design variable.

Variable	Structure #	Wave type (I/R)
Crest height	1, 2, 3	R
	11-I, 12-I	I
	11-III, 12-III	I
	13, 15	I
Crest width	4,5	R & I
	8-I, 10, 15	R
	8-I, 15	I
	11-I, 14	I
Front slope	2, 5	R
	2, 5, 6, 7	I
Block permeability	2, 2-BH	R & I
Structure permeability	9, 10	R
	8, 9	R
Channel length	8-I, 8-III, 8-V, 15	R
	8-0, 8-I, 8-V, 15	I
	11-I, 11-III	I
	12-I, 12-III	I
Coral growth	8-I, 8-I-3D, 8-I-PVC	I

4

DATA PROCESSING HYDRODYNAMIC PERFORMANCE

Box 4.1: KEY TAKEAWAYS

Wave height

⇒ For both regular- and irregular wave tests, the incoming- and reflected wave height is based on the variance of the energy density spectrum (H_{m0}). The lowest included frequency is set to 0.15 hertz and the highest included frequency limit is 3 hertz.

Transmission coefficient

⇒ The transmission coefficient is calculated as the ratio between the transmitted waveheight with- and without a structure. See equation 4.3.

Reflection coefficient

⇒ The reflection coefficient is calculated as the ratio of the reflected waveheight to the incoming waveheight in front of a structure. See equation 4.4.

Wave decomposition method

⇒ For both regular- and irregular waves, the incoming wave at a set of 3 wave gauges is calculated as follows: First subtract the reflected wave signal of Z&S from the total signal at each wave gauge. Secondly, calculate the mean of the variances from the newly composed signals to obtain $H_{m0,i}$

The main goal of this chapter is to explain the method which is used to process the data from the wave-gauges into the performance parameters of the hydrodynamic performance, namely the transmission- and reflection coefficient. The search for the final methodology has been a prominent part of this research and therefore several steps which are considered, but not used, are explained as well.

4.1 DEFINITION WAVE HEIGHT

For the irregular wave tests the significant wave height (H_{m0}) is used to define the transmission- and reflection coefficients. The same is done for the regular wave tests. For both, the waveheight based on the total variance (H_{m0}) is used instead of time domain peak-trough waveheight (H). The main reason is that most studies found in literature use the H_{m0} to define the transmission- and reflection coefficients as well, for example also the DELOS project [Van der Meer et al., 2005]. Another reason is to be able to compare the results more easily to the irregular wave tests. However, results from the tests with regular waves can not be directly compared to results from the tests with irregular wave tests. Due to differences in the type of wave fields for regular and irregular waves. For irregular waves each wave does not only has its own height, but also its own length.

For sinusoidal regular waves, the relationship between H_{m0} and H is $H_{m0} = 4 * \sqrt{m0} = 4 * \sqrt{\frac{1}{8}H^2} = \sqrt{2} * H$. For linear irregular waves with a narrow-banded spectrum conform the Rayleigh distribution the significant wave height $H_{1/3} = H_{m0}$. Nevertheless, in shallow water the Rayleigh distribution is not always valid, but regardless of this it is common practice to use $H_{m0} = 4 * \sqrt{m0}$ as the significant wave height. Actually, the H_{m0} increases if waves become more non-linear and the spectrum broadens, whereas the $H_{1/3}$ remains the same (higher peak, shallower trough). Thus, the ratio of $H_{1/3}/\sqrt{m0}$ decreases if the spectral bandwidth increases [Battjes and Groenendijk, 2000].

All in all, with the use of H_{m0} the amount of energy is expected to be conserved, whereas for $H_{1/3}$ this is not the case.

4.2 DEFINITION TRANSMISSION COEFFICIENT

Different definitions of the wave transmission coefficient K_t are found in literature. For most studies it is expressed as the ratio between the offshore wave height H_i to the transmitted wave height H_t , $K_t = \frac{H_t}{H_i}$ [Van der Meer et al., 2005]. The study of [Ahrens and Cox, 1990] on the other hand used the ratio of the transmitted wave height to the wave height measured at the same location in the absence of a structure.

The transmitted wave height signals from the tests with a structure are partly affected by the foreshore. The effects of the foreshore need to be eliminated to find the transmission effects from only the structure. Therefore, for each wave condition, a test with- and without structure has been conducted. The following abbreviations are used in this research to refer to the different type of tests:

- **f**: test without a structure, giving the effect of the foreshore.

$$- K_t(f) = \frac{H_{m0,i,WG456}(f)}{H_{m0,i,WG789}(f)}$$

- **s,f**: test with a structure, giving the effect of both the structure and the foreshore

$$- K_t(s, f) = \frac{H_{m0,i,WG456}(s, f)}{H_{m0,i,WG789}(s, f)}$$

In Figure 4.1 the results of $K_t(f)$ and $K_t(s, f)$ for all regular wave tests are shown, per type of wave tests.

The definition of the wave transmission should be such that it gives the effect of the structure only $K_t(s)$. Two different methodologies to exclude the effect from the foreshore have been investigated. The chosen method is based on the difference in the incoming waveheight¹ measured at WG789 with- and without a structure. The other method is based on the energy balance when waves travel over a submerged structure. The pros and cons of both methods are explained in the paragraphs below.

¹ The incoming waveheight at WG789 is the same as the transmitted waveheight

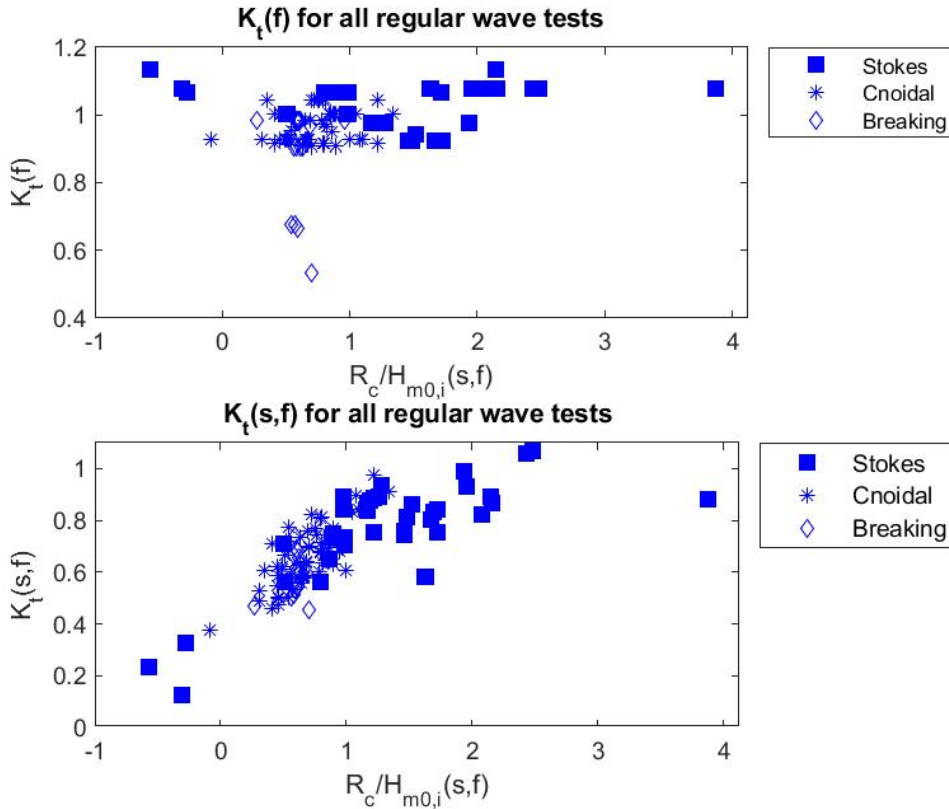


FIGURE 4.1: $K_t(f)$ and $K_t(f,s)$ for all regular wave tests versus the relative submergence $R_c/H_{m0,i}(s,f)$. The type of waves is an additional variables in the graphs.

Foreshore effect from energy balance

The derivations and limitations of this method are explained in Appendix C.1.3. Here, a short introduction is given.

This approach calculates the wave transmission coefficient as the ratio between the incoming wave height $H_{m0,i}$ at the seaward side to the transmitted wave height $H_{m0,t}$ at the lee-ward side, $K_t = \frac{H_{m0,i}}{H_{m0,t}}$. This definition is adopted in most literature studies e.g. [Van der Meer et al., 2005]. The damping effect of the foreshore is included via the energy balance as explained below.

The energy balance is considered between WG456 and WG789, as the effect of the foreshore is significantly smaller between these structures compared to when WG123 would be included. For waves traveling over the submerged structure, the energy balance is written in equation 4.1.

$$E_i = E_t + E_r + E_d \quad (4.1)$$

For linear waves traveling in the same depth, the wave energy is proportional to the squared wave height H^2 and equation 4.1 can be written in terms of waveheights. Combining the energy balances from the tests with- and without a structure results in equation 4.2 to calculate $K_t(s)^s$.

$$K_t(s)^2 = 1 + K_t(s, f)^2 - K_t(f)^2, \quad (4.2)$$

The main limitation of this method is that it assumes that there is an energy balance. Nevertheless, the $H_{m0,i,WG789}$ increases with respect to $H_{m0,i,WG456}$ for many tests without a structure as can be seen from the $K_t(f)$'s above 1 in Figure 4.1. The latter can come from interaction (constructive and destructive) between free and bound waves arising at each higher order harmonic, as the two have different wave numbers and hence different phase velocities. Therefore, this method is not applicable for the non-linear higher order waves which have been tested during these experiments.

Foreshore effect from wave attenuation behind the structure

In this study, equation 4.3 is used to define the transmission coefficient of a structure. This means $K_t(s)$ is defined as the transmitted wave height relative to the scenario without a structure, which is obtained from the following equation:

$$K_t(s) = \frac{H_{m0,i,WG789}(s, f)}{H_{m0,i,WG789}(f)} \quad (4.3)$$

This definition automatically excludes effects of wave reflection and dissipation from the foreshore. This is the same method as for instance [Ahrens and Cox \[1990\]](#) and [van Wesenbeeck et al. \[2021\]](#) used to define K_t .

4.3 DEFINITION WAVE REFLECTION COEFFICIENT

The reflection coefficient is calculated with the formula from equation 4.4. The assumption made for this definition is that the reflection from the wave absorbing system has no impact on the reflection measured in front of the structure.

$$K_r(s) = \frac{H_{m0,r,WG456}(s, f)}{H_{m0,i,WG456}(s, f)} \quad (4.4)$$

4.4 DECOMPOSITION INCOMING AND REFLECTED WAVES

The total signal measured at the wave gauges can be considered as a combination of two wave fields propagating in opposite directions, namely an incident - and reflected wave field. In order to investigate the transmission and reflection, the total signal needs to be decomposed into an incoming- and reflected signal.

There are three different wave separation procedures that use the signals of an array of multiple wave gauges. All three methods are based on the linear wave theory. More information on these methods can be found in Appendix C.1.1. This study uses the method of Zelt & Skjelbreia (Z&S), which is an extension of Mansard and Funke for multiple wave gauges. Z&S separates the total incoming signal into an incident wave field, reflected wave field and a noise signal.

The following aspects can not be processed by the Z&S method and are part of the noise and error: locked harmonics, cross-nodal activities, all non-linear interactions and measurement errors. Measurement errors come from the output of the wave gauges and/or from the measured water depth and space between the wave gauges.

The noise signal of the Z&S method is an indicator of how accurately the method is able to calculate the incoming and reflected waves from the total signal. Hence, to quantify the accuracy, the relative mean square error (RMSE)² for the Z&S is calculated, after the study of [Andersen et al., 2017]. The formula for the RMSE is given in equation 4.5. Here, η_{total} stands for the total measured signal at the wave gauge consisting of $\eta_{i,Z\&S} + \eta_{r,Z\&S} + \eta_{noise,Z\&S}$ ³. $\eta_{calculated}$ is the sum of $\eta_{i,Z\&S}$ and $\eta_{r,Z\&S}$.

$$RMSE = \frac{\overline{\eta_{total} - \eta_{calculated}}^2}{\overline{\eta_{total}}^2} = \frac{\overline{\eta_{noise}}^2}{\overline{\eta_{total}}^2} \quad (4.5)$$

The outcomes of the RMSE for the Z&S method are discussed for irregular and regular waves separately. The main reason behind this is the fact that for regular wave tests, more severe wave conditions have been tested which resulted in more non-linear conditions, a large noise term and therefore a higher maximum RMSE, which can be seen in Figure 4.2⁴.

in Figure 4.3, the regular and irregular tests are plotted onto the diagram of Le Méhauté, visualizing the applicability of different wave theories for periodic water waves. The diagram basically shows the steepness of the tests plotted against the relative water depth [Le Méhauté, 1976]. The symbols used in this Figure referring to the different type of waves (Stokes, cnoidal and breaking) are used throughout the rest of this research.

First, the frequency range included in the Z&S procedure for the regular- and irregular wave tests together is explained in Section 4.4. Thereafter, the applicability of the Z&S method for the regular and irregular tests is discussed in sections 4.4 and 4.4.2.

Frequency limit Z&S

For the method of Z&S an upper- and lower frequency limit is chosen. The same values are chosen for irregular and regular wave tests.

² Note: RMSE is the abbreviation for Relative Mean Squared Error in this study and RtMSE is used as the abbreviation for the Root Mean Squared Error.

³ The total measured signals of WG 4 and 7 are used to calculate the RMSE of Z&S at WG456 and WG 789 respectively

⁴ WG 123 is not included in Figure 4.2, because this data can not be used to determine the incoming- or reflected waves at the toe of the structure, due to the effect of the foreshore.

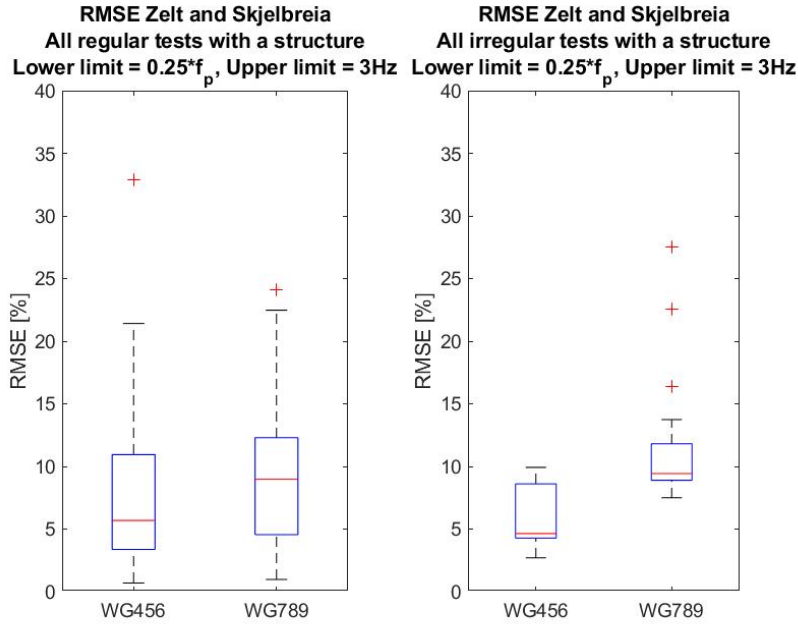


FIGURE 4.2: Boxplot of the RMSE (equation 4.5) for all tests with a structure. Left plot is for the regular tests and right plot for the irregular tests. The same boxplots are given for the reference tests in Appendix C.1.4.

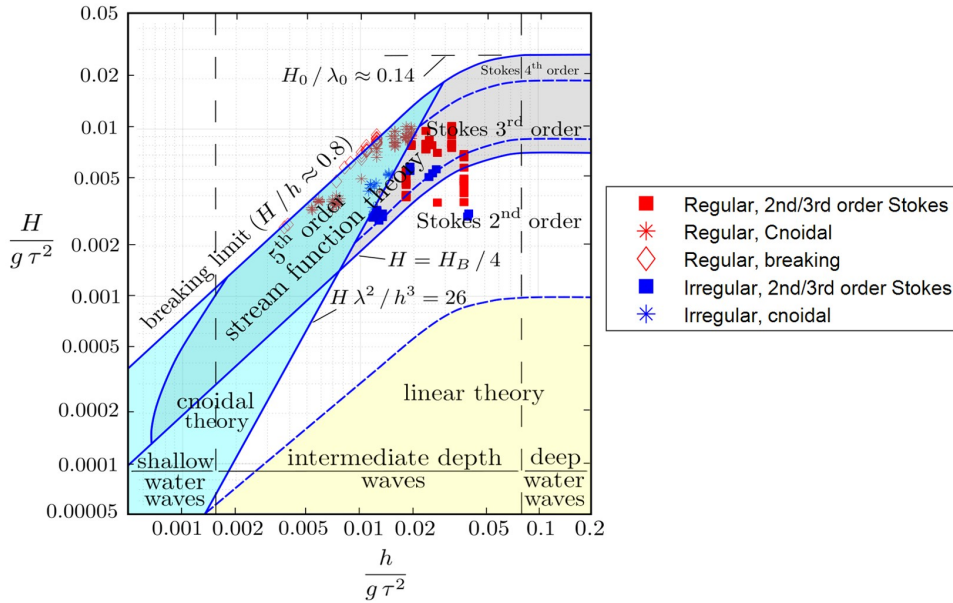


FIGURE 4.3: Describing the non-linearity of the test cases of the incoming waves measured at WG 456, according to Le Méhauté [Le Méhauté, 1976]. The red marks are from the regular wave tests. The blue marks are from the irregular wave tests, where the significant wave height $H_{m0,i}$ is used as H and wave period T is taken as the peak wave period T_p .

The lower limit is set at $0.25 * f_p$. This limit is chosen because there is not a lot of wave energy observed below this threshold. Furthermore, if there is any energy in that range, it can be due to seiching which is not the area of interest for this study. The upper frequency limit is set to 3 Hz. This limit is iteratively chosen as explained in the paragraph below.

Just above the frequency of 3 Hz an erroneous peak in the energy density spectra occurred for many irregular wave tests and for some regular tests. See Figure 4.4 for two examples of such a peak. This peak comes from a measurement error of the Z&S method due to the gauge spacing. According to a study from [Wenneker and Hofland, 2014], the condition number of the least-squares matrix predicts the possible error due to WG spacing. The condition number is a function of the number of wave gauges, the space between the wave gauges and the wave length. It should be 'small' to decrease the inaccuracy. From the pink star in Figure 4.5 it can be seen that the erroneous peak indeed corresponds to a high condition number.

The RMSE has also been computed for smaller and higher upper limit values, which resulted in an increase of the RMSE as can be seen in Appendix C.1.4.

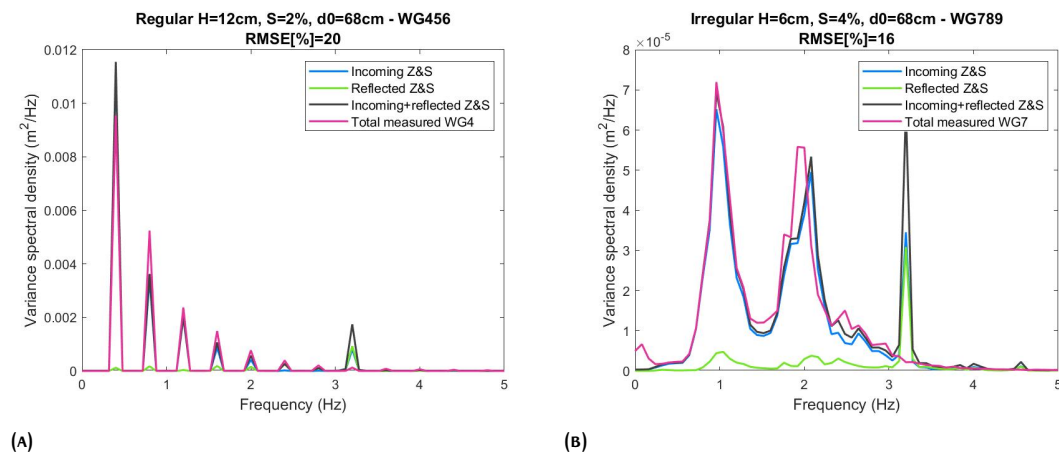


FIGURE 4.4: Comparison of the total - and calculated energy density spectra based on Z&S with an upper frequency limit of 5 Hz. Left figure is an example of WG 456 for a regular wave test. Right figure is an example of WG 789 for an irregular wave test. The erroneous peak at 3.2 Hz is visible.

Applicability of Z&S for regular wave tests

First, the outcomes of the error from the Z&S method for the regular wave tests are discussed.

It is investigated whether the RMSE of the decomposition method is related to the Ursell parameter. The Ursell-parameter (equation 4.6 can describe the degree of non-linearity for regular waves, it combines the steepness of the waves with the relative water depth. If the Ursell number is above 20, when $h/L < 1/8$, the cnoidal wave theory is applicable [Hinis, 2003]. The formula for the Ursell number is shown in equation 4.6⁵. From Figure 4.6 it can

⁵ For the calculation of the Ursell number the $H_{m0,i,Z\&S}$ is used as H and L_p as L

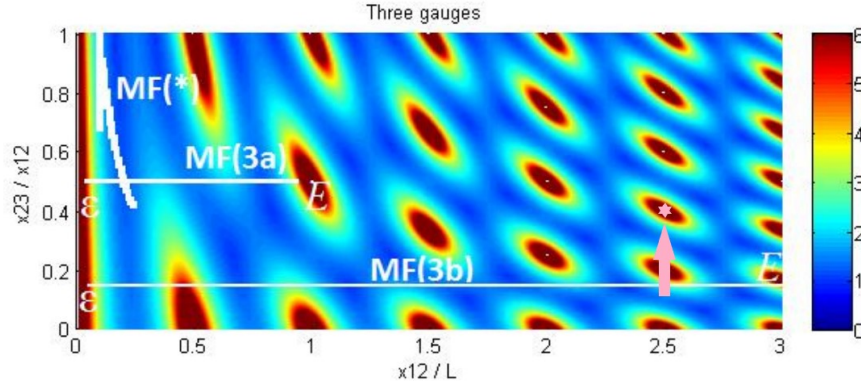


FIGURE 4.5: Matrix condition number for the Z&S method with three wave gauges as a function of x_{12}/L and x_{23}/x_{12} . The pink star represents the location of the erroneous peak found during processing of with the Z&S method. x_{12} is the spacing between the first two wave gauges, this equals 0.38 meters. x_{23} is 0.15 meters, which is the distance between the last two wave gauges. The wavelength L is calculated with the dispersion relation at 3.2 Hz, which equals 0.15 meters for all d_f . For the definitions of E , η , $MF(*)$, $MF(3a)$ and $MF(3b)$ the reader is referred to the study of [Wenneker and Hofland, 2014].

be concluded that the Ursell number is related to the RMSE of Z&S such that there is a trend where an increase in the Ursell number leads to an increase in the RMSE.

$$U = \frac{H_{m0,i}(Z\&S)}{d_f} * \frac{L^2}{d_f^2} \quad (4.6)$$

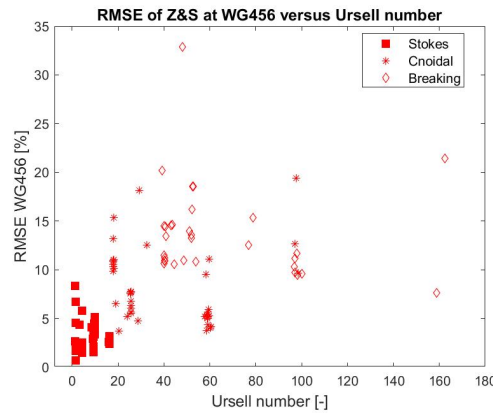
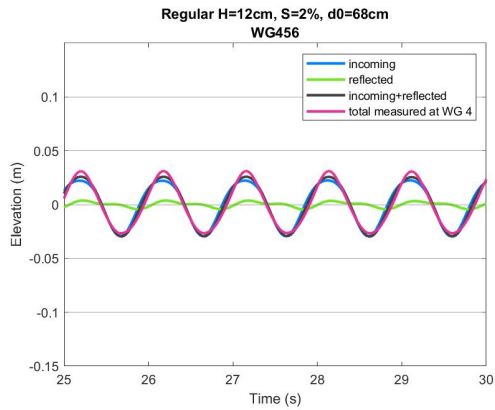


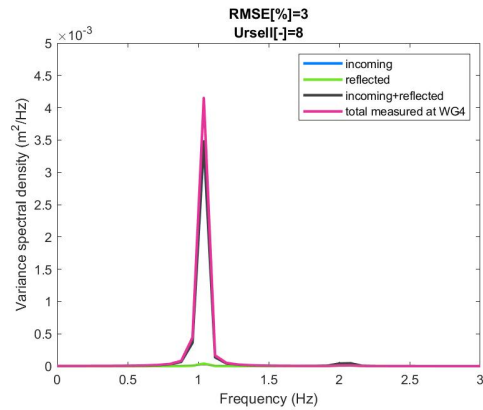
FIGURE 4.6: Relationship between the Ursell-number and the RMSE of the Z&S method. For both the regular and irregular wave tests the $H_{m0,i,Z\&S}$ is used as H and L_p as L , obtained at WG456. The upper limit of Z&S is set to 2.5 Hz.

To visualize the different RMSE outcomes and the Ursell values, Figure 4.7 shows the time signals of the calculated Z&S - and the total signal for different outcomes. It can be concluded that the RMSE is a rough indication of how well the shape of the calculated Z&S (reflected+incoming) wave resembles the total measured wave. Nevertheless, Figures 4.7g,

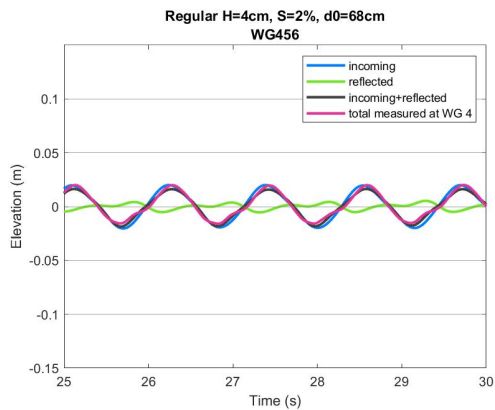
4.7i and 4.7k are examples of tests where the RMSE is similar, while the difference in shape resemblance is big. The Ursell-number is a better indication of the shape resemblance between the total signal and the sum of the calculated signals based on the results shown in Figure 4.7.



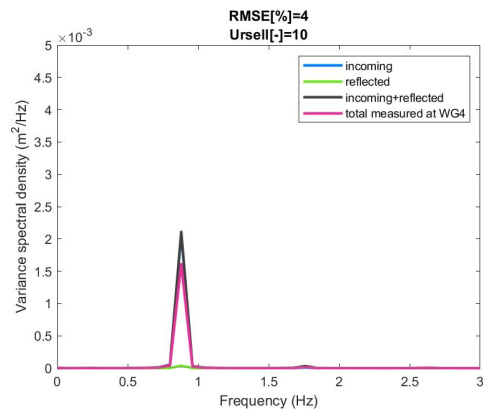
(A) Time signal example 1



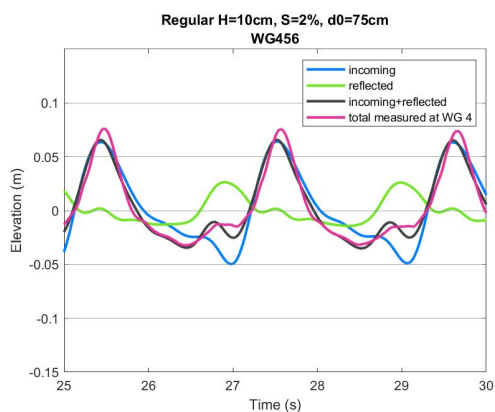
(B) Energy density spectrum example 1



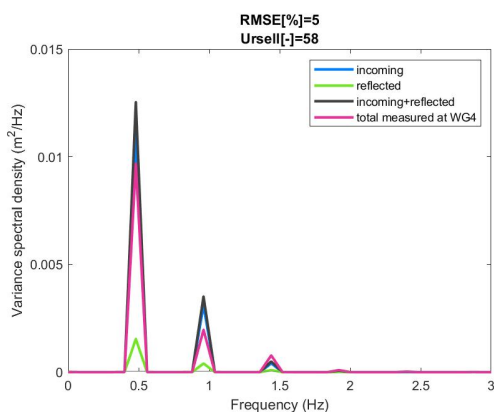
(C) Time signal example 2



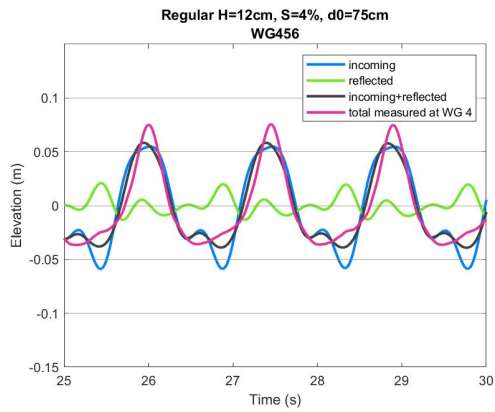
(D) Energy density spectrum example 2



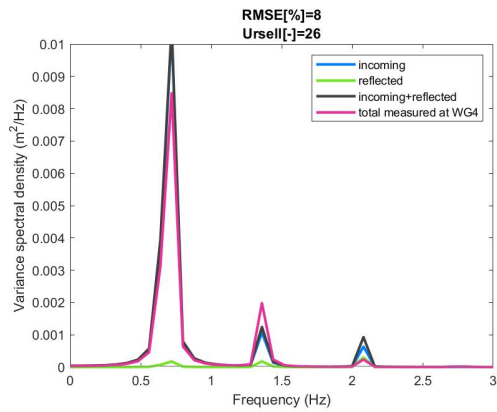
(E) Time signal example 3



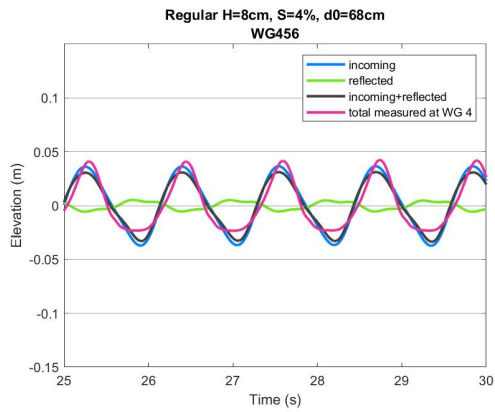
(F) Energy density spectrum example 3



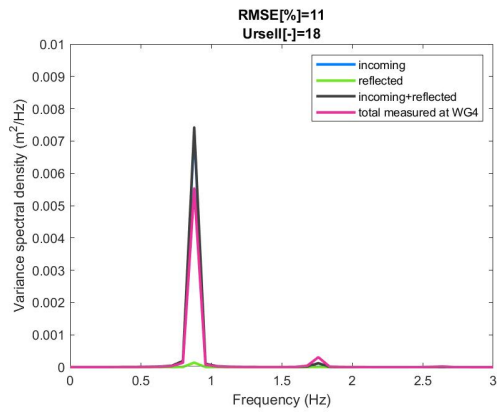
(g) Time signal example 4



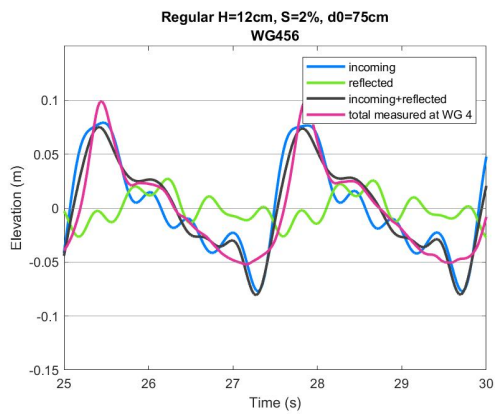
(h) Energy density spectrum example 4



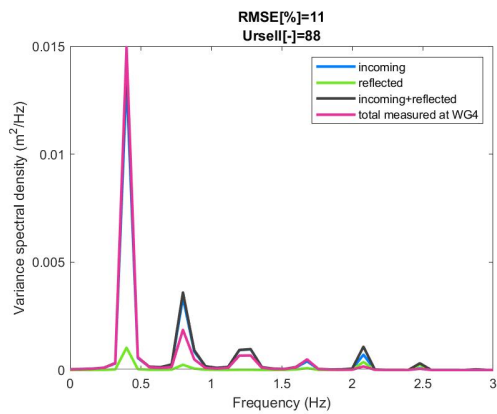
(i) Time signal example 5



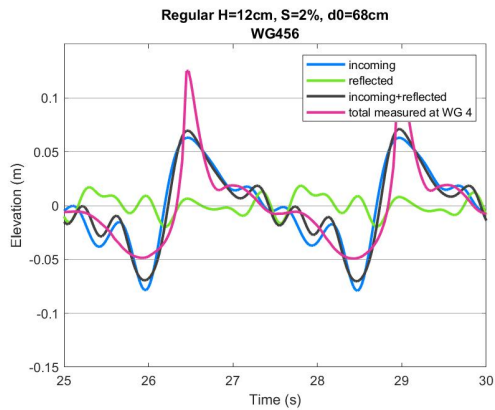
(j) Energy density spectrum example 5



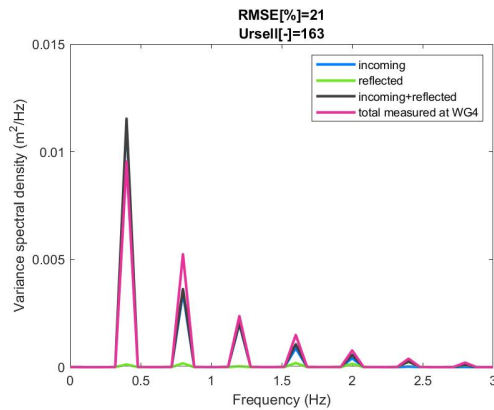
(k) Time signal example 6



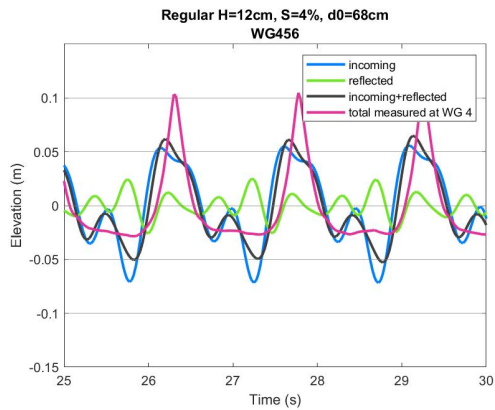
(l) Energy density spectrum example 6



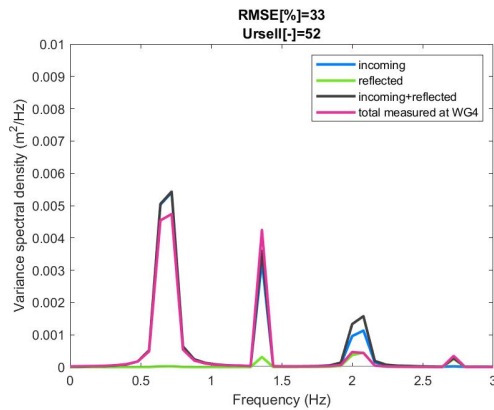
(M) Time signal example 7



(N) Energy density spectrum example 7



(O) Time signal example 8



(P) Energy density spectrum example 8

FIGURE 4.7: Comparison of total - and calculated time signals based on Z&S for regular wave tests with different RMSE at WG456. The relative RMSE is increasing from the top to the bottom and the exact value is given in the title of every sub-figure together with the Ursell number of the test.

The method of Z&S is not used as a final method to define the incoming wave signal for the regular wave tests of this research. The reasons for this are explained in the paragraphs below.

First of all, as can be seen from the figures in Figure 4.7 if the Ursell number exceeds 18, the sum of the Z&S signals result in a very different shape of the wave compared to the total measured signal. At the same time, at WG 4, 5 and 6, for half of the tests, the Ursell number is above 20 (Figure 4.6). Therefore, Z&S often results in a different shape of the wave compared to the total measured signal.

Second of all, from the energy density spectra of examples 3, 4, 5, 7 and 8 in Figure 4.7, it can be seen that Z&S overestimates the first frequency peak and underestimates the second peak. This phenomena can come from the non-linearity's (bound harmonics) which can not be detected with Z&S, but are present in the total signal.

Third of all, in Figures 4.7h, 4.7l and 4.7p an small erroneous peak at a frequency of 2.1-2.2 Hertz is visible. This coincides with point (1.2;0.4) in Figure 4.5, which indeed has a matrix conditions number of 2⁶. If Z&S is used with the flume settings of this research, extra attention needs to be paid for this frequency range as well and perhaps it has to be filtered out for some wave conditions. This will reduce the reliability of the tests in which there is actually some energy present around this frequency.

Consequently, it seems preferable to use the total signal. This is different from the procedure applied in most studies found in literature on 2D wave-transmission of submerged structures. As these studies most often use the Z&S method. However, these studies simulated mostly deep water waves, and hence more linear wave conditions. Furthermore, all experiments in which wave breaking occurred before the structure and/or the wave steepness $s_{0,p}$ exceeded 0.07 were removed [Van der Meer et al., 2005]. This means 82 regular wave and 11 irregular tests conducted during the experiments for this thesis would have not been qualified for further analysis.

4.4.1 Applicability of the total signal for regular wave tests

When using the total signal as an incoming signal, a method needs to be developed to take into account the reflection. Three methods which have been investigated are explained in the following paragraphs. The method referred to as "Reflection based on time signal of Z&S" is chosen.

Reflection based on parameterized K_r

Here, the method is discussed in which the reflection coefficient is parameterized. The incoming $H_{m0,i}$ at a wave gauge is then calculated from the variance of the total wave signal, minus the variance of the parameterized reflection, obtained via equation 4.7 and 4.8. This procedure is applied at every wave gauge and the mean variance is used to calculate the final $H_{m0,i}$.

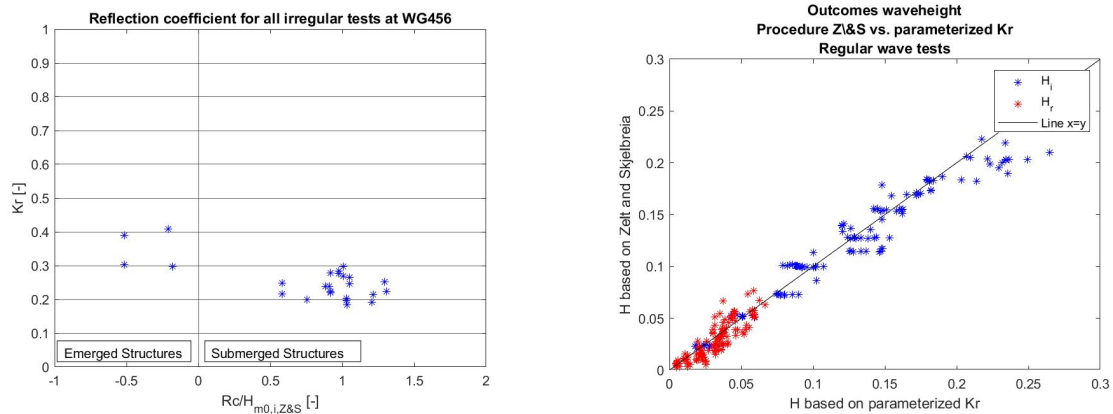
$$K_r = \frac{H_{m0,r}}{H_{m0,i}} = \frac{\sigma_r}{\sigma_i} \quad (4.7)$$

$$H_{m0,i} = 4 * \sqrt{(1 - K_r^2) m0_{total}} \quad H_{m0,r} = 4 * \sqrt{K_r^2 * m0_{total}} \quad (4.8)$$

REFLECTION BASED ON IRREGULARS The first approach which is discussed is to parameterize K_r based on the average K_r of the irregular wave tests. Namely, the RMSE from the irregular tests are smaller, as discussed above. At WG 456 for tests with a structure in place, the K_r of submerged structures appeared to be 0.25 and for emerged structures 0.35, see Figure 4.8a. In Figure 4.8b the outcomes of the $H_{m0,i}$ based on this procedure and from the procedure of Z&S are compared. As can be seen, the outcomes have a good agreement.

Nevertheless, a disadvantage of this method is the fact that it is questionable whether the wave reflection of the irregular waves can be used for the regular wave tests. Namely, for regular

⁶ The dark red areas are the forbidden areas, for the other areas a smaller matrix number is preferred



(A) Wave reflection coefficient from Z&S of all irregular wave tests with a structure.

(B) Comparison outcomes wave-height at WG 456 based on Z&S and a parameterized K_r .

FIGURE 4.8

waves, the superposition of the incoming- and reflected wave field produces a partially standing wave field in front of the structure, see Figure 4.9. This is expected to extent over the whole foreshore area in front of the breakwater [Losada et al., 2003] [Filianoti and Gurnari, 2018]. For irregular waves on the other hand, the wave height only shows a standing pattern close to the structure and this pattern disappears further away from the structure: until about 2 times the local spectral peak length [Klopman and van der Meer, 1999]. Therefore, adding the reflection effect in the form of subtracting the energy potentially under- or overestimates the effect of the reflection in a standing wave pattern.

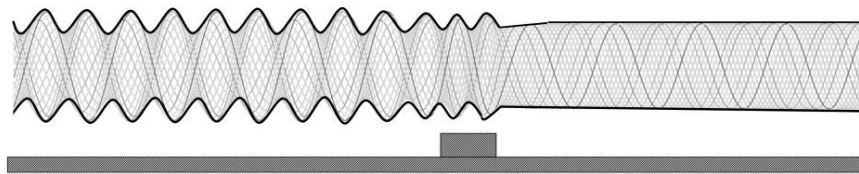


FIGURE 4.9: The envelope of the free surface displacement forming a quasi-standing field around a submerged breakwater [Filianoti and Gurnari, 2018]

REFLECTION BASED ON REGULARS A second approach is to parameterize K_r based on the average K_r of the regular wave tests. As can be seen from Figure 4.10, there is a significant amount of scatter for the K_r around the same relative submergence for tests with a structure. This is also the case when the Stokes type of waves are considered only.

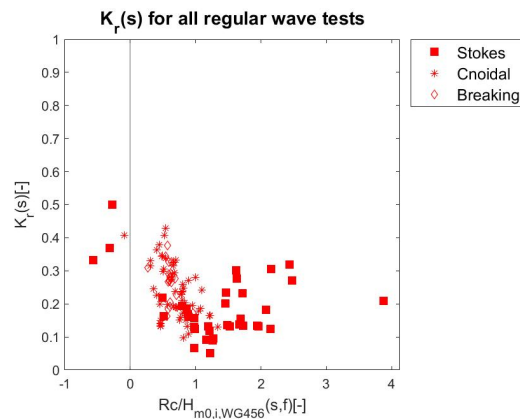


FIGURE 4.10: Wave reflection coefficient from Z&S of all regular wave tests with a structure.

All in all, the methodology of a parameterized reflection is not chosen for this research. The chosen method is discussed next and uses the time signal of the reflected wave from Z&S.

Reflection based on mean of total signals

The position each wave gauge with respect to the quasi standing wave pattern influences the outcomes of the measured wave signal. In the ideal case, the wave gauge with the maximum waveheight would coincide with the quasi-anti-node and with the minimum waveheight with the quasi-node. The reflected waveheight is then the mean of the difference between the anti-node and node waveheight and the incoming waveheight the mean of these [Filianoti and Gurnari, 2018].

Nevertheless, as only three wave gauges have been used during the experiments, for some experiments the wave gauges do not exactly coincide with the node- and anti-node. The spacing of the wave gauges with respect to the tested wavelengths is investigated. This is done by making a sinus wave with the wavelength and height measured at WG456, all plots can be found in Appendix C.1. The found distances between WG 4 to 6 relative to the wavelength are sub-divided into four categories, namely $\frac{1}{8} * \lambda$, $\frac{1}{4} * \lambda$, $\frac{1}{2} * \lambda$ and $\frac{1}{3} * \lambda$. An example of each category with a constructive interaction between the incoming- and reflected wave is shown in Figure 4.11.

As can be seen in Figure 4.11, the estimated wave height based from the wave gauges is different per spacing category and wave gauge positions in the quasi-standing wave pattern. Especially for the longer waves, where the relative distance between WG4 and WG6 is $\frac{1}{8} * \lambda$, the mean of the wave gauges is very different per position of the wave gauges with respect to the quasi-standing wave pattern is. Therefore, this method is not applicable for this research, in which many different wave lengths have been tested and the location from the toe of the structure with respect to the wave gauges was not consistent.

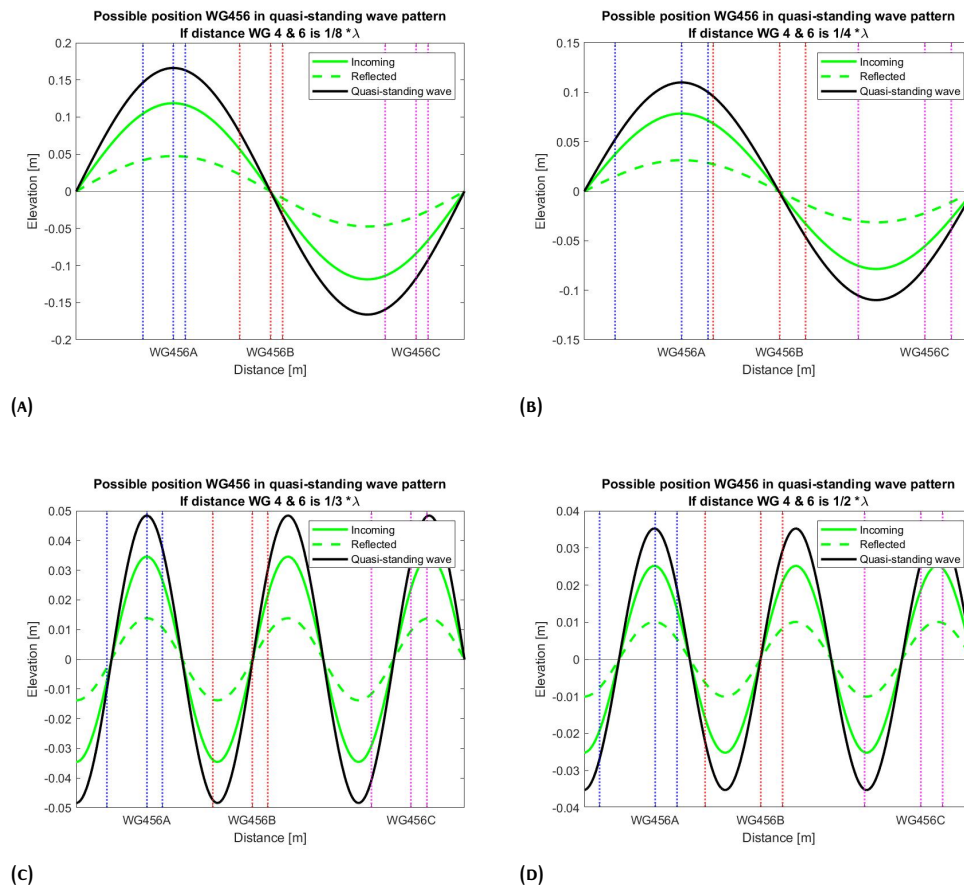


FIGURE 4.11: Examples of the four categories of spacing between wave gauge 4 and 6 with respect to wavelength. For each spacing, three possible positions in the quasi standing pattern are visualised. The reflected wave is visualized as 0.4 times the amplitude of the incoming wave, amplifying the incoming waveheight.

Reflection based on time signal of Z&S

The chosen method is to use the reflected time signal of the Z&S and subtract this from the total time signal. The mean of the variances from the newly composed time signals is used to calculate $H_{m0,i}$ ^{7 8}. The underlying assumption of this is that the Z&S is able to predict the phase of the reflected signal correctly, as this signal is smaller and such more linear. In this way, the impact of the reflection on the standing pattern is in the right direction for every test. Furthermore, the bound harmonics of the total signal are then still considered in the incoming signal.

⁷ In front of the structure the mean of WG 4, 5 and 6. And behind the structure the mean of WG 7, 8 and 9.

⁸ The variance of the newly composed signals is considered for the range above a frequency of 0.15 Hz, as no energy is observed below and the energy if any tests exist in which energy is observed there, it can be due to seicheing or infra-gravity waves and is not of interest for this research.

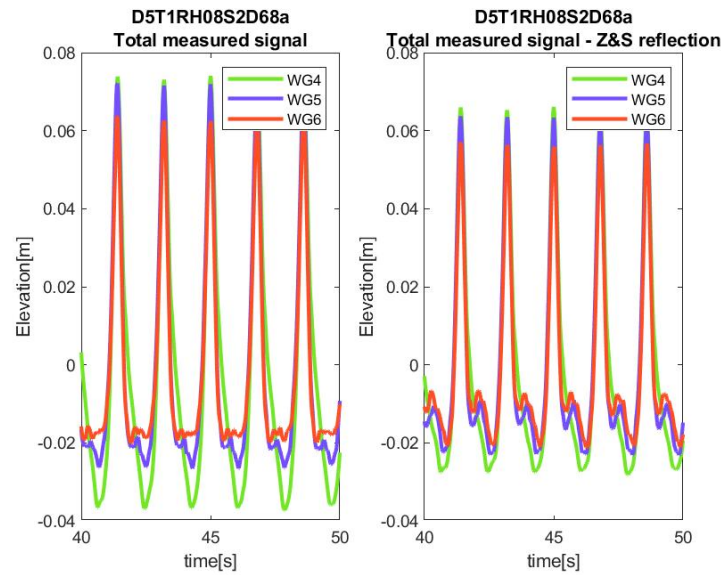


FIGURE 4.12: Example of comparison between total signal and total signal minus the $\eta_{r,Z\&S}(t)$. The crests of the time signals are shifted to overlap them for better comparison.

An example of the application of this approach on the time signal measured during one of the experiments is shown in Figure 4.12. As can be seen in this Figure, there can still be a small difference between waveheight measured at each wave gauge. For this research the mean of the wave gauges is used to find the total incoming waveheight.

4.4.2 Applicability of Z&S for irregular wave tests

Similar as to the regular tests, the RMSE of the Z&S method for the irregular wave tests with a structure in place is plotted in Figure 4.2. The error results are lower compared to the regular wave tests. This was expected, as not many of the irregular wave tests fall within the cnoidal wave theory range (Figure 4.3).

The RMSE error from Figure 4.2 can be explained in numbers as that the error in front of the structure (at WG 4, 5 and 6) for 75 % of the tests is below 8.5 % with a median of 4.6 % and the upper adjacent is at 9.9 % error. Behind the structure (at WG 7, 8 and 9) these values increase again, where the error for 75 % of the tests is below 11.8 % with a median of 9.4 % and an upper adjacent of 13.7 %.

For irregular wave tests, the difference in the calculated Z&S spectra and the total spectra is visualized at WG 456 in Figure 4.13. The corresponding RMSE can be found in the title of every figure. The Ursell number is officially a parameter for periodic waves, therefore only the value of the RMSE is given here.

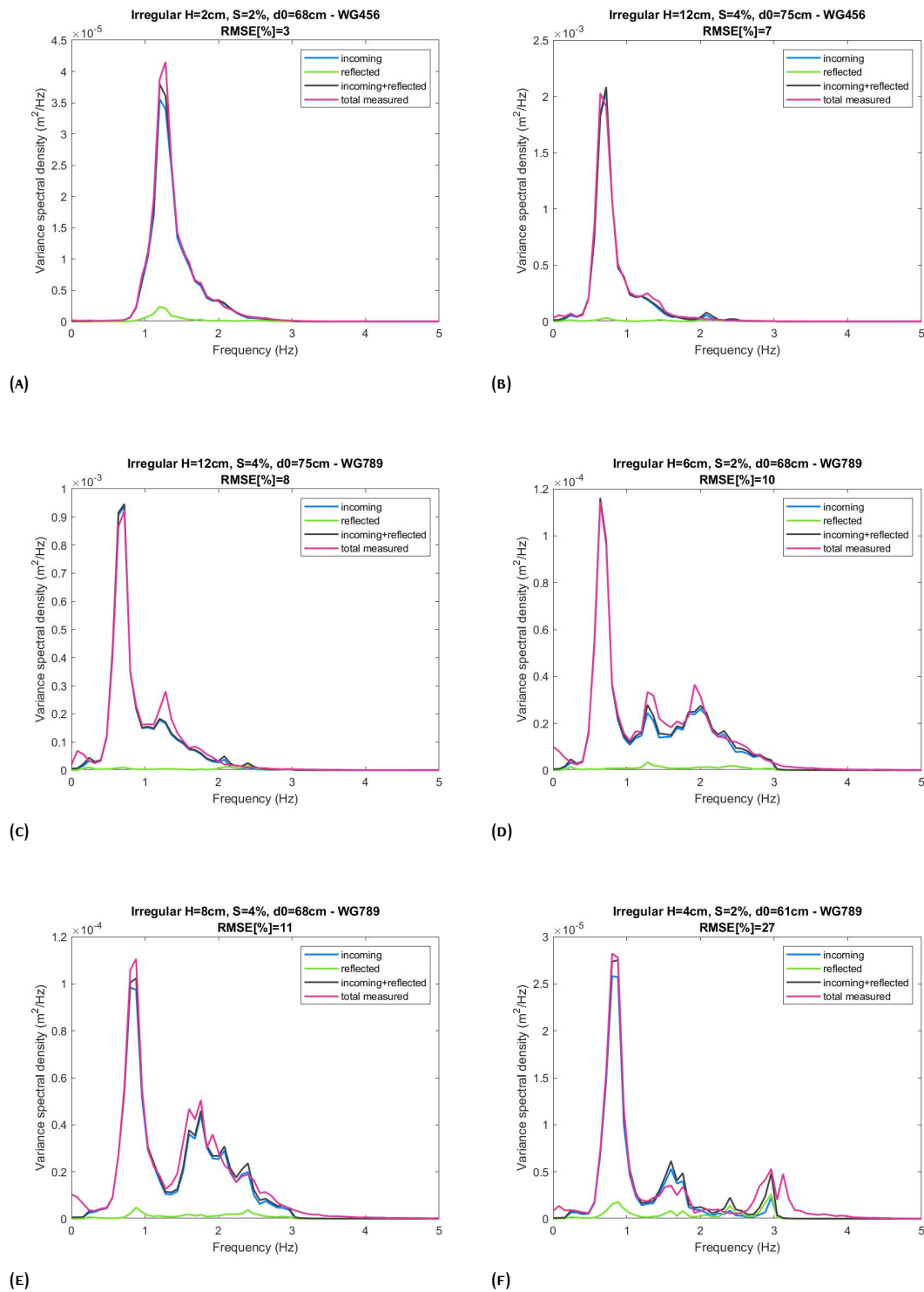


FIGURE 4.13: Comparison of total - and calculated energy density spectra based on Z&S for irregular wave tests with different RMSE. The RMSE is increasing from the top to the bottom and the exact value is given in the title of every sub-figure.

As the RMSE error increases, the spectrum of the sum of Z&S deviates more from the total signal around $1.5 - 2 * f_p$. Therefore for the irregular wave tests, the same procedure as for the regular waves is adopted. This method includes the bound harmonics and results in a reliable distribution of the energy density in the spectrum.

4.4.3 Symbols used per type of wave

In many of the graphs showing the hydrodynamic results, a distinction is made between the symbols for breaking-, cnoidal- and (2dn and 3rd order) Stokes waves. The symbols can be seen in Figure 4.14. The Stokes waves are more linear compared to the breaking- and cnoidal waves, which makes the obtained results more reliable - as these are partly obtained with the linear wave decomposition method of Z&S. Therefore, the matching symbol of the Stokes waves stands out the most.

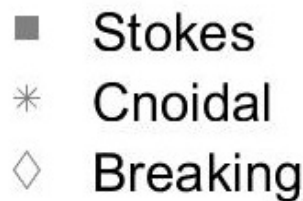


FIGURE 4.14: Symbols used in the graphs from the transmission- and reflection results in Chapter 5. For consistency, the same symbol is used per type of waves.

Dimensionless variables

For the processing of the physical experiment results, the design variables are made dimensionless. For this, the significant incoming waveheight $H_{m0,i}$, local water depth d_f , deep-water wavelength L_0 and fictitious wave steepness $s_{0,m-1,0}$ are used, based on the literature discussed in Chapter 2.1. All in all, this results in the following parameters: $R_c/H_{m0,i}$, h_c/d , $B/H_{m0,i}$, B/L_0 , $\frac{\tan(\alpha)}{\sqrt{s_0}}$ and B/L_0 , similar as can be seen in Table 2.1.

Additional design variables investigated in this research are the permeability of the structure and the distance between two structures. The permeability is investigated with the dimensionless porosity factor, calculated as the volume of voids divided with the total volume. The distance between two structures is investigated relatively to the deep-water wavelength.

5

RESULTS HYDRODYNAMIC PERFORMANCE

The goal of this chapter is to examine the impact of each design variable on the hydrodynamic performance. Based on the conclusion from chapter 2.1, the transmission and reflection are chosen as the hydrodynamic processes which are further investigated in this research. Furthermore, an empirical equation for $K_t(s)$ and $K_r(s)$ of a Reefy structures is derived in this chapter.

The methodology applied in this chapter consists of two steps per design variable. First, the $K_t(s)$ and $K_r(s)$ from the regular wave tests are calculated and visualized graphically. Next, for the irregular wave tests the development of the transmitted- and reflected energy density spectra are analyzed ¹. The outcomes are summarized at the end of each design variable. The key takeaways from the results of each design variable are also briefly stated at the start of the corresponding sub-chapter. At the end of this chapter, the $K_t(s)$ and $K_r(s)$ results are compared to the empirical equations of other researchers. The equation with the best resemblance is optimized with the outcomes of this study using a non-linear least-square optimization process.

5.1 STRUCTURE HEIGHT

Box 5.1: KEY TAKEAWAYS

Note: In this study the freeboard R_c is positive if the crest of the reef is below the water surface. This is in contrast to the definition which is often used in literature.

Transmission

⇒ An increase in the structure height decreases the transmission. If the $R_c/H_{m0,i}$ increases, it has been observed that the $K_t(s)$ increases almost linearly, per d_f .

⇒ If $h_c/d_f \geq 0.83$, the observed $K_t(s)$ is constantly below 0.8 and decreases (almost) linearly with an increase in the fictitious wave steepness $s_{0,m-1,0}$.

Reflection

⇒ An increase in the structure height increases the reflection. Thus, if $R_c/H_{m0,i}$ increases, the K_r decreases.

⇒ h_c/d_f has a weak positive correlation with K_r . If $h_c/d_f \geq 0.83$, the observed $K_r(s)$ decreases almost linearly with an increase in $s_{0,m-1,0}$.

Energy density spectra

⇒ In the transmitted spectra, an increase in h_c results in more dissipated energy around f_p . Furthermore, it has been observed that for (partly) emerged structures, no energy was present above $1.5 * f_p$.

¹ A short introduction into the spectral development over submerged breakwaters can be found in Appendix B.2.1.

⇒ In the reflected spectra, the difference in K_r due to a difference in crest-height is significantly higher for longer waves than for shorter waves.

In literature about the $K_t(s)$ and $K_r(s)$ for submerged breakwaters, two different dimensionless variables are used to take the crest-height into account. Both variables are investigated in this chapter:

1. Relative structure height: h_c/d_f
2. Relative freeboard: $R_c/H_{m0,i}$

5.1.1 Regular waves

In this section, the results from the regular wave tests on structure 1, 2 and 3 are investigated. The height of Structure 1, 2 and 3 consists of respectively 2, 3 and 4 levels of blocks. Structure 1 and 2 are both built of 9 blocks per cross section and structure 2 has 10 blocks per cross section. All structures have the same front slope and porosity, but a different crest width. See Figure 3.7. Table 5.1 gives an overview of the regular wave tests on structure 1, 2 and 3.

TABLE 5.1: Overview regular wave tests for design variable structure height

Structure	d_0	Wave conditions
1	0,68 m	8, 10, 11
1	0,75 m	23, 24, 28, 29, 30, 31
2	0,68 m	8, 10, 11
2	0,75 m	22, 23, 24, 25, 26, 28, 29, 30, 31
3	0,68 m	8, 10, 11
3	0,75 m	23, 24, 28, 29, 30, 31

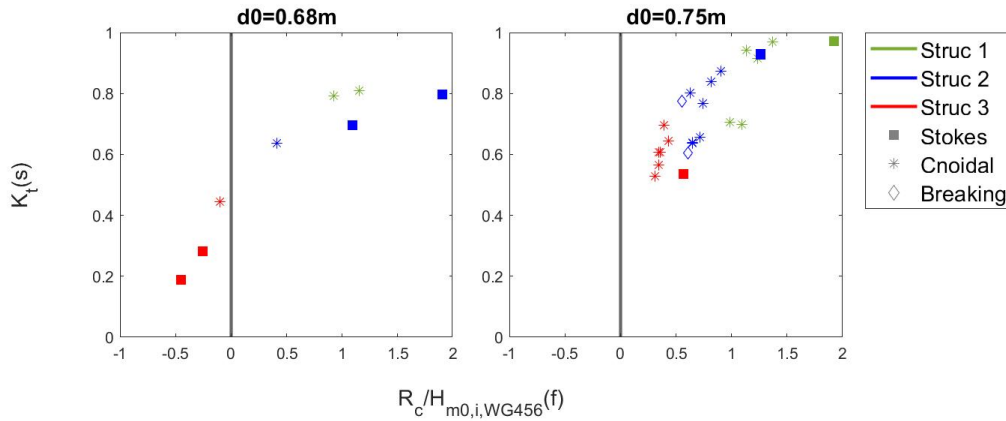
Transmission

RELATIVE FREEBOARD in Figure 5.1a, $K_t(s)$ per $R_c/H_{m0,i}$ is plotted for structure 1, 2 and 3. $K_t(s)$ increases if $R_c/H_{m0,i}$ increases, at first more rapidly and then more slowly. This result had been expected, namely if the structure height is too small for the incoming wave, the waves do not "feel" the breakwater, resulting in ineffective wave attenuation [Armono and Hall, 2003].

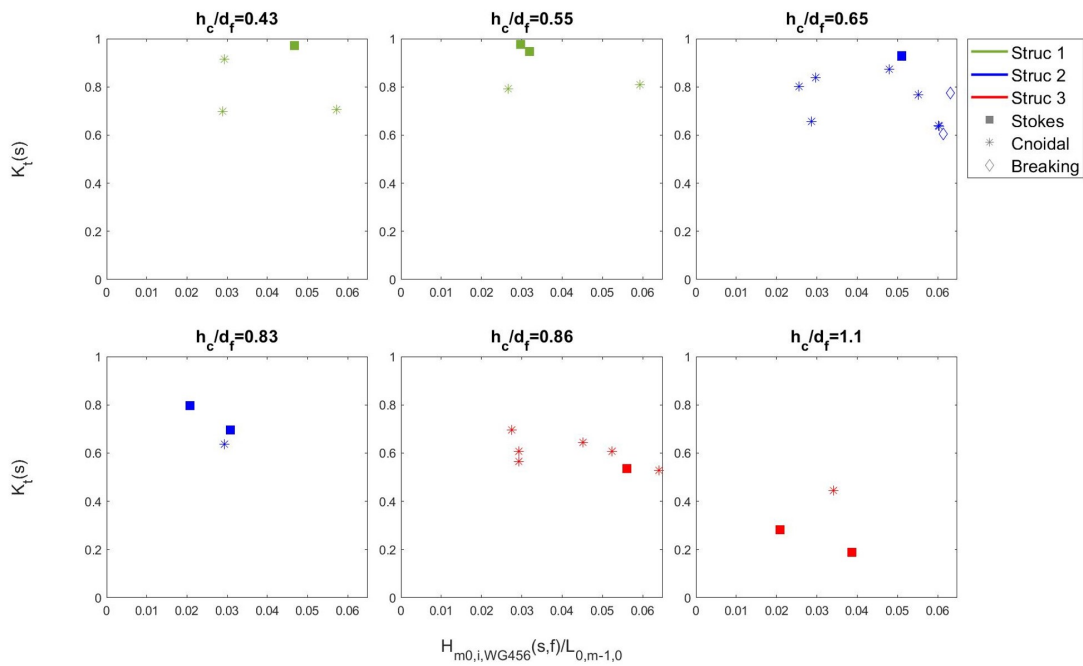
For the area above $R_c/H_{m0,i} = 1$, the difference between the obtained $K_t(s)$ increases. This is probably because the waves mostly dissipate over the crest of the structure in case of $R_c/H_{m0,i} < 1$. On the other hand, when the relative freeboard is larger, other parameters such as the wave steepness and width can affect the $K_t(s)$ outcomes more.

The $K_t(s)$ results around the same $R_c/H_{m0,i}$ can still vary, with have a maximum difference 0.25. This can be due to the inconsistencies between the configurations that were tested. For example, structure 1 has a much wider crest width compared to the others. Furthermore, the period and steepness of the waves are also changing amongst the different wave conditions plotted in the graph.

The graphs in Figure 5.1a distinguish between tests in which $d_0 = 0.68m$ and $0.75m$. This is done to minimize the differences between the tests plotted in each graph. Furthermore, the results suggest that if $R_c/H_{m0,i} > 1$, the tests in $d_0 = 0.68m$ result in lower transmission than the tests in $d_0 = 0.75m$ (for structure 2). However, since also the steepness between the tests is different no firm conclusion can be drawn.



(A) $K_t(s)$ per relative freeboard.



(B) $K_t(s)$ per relative structure height, with $s_{0,m-1,0}$ on the x-axis.

FIGURE 5.1: Transmission results from regular wave tests on structure 1, 2 and 3.

RELATIVE STRUCTURE HEIGHT in Figure 5.1b, $K_t(s)$ per relative structure height is plotted. The smallest transmission results where $K_t < 0.6$ are only found if $h_c/d_f > 0.86$. This can be attributed to the decrease in the transmitted wave energy due to decreasing the area above the structure where the waves can pass. The $K_t(s)$ results around the same h_c/d_f have a maximum difference in magnitude around 0.30. This result implies the relative freeboard has a slightly stronger relationship with $K_t(s)$.²

The term on the x-axis of Figure 5.1b is the fictitious wave steepness $H_{m0,i,WG456}(s,f)/L_0$, in which the local $T_{m-1,0}$ used to calculate L_0 . The steepness has a negative correlation with K_t , which slows down at lower values of h_c/d_f . This can be explained from the fact that a shallow submerged breakwater can induce wave breaking at the incoming waves, if the waves are near the critical wave steepness. Since wave breaking is accompanied by energy losses, steeper waves are more likely to have lower transmission coefficients.

Reflection

RELATIVE FREEBOARD in Figure 5.2a, $K_r(s)$ per $R_c/H_{m0,i}$ is plotted. A trend can be observed in which $K_r(s)$ decreases for an increase in $R_c/H_{m0,i}$. Nevertheless, around the same $R_c/H_{m0,i}$, the $K_r(s)$ results can still differ with a maximum of 0.25 in magnitude. As explained in the transmission part, these differences can be assigned to the inconsistencies between the experiments.

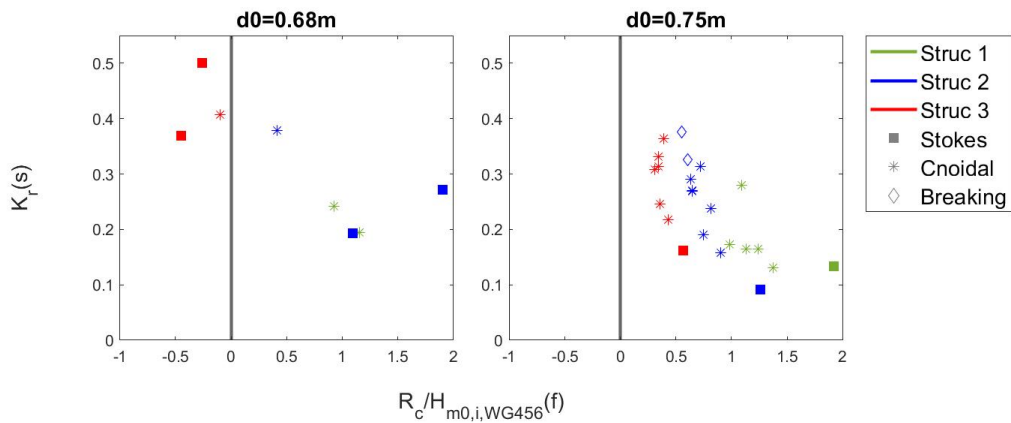
Another result observed from Figure 5.2a is the fact that $K_r < 0.2$ are only obtained for the tests where $d_0 = 0.75m$. This emphasized the positive effect on $K_r(s)$ from the relative structure height.

RELATIVE STRUCTURE HEIGHT The results of $K_r(s)$ per h_c/d_f are plotted in Figure 5.2b. The maximum difference of $K_r(s)$ around the same h_c/d_f is still 0.30.

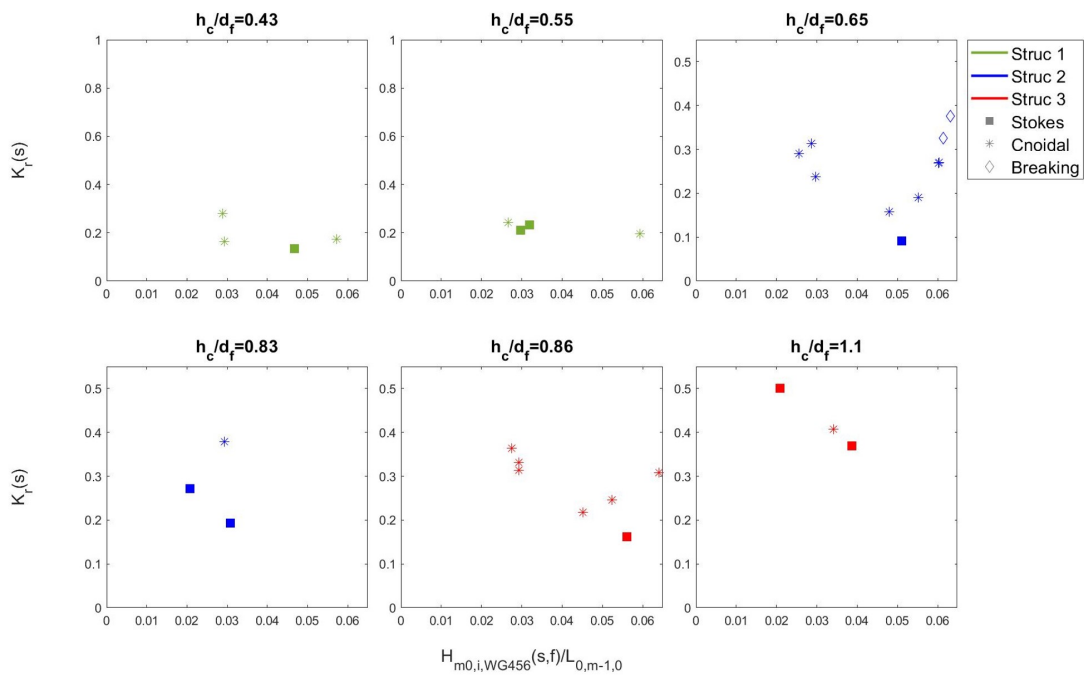
For $h_c/d_f \leq 0.55$, the fictitious wave steepness had no impact on $K_r(s)$. For $h_c/d_f \geq 0.83$, a negative correlation is observed between $s_{0,m-1,0}$ and $K_r(s)$. However, this trend is not completely consistent and no final conclusion can be drawn based on these results.

Lastly, differences in the $K_r(s)$ outcomes per the type of waves are observed. In general, the cnoidal and breaking waves give more reflection than the Stokes waves around the same relative freeboard. This can be due to the fact that cnoidal waves have a small relative water depth and are therefore long waves travelling in shallow water. Both aspects have an increasing impact on the reflection. For the breaking waves, the applied Z&S method to obtain the reflection is not appropriate and therefore the result is not trustworthy.

² In most empirical equations for $K_t(s)$, which are discussed in Chapter 2.1.1, the relative freeboard is used instead of the relative structure height. Some authors, for example [Armono, 2004] and [Srisuwan and Rattanamane, 2015], use the structure height relative to the local water depth



(A) $K_r(s)$ per relative freeboard.



(B) $K_r(s)$ per relative structure height.

FIGURE 5.2: Reflection results from regular wave tests on structure 1, 2 and 3.

Supplementary configuration

One test in wave condition 23 has been performed with a structure that is a combination of structure 2 and 3, see Figure 5.3. This *special* structure has 6 blocks on the fourth level which are unevenly distributed, whereas structure 3 has a complete row of 14 blocks on the highest level. In Figure 5.3, the outcomes of the transmission- and reflection are shown as well. As

can be seen, the $K_t(s)$ from the special structure is 0.04 higher than from structure 3 and 0.04 higher than from structure 2. On the other hand, the K_r from the special structure is slightly lower than from both other structures, with a maximum difference of 0.02. Because only one wave condition has been tested, no firm conclusion can be drawn. Nevertheless, the results suggest that each single block in a series of unevenly distributed blocks on the top level works as effectively in reducing $K_t(s)$, as each block in a compact row of blocks does.

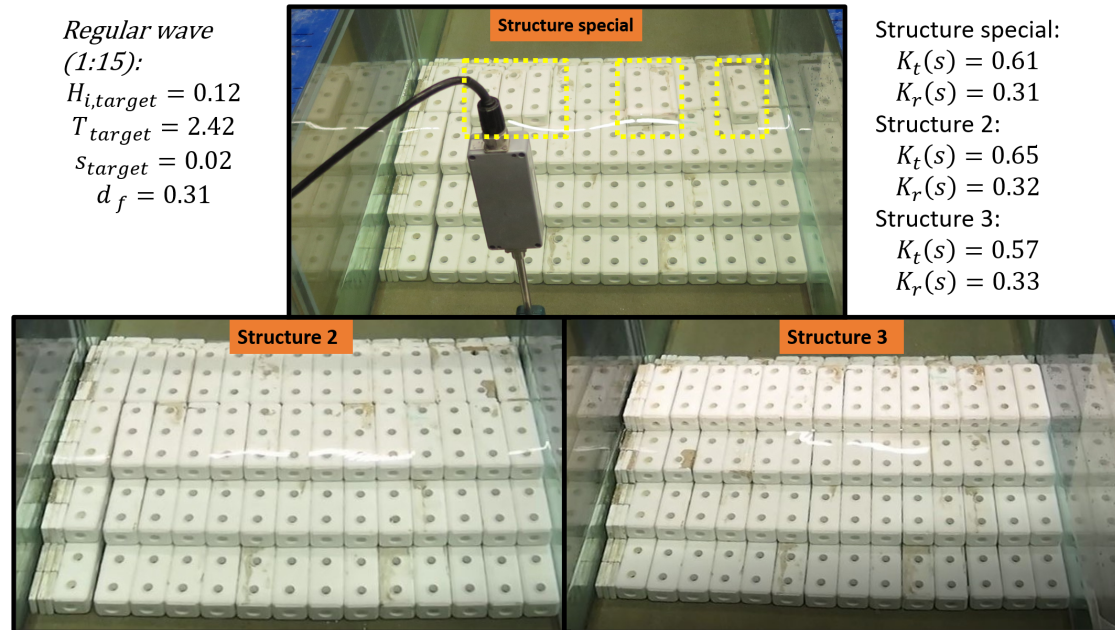


FIGURE 5.3: Picture and outcomes

5.1.2 Irregular waves

The impact of structure height on the development of the energy density spectra is investigated by comparing structure 11-I with 12-I, structure 11-III with 12-III and structure 13 with 15 in different irregular wave conditions. Structure 11 has a height built from 2 blocks, structure 12 and 15 from three blocks and structure 15 from four blocks. See Figure 3.7. An overview of the irregular wave conditions in which the structures are tested is given in Table 5.2.

TABLE 5.2: Overview irregular wave tests for design variable structure height

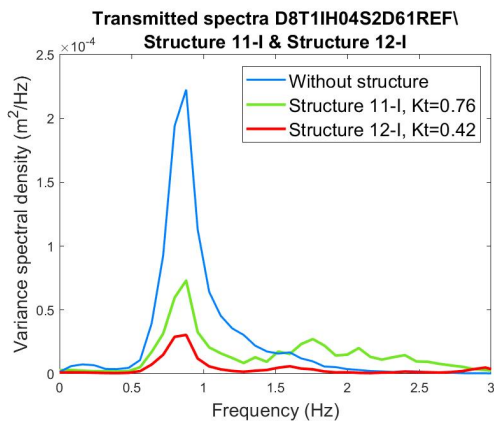
Structure	d_0	Wave conditions
11-I & 12-I, 11-III & 12-III,	0.61 m	5
11-I & 12-I, 11-III & 12-III	0.68 m	18
13 & 15	0.68 m	16

Transmitted spectrum

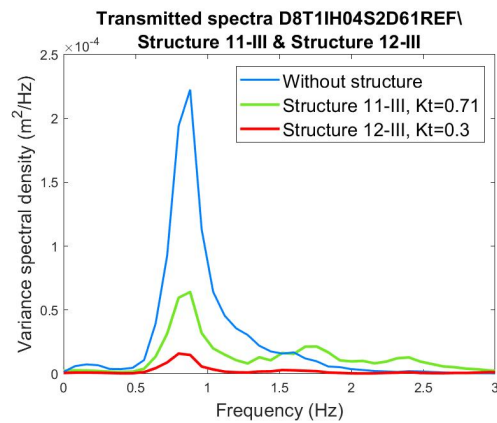
In this section, the energy density spectra measured at WG789 for the tests with- and without a structure are compared. In Figure 5.4, the transmitted spectra are plotted per wave condition.

Only structure 12 in wave condition 5 is emerged, the others are submerged. Furthermore, $K_t(s)$ of each structure can be found in the legend.

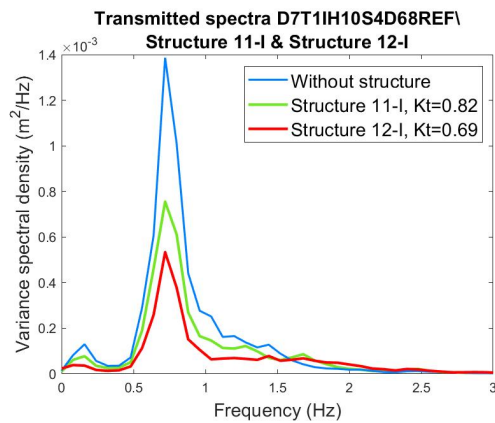
First of all, an increase in h_c reduces the transmitted energy around f_p . Secondly, for all emerged structures (Figures 5.4a, 5.4b), there is no energy present above $1.5 * f_p$. Whereas, for the emerged structures in the same wave condition, there is energy present at these higher frequencies. This implies that without a freeboard, no higher harmonics can be formed. Thirdly, the shape of the transmitted spectrum from the submerged structures is different for each wave condition. Since the results are in line with the outcomes of the regular wave tests, no further discussion is necessary.



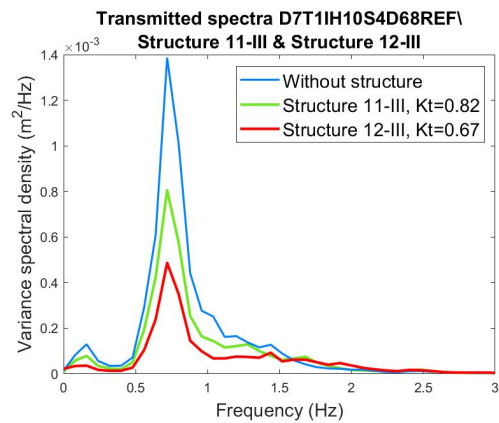
(A) WC 5, Structure 11-I versus 12-I.



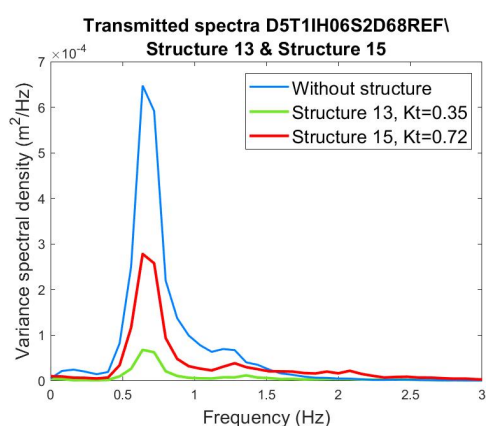
(B) WC 5, Structure 11-III versus 12-III.



(C) WC 18, Structure 11-I versus 12-I.



(D) WC 18, Structure 11-III versus 12-III.



(E) WC 16, Structure 13 versus 15.

FIGURE 5.4: Energy density spectra measured at WG789 for design variable *crest height*.

Reflected spectrum

In this section, the reflected energy density spectra measured at WG456. In Figure 5.5, a comparison is made between the tests with - and without a structure per wave condition. Again, only structure 12 in wave condition 5 is emerged and the $K_r(s)$ of each structure can be found in the legend.

First of all it can be seen that the differences observed depend on the wave condition. For wc 5 and 16, an increase in h_c results in an increase of K_r with 0.10-0.15. On the other hand, for wc 18 the differences in $K_r(s)$ is 0. The common difference between these wave conditions is the target wave steepness, which is 2% for wc 5 and 16 and 4% for wc 18. The results suggest the crest-height has more impact on $K_r(s)$ if the wave steepness is smaller. This is in line to what has been observed in Figure 5.2b, that K_r decreases as the $s_{0,m-1,0}$ increases. However, no firm conclusion can be drawn as the fact that structure 12 is partly emerged in wc 5, whereas all other structures are submerged, probably also plays a role

Despite the fact that the target steepness from wc 5 and 16 is the same, no conclusion can be drawn about the energy distribution of the reflected spectra based on the crest-height distribution.

5.1.3 Conclusion

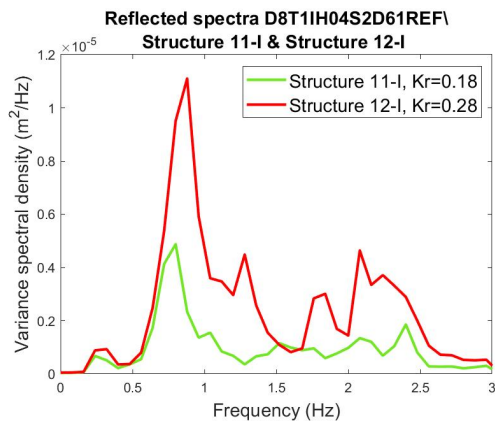
Note that in this study the freeboard R_c is given a positive value for submerged structures.

The relative freeboard has a big impact on both the reflection- and transmission. Roughly said, if $R_c/H_{m0,i}$ increased, the transmission increased and reflection decreased. The opposite correlation has been found for h_c/d_f . Nevertheless, $R_c/H_{m0,i}$ appeared to have a stronger relationship with $K_t(s)$ and $K_r(s)$, than h_c/d_f did. Therefore, it is proposed to use $R_c/H_{m0,i}$ to evaluate the structure's performance in terms of reflection and transmission.

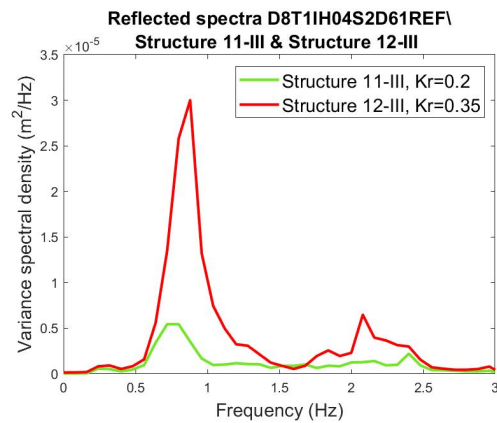
If $h_c/d_f \geq 0.83$, the K_t decreases almost linearly for an increasing $s_{0,m-1,0}$. This indicates that if the crest-height is higher than 80 % of the water depth, the wave steepness has a strong influence on $K_t(s)$.

For the transmitted spectra, an increase in h_c reduces the energy around f_p more. Furthermore, for emerged structures no transmitted energy was present above $1.5 * f_p$. For submerged structures, no relationship has been found for the energy distribution above $1.5 * f_p$.

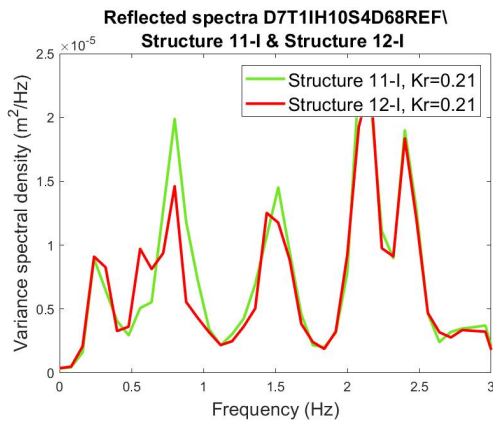
For the reflected spectra the results differed per wave condition and not enough tests are available to draw a firm conclusion.



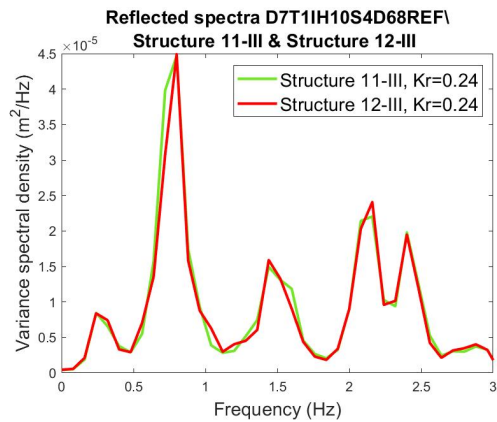
(A) WC 5, Structure 11-I versus 12-I.



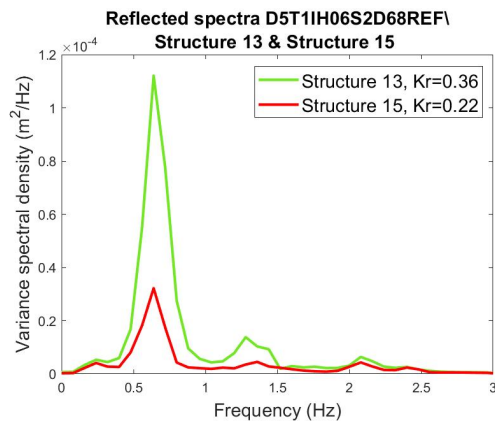
(B) WC 5, Structure 11-III versus 12-III.



(C) WC 18, Structure 11-I versus 12-I.



(D) WC 18, Structure 11-III versus 12-III.



(E) WC 16, Structure 13 versus 15.

FIGURE 5.5: Energy density spectra from reflection measured at WG456 for design variable *crest height*.

5.2 CREST WIDTH

Box 5.2: KEY TAKEAWAYS

Transmission

⇒ An increase in B/L_0 enhances the wave interaction with the submerged structure and decreases the $K_t(s)$. The gradient becomes stronger as the waveheight and/or steepness increases.

Reflection

⇒ No consistent relationship is observed between B/L_0 and $K_r(s)$. However, if $h_c/d_f = 0.65$, the maximum observed difference in K_r per wave condition is only 0.05. The difference increases to 0.07-0.15 for $h_c/d_f = 0.83$.

⇒ The $K_r(s)$ outcomes of the 3D structures are smaller than from the 2DV structures in the same wave condition. This is probably due to the increase in porosity of the structure.

Energy density spectra

⇒ The energy in the f_p of the transmitted waves is more reduced if the B increases. For the tests where $K_t(s) \leq 0.8$, a broader crest results in more energy transferred to the frequency range of $\geq 1.5 * f_p$.

In this part the impact from the crest-width, relative to the wavelength is investigated:

1. Relative width $\frac{B}{L_0}$

The relative width is made dimensionless by dividing it with L_0 , based on $T_{m-1,0}(f)$ at WG456. As for most of the experiments, the larger waveheights coincide with the shorter waves, the

results are similar to $\frac{B}{L_0}$. Therefore, the graphs from the analysis of $\frac{B}{H_{m0,i}}$ are shown in Appendix D.1 and not included here.

5.2.1 Regular waves

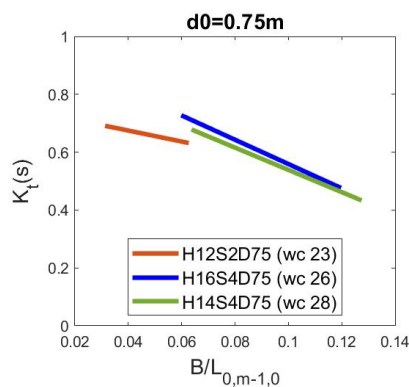
To investigate the impact of the crest width on the performance in regular waves, two comparisons are made. Namely, structure 4 is compared with structure 5 (2DV structures) and structure 8-I, 9 and 15 are compared with each other (3D structures). Structure 5 has a width of 2 blocks and carries 9 blocks per cross-section. Structure 4 has a width of one block and carries 6 blocks per cross-section. Both structures have the same structure height, porosity and front slope. Structure 8-I, 9 and 15 also all have the same structure height, front slope and a similar porosity (45-46%). See Figure 3.7. The regular wave conditions for which the structures are tested can be found in Table 5.3.

TABLE 5.3: Overview regular wave tests structure 4 and 5 for design variable 'crest width'

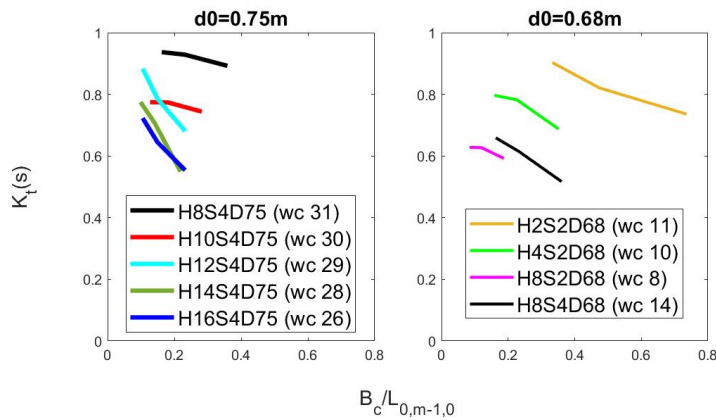
Structure	d_0	Wave conditions
8-I, 10 & 15	0,68 m	26, 28, 29, 30, 31
8-I, 10 & 15	0,75 m	8, 10, 11, 14
4 & 5	0,75 m	23, 26, 28

Transmission

in Figure 5.6a, $K_t(s)$ is plotted over B/L_0 for structure 4 and 5, per wave condition. In general it can be seen that $K_t(s)$ decreases if B/L_0 increases. One of the reasons is the increased friction between the waves and the breakwater surface caused by a longer breakwater width. And this results in a higher loss of energy.



(A) $K_t(s)$ structure 4 and 5.



(b) $K_t(s)$ structure 8-I, 10 and 15.

FIGURE 5.6: Transmission results per relative crest width ratio from regular wave tests. Note that for wc 26, the waves break in front of the structure.

A similar result is observed for structures 8-I, 10 and 15 in Figure 5.6b³. For all wave conditions, $K_t(s)$ decreases when B/L_0 increases. For the test in $d_0 = 0.75m$, the steepest gradients are observed for the conditions with the higher target-waveheight. This is in line with the conclusion from [Ab Razak et al., 2020] and [Van der Meer and Daemen, 1994], which states the effect of B on K_t gets insignificant if the (relative) freeboard is large.

For the tests in $d_0 = 0.68m$, it can be seen that wc 14 results in a steeper decreasing line compared to the other wave conditions. The difference is that wc 14 has a target steepness of 0.04, whereas this is 0.02 for all other conditions in this graph. This can be partly explained with the fact that the transmission through a permeable structure is higher for longer waves [Srisuwan and Rattanamanee, 2015]. However, according to the formulae derived by [Van der Meer et al., 2005] for smooth impermeable structures, see table 2.1, the effect of the crest width on the transmission is only considered if the surf similarity parameter is above 3. An increase in the surf similarity parameter is obtained with an increase in slope steepness or a decrease in fictitious wave steepness. This suggests the opposite, that the effect of the width on K_t is more relevant for longer waves, if the slope remains constant.

According to [Armono and Hall, 2003], the effect of the width on $K_t(s)$ is only noticeable if the relative structure height h_c/d_f is higher than 0.7. Since all tests measured in $d_0 = 0.75m$ have a relative crest-height h_c/d_f equal to 0.65, this study shows the effect is already noticeable for $h_c/d_f = 0.6$ for some values of H_{target} .

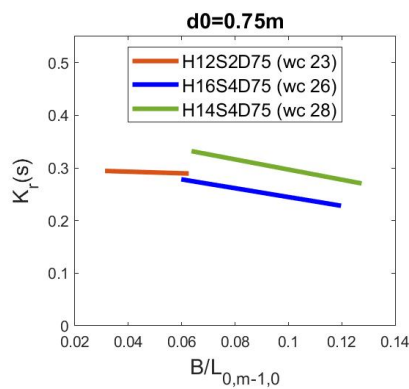
Reflection

in Figure 5.7a, $K_r(s)$ is plotted over B/L_0 for structure 4 and 5, per wave condition. The same is done in Figure 5.7b, for structure 8-I, 10 and 15. The left side of each line comes from the test with the shortest crest width and vice versa for the right side of each line.

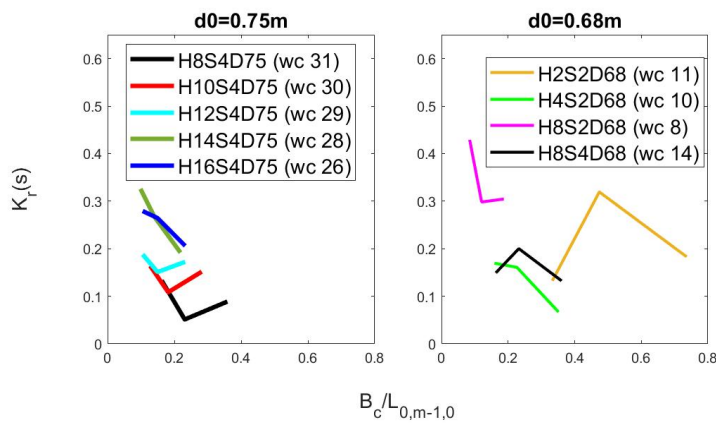
³ Be aware the x-axis here has a broader range than in Figure 5.6a

First of all, it can be observed that the K_r reaches smaller values for the 3D tests Figure 5.7b, than for the 2DV tests in Figure 5.7a. This also holds for the wave condition which has been tested in both figures, namely wc 26 and 28. This is most likely due to the increased porosity from the 3D structure (higher porosity).

On the other hand, no consistent relationship between $K_r(s)$ and B/L_0 can be observed for the other wave conditions. Nevertheless, the impact of the relative width in deeper water ($d_0 = 0.75m$) is not very big, as the variation in K_r is only 0.05. On the other hand, in shallower water ($d_0 = 0.68m$) the variation in K_r is between 0.07-0.15. This is in line with the increasing trend observed for between K_r and h_c/d_f observed in Section 5.1.



(A) $K_r(s)$ structure 4 and 5.



(B) $K_r(s)$ structure 8-I, 10 and 15.

FIGURE 5.7: Reflection results per relative crest width ratio from regular wave tests. Note that for wc 26, the waves break in front of the structure.

5.2.2 Irregular waves

In this section, the spectra of structure 4 & 5, 8-I & 15 and 11-I & 14 are compared. Structure 10 has not been tested for any irregular wave conditions. An overview of the corresponding irregular wave conditions is given in Table 5.4.

TABLE 5.4: Overview irregular wave tests for design variable crest width

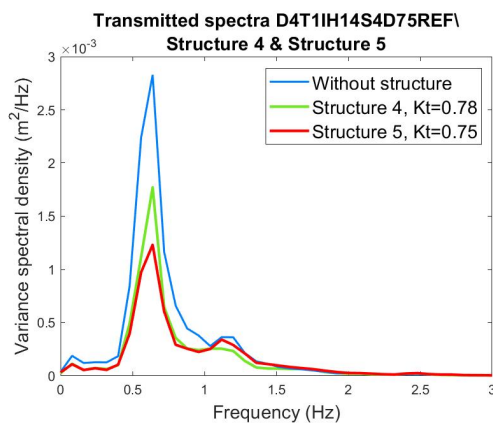
Structure	d_0	Wave conditions
4 & 5	0.75 m	35
8-I & 15	0.68 m	16, 17
11-I & 14	0.68 m	5, 18

Transmitted spectrum

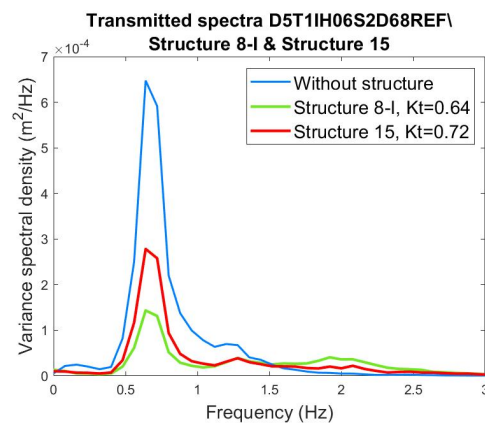
The resulting transmitted spectra measured at WG789 are plotted in Figure 5.8. For all tests, the structure with the smaller crest-width has more energy left around the f_p and a smaller $K_t(s)$. Furthermore, an increase in B often shifts more energy towards the higher harmonic area above $1.5 * f_p$ as a submerged breakwater decomposes the wave into shorter waves. This is observed in Figures 5.8a, 5.8d and 5.8b. Only in Figures 5.8c and 5.8c, this does not happen. Nevertheless, here the K_t of the narrow structure is above 0.9 and therefore the wave is almost not damped by this structure and no valid comparison can be made.

Reflected spectrum

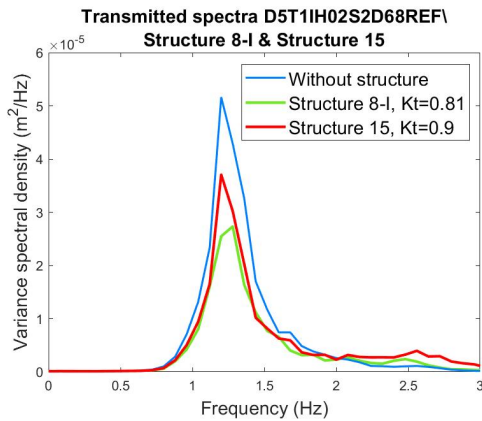
in Figure 5.9, the reflected energy density spectra are compared for the design variable crest-width. The K_r outcome can be found in the legend of each structure. From these outcomes, it can be observed that the wider structure resulted in smaller $K_r(s)$ values, however with a maximum difference of 0.02. Therefore, it can be considered insignificant. An explanation for this could be that a broader structure generally has more blocks and is therefore more "impermeable" for waves to pass through.



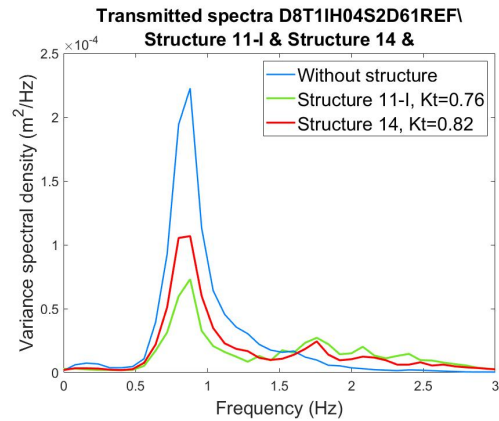
(A) WC 35, Structure 4 versus 5.



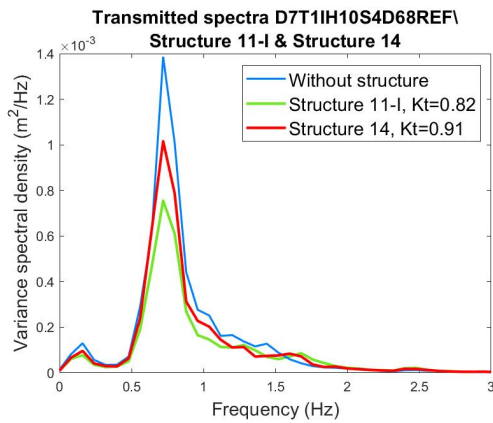
(B) WC 16, Structure 8-I versus 15.



(c) WC 17, Structure 8-I versus 15.



(d) WC 5, Structure 11-I versus 14.



(e) WC 18, Structure 11-I versus 14.

FIGURE 5.8: Energy density spectra measured at WG789 for design variable *crest width*.

5.2.3 Conclusion

The relative crest-width has a decreasing relationship with the $K_t(s)$ outcomes. The gradient steepens if the L_0 and/or $H_{m0,i}$ increases. In the transmitted spectra the same trend is observed, in which a larger B dissipated more energy around f_p . No conclusion can be drawn about the impact of B on the higher harmonics, since the outcomes are inconsistent.

No clear relationship has been observed between $K_r(s)$ and B/L_0 .

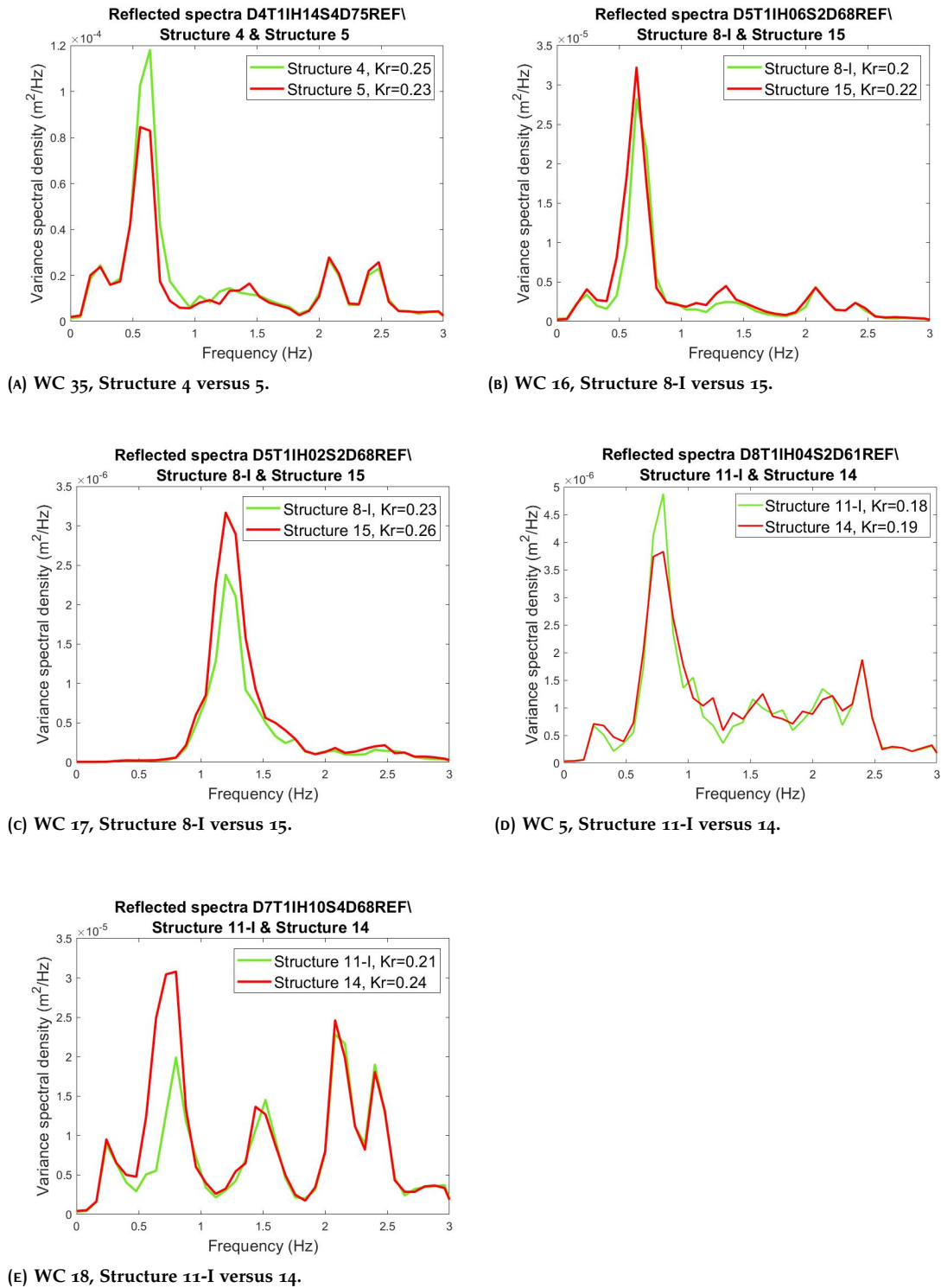


FIGURE 5.9: Energy density spectra from reflection measured at WG456 for design variable *crest width*.

5.3 BLOCKED HOLES

Box 5.3: KEY TAKEAWAYS

Transmission

⇒ The structure with blocked holes gives a maximum decrease in K_t of 0.07.

Reflection

⇒ The structure with blocked holes gives a maximum increase in K_r of 0.02.

⇒ Energy density spectra

The same trends as from the regular tests is observed. The magnitude of the observed difference is also similar. The impact is only visible around f_p .

The effect of blocking the holes vertically with PVC pipes has been investigated here. The outcomes give an indication of the dissipation through the structure and its quantitative contribution to the transmission and reflection. Furthermore, the situation with the PVC pipes mimics vegetation growth in the holes of the structure, a long-term effect.

The results from the regular tests are plotted with $R_c/H_{m0,i}(f)$ on the x-axis to make sure the results with the same x-coordinate have the the same wave condition.

5.3.1 Regular waves

All tests are conducted on structure 2. The test with the PVC pipes in the vertical holes is referred to as Structure 2-BH. Table 5.5 gives an overview of the regular wave conditions in which the tests are conducted.

TABLE 5.5: Overview regular wave test for design variable block porosity The bold wave conditions are compared.

Structure	d_0	Wave conditions
2 & 2-BH	0,75 m	23, 24, 28, 29, 30, 31

Transmission

in Figure 5.10 the $K_t(s)$ results are plotted. Blocking the holes gives the same, or slightly smaller transmission results. The maximum difference is 0.07. This implies that vegetation growth inside the holes will reduce the amount of energy transmitted through the structure. From Figure 5.10, it seems as if the impact increases if the relative freeboard increases. However, based on the number of tests no final conclusion can be made about this.

A side note of this method is the fact that PVC pipes are hollow and therefore not all flow through the structure is prevented.

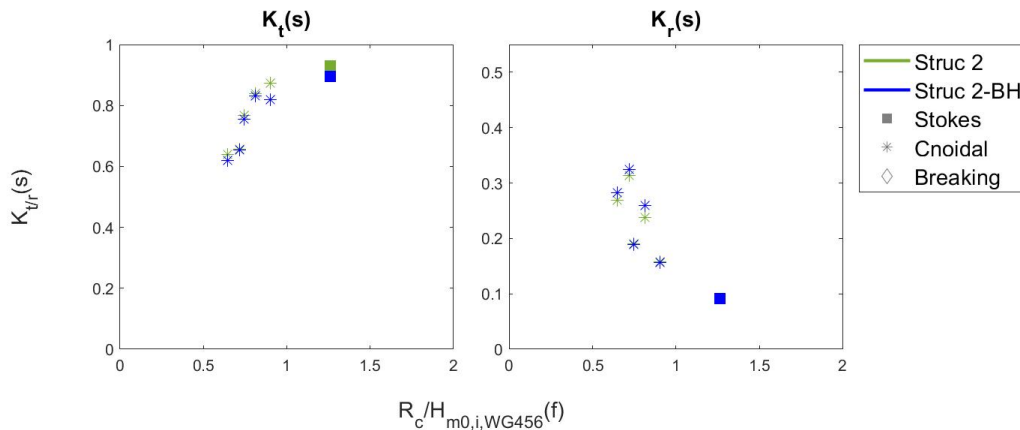


FIGURE 5.10: Transmission and reflection results over the relative freeboard from regular wave tests on structures 2 and 2-BH (with $d_0 = 0.75m$).

Reflection

in Figure 5.10 the reflection over $R_c/H_{m0,i}$ is plotted for the regular wave tests on structure 2 and 2-blocked holes. Blocking the holes gives the same, or slightly increased reflection. However, a maximum difference in $K_r(s)$ of only 0.02 has been observed.

5.3.2 Irregular waves

One irregular wave condition is tested on structure 2 with- and without blocked holes, see table 5.6.

TABLE 5.6: Overview irregular wave test for design variable block porosity

Structure	d_0	Wave conditions
2 & 2-BH	0.75 m	35

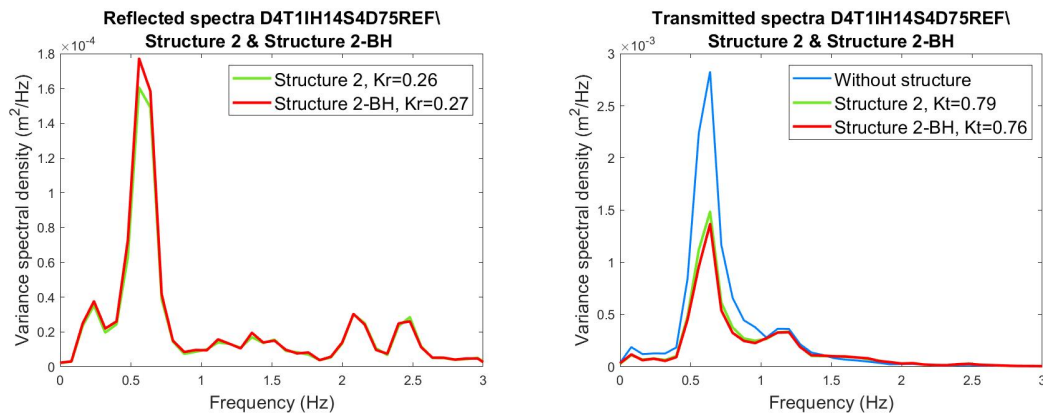
Transmitted spectrum

Only around the peak frequency a very small difference in the transmitted spectrum as a consequence of blocking the holes can be observed, see Figure 5.11b. Namely, the structure with blocked holes has less energy remaining in the f_p and a slightly steeper back slope in f_p . From blocking the holes vertically with PVC pipes, a decrease of 0.03 in $K_t(s)$ is observed for wave condition 35. This is in line with the order of magnitude of the result of the regular wave tests.

Reflected spectrum

The reflected spectra can be found in Figure 5.11a. Again, the difference is only within the area around f_p . From blocking the holes vertically with PVC pipes, an increase of 0.01 in $K_r(s)$ is

observed for wave condition 35. This result is also in line with the results from the regular wave tests.



(A) Reflected spectra measured at WG456

(B) Transmitted spectra measured at WG789

FIGURE 5.11: Energy density spectra for design variable *blocked holes*.

5.3.3 Conclusion

Blocked vertical holes have a positive impact on $K_r(s)$ and a negative impact on $K_t(s)$. Nevertheless, the impact of blocked holes on K_t and K_r is very small for the tested wave conditions. The tests fall within a range of $0.6 < R_c/H_{m0,i} < 1.3$ and $h_c/d_f = 0.65$ and the results are therefore only applicable to this area.

5.4 SLOPE STEEPNESS

Box 5.4: KEY TAKEAWAYS

Transmission

⇒ $K_t(s)$ increases simultaneously with $\zeta_{m-1,0}$. Therefore, a more gentle α_{front} and/or a higher fictitious incoming wave steepness decrease the transmission. Dependency reduces for large values of $\zeta_{m-1,0}$.

Reflection

⇒ Similar as to $K_t(s)$, $K_r(s)$ increases with $\zeta_{m-1,0}$.

Energy density spectra

⇒ The trend from the regular wave tests on K_t is confirmed based on the outcomes of the irregular wave test. Both around the first- and second frequency peak there are differences observed in the transmitted spectra.

⇒ The trend from the regular tests on K_r is also confirmed with the irregular wave test. The reflected spectra only differ around f_p . Furthermore, the shark-tooth orientation (structure 7) gives less reflection than the straight orientation (structure 2).

In this section the impact of the seaward slope steepness α_{front} is investigated. The effect of the slope in empirical equations for K_t and K_r is mostly included in the form of the surf similarity parameter ζ . In this research, this parameter is therefore further investigated:

1. The surf similarity parameter = $\frac{\tan \alpha_{front}}{\sqrt{s_{0,m-1,0}}}$

In which the fictitious wave steepness $s_{0,m-1,0}$ is calculated as $\frac{2 * \pi * H_{m0,i,WG456}(f)}{g * T_{m-1,0,WG456}(f)^2}$ in this study, as also applied by [Heineke and Verhagen, 2009].

5.4.1 Regular waves

From the regular wave tests, a comparison can be made between the performance of structure 2 and 5. Structure 2 has a steeper α_{front} compared to structure 5. Both have been tested for three of the same regular wave conditions, which can be found in Table 5.7. The structures have the same amount of blocks per cross section and the same structure height.

However, it must be noted that the back slope also differs. It is straight for structure 5 and sloping for structure 2. According to [Stauble and Tabar, 2003], the seaward slope has more impact than the leeward slope. And the same is expected based on the empirical relations for K_t and K_r , which only include the seaward slope. However [Stauble and Tabar, 2003] has also reported scour on the landward base can be a consequence of a steep leeward slope for narrow-crested structures. Nevertheless, no further information related to this can be withdrawn from the results here.

TABLE 5.7: Overview regular wave tests structure 2 and 5 for design variable slope steepness

Structure	d_0	Wave conditions
2	0,75 m	23, 26, 28
5	0,75 m	23, 26, 28

Transmission

in Figure 5.12, $K_t(s)$ is plotted over the surf similarity parameter $\zeta_{m-1,0}$ for structures 2 and 5. A relationship can be observed, in which $K_t(s)$ increases when $\zeta_{0,m-1,0}$ increases. Which means either α_{front} increased or $\zeta_{0,m-1,0}$ decreased. This can be explained because a shallower slope causes more severe wave breaking, which results in higher energy losses. This is more likely to occur if the waves are already nearer to the critical steepness.

The observed result shows that an increase around the order of magnitude of 0.25 can be reached if $\zeta_{m-1,0}$ increases from 1.5 to 3. According to [Seabrook and Hall, 1999], the effect of the slope steepness decreases if the submergence increases. This hypothesis can not be verified from these results, as all experiments are conducted for the same submergence.

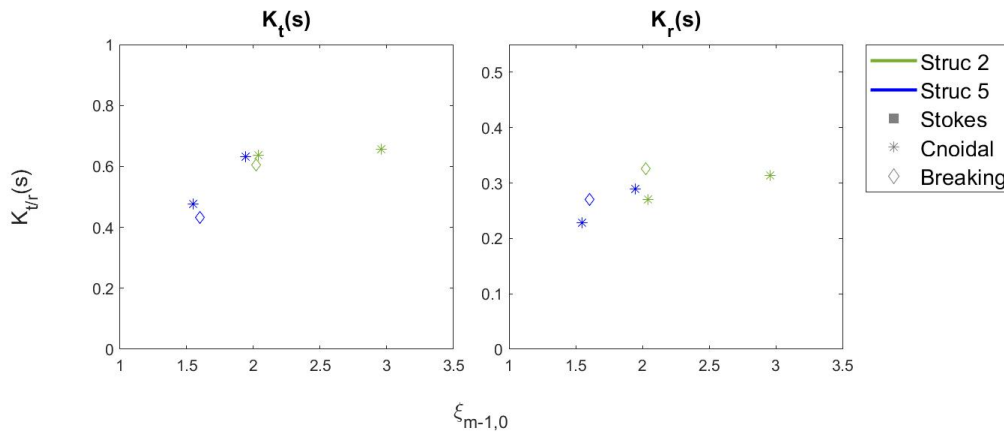


FIGURE 5.12: Transmission and reflection results per surf similarity parameter from regular wave tests on structure 2 and 5.

Reflection

From Figure 5.12, it can be that the relationship between $K_r(s)$ and $\xi_{m-1,0}$ is very obvious. Namely, $K_r(s)$ increases if $\xi_{m-1,0}$ increases. This means both a steeper slope and longer wave can have a positive impact on K_r . The latter can be explained because longer waves can become shallow water waves already for higher values of d_f . And shallow water waves interact with the bottom more as the molecules have a more elliptical orbital path.

The observed result shows that an increase around the order of magnitude of 0.10 can be reached if $\xi_{m-1,0}$ increases from 1 to 3.5.

5.4.2 Irregular waves

For the front slope steepness, one irregular wave condition is tested on structure 2, 5, 6 and 7. Structures 6 has the steepest α_{front} , next structure 2 and lastly structure 5⁴. Structure 7 is a variation of Structure 2, with a shark-tooth top-view, as can be seen in Figure A.18. An overview of the the wave condition is given in Table 5.8.

TABLE 5.8: Overview irregular wave tests structure 2, 5, 6 and 7 for design variable slope steepness

Structure	d_0	Wave conditions
2, 5, 6 & 7	0.75 m	35

Transmitted spectrum

The resulting transmitted spectra are plotted in Figure 5.13.

⁴ $\alpha_{front,Struc2}=0.46^\circ$ - $\alpha_{front,Struc5}=0.32^\circ$ - $\alpha_{front,Struc6}=0.79^\circ$

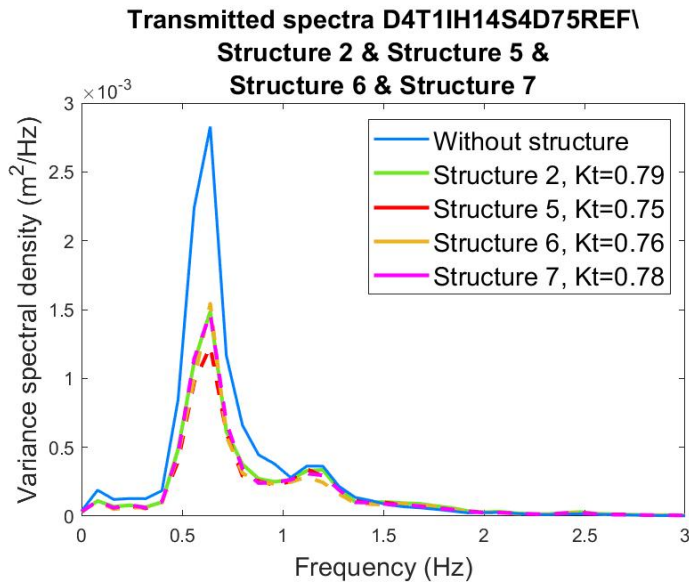


FIGURE 5.13: Energy density spectra measured at WG789 for design variable *front slope*.

First of all, the biggest observed difference in $K_t(s)$ is 0.04 (structures 2 and 5) and thus not very significant. Structure 5, with a shallower front slope compared to structure 2, results in a lower $K_t(s)$. Therefore, this is in line with the trend from the regular wave tests. The small difference can be due to the fact that the h_c/d_f is 0.65, in which the relative crest-height is too small for some waves to feel the structure (see Figure 5.1b).

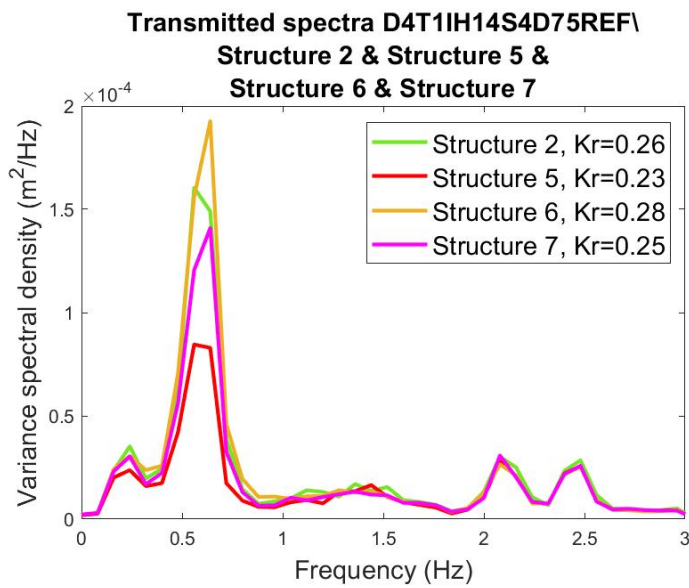
Secondly, the energy difference is mostly observed around f_p , with the smallest peak for structure 5. Around the second order peak structure 6 has a lowest amount of energy than Structure 2, 5 and 7. This suggests a steeper front slope results in less energy shifted towards the higher frequencies.

For Structure 2 and 7, the differences between the transmitted spectra are not very clear. In numbers the transmission coefficient decreases with 0.01.

Reflected spectrum

The resulting reflected spectra are plotted in Figure 5.14. The results are in line with the trend observed from the regular wave tests, in which the steepest front slope gives the highest reflection and vice versa. The shark-tooth orientation of structure 7 reduces the reflection. However, the total reduction in $K_r(s)$ compared to structure 2 is only 0.01 for the tested wave condition. Lastly, it can be observed that the spectra only differ around f_p . The maximum observed difference in $K_r(s)$ is 0.05.

According to [Van der Meer et al., 2005], the influence of the slope angle on the reflection decreases if the structure gets more submerged. Since the $K_t(s)$ is approximately 0.8 and the h_c/d_f is relatively large (0.65), it is expected that the observed effects of the front slope steepness on the K_r and K_t will increase for shallower water conditions or higher structures.



(A) Structure 2, 5, 6 and 7

FIGURE 5.14: Energy density spectrum from reflection measured at WG456 for design variable *front slope*.

5.4.3 Conclusion

All in all, for both the irregular and regular results a decrease of the reflection and transmission coefficient is observed with a decrease in slope steepness. This effect is enhanced if the fictitious incoming wave steepness decreases. The same trends are reported in other studies, such as the study from [Hur et al., 2011] on symmetrical submerged breakwaters.

From the energy density spectrum it can be seen that a decrease in front slope also reduced the amount of energy in the second order peak of the transmitted spectrum. Furthermore, it is observed that a zigzag orientation slightly reduced the amount of energy present in the peak frequency. Nevertheless, since only one wave condition has been tested these conclusions are not very strong.

5.5 POROSITY OF THE STRUCTURE

Box 5.5: KEY TAKEAWAYS

Transmission

⇒ If the width remains equal, but extra blocks are added to the bottom layer of the structure, the structure with the higher porosity results in higher $K_t(s)$ results. The difference is highest for the smallest relative water depth k_0d .

⇒ For the same number of blocks, an increased crest width had a stronger decreasing effect on $K_t(s)$ than a decreased porosity of the bottom layer.

Reflection

⇒ An increase in porosity reduces the $K_r(s)$.

In this section, it is investigated whether the empty spaces inside the structure and/or the location of these voids have an impact on the hydrodynamic performance. The porosity is calculated as follows:

$$\phi = \frac{V_{voids+holes}}{V_{total}} \quad (5.1)$$

5.5.1 Regular waves

For the analysis of the regular waves, structure 9 is compared with structure 10 and with structure 8-I. The porosity ϕ of structure 9 is 31% and from structure 10 it is 46% and from structure 8-I it is 45%. All structures have the same crest-height and front slope. The tests in $d_0 = 0.68m$ have a relative crest-height of $h_c/d_f = 0.50$ and for the tests in $d_0 = 0.75m$ it is $h_c/d_f = 0.65$.

Structure 9 and 10 have the same crest width, but a different porosity and a different number of blocks. Structure 9 has 27 blocks per 3 meter flume width and structure 10 has 21 blocks. On the other hand, structure 9 and 8-I have a different crest width and porosity, but the same number of blocks. The blocks increasing the width of structure 8-I are placed in the voids of the bottom layer for structure 9, increasing its porosity. The corresponding regular wave tests can be found in Table 5.9.

TABLE 5.9: Overview regular wave tests structure 8-I, 9 and 10 for design variable permeability of the structure

Structure	d_0	Wave conditions
8-I & 9 & 10	0,68 m	8, 10, 11, 14
8-I & 9 & 10	0,75 m	26, 28, 29, 30, 31, 32

Transmission

The transmission results are plotted over fictitious deep water wave steepness in Figure 5.15. The waveheight and length from the reference test are used to calculate $s_{0,m-1,0}$, so each specific symbol with the same x-coordinate comes from the same wave condition.

When comparing structure 9 and 10, it can be seen that structure 9 with the lower porosity results in the lowest transmission for all wave conditions. This is due to the fact that a part of the wave energy can travel through the structure for an increased porosity. The maximum observed difference is 0.09.

The differences between structure 9 and 10 are larger for the test in which $d_0 = 0.68m$ and $s_{0,m-1,0} < 0.035$. These are long waves in shallow water and therefore they feel the bottom more (small k_0d). Since the biggest difference in porosity between both structures comes from the bottom layer, the biggest impact is achieved on these waves. For the wave conditions where $d_0 = 0.75m$, the maximum observed difference of 0.04.

Despite the fact that the porosity is lower for structure 8-I, it can be observed that structure 8 has smaller $K_t(s)$ results than structure 9, for all wave conditions. This means a greater part of the incoming wave energy is dissipated over the crest than through the structure. Furthermore, the highest differences are found if $s_{0,m-1,0} > 0.035$, which is in line with the results of the crest width that the crest width has a bigger impact for steeper waves.

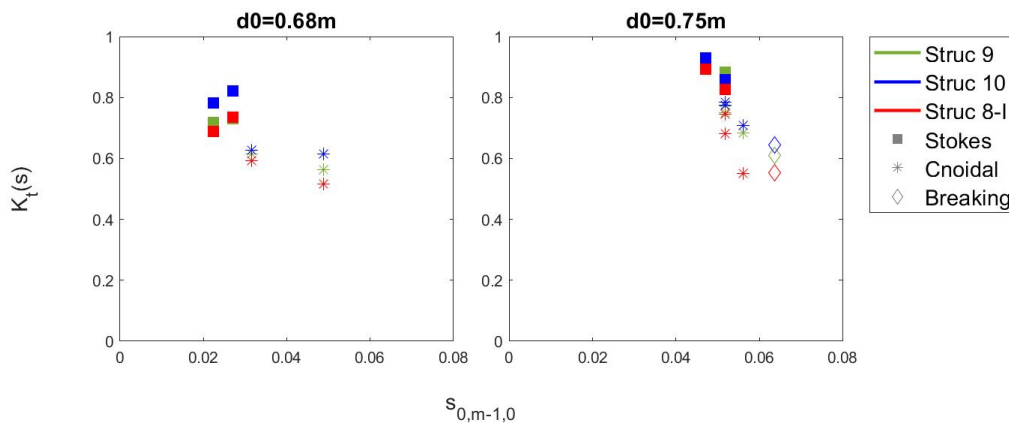


FIGURE 5.15: Transmission results per relative freeboard from regular wave tests on structure 9, 10 and 8-I.

Reflection

The reflection results from structure 9 and 10 are plotted over $s_{0,m-1,0}$ in Figure 5.16. Again, every position on the x-axis represents a specific wave condition.

Comparing structure 9 and 10, it has been observed that a higher porosity results in less reflection for the same wave condition. Comparing structure 9 and 8-I, the same is observed.

More porous structures give less reflection for the same wave condition. The magnitude in the difference of $K_r(s)$ has a maximum of 0.11.

Furthermore, for most of the results structure 8-I gives smaller K_r outcomes than structure 10 as well. Both structures have a similar porosity, structure 8 only has a wider back structure. This indicates if the width of the second structure is increased for the same porosity, the reflection reduces.

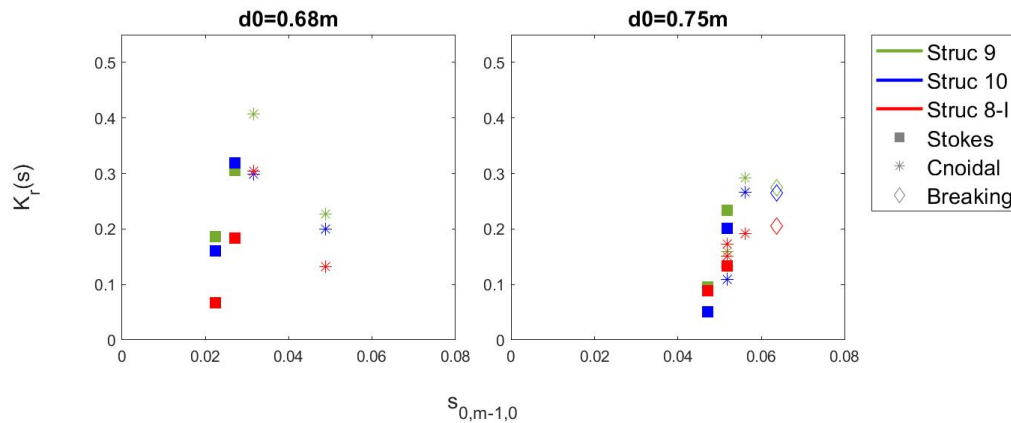


FIGURE 5.16: Reflection results from regular wave tests on structure 9, 10 and 8-I

5.5.2 Conclusion

If the porosity of a breakwater is too high, the energy of long waves can be transmitted through the breakwater. Therefore, the effect of a decreased porosity on K_t is strongest for long waves in smaller water depths. Furthermore, decreased porosity gives higher reflection outcomes.

The effect of an increased crest-width on K_t is stronger than the effect of a decreased porosity. Therefore, for the same amount of blocks it is more efficient to increase the crest width. Furthermore, the results of K_r are smaller if the width of the second structure is increased for the same porosity.

5.6 CHANNEL LENGTH

Box 5.6: KEY TAKEAWAYS

Transmission

⇒ The maximum difference in $K_t(s)$ resulting from a different S_{ch} in the same wave-condition is 0.10. Neither an optimum nor a trend for S_{ch}/L_0 and $K_t(s)$ has been identified.

Reflection

⇒ $K_r(s)$ has a positive correlation with S_{ch}/L_0 . Thus, a bigger part of the wave energy is

reflected by the second structure if L_{ch} increases and then flows through the first structure. A maximum difference in $K_r(s)$ in the same wave-condition is 0.15.

Energy density spectra

⇒ The differences in the transmitted spectra per channel length are small around f_p for the submerged structures. In the second order peak an increase in channel length reduces the amount of energy present for some wave conditions. For others, no difference is observed around the higher harmonics.

⇒ From the reflected spectra, the same trends is observed as for the regular wave tests. An increase in channel length simultaneously increases the amount of reflected energy around f_p .

Another study on the impact of the distance between two submerged breakwaters has been found, which measured the channel length as the distance between half of the crest-width at each side and called it spacing S [Liang et al., 2015]. The same definition is adopted here. The corresponding dimensionless variable is referred to as "the relative channel spacing":

- The relative channel spacing: S_{ch}/L_0

The channel length is made dimensionless by dividing it with L_0 , based on the local $T_{m-1,0}(f)$. The impact of this "relative channel length" on the transmission and reflection is further investigated in the next sections section.

5.6.1 Regular waves

The regular wave conditions for which structure 8-I, 8-III and 8-V have been tested are presented in table 5.10. Structure 8-0, 11-I, 11-III, 12-I, 12-III and 14 have only been tested for irregular wave conditions.

TABLE 5.10: Overview regular wave test for design variable Channel length

Structures	d_0	Wave conditions
8-I, 8-III, 8-V & 15	0.68 m	8, 10, 11, 14
8-I, 8-V & 15	0.75 m	26, 28, 29, 30, 31, 32
8-III	0.75 m	26, 28, 29, 30, 32

Transmission

The $K_t(s)$ results per S_{ch}/L_0 are plotted in the upper row of Figure 5.17. For each set of symbols, the left symbol represent 8-I, the middle one 8-III and the right one 8-V.

From the results no optimum S_{ch}/L_0 has been found. Furthermore, it can be seen that the maximum difference in $K_t(s)$ resulting from a different S_{ch} in the same wave-condition is 0.10. This is in line with the conclusion of [Rambabu and Mani, 2005], that the spacing has a minimal impact on the transmission.

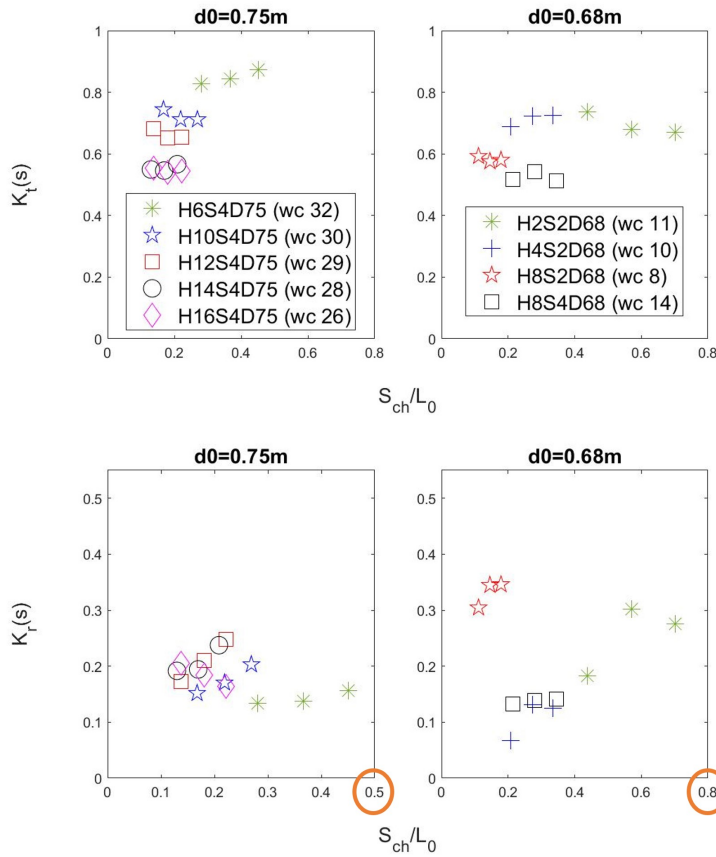


FIGURE 5.17: Transmission and reflection results per relative channel spacing, from regular wave tests on structure 8-I, 8-III and 8-V. Note that for wc 26, the waves break in front of the structure.

On the other hand, according to [Liang et al., 2015], the spacing is able to reduce $K_t(s)$ with 0.25 compared to the highest observed $K_t(s)$ in the same wave conditions. This study stated if S_{ch}/L_0 lies around 1.11, an optimum in reducing $K_t(s)$ is observed. In this research, S_{ch}/L_0 varied from 0.1 to 0.45. The hypothesis of [Liang et al., 2015] can therefore not be investigated.

in Figure 5.17 it is visible that $K_t(s)$ increases if the H_{target} from the wave-conditions decreases. Because R_c remains equal per sub-figure, it means R_c/H_i increases. Therefore, this result was expected and explained in the section about "structure height".

Reflection

in Figure 5.17, the bottom row show the reflection results from the regular wave tests on structure 8-I, 8-III and 8-V, with S_{ch}/L_0 on the x-axis. For each Figure, the R_c remains constant and each symbols represents different wave conditions. The left symbol coincides with the smallest S_{ch} (8-I) and vice versa for the right symbol (8-V).

From the results it can be seen that S_{ch}/L_0 impacted the $K_r(s)$ outcomes. With the maximum difference of 0.15 for the same wave condition. In general, Structure 8-I resulted in less reflection than structures 8-III and 8-V⁵. Between structure 8-III and 8-V less difference is observed if $d_0 = 0.68m$. For the tests in $d_0 = 0.75m$, $K_r(s)$ decreases with a decreasing channel length.

All in all, the results mean that a bigger part of the wave energy is reflected by the second structure if L_{ch} increases. And that the reflected wave from the second structure does not get fully dissipated when travelling between the structures, but instead flows back through the first structure.

This results differs from the study of [Liang et al., 2015], where the spacing did not influence $K_r(s)$. One explanation is that [Liang et al., 2015] modelled impermeable structures. The Reefy structure is more permeable and therefore more of the reflected wave can flow through the front structure. A second explanation is the fact that the front slope from the second structure in the study of [Liang et al., 2015] is 1:2, whereas the second structure from Reefy has a straight front slope. And steeper front slope gives more reflection.

5.6.2 Irregular waves

In this section the development of the energy density spectra is investigated for the channel length by comparing structures 8, 11 and 12 for different channel lengths. An overview of the irregular wave conditions in which the structures are tested is given in Table 5.11.

TABLE 5.11: Overview irregular wave tests for design variable channel length

Structure	d_0	Wave conditions
11-I & 11-III, 12-I & 12-III,	0.61 m	5
11-I & 11-III, 12-I & 12-III,	0.68 m	18
8-0, 8-I, 8-V	0.68 m	16, 20

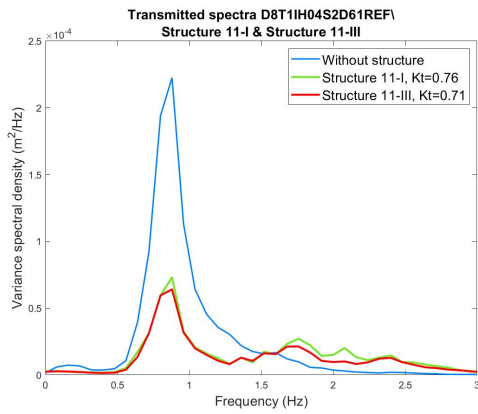
Transmitted spectrum

Here, the energy density spectra at WG789 are compared for tests with- and without a structure.

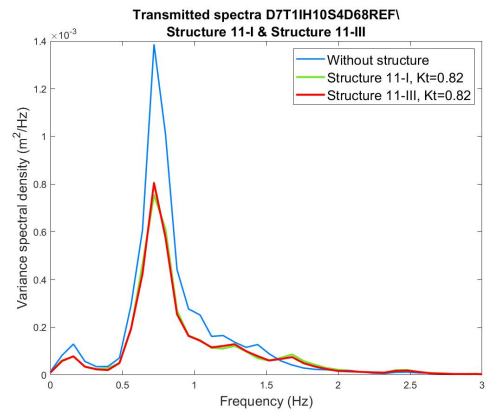
Around f_p , for the emerged structures (Figure 5.18c) an increase of the channel length reduces the energy in f_p . For all the other tests the structures are submerged, the difference of the energy around f_p is very small for different channel lengths.

Above $1.5 * f_p$, the amount of energy is smallest for the longest channel length in Figures 5.18a, 5.18e, and 5.18f. This is only not observed for wave condition 18. This is different to the result of [Liang et al., 2015], where an increase in channel length resulted in more energy shifted towards the super harmonic domain, defined as $1.5 - 3.5 * f_p$. Nevertheless, as discussed before, the range of S_{ch}/L_0 in which [Liang et al., 2015] tested is much bigger.

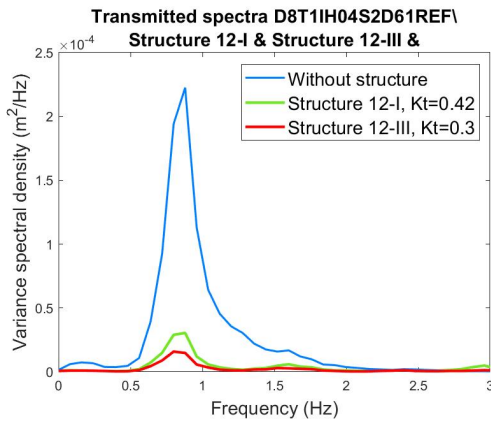
⁵ Except for wc 26, however because wave condition 16 results in breaking waves before the structure this result is considered to be less reliable.



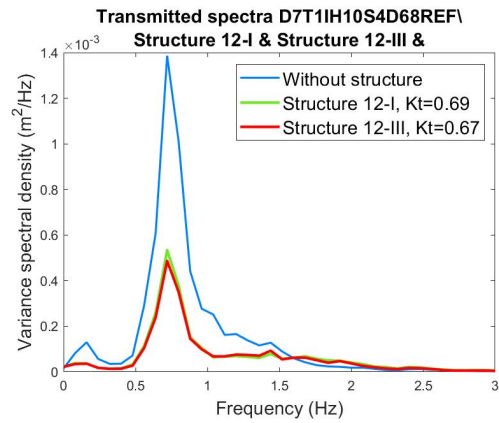
(A) WC 5, Structure 11-I, 11-III and 14.



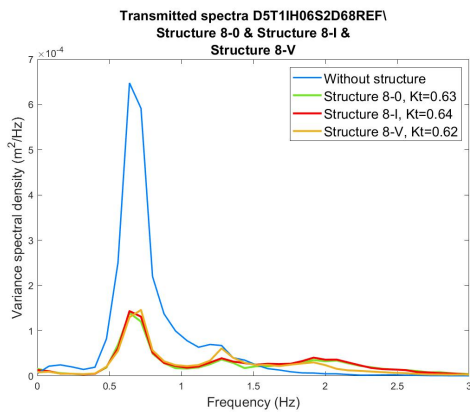
(B) WC 18, Structure 11-I, 11-III and 14.



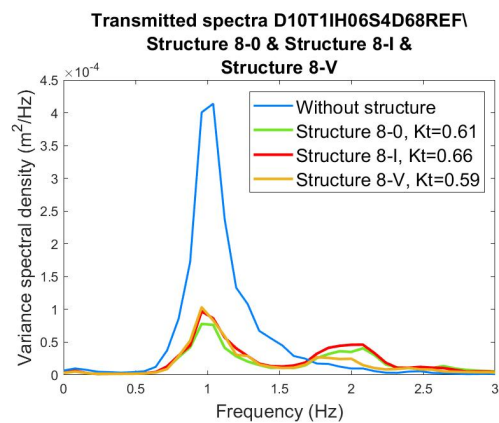
(C) WC 5, Structure 12-I and 12-III.



(D) WC 18, Structure 12-I and 12-III.



(E) WC 16, Structure 8-0, 8-I and 8-V.



(F) WC 20, Structure 8-0, 8-I and 8-V

FIGURE 5.18: Energy density spectra measured at WG789 for design variable *channel length*. The $K_t(s)$ of each structure can be found in the legends. Structures in Figure 5.18c are emerged, the others submerged.

Reflected spectrum

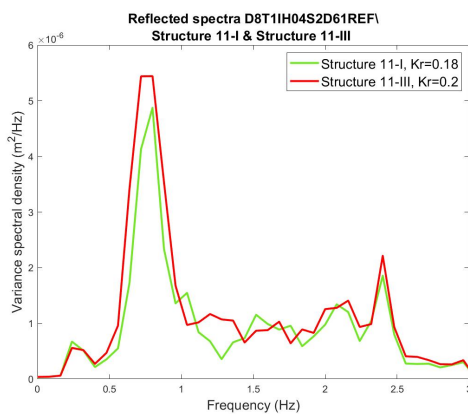
Here, the reflected energy density spectra in front of the structure are compared for tests with a structure. The results can be found in Figure 5.19.

It is visible that in each wave condition, the structure with the longest channel has resulted in the highest $K_r(s)$. The energy differences are the highest in the area around f_p . The maximum $K_r(s)$ difference which has been found is 0.07.

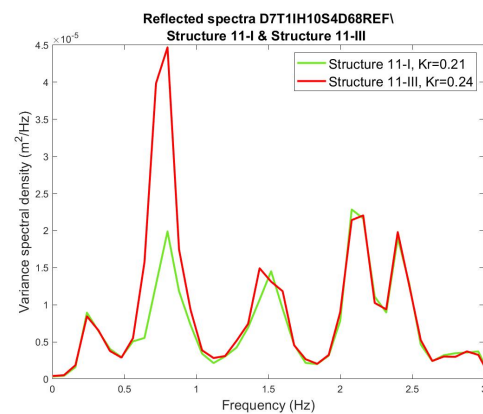
5.6.3 Conclusion

No consistent correlation has been observed between the relative channel spacing parameter and the transmission. Moreover, the impact of S_{ch}/L_0 on $K_t(s)$ reached a maximum of 0.1 for the same regular wave condition. For the irregular wave conditions the maximum is 0.07. Therefore, it can be concluded that S_{ch}/L_0 does not have a significant impact $K_t(s)$ within the range of $0.1 < S_{ch}/L_0 < 0.8$.

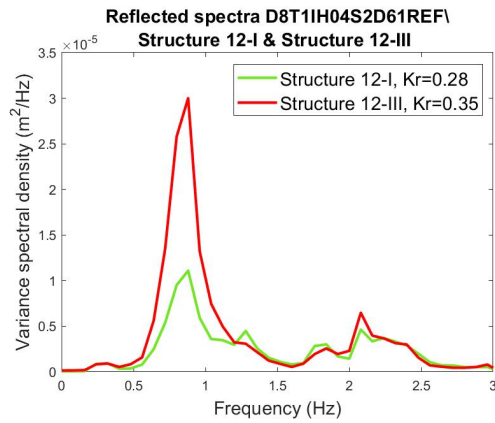
On the other hand, the $K_r(s)$ increased for an increase in S_{ch}/L_0 . With the maximum difference of 0.15 for the same regular wave condition. The same is observed for the irregular wave conditions, in which the energy around f_p is affected from the channel.



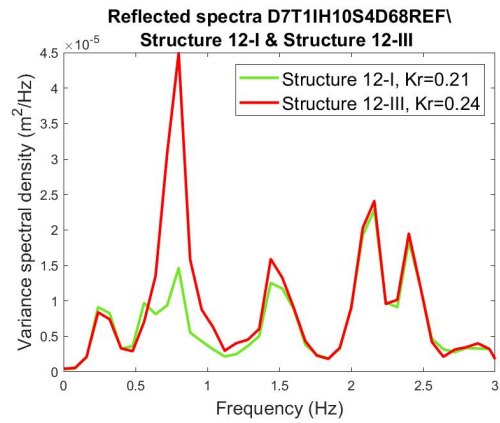
(A) WC 5, Structure 11-I, 11-III and 14.



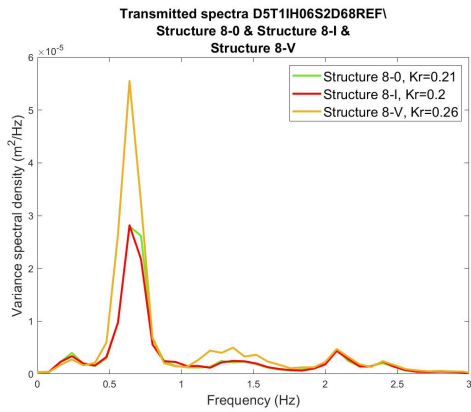
(B) WC 18, Structure 11-I, 11-III and 14.



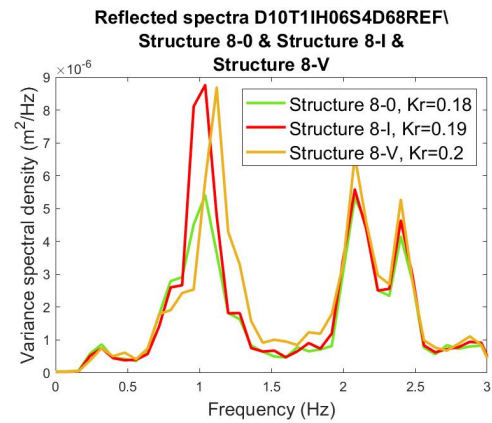
(c) WC 5, Structure 12-I and 12-III.



(d) WC 18, Structure 12-I and 12-III.



(e) WC 16, Structure 8-0, 8-I, 8-V and 15.



(f) WC 20, Structure 8-0, 8-I, 8-V and 15.

FIGURE 5.19: Energy density spectra from reflection measured at WG456 for design variable *channel length*. Structures in Figure 5.19c are emerged, the others submerged.

5.7 SURFACE ROUGHNESS

Box 5.7: KEY TAKEAWAYS

Transmission

⇒ For $h_c/d_f = 0.27$, no effect of the increased surface roughness on K_t is observed.

⇒ For $h_c/d_f = 0.83$, K_t decreases for an increase in outer surface roughness. The observed impact on K_t is 0.06 – 0.12 for 8-I-PVC(169), 0.02 for 8-I-PVC(69) and 0.09 for 8-I-3D.

⇒ The increased surface roughness affects the transmitted spectrum both in the first- and second harmonic.

Reflection

⇒ There is no consistent trend of the impact of increased outer surface roughness on K_r . However, the maximum difference obtained is only 0.03.

The effect of increased the surface roughness, which can occur in real life due to the growth of vegetation, has been investigated here. Only irregular waves are tested with increased surface roughness.

5.7.1 Irregular waves

Structure 8-I has been modified by adding different amounts of 4cm tall PVC pipes out of holes on top of the structure. Respectively 37, 69 and 169 pipes have been added, referred to as for example 8-I-PVC(37). The roughness of structure 8-I-PVC(169) is higher than for 8-I-PVC(37). Also 3D corals are printed and added to structure 8-I. Pictures of these structures can be found in Appendix A. Table 5.12 gives an overview of the regular wave conditions in which the tests are conducted.

TABLE 5.12: Overview irregular wave tests structure 8-I, 8-I-PVC(x) and 8-I-3D for design variable Surface roughness

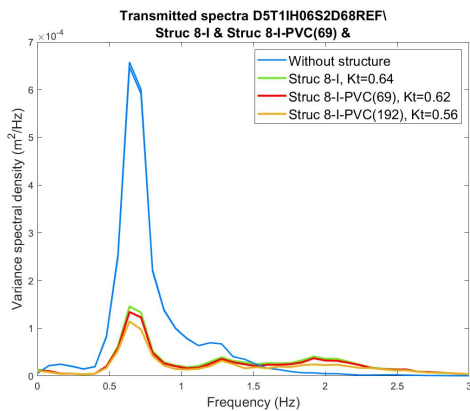
Structure	d_0	Wave conditions
8-I & 8-I-PVC(32) & 8-I-PVC(69) & 8-I-PVC(169)	0,75 m	35
8-I & 8-I-PVC(69) & 8-I-PVC(169)	0,68 m	16
8-I & 8-I-PVC(169)	0,68 m	17, 19
8-I & 8-I-PVC(169) & 8-I-3D	0,68 m	20

Transmitted spectrum

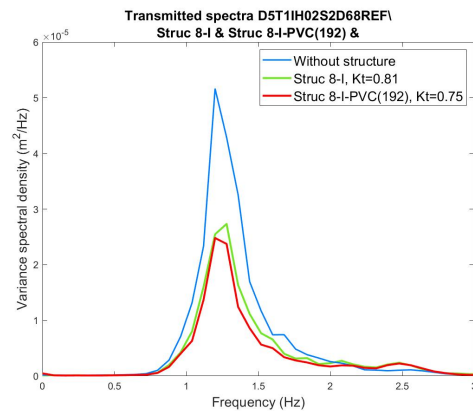
The transmitted spectra are shown in Figure 5.20. For a small relative structure height ($h_c/d_f = 0.27$), no effect of the increased surface roughness on K_t is observed. On the other hand, if the relative structure height is high enough (e.g. $h_c/d_f = 0.83$), an increased roughness decreases the transmitted energy. This can be explained by the fact that the roughness creates turbulence in the waves, which dissipates energy. The effect can be observed in both the first- as second harmonic. The latter can be explained by the fact that steeper/shorter waves are more affected

by the width of the crest, and thus as increased roughness of the crest has an impact on the higher harmonics as well.

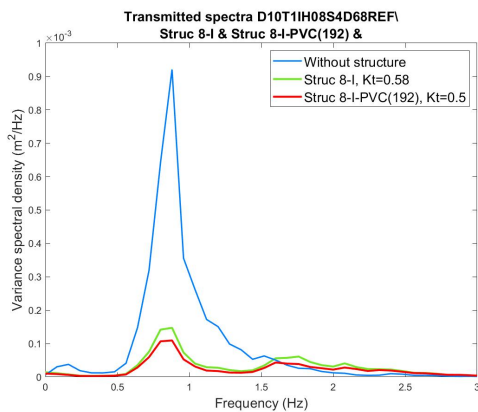
The significance of the impact increases if the amount of pipes increases. Furthermore, the results suggest the impact increases if the target wave steepness increases. Namely, comparing the results of two wave conditions in which only s_{target} differs ⁶, the decrease in $K_t(s)$ is higher for the highest target steepness. The maximum difference in $K_t(s)$ from an increased roughness is 0.12, observed for structure 8-I-PVC(169) in wc 20. Structure 8-I-3D in the same conditions decreases $K_t(s)$ with 0.09. Nevertheless, for structure 8-I-3D, an extra block has accidentally been placed on top of the front structure, see Figure A.3d in Appendix A. Thus, the 3D corals together with an extra block decreased $K_t(s)$ less than 169 PVC pipes by itself did.



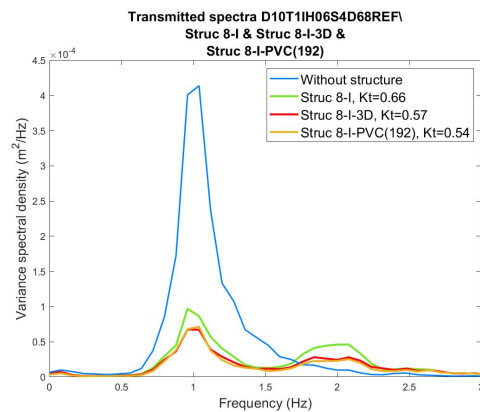
(A) WC 16, Structure 8-I, 8-I-PVC(69) and 8-I-PVC(169).



(B) WC 17, Structure 8-I and 8-I-PVC(169).

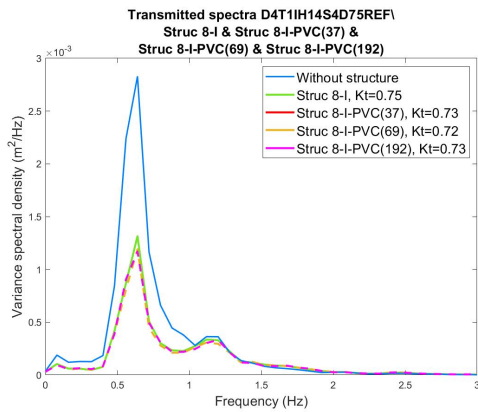


(C) WC 19, Structure 8-I and 8-I-PVC(169).



(D) WC 20, Structure 8-I, 8-I-3D and 8-I-PVC(169).

⁶ Compare Figure 5.20a from wc 16 ($s_{target} = 0.02$) with Figure 5.20d wc 20 ($s_{target} = 0.02$)



(E) WC 35, Structure 8-I, 8-I-PVC(38), 8-I-PVC(69) and 8-I-PVC(169).

FIGURE 5.20: Energy density spectra measured at WG789 for design variable *surface roughness*. The $K_t(s)$ of each structure can be found in the legends. Structures in Figure 5.20e have a relative structure height around 0.27, the others around 0.83

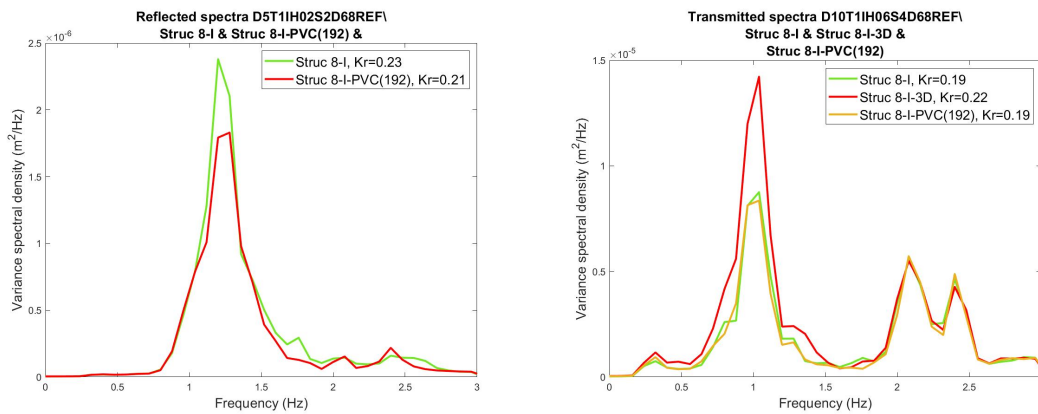
Reflected spectrum

The impact of the increased surface roughness on the reflected spectra is not consistent, as can be seen in Figure D.2. Only two spectra are shown, the others can be found in Appendix ???. The reason behind this is the insignificant impact on K_r which is measured from the increased surface roughness, with a maximum observed difference of 0.03 in K_r .

5.7.2 Conclusion

It has been observed that the increased surface roughness on the outer layer of the structure decreases the energy in the transmitted spectra, given the relative structure height is "high enough". This effect is both visible in the first- and second harmonic. The impact on the K_t of irregular waves reaches a maximum of 0.12 and is observed to increase if s_{target} increases and/or the roughness increases.

On the other hand, for the reflected spectra no consistent relation has been observed between an increased roughness and K_r . The maximum observed difference in K_r is 0.03.



(A) WC 17, Structure 8-I and 8-I-PVC(169).

(B) WC 20, Structure 8-I, 8-I-3D and 8-I-PVC(169).

FIGURE 5.21: Reflected energy density spectra measured at WG456 for design variable *surface roughness*. The $K_r(s)$ of each structure can be found in the legends. Both have a relative structure height of 0.83

5.8 NEW EMPIRICAL FORMULAE

5.8.1 Transmission

In this section, the empirical equations from table 2.1 in Chapter 2.1.1 are compared with the test results from the regular wave tests. The results are shown in Figure 5.22. Thereafter, the empirical equation with the best fit is optimized for the Reefy structure.

Method comparison literature

DATASET For the comparison with the equations from other studies, first all the tests conducted in breaking wave conditions are removed from the dataset. The breaking waves behave different from the cnoidal and stokes waves, for example because they show no correlation with the relative freeboard⁷. Therefore they are not included. In addition to that, this is also done by the DELOS project for the DELOS database. The breaking wave conditions are wc 6, 12 25 and 26.

Many studies from table 2.1 defined an applicability range in which this formula is tests. Some adjustments are made in order to decrease the error. Namely, the limiting upper boundary of 0.8 for K_t from [Van der Meer and Daemen, 1994], [Van der Meer et al., 1996] and [Van der Meer et al., 2005] is not taken into account. Namely, many experiments of this research have a K_t above this threshold. The maximum is therefore imposed as 1. Furthermore, the applicability ranges based on D_{n50} from the studies of [Van der Meer and Daemen, 1994] and [Seabrook and Hall, 1999] are also not included, as the D_{n50} of a Reefy block is not comparable to a rubble mound breakwater and this range would discard many test results. The other applicability ranges are still applied and if an experiment is not within this range this test is not included.

⁷ This can be seen in Figure D.3a of Appendix D.3

INPUT VARIABLES The special input variables for the equations from table 2.1 are shortly repeated in this alinea. The D_{n50} of a block is set to 0.09 m. This is based on the $(\frac{M_{50,saturated}}{\rho_{saturated}})^{1/3}$. The surf similarity parameter is based on the spectral wave period $\zeta_{0,m-1,0}$. Furthermore H is based on $H_{m0,i,WG456}(s, f)$.

STATISTICAL ERROR MEASURES The prediction capabilities of each empirical equation are expressed for three different statistical measures. First of all, the coefficient of determination R^2 is calculated, which says something about how well the formula predicts the real observations. A value of 1 indicates a perfect fit. Secondly, the root mean squared error $RtMSE$ ⁸ is computed, this is the squared root of the quadratic mean of the differences between the predicted- and measured values. A value of zero would indicate a perfect fit. Lastly, the mean absolute error MAE is calculated, which is the average of the absolute errors and is therefore easy to interpret. The results are shown per empirical formula in Figure 5.22.

Results comparison literature

The results are plotted per equation in Figure 5.22. With on the x-axis the predicted K_t and on the y-axis the measured $K_t(s)$.

The empirical equation from [Van der Meer et al., 2005] for smooth impermeable breakwaters has the best fit with the results from the experiments. With a R^2 of 0.7, $RtMSE$ of 0.07 and MAE of 0.07. Furthermore, no limiting applicability ranges are defined for this equation, thus all tests are included in the comparison. In the next step, the formula is optimized to find the smallest RMSE.

Optimization method

In this part, both the equations are optimized with the `lsqnonlin` function in matlab, which solves nonlinear least-squares problems. For each coefficient, a starting point, upper- and lower limit is defined. The function is looped to execute the optimization hundred times and for each run the starting point is randomly generated within the boundaries from that coefficient. For the first execution, the upper- and lower boundary are very sparse and for the following executions they are each time adjusted closer to the generated coefficient. This process is repeated until the R^2 , MAE and $RtMSE$ are not improving anymore.

The equations of [Van der Meer et al., 2005] for impermeable low-crested breakwaters is repeated here, with the coefficients numbered as $c(1)$, $c(2)$, $c(3)$ and $c(4)$:

$$\text{For } \zeta < 3 \quad K_t = c(1) \frac{R_c}{H_{s,i}} + c(2)(1 - e^{c(4)\zeta}) \quad (5.2)$$

$$\text{For } \zeta \geq 3 \quad K_t = c(1) \frac{R_c}{H_{s,i}} + c(2) \left(\frac{B}{H_{s,i}}\right)^{c(3)} (1 - e^{c(4)\zeta}) \quad (5.3)$$

⁸ Often RMSE is the used abbreviation for the Root Mean Squared Error, however this is already used in Chapter 4 as the Relative Mean Squared Error.

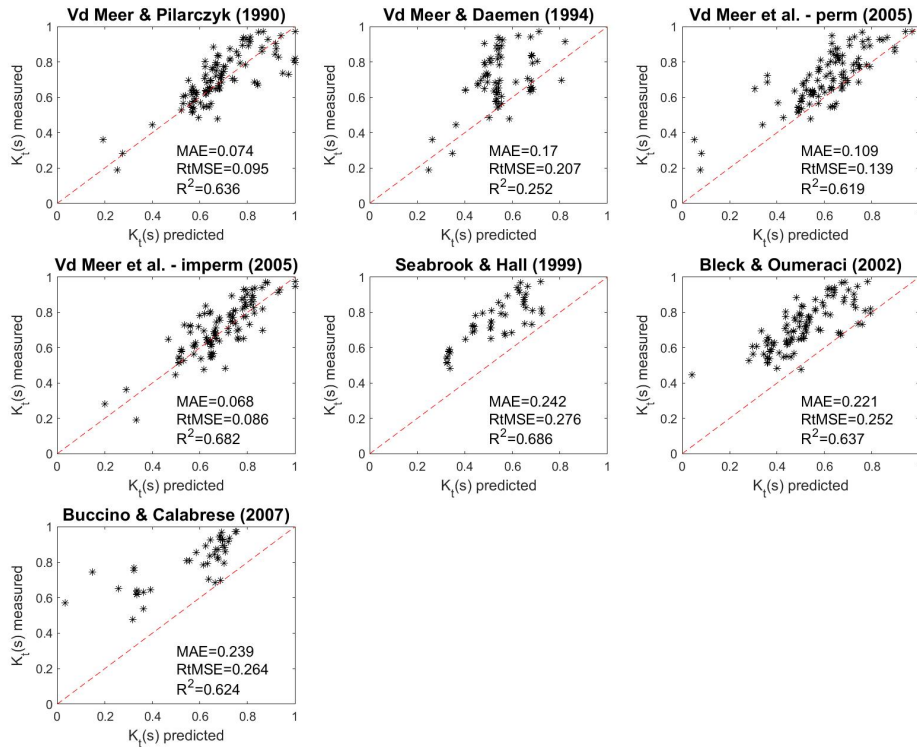


FIGURE 5.22: Comparison between the measured K_t outcomes and the predicted K_t from the empirical formulas of table 2.1

The original values of the coefficients are shown in Table 2.1, namely $c(1) = 0.3$, $c(2) = 0.75$, $c(3) = -0.31$ and $c(4) = -0.5$.

Results optimized equation

First, equation 5.3 improved. For this, only data with $\zeta_{0,m-1,0} \geq 3$ is included. It has been investigated whether replacing $B/H_{m0,i}$ with $B/L_{0,m-1,0}$ would generate an improved equation. The results show that this is the case, as can be seen in Figure 5.23. The obtained R^2 is 0.83, $RtMSE$ is 0.056 and MAE is 0.046. The new empirical formula yields:

$$\text{If } \xi \geq 3 \quad K_t = 0.34 * \frac{R_c}{H_{s,i}} + 0.287 * \left(\frac{B}{L_0}\right)^{-0.33} (1 - e^{(-0.505)\xi}) \quad (5.4)$$

Note that the freeboard R_c is positive for submerged structures in equation 5.4, as this formulation is used throughout the whole report. However, it is in contrast to the original definition by [Van der Meer et al., 2005].

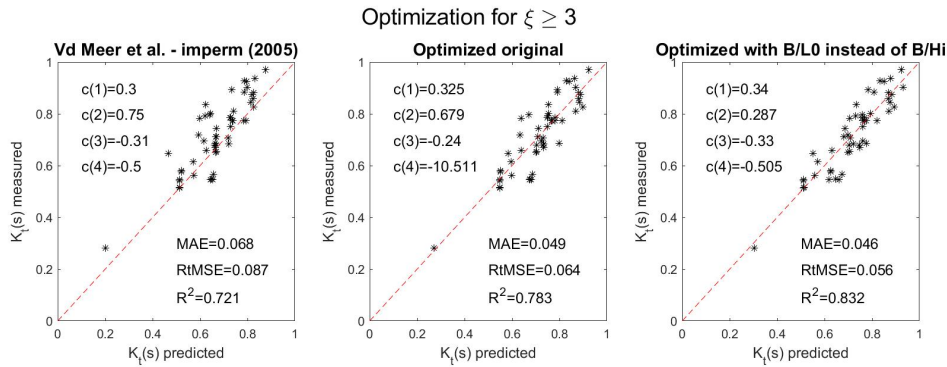


FIGURE 5.23: Comparison between the measured K_t outcomes and the predicted K_t from the optimized formulas for regular waves, based on [Van der Meer et al., 2005] for $\zeta_{0,m-1,0} \geq 3$.

Secondly, equation 5.2 for $\zeta_{0,m-1,0} < 3$ is considered. It has been investigated whether replacing h_c/d_f to the position of $B/H_{m0,i}$ in equation 5.3 would generate a smaller RMSE. The results are shown in Figure 5.24, and it can be concluded that the addition of the relative structure height indeed results in smaller error indicators. The obtained R^2 is 0.743, $RtMSE$ is 0.079 and MAE is 0.064. The new empirical formula yields:

$$\text{If } \zeta < 3 \quad K_t = 0.189 \frac{R_c}{H_{s,i}} + 0.498 \left(\frac{h_c}{d_f} \right)^{-0.358} (1 - e^{(-1.919)\zeta}) \quad (5.5)$$

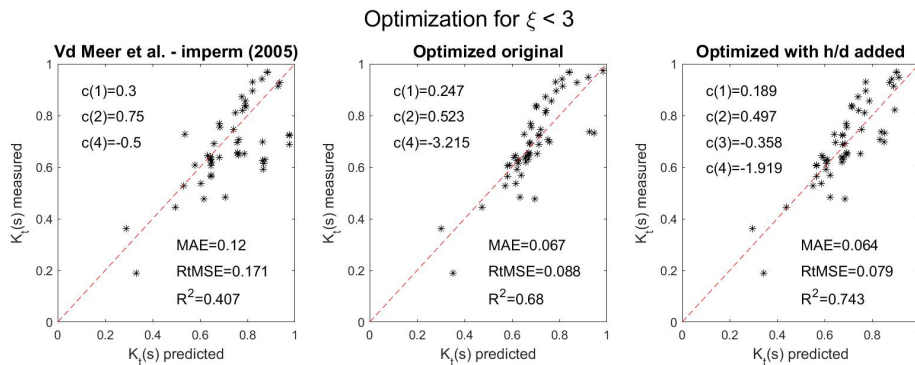


FIGURE 5.24: Comparison between the measured K_t outcomes and the predicted K_t from the optimized formulas based on [Van der Meer et al., 2005] for $\zeta_{0,m-1,0} < 3$.

5.8.2 Reflection

Method comparison literature

For the reflection analysis, the same dataset as for the transmission analysis is used, with the wave conditions in which the waves break before the structure removed. The empirical equations which are included in the analysis can be found in Table 2.3.

The formula referred to as Rock Manual B requires a notional permeability factor P , which characterizes the permeability of the structure. [Van der Meer et al., 2005] represent three values for this factor, based on armor stability model tests with three armor layer compositions. For overtopped rubble mound structures a factor 0.4-0.6 is expected. Because these values are in the order of magnitude of the porosity of the structure, the porosity as shown in Table 3.5 is used as an input for P . Furthermore, in the equation the K_r is negatively proportional to P which also holds for the porosity. Secondly, for the roughness parameter γ_f in the formula from [Zanutigh and Van der Meer, 2008], 0.47 is based which is calculated for 2 layers of antifer by [Bruce et al., 2007]. Antifer is chosen as this has a relatively high roughness parameter and therefore less reflection. Due to the permeability of the Reefy structure the reflection is expected to be lower than for conventional breakwaters. This is also confirmed in Figure 5.25.

Lastly, the same statistical measures are used as for the transmission part: R^2 , $RtMSE$ and MAE .

Results comparison literature

The results are plotted in Figure 5.25 for each equation. The predicted K_r is plotted on the x-axis and on the y-axis the measured $K_r(s)$. As can be seen from the results, none of the existing equations results in a relative good fit with the measured K_r . Therefore, all three equations are investigated in a non-linear least-square optimization process.

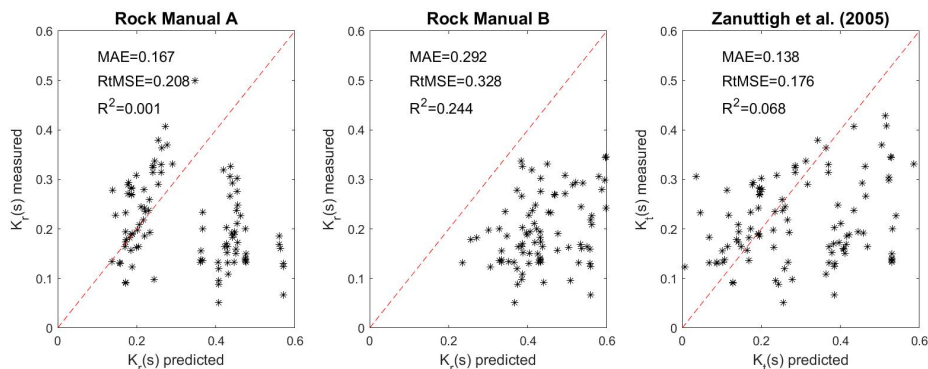


FIGURE 5.25: Comparison between the measured K_r outcomes and the predicted K_r from the empirical formulas of table 2.3

Optimization method

The same method as discussed in the transmission part is applied here to the empirical equations from table 2.3. The form of the different equations with the coefficients numbered as $c(1)$, $c(2)$ etc, are written in equations 5.6, 5.7 and 5.8. Equations 5.6 "Rock Manual A" and 5.7 "Rock Manual B" are from [Van der Meer et al., 2005]. Equation 5.8 is from [Zanutigh and Van der

Meer, 2008]. The values of the coefficients in the original formulas are summarized in Table 5.13.

$$K_r = (c(1) \frac{R_c}{H_{s,i}} + c(2))c(3)\zeta_{0,m-1,0}^{c(4)} \quad (5.6)$$

$$K_r = (c(1) \frac{R_c}{H_{s,i}} + c(2))c(3)P^{c(4)} \cot(\alpha_{front})^{c(5)} \zeta_{0,m-1,0}^{c(6)} \quad (5.7)$$

$$K_r = \tanh((c(1)(1 - \exp(c(2) * \gamma_f)))\zeta_{0,m-1,0}^{c(3)(\gamma_f+c(4))^2+c(5)})(c(6) + c(7) * \frac{R_c}{H_{s,i}}) \quad (5.8)$$

TABLE 5.13: Coefficients from original K_r formulas as can be found in Table 2.3

Author	c(1)	c(2)	c(3)	c(4)	c(5)	c(6)	c(7)
Rock Manual A (2005)	-0.2	0.9	0.14	0.73	N/A	N/A	N/A
Rock Manual B (2005)	-0.2	0.9	0.071	-0.82	-0.62	-0.46	N/A
Zannutigh et al (2008)	0.167	-3.2	1.49	-0.38	0.86	0.67	-0.37

Results optimized equation

From the Figure 5.25, it can be seen that the best optimization fit comes from Rock manual B. The corresponding coefficients of each graph are summarized in Table 5.14. The obtained R^2 is 0.462, $RtMSE$ is 0.064 and MAE is 0.049. Nevertheless, for all expressions the performance is clearly less than those for wave transmission.

TABLE 5.14: Output coefficients from optimized K_r formulas

Author	c(1)	c(2)	c(3)	c(4)	c(5)	c(6)	c(7)
Rock Manual A (2005)	-0.233	0.986	0.307	-0.081	N/A	N/A	N/A
Rock Manual B (2005)	-0.234	0.837	0.055	-0.173	-0.007	-0.4866	N/A
Zannutigh et al (2008)	0.413	0.677	-0.140	0.305	0.003	-1.970	0.466

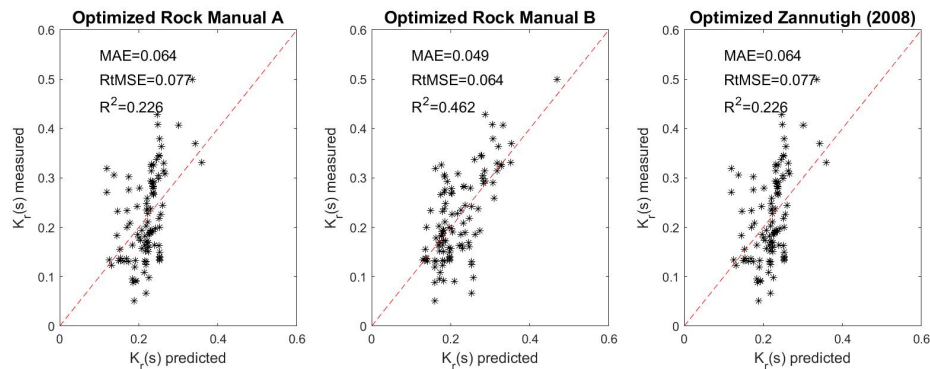
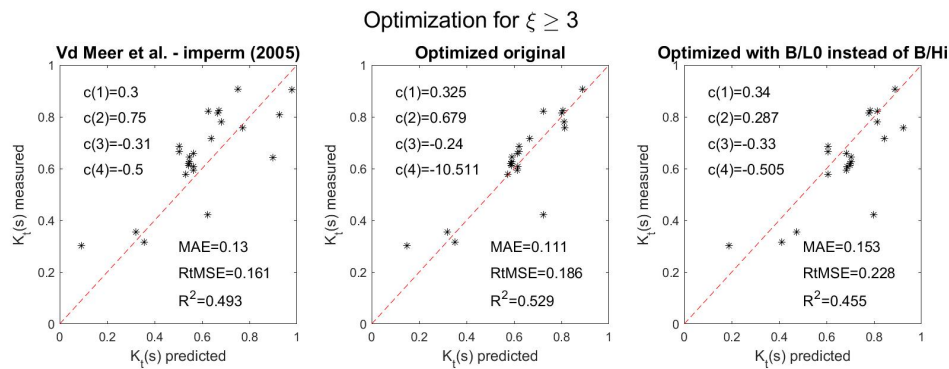


FIGURE 5.26: Comparison between the measured K_r outcomes and the predicted K_r from the optimized formulas for regular waves.

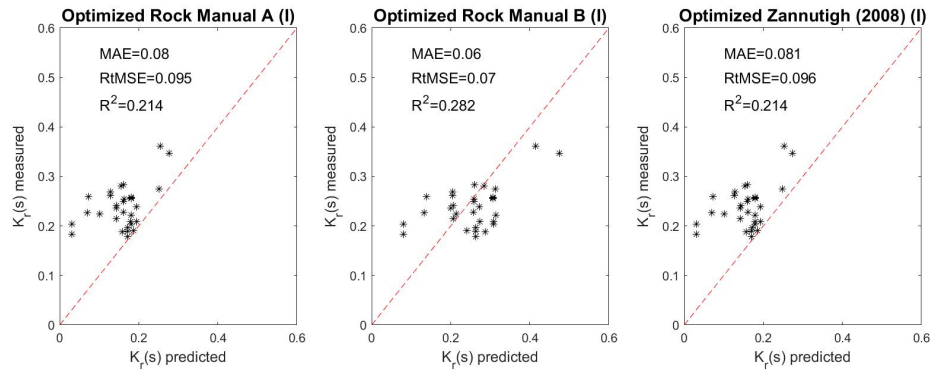
5.8.3 Applicability new formulae for irregular wave conditions

Here, the obtained optimized formulae for the regular tests are applied to the outcomes of the irregular tests. The outcomes can be seen in Figure 5.27a for the transmission formula en in Figure 5.27b for the reflection formula. For the transmission coefficient, only the optimized formula for $\zeta_{0,m-1,0} \geq 3$ is investigated because for only four irregular wave tests ζ appeared to be below 3.

As can be seen, for the reflection formula, the optimized Rock Manual B results in the best fit. For the transmission formula, the optimized original [Van der Meer et al., 2005] results in the best fit, thus it is better not to use the version with the width to wavelength ratio.



(A) Optimized formulae predicting K_t of regular waves based on the formula of [Van der Meer et al., 2005] for $\zeta_{0,m-1,0} \geq 3$ applied to the irregular wave tests.



(B) Optimized formulae predicting K_r of regular applied to the irregular wave tests.

FIGURE 5.27: Applicability of the obtained optimized formulae from the regular tests for the irregular tests.

The formula of [Van der Meer et al., 2005] for $\zeta_{0,m-1,0} \geq 3$ is also optimized for the irregular wave tests only. The results can be seen in Figure 5.28. Compared to applying the optimized formula for regular waves to the irregular waves in Figure 5.27a, this shows better statistical resemblance.

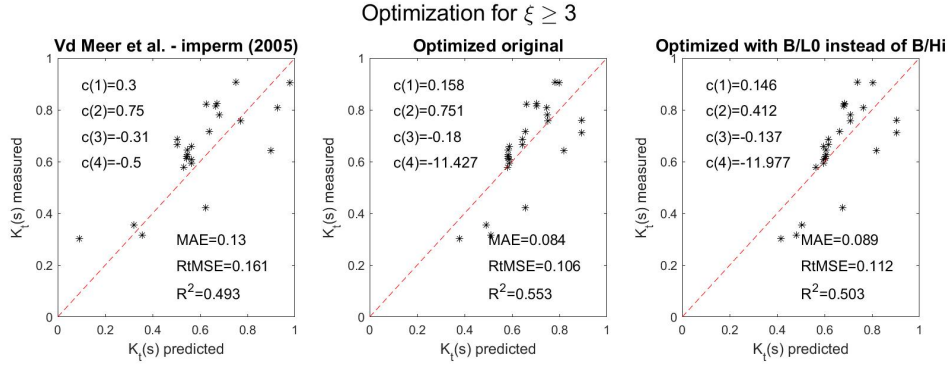


FIGURE 5.28: Comparison between the measured K_t outcomes and the predicted K_t from the optimized formulas for irregular waves, based on [Van der Meer et al., 2005] for $\xi_{0,m-1,0} \geq 3$.

Conclusion optimization empirical formulae

The final optimized formulae for $K_t(s)$ yield:

$$\text{If } \xi \geq 3 \quad K_t = 0.325 \frac{R_c}{H_{s,i}} + 0.679 \left(\frac{B}{H_{s,i}} \right)^{-0.24} (1 - e^{(-10.511)\xi_{0,m-1,0}}) \quad (5.9)$$

$$\text{If } \xi < 3 \quad K_t = 0.189 \frac{R_c}{H_{s,i}} + 0.498 \left(\frac{h_c}{d_f} \right)^{-0.358} (1 - e^{(-1.919)\xi_{0,m-1,0}}) \quad (5.10)$$

Equation 5.9 is based on the results for both irregular- and regular waves. Equation 5.10 is based on the results for only regular waves.

It can be concluded that for all surf similarity parameters the freeboard relatively to the incoming waveheight has the biggest impact on the transmission coefficient. In which the transmission coefficient decreases if the relative freeboard decreases. Furthermore, the multiplication factor with the relative freeboard is lower if the surf similarity parameter is $\xi_{0,m-1,0} < 3$. As such, if the ratio between the front slope relative to the fictitious wave steepness decreases a certain threshold, the relative freeboard has more impact on K_t .

Moreover, the impact of the structure height relative to the local water depth only plays a role in the predicting equation if the surf similarity parameter is $\xi_{0,m-1,0} < 3$. In which the transmission coefficient decreases if the relative structure height increases. The impact of the relative structure height is dependent on the magnitude of ξ . In which the impact increases if ξ decreases.

Whether the crest-width plays an important role in the prediction of the transmission coefficient depends on the surf similarity parameter. For the tests in which $\xi_{0,m-1,0} \geq 3$, the impact of the crest width comes into play, whereas it is not included in the predictive empirical formula for $\xi_{0,m-1,0} < 3$. Therefore, the crest width has more impact on K_t waves if the ratio between the front slope relative to the fictitious wave steepness increases a certain threshold of $\xi_{0,m-1,0} \geq 3$. Furthermore, the results show that once the threshold of $\xi_{0,m-1,0} = 3$ is reached, an increase in

$\zeta_{0,m-1,0}$ has (almost) no impact on the magnitude of the influence of the crest width anymore. For example, the multiplication factor $(1 - e^{(-10.511)\zeta_{0,m-1,0}})$ is 1,00 for both $\zeta = 3$ and $\zeta = 18$ ⁹.

The role of the slope steepness is investigated through the surf similarity parameter and as explained above plays a role in determining the impact of the relative freeboard, crest width and relative structure height. However, as soon as the threshold of $\zeta_{0,m-1,0} \geq 3$ is reached, the multiplication factors for the relative freeboard and crest width are not changing with the front slope anymore. Whereas, if $\zeta_{0,m-1,0} < 3$, the multiplication factor for the relative structure height decreases for a decreases in front slope relative to the fictitious wave steepness, thereby reducing the transmission coefficient.

The final optimized formulae for $K_r(s)$ yield:

$$K_r = \left(-0.234 \frac{R_c}{H_{s,i}} + 0.837\right) * 0.055 P^{-0.173} \cot(\alpha_{front})^{-0.007} s_{0,m-1,0}^{-0.487} \quad (5.11)$$

The performance of this equation is less compared to the equations for the transmission coefficient. Nevertheless, from the equation of the parameters it can be concluded that the reflection coefficient decreases is the relative freeboard increases, the porosity increases, the front slope decreases and/or the fictitious wave steepness decreases. It can be seen that the impact of the fictitious wave steepness is higher than from the front slope steepness. This is opposite to the original equation. An explanation could be that for the 3D structures the slope was often much steeper, nevertheless the porosity much smaller.

⁹ The example of $\zeta = 18$ is chosen, because the maximum tested $\zeta_{0,p}$ was 18.49 (see table 2.2).

6

DATA PROCESSING ECOLOGICAL PERFORMANCE

Box 6.1: KEY TAKEAWAYS

Scope

⇒ For the ecological enhancement part, only the irregular wave tests and the peak horizontal velocities are considered. All measurements are taken 75 cm above the bottom of the foreshore (1:1 scale). The exact locations of the EVM measurements with respect to a structure can be found in Figure 3.2 and are referred to with *Back-* and *Channel* location.

Amplitude spectra

⇒ The frequencies above 3 Hz are removed from the horizontal velocity signal. All frequencies below this limit are included. Therefore frequencies present below the $0.25 * f_p$ limit are included as well, because these are expected to occur in natural conditions as well.

Tranquility index

⇒ Three tranquility indexes Tr are calculated, based on respectively the 30th, 50th and 95th percentile of the absolute peak velocities. The tranquility indexes compare these percentile values in the wake of a structure with the percentile values without a structure, for the same wave condition. A higher Tr corresponds to a more tranquil wake region.

Safety score

⇒ The safety score compares the orbital velocity for which a branching coral will break with the 95th percentile value of the peak velocities measured by the EVM. The safety score is below 1 if the breaking limit is exceeded and above 1 if the breaking limit is not exceeded by 5% of the maximum peak velocities.

The main goal of this chapter is to explain the data processing from the electromagnetic liquid velocity meter (EVM) into the performance parameters of the ecological performance, namely the tranquility index and the safety score. In Section 6.1, these performance parameters are explained and the used formulae are introduced. In Section 6.2, the steps which are undertaken to process the EVM data into the information needed for the performance parameters are discussed. Lastly, in Section 7.3, an example of an ink-injection is analyzed and compared to the information gained from the processing of the electromagnetic liquid velocity meter.

6.1 PERFORMANCE PARAMETERS

During the experiments, tests have been conducted to measure the velocities near the bottom at the lee-side of the structure. The location of the EVM with respect to the structure and the

flume is visualised in Figure 3.2. In this section, the performance parameters which are used to assess these velocities are introduced.

6.1.1 Tranquility index

For the ecological enhancement assessment, a tranquility index Tr is computed to assess the tranquility in the wake region and investigate the impact of the design variables on this index. An increase of the tranquility index means the flow circumstances are more tranquil in the wake region, which is important for certain species to use this region as an energy saving zone. The index is based on a similar index introduced by [Kim et al., 2016]. In short, the tranquility index is based on a reference velocity divided by the velocity in the wake region, both in stream-wise (horizontal) x -direction. The original formula can be found in equation 2.2 from Chapter 2.2. Compared to this definition, a few adaptations are made due to different testing conditions:

1. The reference velocity is not measured at the sea-side from the structure, but it is obtained from the test without a structure around the same location.¹ The reasons behind this are to use a similar method as is used when computing K_t and because not enough data was available in which the EVM was placed in front of the structure.
2. For this thesis waves were present around the structure and not water flow. Therefore, the peak orbital velocities in horizontal direction ($|U_{x,peak}|$) are considered here instead of the mean flow velocity.
3. The tranquility index is computed for the 30-th, 50-th and 95-th percentile of $|U_{x,peak}|$. These percentiles are abbreviated as for example $|U_{x,peak,30\%}|$. In which $|U_{x,peak,30\%}|$ refers to the value to which 30% of the horizontal peak velocities is equal or below, etc.

The final formulas can be found in equations 6.1, 6.2 and 6.3. In these formulas, the notation (f) is used to show that a value is measured during the test without a structure and the notation (s,f) is used to show that a value is measured during a the test with a structure².

$$Tr_{30\%} = \frac{|U_{x,peak,30\%}(f)|}{|U_{x,peak,30\%}(s,f)|} \quad (6.1)$$

$$Tr_{50\%} = \frac{|U_{x,peak,50\%}(f)|}{|U_{x,peak,50\%}(s,f)|} \quad (6.2)$$

$$Tr_{95\%} = \frac{|U_{x,peak,95\%}(f)|}{|U_{x,peak,95\%}(s,f)|} \quad (6.3)$$

¹ The exact location of the EVM during a reference test was not consistent. Nevertheless, the EVM during the reference test was close to the location of the structure. Thus, this method assumes that the horizontal particle velocities in the scenario without a structure are quite consistent around the location of interest.

² This notation is also used in the investigation of the hydrodynamic performance. The reason behind these letters is as follows: with a structure in place the measurements can include effects from both the foreshore (f) and the structure (s). Without a structure, the measurement includes the effect of the foreshore (f) only.

The outcomes provide insight in the reduction of the lowest 30% of the peak velocities (6.1), the reduction of the median from the peak velocities (6.2) and the reduction of the lower limit from the 5% highest peak velocities (6.3). In Section 6.2, the steps undertaken to process the EVM data into the percentile values of $|U_{x,peak}|$ are described.

6.1.2 Safety score

For the ecological enhancement assessment, a safety score is computed to investigate whether the branching coral³ is expected to break based on the maximum peak velocities measured from the EVM data per test. The safety score is based on the study from [Baldock et al., 2014]. This study concluded the limiting orbital velocity in which a branching coral is expected to break equals $0.5m/s$ ($|U_{x,limit}|$). The safety score is calculated from equation 6.4, in which n_l stands for the length scale factor of the experiments ($n_l = 15$)⁴. If the score is below 1, breaking is expected to occur during the highest 5% of the peak velocities. And the opposite holds if the score is above 1.

$$safety\ score = \frac{|U_{x,limit}|}{|U_{x,peak,95\%}| * \sqrt{n_l}} \quad (6.4)$$

From equation 6.4, it can be seen that the score compared the limit velocity to the 95-th percentile value of the peak velocities. The high percentile value is used, because the velocity measurements are taken $0.75m$ above the bottom (real life scale). The peak orbital velocities are expected to be higher at the crest of the structure. Therefore, using a high percentile assures the score is more representative for the conditions occurring at the crest. Furthermore breaking is a severe damage which can not be reversed. If for example the safety score for feeding mechanisms needs to be evaluated, it can be considered to use a lower percentile value.

6.2 DATA PROCESSING ELECTROMAGNETIC LIQUID VELOCITY METER

In this section the data processing steps of the EVM data is explained.

Step 1: Selection of tests

It is decided to look only at the irregular wave test as these are closer to real-life conditions and the EVM was placed behind the structure more often with irregular waves. Furthermore, only the conditions in which the EVM has been placed in the wake of a structure are considered. This is the case for wave conditions number 5, 16, 18, 19, 20 and 35. As a next step, the velocity time signals from the considered test are investigated and spuriousities are removed.

³ The branching type of coral named *Acropora intermedia* is used for this comparison.

⁴ This factor converts the obtained velocities to a real life scale, based on the Froude scaling laws as are shown in Table 3.1.

Step 2: Remove spuriousities

TIME SPAN For some experiments, the EVM recording started before there were waves present. This time interval is removed for the further analyses. Moreover, for some tests a few erroneous peaks (with unrealistic magnitudes) were visible, possibly because of ink-injections close to the EVM. These peaks were also removed from the time-series. Examples of these two phenomena can be found in Appendix C.2.

Thereafter, the velocity amplitude spectra are plotted for the considered test. Examples of such spectra measured at different locations around the structure can be found in Figure 6.1.

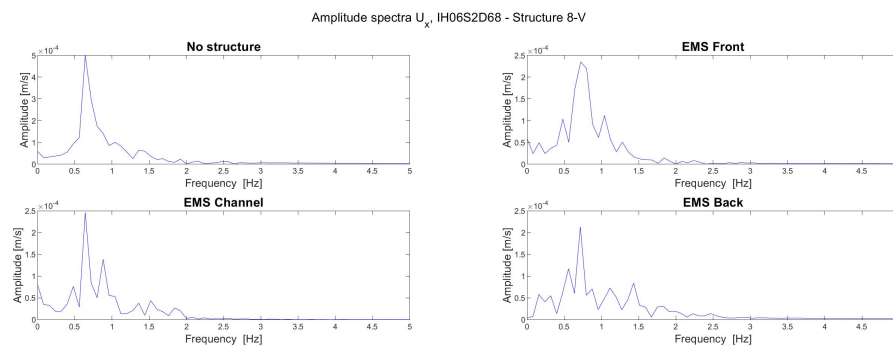


FIGURE 6.1: Examples of raw amplitude spectra of horizontal velocity measured in wave condition 16. The spectrum for the test without a structure is given together with the spectra for different locations of the EVM around structure 8-V.

HIGH FREQUENCIES From the results it can be seen that for some spectra (at the back, in the front and in the channel), frequencies above 3 Hertz are observed. These frequencies are removed. Namely, they create spurious peaks and troughs in the velocity time signal. The latter can be seen in the upper row of graphs in Figure 6.2. Therefore, it is assumed to be high frequency noise generated from for example breaking waves. A low-band pass frequency filter is applied to get rid of these spurious peaks and troughs and thereby improve the signal-to-noise ratio. This filter removes all the data with a frequency above a chosen frequency limit. The limit is set to 3 Hz, because this is the same limit which has been used in the spectral analysis from the wave gauge data. Furthermore, after applying a limit at 3 Hz, most spurious peaks and troughs are removed for all of the investigated wave conditions. An example of the improved peak detection can be seen in the bottom row of Figure 6.2.

Step 3: Interpretation cleaned up signal

After the spuriousities explained above are removed, the resulting signal is further analyzed and interpreted. In this section, the phenomena observed are summarized. For this, the tests from Figure 6.1 are used as an example. In appendix C.2, the analysis from all the other wave conditions that are analyzed for the ecological enhancement can be found.

MEAN VELOCITY First of all, it is observed that the mean of the velocity signal is negative for all locations, indicating the flow has a mean seaward direction from for example an undertow.

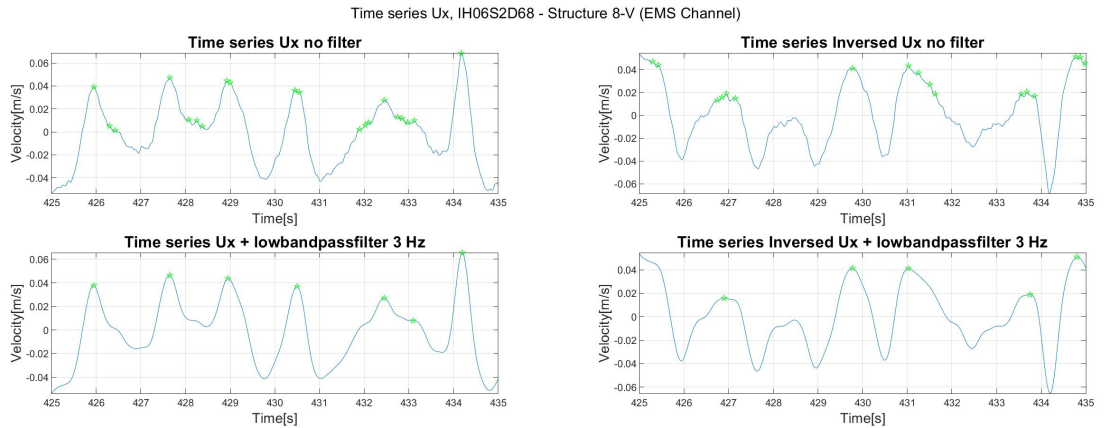


FIGURE 6.2: Zoomed-in view of the horizontal velocity time signal from the same wave condition and structure as in Figure 6.1. The graphs in the upper row show the actual signals. The graphs in the bottom row show the signals after the addition of a low-band pass filter at 3 Hz.

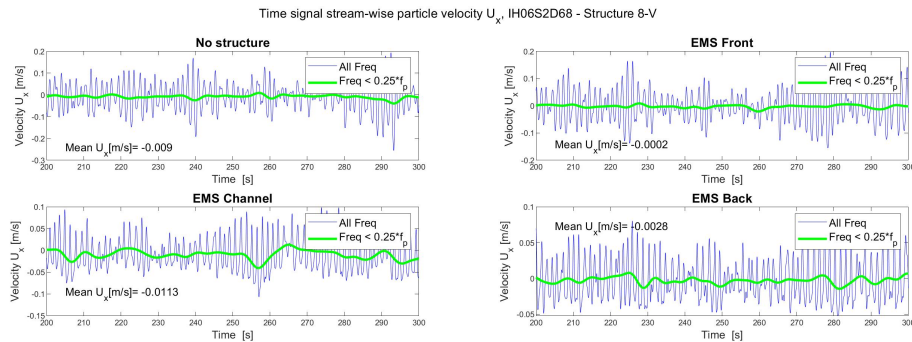


FIGURE 6.3: Comparison of the horizontal velocity time-signal from the lower frequencies ($0.25 * f_p = 0.18$) and the total time-signal. Based on filtered signal from the bottom row in Figure 6.2, from wave condition 16. The time series for the test without a structure is given together with the time series different locations of the EVM around structure 8-V.

In front of a structure (top right), the mean velocity is smaller compared to the other locations. Furthermore, from the analysis of other wave conditions it is observed that the mean seaward flow velocity at the back of a structure decreases if the channel length increased C.2. This could be explained with the fact that bigger a part of the wave energy is reflected by the second structure if the channel length is increased, as has been concluded from the investigation of the reflection coefficient.

LOW FREQUENCIES Secondly, from the velocity amplitude spectra the frequencies below $0.25 * f_p$ are investigated.⁵ These frequencies are not removed from the velocity signal, as is explained in this paragraph. In Figure 6.3, the time signal of the low frequencies is plotted on top of the time signal of the total waves. For the tests without a structure (top left) it is observed

⁵ This limit is chosen, because for the wave decomposition method with Z&S the wave energy below $0.25 * f_p$ is (if present) not included.

that the trough of the lower frequency signal coincides with the largest waves in the short wave group. This suggests a bound infra gravity wave is present during a test without a structure. For the measurements in the back and channel (bottom left and right), the wave group and the lower frequency signal both fluctuate a lot. This could be explained from the fact that the conditions in these wake regions are turbulent. Above that, the low frequency troughs still have a tendency to occur simultaneously with the largest waves in the wave group. Behind a submerged obstacle this phenomena is also associated with the mass influx transport over the structure which is linked with the wave group. All in all, it is decided to include these lower frequencies, as all phenomena can be explained and are expected to be present in real life as well.

Step 3: Obtain the performance indexes

After the spuriousities are removed from the data, the absolute peak velocities are obtained from the horizontal orbital velocity ($|U_{x,peak}|$). Next, empirical cumulative distribution function (eCDF) of these peaks is computed. From the eCDFs, the 30-th, 50-th and 95-th percentile values of $|U_{x,peak}|$ with- and without a structure are compared. The comparison is done by calculating the corresponding tranquility indexes $Tr_{x\%}$: see equation 6.1 for $Tr_{30\%}$, 6.2 for $Tr_{50\%}$ and 6.3 for $Tr_{95\%}$. Furthermore, the 95-th percentile value of the peak velocities is used to give a safety score with respect to the breaking expectancy for a branching coral. The equation for this score can be found in equation 6.4.

Box 7.1: KEY TAKEAWAYS**General notions**

⇒ If the tranquility increases it means the horizontal peak velocities in the wake of the structure decrease with respect to the scenario without a structure.

⇒ The tranquility index abbreviation $Tr_{x\%}$ is used to refer to $Tr_{30\%}$, $Tr_{50\%}$ and $Tr_{95\%}$ together. Detailed information can be found in Chapter 6. Equation 6.1 corresponds to $Tr_{30\%}$, equation 6.2 corresponds to $Tr_{50\%}$ and equation 6.3 corresponds to $Tr_{95\%}$.

⇒ The difference in the outcomes of the tranquility index between different structures and in the same wave condition is referred to as ΔTr_x . Here, $Tr_{30\%}$ from a structure is compared to $Tr_{30\%}$ from another structure, etc.

Tranquility index

⇒ It has been observed that the tranquility index $Tr_{x\%}$ increases for an increase in crest width, structure height or surface roughness; and for a decrease in block porosity or front slope steepness.

⇒ No consistent relationship is observed between the channel length and/or the location within the structure (back vs. front) and $Tr_{x\%}$.

⇒ The induced change in the tranquility index by each design variable ΔTr_x varies per test condition. The design variables are ranked from highest to lowest $\Delta Tr_{x,max}$ in Table 7.1

⇒ No general rule is found on whether the lower or higher peak velocities are more reduced in a wake region. It appears that this varies per test condition.

Safety score

⇒ An example is given on how the safety against breaking for a coral can be predicted.

In this chapter, the results on the ecological performance are discussed. For this the cumulative distribution functions of the horizontal peak velocities are investigated $|U_{x,peak}|$, as is explained in Chapter 6. These velocities are measured in the wake of a structure and in the scenario without a structure. The exact location of the EVM with respect to the water column and the structure are shown in Figure 3.2 from Chapter 3.

In Section 7.1, the impact of different design variables on the tranquility index $Tr_{x\%}$ is investigated. The variables which are investigated are the structure height, crest width, blocked holes, slope steepness, channel length, location around the structure (channel vs. back) and outer surface roughness. In Section 7.1.7, a summary is given from the impact of the design variables on the tranquility. Thereafter, in Section 7.2 the safety score results are discussed for branching

corals. This provides a second tool on how to interpret the empirical cumulative distribution graphs from $|U_{x,peak}|$ and link this to the velocity limits an organism can withstand.

7.1 TRANQUILITY INDEX

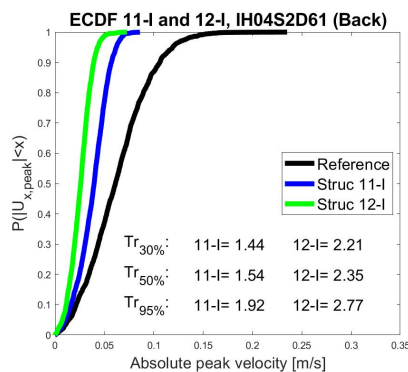
7.1.1 Structure height

In this section, the tranquility is compared for two structures with a different structure height, namely structures 11 (2 levels) and 12 (3 levels). In Figures 7.1a and 7.1b, the cumulative distribution functions of $|U_{x,peak}|$ at the back of structures 11-I and 12-I are compared and in Figure 7.1c the same is done in the channel of structures 11-III and 12-III.

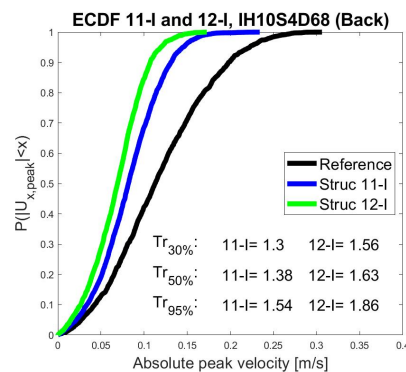
First of all, from the results it is observed an increase in structure height increases the tranquility index $Tr_{x\%}$ in all scenarios. A higher structure dissipates and reflects more wave energy, thus less mass and energy is present behind the structure. Therefore, smaller peak velocities are measured in the wake.

The impact of a change in structure height on the tranquility (ΔTr_x) outcome is significantly higher if one of the structures is emerged and the other submerged. The latter is the case in Figures ?? and 7.1c, where structure 12 is emerged and structure 11 is not. The ΔTr_x in these figures lies between 0.7 and 0.85. In Figure 7.1b, bot structures are submerged and ΔTr_x here lies between 0.25 and 0.32. Nevertheless, since also the wave conditions differ, no firm conclusion can be withdrawn from this. Namely, in the test where both structures are submerged (Figure 7.1b), the wave conditions are also much more stormy compared to the other two tests.

For the results of the wake region in the back, it can be seen than the $\Delta Tr_{95\%}$ is higher than $\Delta Tr_{50\%}$ and $\Delta Tr_{30\%}$. This suggest that in these cases, the same increase in crest height reduced the highest 95th percentile of the peak velocities more than the 50th- and 30th percentiles. Nevertheless, this is not the case for the measurements in the channel. Therefore, more data would be needed to see if there is a consistency about on which percentile an increase in crest height has the biggest impact and whether this is different in the channel and at the back.



(A) Structure 11-I and 12-I, wc 5



(B) Structure 11-I and 12-I, wc 18

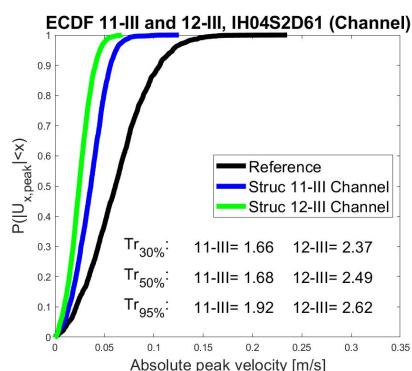
(c) Structure 11-III and 12-III, w_c 5

FIGURE 7.1: Comparison between the eCDF of the horizontal peak velocities for different structure heights during the same test conditions. The structure number, wave condition and location of the EVM can be found in the title of each figure and the tranquility index is plotted in the graph.

7.1.2 Crest width

In this section, the tranquility index is compared at the back of two structures with a different crest width. In Figure 7.2a, structure 4 ($B = 0.2\text{m}$) and 5 ($B = 0.4\text{m}$) are compared, which are two 2DV structures. In Figure 7.2b, structure 11-I ($B = 0.73\text{m}$) and 14 ($B = 0.33\text{m}$) are compared, which are 3D structures ¹. In Figure 7.2c, structure 8-0 ($B = 0.73\text{m}$) and 15 ($B = 0.33\text{m}$) are compared, which are also 3D structures ². Each comparison has a different wave condition.

In general, it can be observed that an increase in B decreases Tr . This can be explained because a wider structure dissipates more wave energy over the crest. Therefore, less (kinetic) energy is present behind the structure and thus smaller peak velocities are measured in the wake at the back of the structures.

The results suggest that an increase in crest width decreases the $Tr_{x\%}$ more for 2DV structures than for 3D structures. Namely, from the comparison between structures 4 and 5, $\Delta Tr_{x,max} = 0.98$ and $\Delta Tr_{x,min} = 0.86$ are observed. On the other hand, from the comparison between structure 14 versus 11-I the results were $\Delta Tr_{x,max} = 0.04$ and $\Delta Tr_{x,min} = 0.01$ and for structure 15 and 8-0 the results were $\Delta Tr_{x,max} = 0.35$ and $\Delta Tr_{x,min} = 0.19$. An explanation could be the increased porosity of 3D structures compared to the 2DV ones. This allows more water to flow through the structure and thus results in more kinetic energy present behind the structure, regardless of the crest width. Nevertheless, because more aspects are different between the tests (the structures and the wave conditions), the validity of this outcome can not be confirmed in this study.

Lastly, for the results of structure 4 vs. 5 and 15 vs. 8-0, $\Delta Tr_{95\%}$ is bigger than $\Delta Tr_{50\%}$ and $\Delta Tr_{30\%}$. This suggests an increase in crest width reduces the 5% highest peak velocities the most. However, this is not the case for structure 11-I vs, 14, for which the ΔTr_x is relatively low

¹ Structure 14 is a single structure and structure 11 is a double structure. Structure 14 is the front structure of structure 11.

² Structure 15 is a single structure and structure 8 is a double structure. Structure 15 is the front structure of structure 8.

in general. All in all, more data would be needed to conclude whether there is a consistency for which percentile of the peak velocities an increase in crest width has the biggest impact.

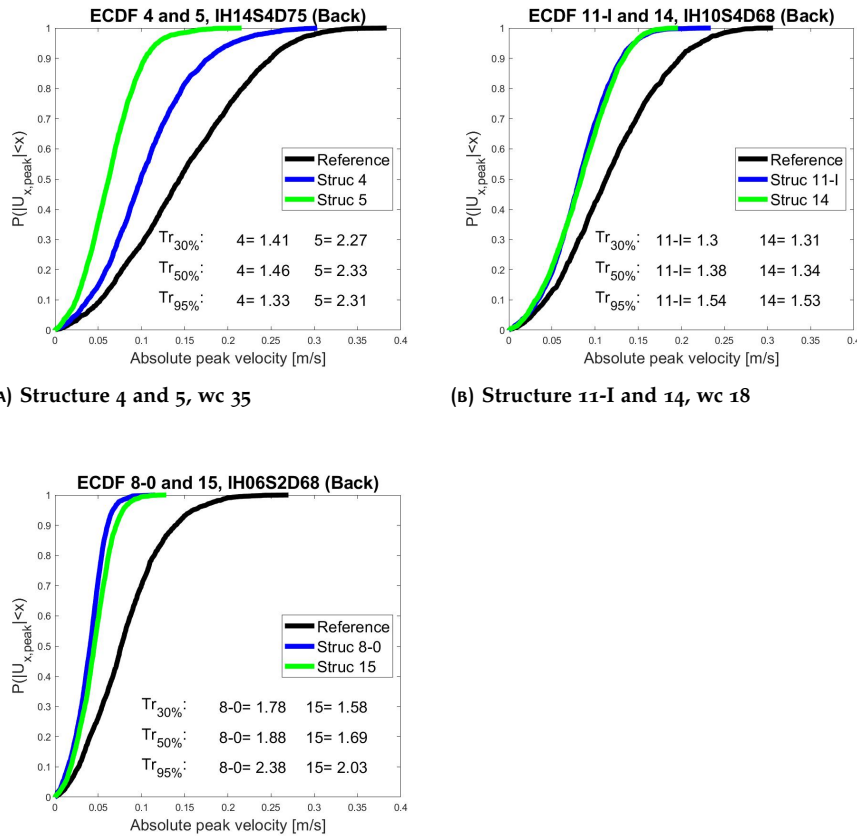


FIGURE 7.2: Comparison between the eCDF of the horizontal peak velocities for different crest widths during the same test conditions. The structure number, wave condition and location of the EVM can be found in the title of each figure and the tranquility index is plotted in the graph.

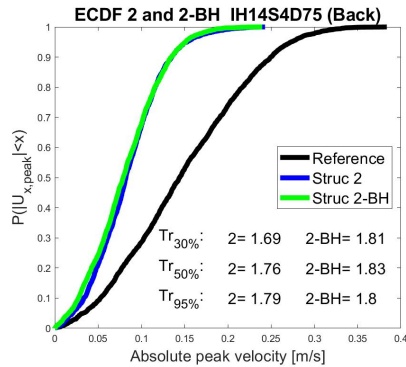
7.1.3 Blocked holes

In this section, the tranquility behind structure 2 is compared for a scenario with- and without PVC pipes blocking the vertical holes. The scenario for which the holes are blocked and thereby the block porosity is reduced, is referred to with BH. The results are shown in Figure 7.3a.

From the results it can be seen that the decreased block permeability reduces Tr . This can be explained because less water can flow through the structure if the holes are blocked, which decreases the peak velocities behind the structure at the lower part of the water column. This phenomena was also identified by [Jiang et al., 2020].

The maximum- and minimum difference in tranquility indexes between structure 2 and 2-BH are $\Delta Tr_{x,max} = 0.12$ and $\Delta Tr_{x,min} = 0.01$. Moreover, the results suggest that a reduced

porosity decreases the smaller peak velocities more than the higher peak velocities, because $\Delta Tr_{30\%} > \Delta Tr_{50\%} > \Delta Tr_{95\%}$. However, only one condition is available and thus more tests are needed to confirm whether this observation is consistent.



(A) Structure 2, 5, 6 and 7, wc 35

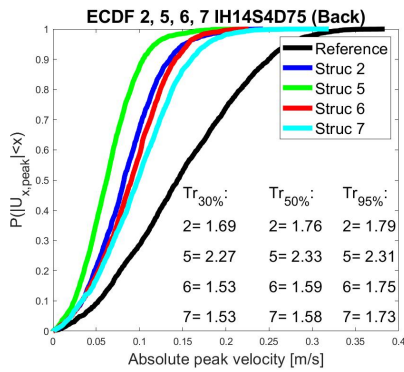
FIGURE 7.3: Comparison between the eCDF of the horizontal peak velocities for different permeability of the blocks during the same test condition. The structure number, wave condition and location of the EVM can be found in the title and the tranquility index is plotted in the graph.

7.1.4 Slope steepness

The results of the tranquility at the back of structures with a different front slope can be found in Figure 7.4a. Structure 5 has the shallowest front slope (1:3), next structure 2 (1:2) and structure 6 has the steepest front slope (1:1). The opposite holds for the back-slope of the structures, where structure 5 has a straight back slope, structure 2 has a back slope of 1:1 and structure 6 has a back slope of 1:2. Structure 7 has the same slope steepness as structure 2 (1:2), with a zigzag orientation (see Figure A.1g).

From the results it can be seen that a decrease in front slope increases $Tr_{x\%}$ and vice versa. This can be explained from the fact that a shallower front slope causes more wave breaking and thus less energy present in the wake region. The maximum observed difference $\Delta Tr_{x,max}$ between structure 5 and 6 is 0.74 and the smallest observed difference $\Delta Tr_{x,min}$ is 0.56. Moreover, the result shows that a zigzag orientation decreases the $Tr_{x\%}$ compared to a straight orientation.

The following difference in tranquility indexes between structure 2 and 7 are found: $\Delta Tr_{30\%} = -0.16$, $\Delta Tr_{50\%} = -0.18$ and $\Delta Tr_{95\%} = -0.06$. This suggests the slope orientation had less impact on the highest 5% of the peak velocities, compared to the lowest half of the peak velocities. Furthermore, from comparing structure 2, 5 and 6 with each other it appeared that $\Delta Tr_{30\%} \& \Delta Tr_{50\%} > \Delta Tr_{95\%}$. This suggests the slope steepness had less impact on the highest 5% of the peak velocities as well. Because only one wave condition is tested, no firm conclusion can be made.



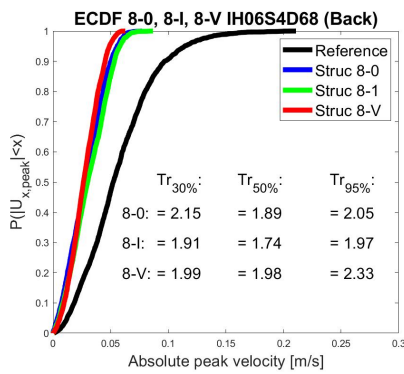
(A) Structure 2, 5, 6 and 7, wc 35

FIGURE 7.4: Comparison between the eCDF of the horizontal peak velocities for different front slope during the same test condition. The structure number, wave condition and location of the EVM can be found in the title and the tranquility index is plotted in the graph.

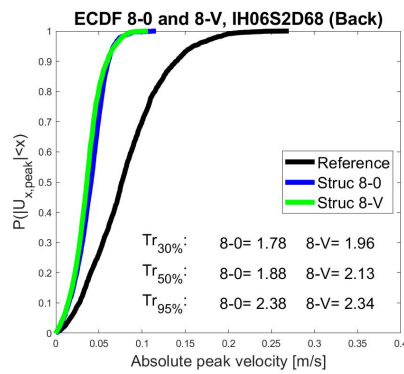
7.1.5 Channel length

The results of the tranquility at the back of the structure for different channel lengths are analyzed here. In Figures 7.5a and 7.5b, the cumulative distribution functions of $|U_{x,peak}|$ at the back of structures 8-0, 8-I and 8-V are shown³. In Figure 7.5c, the same is done for structure 12-I and 12-III.

From the results it can be observed that there is no consistent trend between an increase in channel length and the change in the tranquility indexes. The maximum measured difference $\Delta Tr_{x,max}$ for the same wave condition and a different L_{ch} is 0.36, the minimum observed difference $\Delta Tr_{x,min}$ is 0.04. Furthermore, also no consistency is observed in which index ($Tr_{30\%}$, $Tr_{50\%}$ or $Tr_{95\%}$) is mostly affected from a change in channel length.

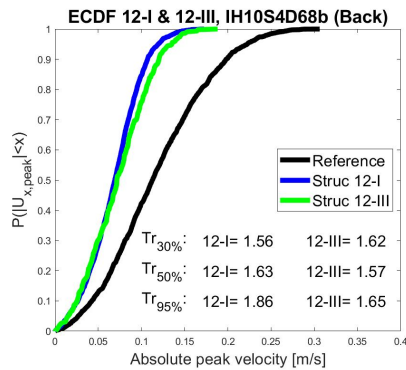


(A) Structure 8-0, 8-I and 8-V, wc 20



(B) Structure 8-0 and 8-V, wc 16

³ The 0 refers to no channel, I refers to one meter channel and V to a five meter channel on a 1:1 scale.



(c) Structure 12-I and 12-III, wc 18

FIGURE 7.5: Comparison between the eCDF of the horizontal peak velocities for different channel lengths during the same test conditions. The structure number, wave condition and location of the EVM can be found in the title of each figure and the tranquility index is plotted in the graph.

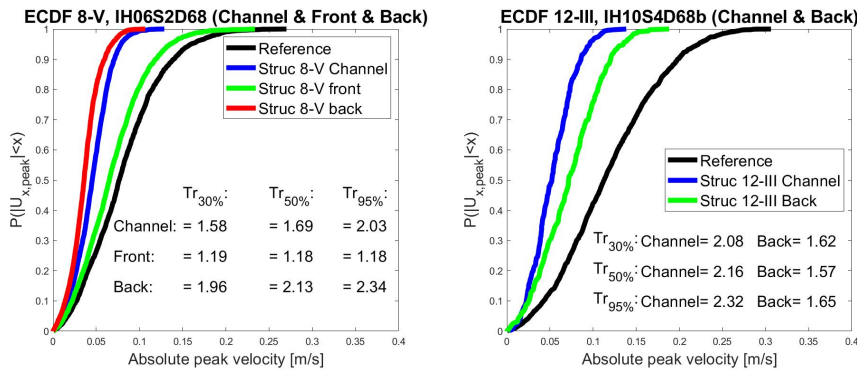
Additional note: It can be seen that the eCDF of wc 18 is less smooth. This is due to the fact that the EVM changed location during the test and therefore time record shortened. See appendix C.2.

7.1.6 Channel vs. back

In this section, the tranquility index is compared in the back and in the channel of the same structure and the same wave condition. In Figure 7.6a, structure 8-V is analyzed. In Figure 7.6b, structure 12-III.

From the results, no consistency is observed between location of the EVM and the tranquility indexes $Tr_{x\%}$. Namely, the $Tr_{x\%}$ is higher at the back than in the channel for structure 8-V, whereas the opposite holds for structure 12-III. From a change in channel length the maximum and minimum impact on the indexes are found to be $\Delta Tr_{x,max} = 0.67$ and $\Delta Tr_{x,min} = 0.31$. Furthermore, also no consistency is observed in which index ($Tr_{30\%}$, $Tr_{50\%}$ or $Tr_{95\%}$) shows the biggest difference between the two locations.

All in all, it can be concluded there exist no general rule of thumb about the change in $Tr_{x\%}$ between the two locations. Since the wave conditions, the tested structures and the tested channel lengths are different between both test, no speculations can be done about the cause of the outcome.



(A) Structure 8-V, wc 16

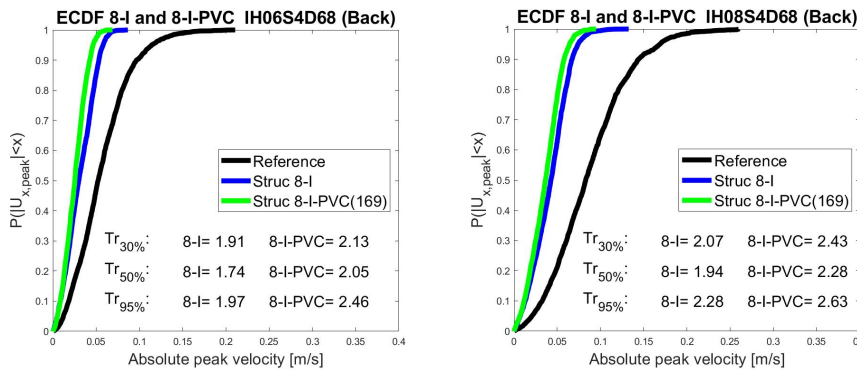
(B) Structure 12-III, wc 18

FIGURE 7.6: Comparison between the eCDF of the horizontal peak velocities at different locations during the same test conditions. The structure number and wave condition can be found in the title of each graph and the tranquility index is plotted in the graph.

7.1.7 Outer surface roughness

In this section, the results on T_r are discussed for structure 8-I, in a scenario with- and without increased roughness. The roughness is increased with 4cm tall PVC pipes that come out of each hole on top of the structure (169 in total), see Figure A.3c. The results of $Tr_{x\%}$ and the cumulative distribution functions of $|u_{x, peak}|$ are shown in Figures 7.7a and 7.7b.

For both test it is observed that an increase in surface roughness results an increase of $Tr_{x\%}$. This can be explained because more energy is dissipated from the interaction with the outer surface. The change in $Tr_{x\%}$ between structure 8-I and 8-I-PVC varies between $\Delta Tr_{x,max} = 0.49$ and $\Delta Tr_{x,min} = 0.22$. Nevertheless, no consistency is observed in the different magnitudes from $\Delta Tr_{30\%}$, $\Delta Tr_{50\%}$ and $\Delta Tr_{95\%}$.



(A) Structure 8-I and 8-I-PVC, wc 20

(B) Structure 8-I and 8-I-PVC, wc 19

FIGURE 7.7: Comparison between the eCDF of the horizontal peak velocities for different crest surface roughness during the same test condition. The structure number, wave condition and location of the EVM can be found in the title and the tranquility index is plotted in the graph.

Conclusions tranquility index results

First of all, for the *channel length* and the *wake location*, the results are different per test and no clear trend is observed on the relationship with $Tr_{x\%}$. For the channel length a maximum difference in the tranquility index ($\Delta Tr_{x,max}$) measured at the back of 0.36 has been observed. Therefore, the channel length is of minor importance for the $Tr_{x\%}$ at the back compared to the other tested variables. On the other hand, for the location (back versus channel) a $\Delta Tr_{x,max} = 0.67$ has been observed. Therefore, the tranquility differs more for different locations and additional experiments or 3D modelling could give valuable information about this.

For the variables of the *block porosity* and *slope steepness*, only one wave condition was available. Therefore, it is not possible to draw a conclusion, nevertheless the results are shortly described. The results of the block porosity suggest that the $Tr_{x\%}$ increased if the holes are blocked (block porosity decreased). The result of the slope steepness suggest that $Tr_{x\%}$ increases if the front front slope steepness decreases (and back slope increases). Above that, the results suggest that a zigzag orientation decreased the tranquility compared to a straight orientation. Furthermore, the results of the slope steepness and orientation suggest that the impact of a change in slope is more felt for $Tr_{50\%}$ and $Tr_{30\%}$ than for $Tr_{95\%}$.

For the other variables, more tests are available and the observed relationship with $Tr_{x\%}$ was consistent. Namely, the $Tr_{30\%}$, $Tr_{50\%}$ and $Tr_{95\%}$ increase if the *structure height*, *crest width* or *outer surface roughness* increases. The ranking of the design variable with the highest observed $\Delta Tr_{x,max}$ to the lowest observed $\Delta Tr_{x,max}$ can be found in Table 7.1. From this table it can be seen that the highest $\Delta Tr_{x,max}$ are found for a change in the structure height, crest width and slope steepness. This indicates these variables can have a big impact on the tranquility in the wake. However, for the structure height and crest width the $\Delta Tr_{x,min}$ is much smaller than $\Delta Tr_{x,max}$. From the results of the crest width it is suggested that ΔTr increases a lot if the porosity of the structure decreases (from a 3D to a 2D structure). From the results of the structure height it is suggested that ΔTr increases a lot if one of the structures is emerged. Nevertheless, more data is needed to verify if these suggestions are indeed the cause of the large range of ΔTr .

All in all, the attentive reader might have noticed that the trends between the design variables and $Tr_{x\%}$ are related to the relationship between those variables and $K_t(s)$. Such that in general, Tr increases for an increase in the design variables that were inversely proportional related to K_t . This can be explained, because if more (kinetic) energy is transmitted, the peak velocities increase. The plots of $Tr_{30\%}$, $Tr_{50\%}$ and $Tr_{95\%}$ over $K_t(s)$ can be found in Figure 7.8. From comparing the coefficient of correlation which is shown behind $R =$ in each plot, it can be concluded that the correlation is strongest between $K_t(s)$ and $Tr_{95\%}$.

Lastly, no general rule is found on whether the lower or higher peak velocities are more reduced in a wake region. It appears that this varies per test condition.

TABLE 7.1: Variables ranked from highest to lowest $\Delta Tr_{x,max}$. The impact of each design variable on $Tr_{x\%}$ is explained as the maximum - and minimum observed difference in $Tr_{x\%}$ for the same wave conditions

Variable	# of tests	$\Delta_{max} (Tr_{x\%})$	$\Delta_{min} (Tr_{x\%})$
Crest width	3	0.98	0.01
Structure height	3	0.85	0.25
Slope steepness	1	0.74	0.56
Channel vs. Back	2	0.67	0.31
Surface roughness	2	0.49	0.22
Channel length	3	0.36	0.04
Blocked holes	1	0.12	0.01

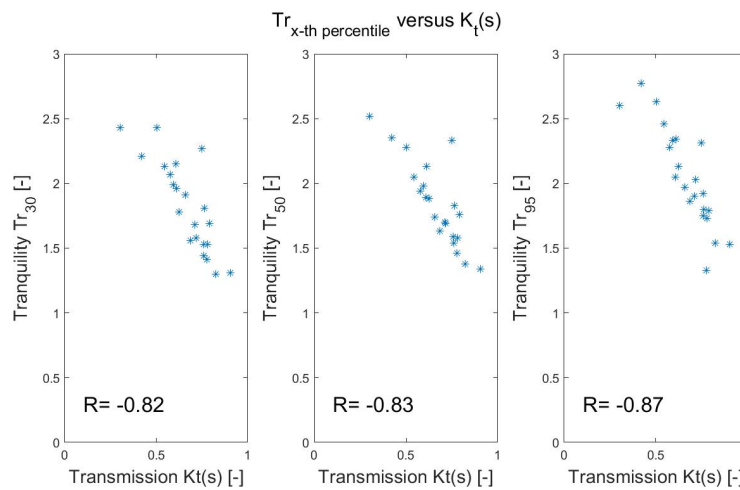


FIGURE 7.8: Graphs from the tranquility indexes $Tr_{x\%}$ versus the transmission coefficient $K_t(s)$. From left to right the graphs correspond to the following index: $Tr_{30\%}$, $Tr_{50\%}$ and $Tr_{75\%}$. The tests in which $Tr_{x\%}$ is measured in the back- as well as in the channel are included.

7.2 SAFETY SCORE

The method applied in this section gives an example of how to interpret the empirical cumulative distribution graphs from $|U_{x,peak}|$ that are provided in the section above 7.1⁴ and link this to the velocity limits an organism can withstand. The same procedure can be applied for the limiting velocities from other reef inhabitants, as are summarized in Figure 2.4 from Chapter 2.

7.2.1 Branching corals

This section shows an example of how to predict the safety against breaking for a branching coral type, named the *Acropora intermedia*. An introduction to this coral type is given in Chapter 2.2. In Figure 7.10, the outcomes of the safety scores are shown per test condition. The

⁴ The 95-th percentile value of $|U_{x,peak}|$ which is used to calculate the safety score can be found in the eCDF graphs.

formula from how the safety score is calculated can be found in equation 6.4 from Chapter 6. For a score above 1, the breaking limit velocity of the coral is not exceeded by the highest 5% of the peak velocities and vice versa for a score below one. The target input variables of the corresponding wave conditions are given for a 1:1 scale.

As can be seen from the results, the safety score increases in the wake of a structure compared to the situation without a structure for all wave conditions. Furthermore, it can be observed that for some wave conditions, the safety score is already above 1 in the situation without a structure.

7.3 INK INJECTION

Ink injections are used as a passive scalar source during some irregular wave conditions. The observations can be used to investigate for example how the nutrients are transported and mixed around- and within the structure.

Figures 7.9a and 7.9b show the results of two different ink injections conducted during the same irregular wave test. The tests are done in wc 35 and in front of structure 8-I-PVC(69). This wave condition resembles a quite stormy wave environment. The pictures show that the dilution time (time until the water has no blue color anymore) varies per time interval for the same location and test. Furthermore, the dilution time differs per location in the water column. Lastly, the direction of the mean flow differs if different for both time intervals as well.

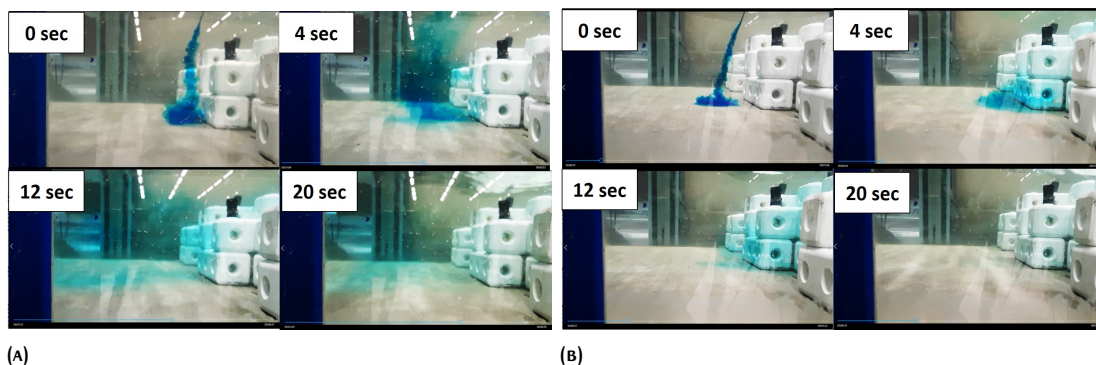


FIGURE 7.9: Pictures from two different ink injections in the same test and location: front of structure 8-I-PVC(69) in wave condition 35.

Assessment of expected breakage for a coral named <i>Acropora intermedia</i>																
Wave condition [1:1] Target values	Structure number															
	(REF)	2	2-BH	5	6	7	8-0	8-I	8-I-PVC (169)	8-V	11-I	11-III	12-I	12-III	14	15
#: 5 $H_{i,mo} = 0.6\text{ m}$ $s = 0.02$ $T_p = 4.5\text{ sec}$ $d_f = 2.55\text{ m}$	1.08	N.T.	N.T.	2.08 Back	N.T.	3.00 Back	N.T.	N.T.	N.T.							
											N.T.	2.08 channel	N.T.	1.84 Back		
#: 16 $H_{i,mo} = 0.9\text{ m}$ $s = 0.02$ $T_p = 5.7\text{ sec}$ $d_f = 3.6\text{ m}$	0.81	N.T.	N.T.	N.T.	N.T.	N.T.	1.92 back	N.T.	N.T.	1.89 back	N.T.	N.T.	N.T.	N.T.	N.T.	1.64 back
										1.64 channel						
#: 18 $H_{i,mo} = 1.5\text{ m}$ $s = 0.04$ $T_p = 5.1\text{ sec}$ $d_f = 3.6\text{ m}$	0.58	N.T.	N.T.	0.89 back	N.T.	1.08 back	0.96 back	0.89 back	N.T.							
												1.04 channel	1.35 channel			
#: 19 $H_{i,mo} = 1.2\text{ m}$ $s = 0.04$ $T_p = 4.5\text{ sec}$ $d_f = 3.6\text{ m}$	0.77	N.T.	N.T.	N.T.	N.T.	N.T.	N.T.	1.74 back	2.01 back	N.T.	N.T.	N.T.	N.T.	N.T.	N.T.	N.T.
#: 20 $H_{i,mo} = 0.9\text{ m}$ $s = 0.04$ $T_p = 3.8\text{ sec}$ $d_f = 3.6\text{ m}$	1.13	N.T.	N.T.	N.T.	N.T.	N.T.	2.32 back	2.22 back	2.78 back	2.63 back	N.T.	N.T.	N.T.	N.T.	N.T.	N.T.
#: 35 $H_{i,mo} = 2.1\text{ m}$ $s = 0.04$ $T_p = 6.2\text{ sec}$ $d_f = 4.65\text{ m}$	0.47	0.84 back	0.85 back	1.09 back	0.83 back	0.72 back	N.T.	N.T.	N.T.	N.T.	N.T.	N.T.	N.T.	N.T.	N.T.	N.T.

Score = $\frac{U_{x,limit\ of\ coral: 0.5m/s}}{95^{th}\text{-percentile value of } |U_{peak,x}|}$, if < 1 : breaking limit exceeded, if > 1 : within breaking limit
 N.T. means Not Tested Back/Channel = location EVM

FIGURE 7.10: Safety score for different test conditions. The score is calculated from equation 6.4. If the breaking velocity is exceeded, the score is below 1 and a red color is given. If the breaking velocity is not exceeded to 95 per cent of the horizontal peak velocities, the score is above 1 and the block is given a green color. The location of the EVM is 0.75 meter above the bottom (1:1 scale) for all tests. In Figure 3.2, a sketch of the EVM locations with respect to the structure can be found.

8

DISCUSSION, CONCLUSION AND RECOMMENDATIONS

This section contains a discussion on the methods and results of the research and the associated implications for the main conclusions.

The experiments and literature search described in this thesis provide insight and are helpful to develop design guidelines for hydrodynamic and ecological functionalities of Reefy design configurations under wave loading. The impact of different design variables on the hydrodynamic performance has been investigated, based on the transmission- and reflection coefficients. The literature study provides insight into the current state of knowledge on hydrodynamic- and ecological performance considerations for living breakwaters. Compared to other empirical equations for K_t and K_r in literature, the formulae of [Van der Meer et al., 2005] showed the best agreement and in this thesis an optimized-version of this equation has been proposed for the Reefy structure. Furthermore, the maximum near-bottom stream-wise velocities are investigated in the wake of the structure to provide insight in the impact of different designs on the ecological performance. The latter was based on a performance index introduced by [Kim et al., 2016] called the tranquility index Tr , for which some adaptations were made to take the presence of waves into account.

8.1 DISCUSSION

In the next paragraphs, the findings as well as limitations and strengths of the experiments, processing methods and outcomes are discussed.

Location of the measurements

When looking at the outcomes of the transmission coefficient, one should keep in mind that this is a point-specific value, only valid close to the structure¹. However, for practical applications the information closer to the beach can be relevant as well. These outcomes can be different. Namely, in the zone between WG789 and the wave-damper, wave-height and period evolution occurs. An example can be seen in Figure 8.1, in which the effect of an increase of the crest-width on the transmitted waveheight is compared for the region close to the structure compared to close to the beach. As can be seen, the transmitted waveheight decreases with an increase in crest width close to the structure, whereas further away from the structure more fluctuations are observed. All in all, additional experiments with measurements closer to the beach or numerical models are recommended, to investigate the impact of each design variable on the wave-height evolution at different locations. This might also be important for the prediction of the sediment distribution after the placement of a Reefy structure.

¹ The front of the structure is kept at approximately $x = 25m$ in the wave-flume. Likewise, the distance from the back of a structure to WG 7 varied between 1 and 2 meters. And the distance between WG 9 and the wave damper is above 20 meters.

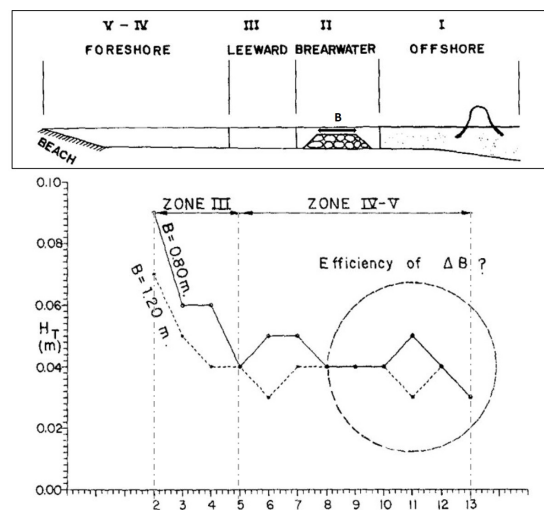


FIGURE 8.1: Example of transmitted wave height evolution [Pina and de Alarcón, 1991]

Angle of wave incidence

In the current research, the angle of the wave attack is perpendicular to the orientation of the structure. However, in real life, the dominant angle of wave attack does not have to be perpendicular and the dominant wave direction can also vary per storm or during the year. The study of [Seabrook and Hall, 1999] conducted experiments with an oblique wave attack of 30 degrees and concluded the transmission coefficient is not related to the incident wave angle. [Van der Meer et al., 2005] confirms that the angle of wave attack has minor influence on the transmission coefficient for rubble mound breakwaters, but adds the fact that this is not the case for impermeable breakwaters. For the latter, the transmission decreases with increasing incident wave angle. As the Reefy structure is a new category of breakwaters, it is recommended for further research to investigate the impact of oblique wave attack on the Reefy structure.

Multitude of design variables

In the current experiments, multiple variables are changed within each experiment. Namely, for each wave condition the height- and period changed. And also for the investigation of a design variable, often multiple variables were changed within the structures. For example, for the comparison of the front slope, structure 2, 5 and 6 are compared. Beside the different front slope, also the back slope of each structure is different. This complicated the investigation of the impact of each design variable on the performance, as the observed differences could be the consequence of multiple changing conditions. For future research on the impact of the design on the performance, it is recommended to change less variables in each experiment, but focus on one variable and test this in different wave conditions. However, the strength of this research approach is the fact that I was able to look at many design variables possibly influencing the hydrodynamic- and ecological performance.

On an additional note, the definition of each design variable is based on a subjective interpretation. For example, the front- slope of a structure is variable, as shown in Figure 8.2. But for

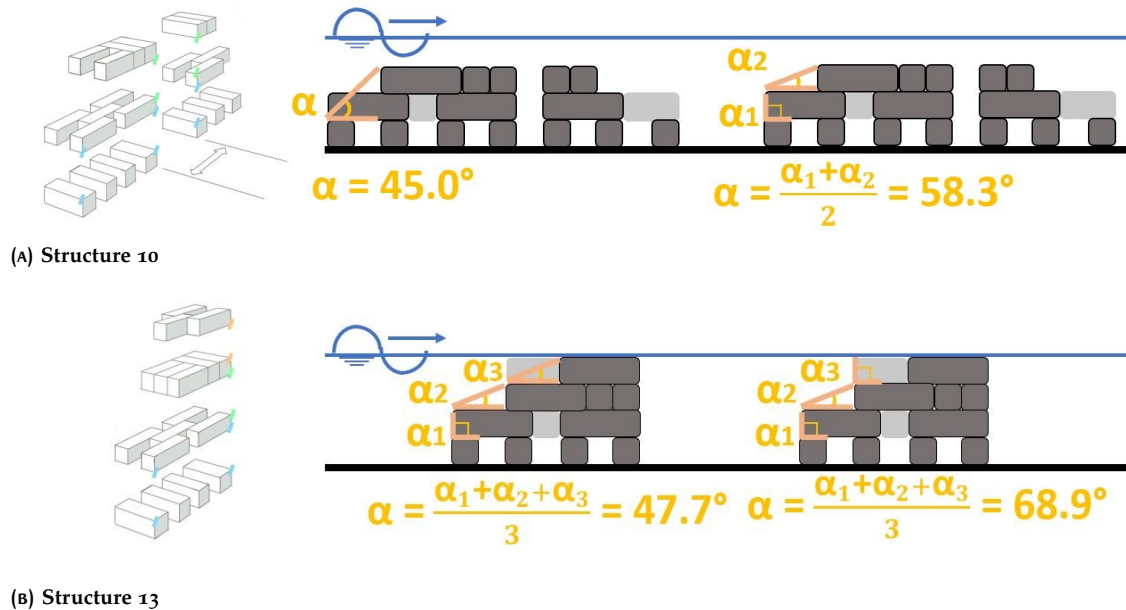


FIGURE 8.2: Example of different methods to calculate the front slope steepness. In Figure 8.2a, the first consideration is explained. The method on the right side, in which α is calculated as the mean of the stepped slopes, is used in this study. In Figure 8.2b, the second consideration is visualized. At some levels, the front of the block differs over the width of the structure. The method on the right side is used in this study, meaning the most forwardly projecting block is used to calculate the slope.

calculation purposes, one value needed to be assigned to each structure. The methodology of how this is calculated is explained in the caption of the figure. The final slope steepness value has an impact on the surf similarity parameter and therefore a different definition of the front slope would result in for example a different empirical equation.

In the next paragraphs, the limitations and strengths of the data processing methodology will be discussed.

Wave decomposition

The final method which is chosen for the decomposition of the wave gauge data into a reflected- and incoming wave field, is based on the total signal in combination with the reflected time signal of Z&S. A few assumptions are made in order for this method to be valid. First of all, it is assumed that the Z&S method is able to give a good estimate of the reflected wave-height and phase. This assumption is based on the fact that the reflected wave is small and therefore more or less linear. However, if the reflected wave was highly non-linear, the outcomes might be unreliable. This could be the case for extreme wave conditions. Therefore, a distinction has been made between the symbols for breaking-, cnoidal and stokes waves and only the last two are included in the optimization process of the empirical equations. Furthermore, if the Z&S method is not able to predict the phase of the reflected waves well, this can result in an under- or over prediction of the incoming waveheight in a partially standing wave pattern. Lastly, if

there is a bound-harmonic within the reflected wave, this is not detected by the Z&S method and could result in a slightly underestimated reflected wave-height and overestimated incoming wave height.

Transmission coefficient definition

The transmission coefficient in this study is calculated from the transmitted waveheight with- and without a structure, whereas most studies calculate it from the incoming- and transmitted waveheight. These methods can give different outcomes, if the "transmitted" wave-height without a structure differs from the incoming waveheight with a structure. This is the case if for example the waveheight in front of the structure is higher due to interference between the reflected- and incoming waves, or due to energy dissipation from friction with the foreshore between WG456 and WG789 [Pina and de Alarcón, 1991]. Both phenomena result in a higher transmission coefficient based on the current definition, compared to the *main-stream* method. The incoming waveheight in front of the structure is used in the optimized prediction equations of the transmission coefficient ². Therefore, the outcomes of the current research results can be viewed as a conservative estimation of the transmission coefficient.

Furthermore, it must be mentioned that a consequence of this method the dissipation coefficient of a structure can not be derived from the energy balance with K_t and K_r anymore, as K_t is not based on the incoming waveheight at WG456, whereas K_r is.

Reflection coefficient definition

The reflection coefficient is calculated as the reflected-waveheight divided by the incoming-waveheight in front of the structure. Depending on the local situation and permeability of the structure, in real life this might be a realistic observation of the reflection. However, no adjustment is made for the possibility of a reflected wave from the foreshore and/or wave damper, which travels through the structure(s) and adds up the reflection measured in front. This assumption is made as the reflection from the wave damper is expected and observed to be very low. Furthermore, for the regular wave tests, which have a duration of approximately one minute, a high chance exists that the reflected wave from the beach has not yet reached WG 456. However, for the irregular tests with a very permeable structure, the reflection coefficient might be over-estimated as a part could be originated from the beach. This should be kept in mind when interpreting these results. However, it could also be argued that the reflection from the beach is also present in real life conditions.

Lower frequencies observed in horizontal velocity signal

For the velocity measurements near the bottom surface in the wake as well as without a structure, there is energy present at lower frequencies. After applying a low-band pass filter it is observed that the lower frequencies wave signal have a cyclic pattern. For the experiments without a structure, a clear pattern can be observed in which the trough of the lower peak

² Namely, in these equations, the relative freeboard, relative structure height and relative crest width are based on the $H_{m0,i,WG456}$

signal coincides with the biggest waves in the short wave group. This behaviour is most likely coming from bound infra-gravity waves. The cyclic pattern is less obvious in the wake regions, where the signals from the wave group and from the lower frequencies are more fluctuating. This can be explained because the conditions in the wake are more turbulent compared to the situation without a structure. However, a cyclic pattern can sometimes still be observed in the wake region. In this situation, also a return flow from the mass transport over a structure is known to cause these cyclic patterns with the wave groups. As all these phenomena are expected to be present in real life as well, it is decided to include the lower frequencies. For the observed mean flow in seaward direction, it could also be argued that in real life, a larger part of this return flow will follow the path of the least resistance and therefore return back by the sides of the breakwater [Losada et al., 2003].

From the fact that the lower frequencies are often also observed in the channel- and in front of the structure, it is suggested that a return flow is able to flow through the structure. On a positive note, this indicates the permeability of the structure is high enough to allow for water circulation and thereby maintain a high water quality in the lee-side of the structure.

Additionally, there is a physical explanation for the fact that in the spectrum of the bottom velocity the peak frequency is shifted towards a lower frequencies than in the spectrum of the surface elevation. Namely, for longer waves (smaller frequencies) the orbital velocities near the bed are bigger than for shorter waves (higher frequencies) [Soulsby, 1987].

Tranquility index definition

The tranquility index of a wake region increases if the flow is more tranquil and is related to the stream-wise peak-velocities $|u_{x,peak}|$ with- and without a structure. The investigation for the tranquility index provided insight in the qualitative relationship between some design variables and the reduction of the maximum velocities near the bottom of the wave flume. The approach of this study - focusing on the maximum velocities - is rather new and therefore relevant addition to the existing literature, which focuses on the mean velocities. Namely, most marine species are sensitive to deviations from the mean velocities as for example the maximum velocities can dislodge epibiota Kontaxi and Memos [Diplarakos, 2017].

However, it must be emphasized that an optimal Tr value does not exist, and that a higher Tr should not be associated with a better ecological performance by definition. This is because there are both pros and cons of a tranquil flow zone, and the preference of flow velocities differs per species. Therefore, as a first step the absolute values of $u_{x,peak}$ need to be compared to the optimal living conditions of the existing/wanted marine life. Then, as a second step the knowledge of how to influence the Tr can be applied to modify the velocities and optimize the design.

Furthermore, according to [Kim et al., 2016], the tranquility and absolute velocities are not related to the actual volume of the wake. Therefore, if the aim is to increase the area of recirculating flow or if knowledge is wanted about the distance needed between multiple breakwaters, additional studies should be conducted about the volume of the wake.

Safety score definition

In this study, the safety score compares the limit velocity for which breaking of a branching coral is expected, to the 95-th percentile value of the peak velocities. This procedure from how the safety score is calculated can also be applied for the limiting velocities of other reef inhabitants, as are summarized in Figure 2.4 from Chapter 2. For this, a distinction should be made between the type of consequence which is associated with the limiting velocity. For example, in the safety factor for the breakage of branching corals, the 95-th percentile of $|u_{x,peak}|$ is used. Namely, breaking is associated with an irreversible failure mechanism and this high percentile will result in a conservative estimate. On the other hand, if the velocity limit is related to the feeding behaviour of a species, the 30 - th percentile can be used as the associated consequence is less severe.

Secondly, it is important to mention that the velocities are measured 75 cm above the bottom of the foreshore. Thus, for deep- to intermediate water depths, the velocities are expected to be higher near the crest of the structure. For future research, it could be useful to calculate the safety factor for different locations within the water column. As a first step, an indication of the expected 95-th percentile value from $|U_{x,peak}|$ at the crest of the structure can be calculated using the orbital velocity formula from linear wave theory (see equation B.4) [Holthuijsen, 2010].

In the next paragraphs, the limitations and strengths of the results will be discussed.

Optimized equations of K_t

From the optimization process of the equations from [Van der Meer et al., 2005] for the transmission coefficient K_t , two new formulae are derived. These results show that if the surf similarity parameter $\zeta_{0,m-1,0} \geq 3$, the K_t can be predicted from the relative freeboard and crest width, whereas the exact value of $\zeta_{0,m-1,0}$ has no influence on the outcome of K_t . On the other hand, for conditions in which $\zeta_{0,m-1,0} < 3$, the K_t can be predicted from the relative freeboard, - structure height and $\zeta_{0,m-1,0}$, whereas the energy dissipation occurring over the width of the crest is less significant here.

When interpreting these formulae, there is an important bias in the distribution of structures included per formula. A table with an overview on which structures each formula is based can be seen in Table 8.1. This table is discussed below. Figure 3.7, with sketches of the cross-section of every structure and Table 3.5, with the dimensions and details of every structure, are useful when reading the discussion.

Firstly, it can be seen 87% of the structures on which the formula for $\zeta_{0,m-1,0} \geq 3$ is based have the same front slope of $\alpha_{front} = 58.3^\circ$ ³. Thus, the fact that the front slope steepness has no influence on the outcomes of K_t if $\zeta_{0,m-1,0} \geq 3$ is probably due to the fact that the majority of the tests included have the same (steep) front slope. However, the fact that $\zeta_{0,m-1,0}$ has no impact on K_t does show that the fictitious wave steepness had no impact on the transmission for these structures.

³ Structure 8, 9, 10, 15. For these structures, the surf similarity parameter $\zeta_{0,m-1,0}$ will constantly be ≥ 3 . Namely, the opposite can only be obtained if $s_{0,m-1,0} > 0.28$ and this is outside the range of the experiment as can be seen in Table 2.2.

TABLE 8.1: Percentages of number of tests per structure which are included in the optimization process of the two equations for $K_t(s)$. The total number of tests included is 64 for the equation of $\zeta_{0,m-1,0} \geq 3$ and 45 for the equation of $\zeta_{0,m-1,0} < 3$. The optimization process is based on regular wave tests (not all structures are tested in regular waves).

	Equation for $\zeta_{0,m-1,0} < 3$	Equation for $\zeta_{0,m-1,0} \geq 3$
2DV:		
Structure 1	20%	2%
Structure 2	38%	3%
Structure 3	19%	3%
Structure 4	4%	0%
Structure 5	4%	0%
3D:		
Structure 8	0%	45%
Structure 9	0%	14%
Structure 10	0%	14%
Structure 11	13%	5%
Structure 12	2%	0%
Structure 15	0%	14%
Total %	100%	100%

Secondly, in Table 8.1 it can be seen that 67% of the structures on which the formula for $\zeta_{0,m-1,0} < 3$ is based have a crest width smaller than 4 meters (1:1 scale)⁴. Whereas 80% of the structures on which the formula for $\zeta_{0,m-1,0} \geq 3$ is based have a crest width bigger than 7 meters. Thus, the fact that the width does not need to be included in the equation for $\zeta_{0,m-1,0} < 3$ can not only be explained by the fact that the width becomes more important for steeper waves. Namely, also the fact that the structures which are included in this group have a relatively small crest width plays a role.

In a practical sense this has a consequence when the transmission of new Reefy configurations is predicted from these formulae. For example, if the design of a complex structure changes such that the front slope is decreased to for example 1 : 3, while the crest width > 7 meters (1:1), the equation for $\zeta_{0,m-1,0} < 3$ will probably overestimate K_t as the impact of the crest width is not included. Furthermore, the equation for $\zeta_{0,m-1,0} \geq 3$ probably also overestimates K_t in this scenario, because this formula does not change for a shallower slope steepness.

Predicted hydrodynamic performance shallow, complex structure

From the investigation of the hydrodynamic performance it has been concluded that the transmission coefficient is strongly related to the relative freeboard $R_c/H_{m0,i}$. Thus, a structure probably with its crest near the water surface is protects the coast best against high wave forces. Above that, it has been concluded that for ecological considerations a complex (3D) structure is preferred. In this discussion part, the performance of a complex, shallow Reefy structure with a relative freeboard between $0.2 < R_c/H_{m0,i,WG456}(s, f) < 0.5$ is investigated and elaborated.

⁴ Structure 2, 3, 4, 5 and 12. The only structures on which the equation for $\zeta_{0,m-1,0} < 3$ is based with a crest width > 4 , are structure 11 and 2. However, these have a 1 meter lower structure height than the other structures considered.

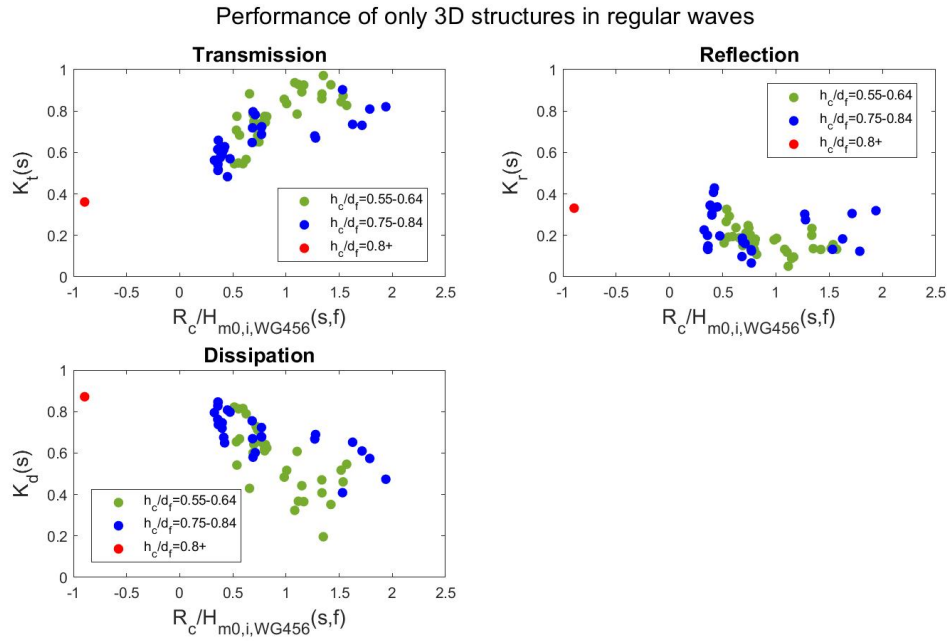


FIGURE 8.3: Graph of transmission, reflection and dissipation coefficients from 3D structures in regular waves. On the x-axis the relative freeboard can be found and the relative structure height is given as an extra parameter. The tests in which wave breaking occurred in front of the structure are excluded.

In Figure 8.3, the hydrodynamic performance parameters are plotted over the relative freeboard $R_c/H_{m0,i,WG456}(s,f)$ for all regular tests with complex 3D structures. The tests in which wave breaking occurred in front of the structure are excluded and the relative structure height is given as an extra variable. $K_d(s)$ is calculated from equation C.5 based on the energy conservation law.

The following 95% confidence intervals have been found for the hydrodynamic performance parameters within $0.2 < R_c/H_{m0,i,WG456}(s,f) < 0.5$:

1. [0.560.61] for $K_t(s)$. Thus, the predicted decrease of the transmitted waveheight by a shallow, complex Reefy structure lies around 40%. The transmission results are more widespread outside this range or relative freeboard. Thus, the optimized formulae, including the impact of the other design variables, need to be used to predict the transmission then.
2. [0.220.31] for $K_r(s)$. Thus, the predicted percentage of the incoming wave that is reflected seaward by a shallow, complex Reefy structure lies around 27%. Nevertheless, still a lot of variation in $K_r(s)$ is observed within the considered area. The outcomes of the reflection analysis showed that the reflection for small relative submergences depends on the fictitious wave steepness a lot, and it increased for smaller fictitious wave steepness.
3. [0.730.78] for $K_d(s)$. Thus, the predicted percentage of energy dissipation from the a shallow, complex Reefy structure lies around 75%.

Furthermore, these results suggests that in all tested conditions a minimum of 40% of the incoming wave energy is dissipated if the relative crest height of a complex structure is higher than $h_c/d_f = 0.75$

8.2 CONCLUSIONS

8.2.1 Hydrodynamic performance

The placement of a Reefy structure induces four main 2D local physical processes related to the hydrodynamic performance in shallow water conditions. These processes are the **dissipation** - and the **reflection** of a part of the incoming wave energy, the occurrence of **non linear wave phenomena** as waves travel over the structure and the **variation of the mean water level** at the lee-side of the structure.

In this study, the wave **transmission- and reflection coefficient** K_t and K_r are further evaluated to investigate the hydrodynamic performance of a Reefy breakwater. These parameters are related to the dissipative capabilities of a structure through the energy conservation law. Both regular- and irregular wave tests are considered and for the irregular waves, the development of the reflected- and transmitted wave spectra are investigated as well.

The transmission coefficient is calculated from the transmitted waveheight behind the structure divided by the transmitted waveheight without a structure, at the same location. This definition excludes all possible effects of the foreshore on the transmission. The reflection coefficient is calculated from the ratio between the reflected- and incoming waveheight in front of the structure.

For these coefficients, the incoming- and reflected wave fields measured at the wave gauges need to be separated. The tested shallow water conditions resulted in highly non-linear waves. As a result, the usual decomposition method of Zelt & Skjelbreia (Z&S) based on the linear wave theory wrongly predicted the shape of the incoming wave field. The Ursell-number appeared to be a good indication of the shape resemblance between the total signal and the sum of the incoming- and reflected waves based on Z&S. Better than the Relative Mean Squared Error. If the Ursell number exceeded 26, the method of Z&S was not able to produce reliable results of the incoming wave field. For approximately half of the tests, the Ursell number was higher than 26.

As a consequence, a new method to decompose the wave field for shallow water conditions has been defined in this study. The incoming wave at a set of 3 wave gauges is obtained from subtracting the reflected wave signal based on Z&S from the total signal at each wave gauge. The mean of the variances from the newly composed signals is used to obtain the incoming significant waveheight $H_{m0,i}$. This procedure assumes that Z&S is able to predict (the phase of) the reflected signal correctly, as this signal is smaller and much more linear.

This study investigated the impact of several design variables on K_t and K_r . The design variables which are analyzed for the hydrodynamic performance are: the relative structure height (h_c/d_f),

relative freeboard ($R_c/H_{m0,i}$), relative crest width (B/L_0), porosity of the block and - structure (ϕ), the surf similarity parameter ($\frac{\tan(\alpha_{front})}{\sqrt{s_{0,m-1,0}}}$), the relative channel spacing S_{ch}/L_0 and the surface roughness.

Furthermore, the existing formulae for the K_t and K_r are compared to results of the hydrodynamic performance. The one with the best resemblance is optimized using a non linear regression analysis. For both the transmission- and reflection the equations proposed by [Van der Meer et al., 2005] resulted in the best fit.

For the transmission coefficient K_t two optimized empirical equations are defined, each applicable to another range of the surf similarity parameter⁵:

$$\text{If } \zeta \geq 3 \quad K_t = 0.325 \frac{R_c}{H_{s,i}} + 0.679 \left(\frac{B}{H_{s,i}} \right)^{-0.24} (1 - e^{(-10.511)\zeta}) \quad (8.1)$$

$$\text{If } \zeta < 3 \quad K_t = 0.189 \frac{R_c}{H_{s,i}} + 0.498 \left(\frac{h_c}{d_f} \right)^{-0.358} (1 - e^{(-1.919)\zeta}) \quad (8.2)$$

The optimized equations have a Mean Average Error of 0.05&0.07, a Root Mean Squared Error of 0.06&0.09 and a coefficient of determination of 0.78&0.68 with the regular wave tests. The first number is related to $\zeta \geq 3$ and vice versa. Thus, the performance of these equations is reasonable.

Structural design variables included in these equations are the height of the structure, crest width and front slope. Although to a lesser extent, the increase of roughness of the outer surface and the increase of porosity of the structure are identified to affect K_t as well. First of all, if the roughness increases, the transmission decreases. This impact has been observed to be higher for steeper waves. Secondly, an increase in porosity of the structure increases K_t , especially for longer waves in shallower water. However, if the relative water depth increases, a wider crest instead of a decreased porosity gave smaller K_t results, for a structure with the same amount of blocks. Furthermore, decreasing the block porosity by adding PVC pipes in the vertical holes slightly reduces the K_t as well.

On the contrary, neither an optimum, nor a trend has been found between the transmission and the relative channel spacing. However, the impact on K_t due to a different channel length is small (maximum 0.1).

The trends observed from the regular wave tests are confirmed with the transmitted spectra. Furthermore, some interesting phenomena are observed based on the spectra. Firstly, for (partly) emerged structures, if the structure height exceeds the water level, there is no energy transfer anymore towards the second harmonic or higher. Secondly, an increasing crest width transfers more energy towards the higher harmonics, given the transmission coefficient is below 0.8. The same phenomena is observed for a decrease in slope steepness. Thirdly, an increase in channel length either decreases the energy present at the second harmonic, or has no impact on the energy there. Fourthly, the increased surface roughness reduces the energy in both the

⁵ Note that the freeboard is assumed to be negative for submerged structures in this study. This is in contrast to the definition of the freeboard which is most often used in other studies.

first- and second harmonic. Lastly, the zigzag orientation (structure 7) had no impact on the transmitted spectrum.

For the reflection coefficient K_r the final optimized formulae is defined as follows⁶:

$$K_r = \left(-0.234 \frac{R_c}{H_{s,i}} + 0.837\right) * 0.055 P^{-0.173} \cot(\alpha_{front})^{-0.007} S_{0,m-1,0}^{-0.487} \quad (8.3)$$

The equation has a Mean Average Error of 0.05, a Root Mean Squared Error of 0.06 and a coefficient of determination of 0.5. Thus, the performance of this equation is less compared to the equations for the transmission coefficient.

Additionally, it has been concluded that the reflection increased for an increase in relative channel length. Also a decreased block porosity resulted in slightly more reflection, however the impact is negligible compared to the other variables. Lastly, it has been observed that cnoidal an breaking waves give more reflection around the same submergence.

On the other hand, between the relative crest width and the reflection, no consistent relationship has been observed. However, the maximum observed difference in K_r was 0.02. Similarly, from the increased surface roughness no consistent impact on K_r has been identified and a the maximum observed difference was 0.03. Therefore these design considerations are considered to have an insignificant impact on the reflection.

The trends observed from the regular wave tests are confirmed by the reflected spectra. Furthermore, some interesting observations are made. Firstly, a shark-tooth orientation gave less reflection than a straight orientation (structure 7 vs 2). Secondly, the channel length mostly affects the reflected spectra around f_p .

8.2.2 Ecological performance

For the ecological performance, the placement of a Reefy structure is associated with a number of phenomena which can enhance the existing ecosystem and increase the abundance and biodiversity of organisms in the structure. These phenomena are mostly related to the flow field in- and around the structure. In short, the **sheltered areas**, the **circulation of flow** in- and around the structure, the **low-flow zones** in the wakes of a structure and the **renewal of coastal water** through the structure are all phenomena which are associated with a positive ecological potential. Above that, the local maximum velocities to which an artificial reef is exposed is the most important factor determining the abundance of species.

As a first step, this study investigates the decrease of the stream-wise velocities behind a structure under wave loading. The velocity measurements are taken 75 cm above the bottom of the structure (1:1) scale and only irregular wave tests are considered. The tranquility index Tr is calculated from the ratio between the stream-wise peak velocities $|u_{x,peak}|$ without a structure and in the wake of a structure. The 30 – th-, 50 – th and 95 – th percentile values are used to calculate respectively $Tr_{30\%}$, $Tr_{50\%}$ and $Tr_{95\%}$.

⁶ Note that the freeboard is assumed to be negative for submerged structures in this study. This is in contrast to the definition of the freeboard which is most often used in other studies.

In general, Tr increased for an increase in the design variables that were inversely proportional related to K_t . The structural design variables with the biggest impact on Tr were: the structure height, crest width and slope steepness. The results show that in general, the Tr indexes increase for an increase in crest height and crest width, or a decrease in front slope (which is accompanied by an increase in back slope). However, the magnitude of the impact of each design variable varies a lot for different test conditions. The variation found in the impact of the width on Tr suggest that the porosity of a structure is very important for the tranquility. Such that a decreased porosity increases Tr . Furthermore, the results suggest that the zigzag orientation decreased the tranquility in the wake. However, due to the shortage in the amount of tests available for the analysis, no firm conclusions can be made.

As a second step, a so called safety score is given to the wake region of each test. This score compares the limiting velocity for which a branching coral is expected to break, to the measured 95 – th percentile value of $|u_{x,peak}|$. A score above 1 indicates no coral breakage is expected to occur and vice versa for a score below one. It can be seen that the safety score differs per wave condition and structure.

8.3 RECOMMENDATIONS

Based on the discussed limitations, strengths and the conclusions, recommendations for further research and for the design of the Reefy structure can be made. These recommendations are discussed in this section.

8.3.1 Future research

Stability

Firstly, a study on the stability of the structure is needed. Right now, the failure of many artificial reefs is due to instabilities during storms. The positive ecological impact of a Reefy structure is at risk if failure occurs and loose blocks demolish the bottom of the seafloor. During the experiments, no complete failure conditions have been tested. Nevertheless, some rocking of single blocks or from the whole structure is observed. Therefore, the stability analysis can already partly be done based on the performed experiments for this research. Furthermore, other failure mechanisms and mitigation measured need to be investigated as well. For example, a scour protection might be needed to prevent scouring of the structure from for example reflection or the return flow. Namely, maintenance as well as failures have an adverse effect on the ecology and are costly.

Shoreline response mode

The study from [Ranasinghe et al., 2006] concluded that 70 per cent of submerged structures constructed for beach protection have resulted in unexpected net erosion of the shoreline. Therefore, the shoreline response mode of the structure needs to be predicted in order to be sure that no erosive patterns are expected in the lee of a structure. This can be done either

with the empirical equations discussed in Appendix B.1.2 or with a 3D numerical model, implementing the hydrodynamic performance parameters obtained from the optimized Reefy formulae derived in this study. The main goal of this investigation should be to prevent erosion. Furthermore, it should be kept in mind that for an ecological point of view it is beneficial to build the structure further offshore, as this increases the biodiversity because more different flow conditions will exist around the structure. But of course, also navigation routes need to be kept in mind.

Slope orientation

The results of this research showed that a zigzag slope orientation reduced the reflection and the tranquility, without having an impact on the transmission. However, only one irregular wave test is performed with the zigzag slope, in a relatively large submergence $h_c/d_f = 0.65$. According to [Van der Meer et al., 2005], the influence of the slope steepness on the reflection decreases if the structure gets more submerged. This could mean that also the impact of the slope orientation increases for lower submergences. Furthermore, for the 3D structures no tests are performed on structures with a similar structure height and crest width, but with a different slope steepness α_{front} . Thus, more physical experiments on the impact of the slope orientation as well as on the slope steepness of complex structures are recommended to draw firm conclusions with regard to this. And to obtain a better performance of the prediction formulae.

Wave decomposition method

The limitations of the current wave decomposition method has been discussed in the discussion part of this chapter. For future research it would be interesting to process the wave gauge data with the wave separation method for non-linear regular waves from [Andersen et al., 2017]. Nevertheless this method is not suited for irregular waves and out of the scope of this research. Therefore, an investigation in wave decomposition methods for irregular non-linear waves is recommended for future research.

Complexity and porosity limit

From an ecological point of view, the complexity of a structure should be increased to enhance the ecological potential. This suggests a 3D structure is preferred over a 2DV -. Nevertheless, until now these two type of configurations are not directly compared. Namely, only structures that resembled each other in (most of) the design variables except for the variable which was investigated are compared ⁷. Because this prerequisite does not hold for any combination of 2DV- with 3D structures (see Table 3.5), no comparison has been made. Nevertheless, the impact of the porosity of a structure has been investigated, but this was based on 3D structures with a different porosity.

Here, structure 2 (2DV) and 8 (3D) are compared. There are some regular wave conditions available in which both structures have been tested. These conditions are summarized in Table

⁷ The second prerequisite was that both structures were tested for the same wave condition.

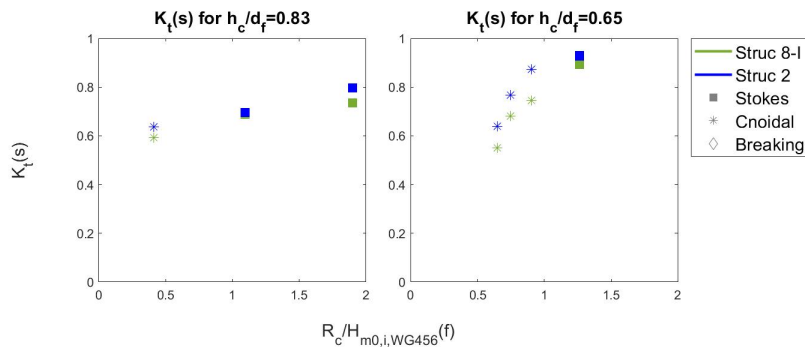
8.2. They both have the same number of blocks and structure height, but a different crest width, front slope steepness and porosity. Structure 2 has a porosity of 0.2 and structure 8-I has a porosity of 0.45⁸. In Figure 8.4a, the transmission results are compared between these structures. The same is done for the reflection results in Figure 8.4b. Each test with the same x - value corresponds to the same wave condition.

TABLE 8.2: Overview regular wave tests structure 8-I and 2 for design variable '2DV versus 3D'

Structure	d_0	Wave conditions
8-I & 2	0,68 m	8, 10, 11
8-I & 2	0,75 m	28, 29, 30, 31

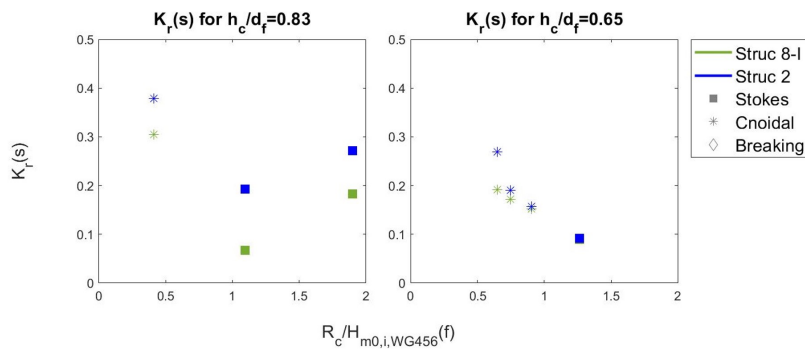
As can be seen from Figure 8.4a, for the same number of blocks and structure height, a 3D structure (structure 8-I) is able to obtain similar, and for some conditions even lower, transmission results as a 2DV structure (structure 2). Furthermore, from the results of Figure 8.4b it can be observed that most often the 3D structure gave less reflection.

These results shows that for the same number of blocks, a more complex structure can be built without making a compromise in the hydrodynamic performance, based on the reflection- and transmission coefficient. More physical experiments will be helpful to investigate if this conclusion holds, even when the porosity is increased further than 0.45. Namely, a structure becomes financially more interesting if the number of blocks per width are reduced, which can be obtained by increasing the porosity.



(A) $K_t(s)$ results

⁸ The detailed information of these structures can be found in Table 3.5.



(b) $K_r(s)$ results

FIGURE 8.4: Hydrodynamic performance results per relative freeboard from regular wave tests on structure 8-I and 2. Each result with the same x-value is related to the same wave conditions. The left graph shows the results from the tests in $d_f = 0.24m$ and the right graphs shows the results from the tests in $d_f = 0.31m$.

Channel length between a double structure

Implementing a distance/channel in between the structure is beneficial for marine life as it adds complexity to the structure and therefore increases the biodiversity of the inhabitants of the structure. In this study the impact of the added empty space (channel) is investigated. It is concluded that the reflection increases as the distance increases. On the other hand, no consistent relationship between the channel length and the transmission or tranquility is found. Based on these results, it is advised to minimize the channel length or not to include it at all.

However, only three variations of channel lengths are considered,⁹ and the outcomes could be different if the channel length is increased further. Namely, in the study of [Liang et al., 2015] the reflected wave from the second structure was already dissipated when travelling back from the second to the first structure. Furthermore, other studies mention an optimal spacing for hydrodynamic and ecological considerations [Liang et al., 2015] [Rambabu and Mani, 2005] [Jordan et al., 2005]. Therefore, it is recommended to further investigate the optimal spacing for the site-specific wave conditions by more thoroughly investigating the wake region in the channel- and at the back as well as the hydrodynamic processes. This can be done with a numerical model or with additional experiments using the Particle Image Velocimetry technique.

Implementation management

Last but not least, a study on the building- and implementation phase of the Reefy structure is needed. Building a Reefy structure block by block can be difficult and perhaps some parts of this process can be conducted on the land. Furthermore, as mentioned in the part on ecology, before building a structure, an investigation of the ecosystem needs to be done for the whole coast and a plan should be made on how to monitor the ecological performance of the structure.

⁹ The channel lengths which are investigated are 0, 1, 3 and 5 meters (1:1) scale.

8.3.2 Design of a Reefy structure

For the design of the submerged structure, an increase in structure height both reduces the transmission as well as it enhances ecology. The latter occurs due to the increase in surface area to which epibiota can attach, as well as by increasing the length of the low-flow zone at the lee of the structure [Takeuchi, 1991]. When designing a Reefy structure to protect the coast against severe wave attack, it is a safe choice to design the relative structure height (h_c/d_f) based on the water depth expected during high tide, plus an extra storm surge of for example a 1 : 10 years return period. With respect to this, it might be useful to include expected sea-level rise in the design water depth as well. A guideline from the transmission results of the present study would be to choose a minimum relative structure height around 0.75.

From another perspective, if the crest of the structure is close to the water surface during high tides, there is a change that the structure becomes visible during low tides, depending on tidal differences. In this scenario, attention should be paid to make sure that there is still enough water circulating to maintain a good water quality behind the structure. For example, circulation then needs to occur regularly during high tides, through/along the sides of the structure and/or over the parts of the crest, if the top layer includes empty spaces as well and the structure is "partially" submerged.

Furthermore, the structure height increases the reflection, which in its place decreases the dissipation capacity of the structure. Nevertheless, the amount of reflection still varies a lot if $h_c/d_f > 0.8$, depending on the fictitious wave steepness. Furthermore, in the next paragraphs other design possibilities are discussed which will reduce the reflection.

A shallow front slope of a structure is recommended as this decreases the transmission and reflection as well as it increases the tranquility index. The front slope of structure 5 ($\alpha = 1 : 3$) showed very promising results. Moreover, a zig-zag orientation (see structure 7) had no impact on the transmission, but it decreases both the reflection and the tranquility. Since reflection can result in scouring, which has a very negative impact on the ecology, the zig-zag orientation is recommended to be adopted in the final design.

With respect to the distance between a double breakwater (called channel in this thesis), it is advised to minimize the distance or not to include it at all. Namely, an increase in channel length results in an increased reflection and had no significant impact on the transmission and the tranquility.

For the porosity of the structure, it is recommended to increase the porosity to allow a return flow through the structure and improve the water circulation and decrease the reflection. The investigation of the design variable *porosity of a structure* showed that, for the same number of blocks, an increase in crest width decreased the transmission more than a reduced porosity of the bottom layer did. An increased complexity, which is often accompanied with increased porosity, is an important asset for the ecological potential of a structure as well. Namely, complexity creates circulating flow patterns and turbulence within the structure. Therefore, it is advised to build a complex 3D configuration instead of a compact 2DV structure.

On the other hand, increased porosity showed to decrease the tranquility in a wave region. However, a higher Tr is not associated with a better ecological performance by definition. Therefore, the velocity field in the wake must be further investigated for the final design. If the velocities are too high, either the porosity or the slope steepness can be reduced a bit, or the structure height can be increased. With respect to the crest width, the results suggest that an increase in crest width is not an effective measure to reduce the tranquility behind 3D structures.

An example of a potentially improved design can be found on the left side of Figure 8.5. This structure is complex, with a shallow front slope of 1 : 3 and a built-in zig-zag orientation. The structure has the same amount of blocks per meter of flume width as structures 1, 2, 5, 6, 7, 8 and 9 have. On the other hand, the crest width of this structure is wider than from all configurations tested during the experiments. Additionally, the structure can be built from three sub-compositions of blocks only. These can be built on-shore and thereby ease the building process. On the right side of Figure ??, a second improved design is proposed, with the same front slope, slope orientation and number of blocks. Nevertheless, for this structure two blocks are removed from the back of the structure and added on the crest. Depending on the tidal- and wave conditions, the design and height of a structure has to be adapted accordingly.

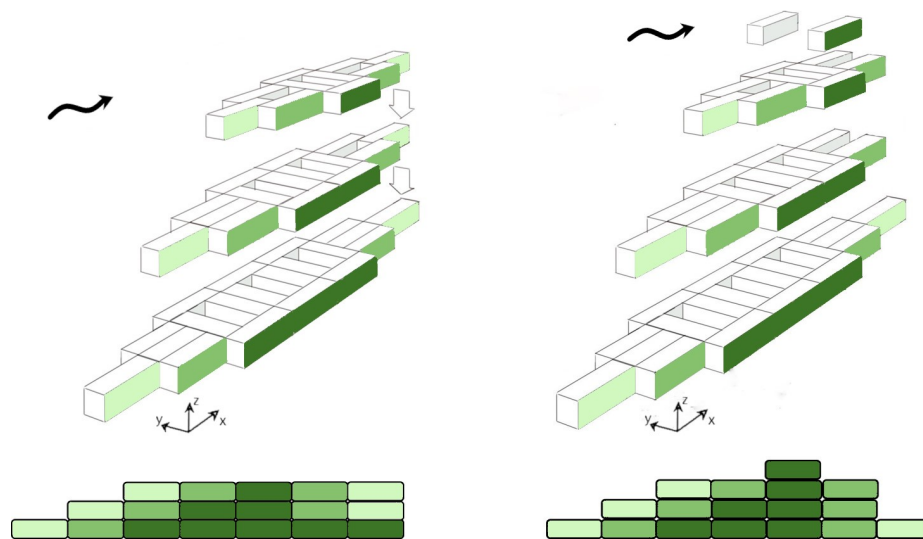


FIGURE 8.5: Two newly proposed configurations for a Reefy structure. The top sketches are 3D and the bottom sketches show the corresponding cross-section. Each block has the dimensions of $1 \times 1 \times 3$ meters (1:1). It must be realized that the holes inside the blocks are not visible in these sketches.

BIBLIOGRAPHY

- M. S. Ab Razak, B. Yusof, S. M. Desa, et al. The performance of narrow and broad-crested submerged breakwaters in dissipating wave heights. *Jurnal Teknologi*, 82(3), 2020.
- J. Aberg, S. Granhag, M. Gacia, S. Martin, T. Frost, and M. Hawkins. Background knowledge and tools for prediction of ecological impacts.
- M. Ahmed and R. Anwar. Experimental study on the performance of submerged breakwater as shore protection structure. In *International Conference on Environment and BioScience, IACSIT Press, Singapore*, pages 156–160, 2011.
- J. Ahrens and J. Cox. Design and performance of reef breakwaters. *Journal of Coastal Research*, pages 61–75, 1990.
- L. Airoidi, M. Abbiati, M. W. Beck, S. J. Hawkins, P. R. Jonsson, D. Martin, P. S. Moschella, A. Sundelöf, R. C. Thompson, and P. Aberg. An ecological perspective on the deployment and design of low-crested and other hard coastal defence structures. *Coastal engineering*, 52 (10-11):1073–1087, 2005.
- A. C. Alfaro and R. C. Carpenter. Physical and biological processes influencing zonation patterns of a subtidal population of the marine snail, *astraea (lithopoma) undosa* wood 1828. *Journal of Experimental Marine Biology and Ecology*, 240(2):259–283, 1999.
- T. L. Andersen, M. R. Eldrup, and P. Frigaard. Estimation of incident and reflected components in highly nonlinear regular waves. *Coastal Engineering*, 119:51–64, 2017.
- M. E. Anderson, J. M. Smith, and S. K. McKay. Wave dissipation by vegetation. 2011.
- A. Anonymous. Identification of design features to maintain biodiversity of epibiota. Technical Report Delos report D46, University of Bologna, July 2003. URL <https://repository.tudelft.nl/>.
- H. Armono and K. Hall. Wave transmission on submerged breakwaters made of hollow hemispherical shape artificial reefs. In *Canadian coastal conference*, pages 313–322, 2003.
- H. Armono, K. Hall, and A. Swamidas. Wave field around hemispherical shape artificial reefs used for fish habitat. In *Canadian coastal conference*, 2001.
- H. D. Armono. *Flow field around single and multiple hollow hemispherical artificial reefs used for fish habitat*. PhD thesis, Memorial University of Newfoundland, 1999.
- H. D. Armono. Artificial reefs as shoreline protection structures. In *Seminar Teori dan Aplikasi Teknologi Kelautan IV*, pages 1–14, 2004.
- T. E. Baldock, H. Karampour, R. Sleep, A. Vyltla, F. Albermani, A. Golshani, D. P. Callaghan, G. Roff, and P. J. Mumby. Resilience of branching and massive corals to wave loading under sea level rise—a coupled computational fluid dynamics-structural analysis. *Marine pollution bulletin*, 86(1-2):91–101, 2014.
- J. A. Battjes and H. W. Groenendijk. Wave height distributions on shallow foreshores. *Coastal engineering*, 40(3):161–182, 2000.

- M. W. Beck, I. J. Losada, P. Menéndez, B. G. Reguero, P. Díaz-Simal, and F. Fernández. The global flood protection savings provided by coral reefs. *Nature communications*, 9(1):1–9, 2018.
- K. P. Black and C. J. Andrews. Sandy shoreline response to offshore obstacles part 1: Salient and tombolo geometry and shape. *Journal of coastal research*, pages 82–93, 2001.
- M. Blacka, T. Shand, J. Carley, and A. Mariani. A review of artificial reefs for coastal protection in nsw. 2013.
- M. Bleck. Wave attenuation by artificial reefs. *PIANC magazine" on course" nr 125*, 2006.
- M. Bleck and H. Oumeraci. Wave damping and spectral evolution at artificial reefs. In *Ocean Wave Measurement and Analysis (2001)*, pages 1062–1072. 2002.
- J. A. Bohnsack. Are high densities of fishes at artificial reefs the result of habitat limitation or behavioral preference? *Bulletin of Marine Science*, 44(2):631–645, 1989.
- B. W. Borsje, B. K. van Wesenbeeck, F. Dekker, P. Paalvast, T. J. Bouma, M. M. van Katwijk, and M. B. de Vries. How ecological engineering can serve in coastal protection. *Ecological Engineering*, 37(2):113–122, 2011.
- T. Bruce, J. Van der Meer, L. Franco, and J. M. Pearson. A comparison of overtopping performance of different rubble mound breakwater armour. In *Coastal Engineering 2006: (In 5 Volumes)*, pages 4567–4579. World Scientific, 2007.
- M. Buccino and M. Calabrese. Conceptual approach for prediction of wave transmission at low-crested breakwaters. *Journal of waterway, port, coastal, and ocean engineering*, 133(3):213–224, 2007.
- I. Cáceres, A. Sánchez-Arcilla, B. Zanuttigh, A. Lamberti, and L. Franco. Wave overtopping and induced currents at emergent low crested structures. *Coastal Engineering*, 52(10-11):931–947, 2005.
- M. Calabrese, D. Vicinanza, and M. Buccino. 2d wave setup behind submerged breakwaters. *Ocean Engineering*, 35(10):1015–1028, 2008.
- D. Cardenas-Rojas, E. Mendoza, M. Escudero, and M. Verduzco-Zapata. Assessment of the performance of an artificial reef made of modular elements through small scale experiments. *Journal of Marine Science and Engineering*, 9(2):130, 2021.
- H.-C. Chan, J.-M. Leu, and C.-J. Lai. Velocity and turbulence field around permeable structure: Comparisons between laboratory and numerical experiments. *Journal of Hydraulic Research*, 45(2):216–226, 2007.
- H. Chanson and C. A. Gonzalez. Physical modelling and scale effects of air-water flows on stepped spillways. *Journal of Zhejiang University-Science A*, 6(3):243–250, 2005.
- E. Charbonnel, C. Serre, S. Ruitton, J.-G. Harmelin, and A. Jensen. Effects of increased habitat complexity on fish assemblages associated with large artificial reef units (french mediterranean coast). *ICES Journal of Marine Science*, 59(suppl):S208–S213, 2002.
- C. CIRIA, CUR. *The Rock Manual. The use of rock in hydraulic engineering (2nd edition)*. 01 2007.

- I. Daemen. Wave transmission at low-crested structures. 1991.
- K. A. Dafforn, T. M. Glasby, L. Airoidi, N. K. Rivero, M. Mayer-Pinto, and E. L. Johnston. Marine urbanization: an ecological framework for designing multifunctional artificial structures. *Frontiers in Ecology and the Environment*, 13(2):82–90, 2015.
- M. De Rijcke. Artificial reefs, Jul 2011. URL http://www.coastalwiki.org/wiki/Artificial_reefs.
- S. Degraer, D. A. Carey, J. W. Coolen, Z. L. Hutchison, F. Kerckhof, B. Rumes, and J. Vanaverbeke. Offshore wind farm artificial reefs affect ecosystem structure and functioning. *Oceanography*, 33(4):48–57, 2020.
- N. Diplarakos. Velocity measurements in and around a permeable breakwater. 2017.
- J. E. Eckman and D. O. Duggins. Effects of flow speed on growth of benthic suspension feeders. *The Biological Bulletin*, 185(1):28–41, 1993.
- P. G. F. Filianoti and L. Gurnari. Wave diffraction and transmission by a submerged breakwater. *Coastal Engineering Proceedings*, (36):27–27, 2018.
- L. E. Frostick, S. J. McLelland, and T. G. Mercer. *Users guide to physical modelling and experimentation: Experience of the HYDRALAB network*. CRC Press, 2019.
- F. Gallerano, G. Cannata, and F. Palleschi. Hydrodynamic effects produced by submerged breakwaters in a coastal area with a curvilinear shoreline. *Journal of Marine Science and Engineering*, 7(10):337, 2019.
- C. Geierman. *Barnacle Feeding: Comparing Cirral Anatomy, Feeding Behavior, Reynolds Numbers, and Cirral Fan Leakiness Across Three Size Classes of Three Species of Common Acorn Barnacles*. PhD thesis, University of Oregon, 2007.
- Y. Goda and Y. Suzuki. Estimation of incident and reflected waves in random wave experiments. In *Coastal Engineering 1976*, pages 828–845. 1977.
- M. C. Haller, R. A. Dalrymple, and I. A. Svendsen. Experimental study of nearshore dynamics on a barred beach with rip channels. *Journal of Geophysical Research: Oceans*, 107(C6):14–1, 2002.
- W. Hammond and C. Griffiths. Influence of wave exposure on south african mussel beds and their associated infaunal communities. *Marine Biology*, 144(3):547–552, 2004.
- A. Hashish, M. Gad, M. ElKamash, M. G. El-Rab, and M. N. El-Din. Impacts of different breakwater configurations on the water quality; case study: Mandrah beach.
- T. Hata, J. S. Madin, V. R. Cumbo, M. Denny, J. Figueiredo, S. Harii, C. J. Thomas, and A. H. Baird. Coral larvae are poor swimmers and require fine-scale reef structure to settle. *Scientific reports*, 7(1):1–9, 2017.
- M. Hattori and H. Sakai. Wave breaking over permeable submerged breakwaters. In *Coastal Engineering 1994*, pages 1101–1114. 1995.
- S. J. Hawkins, H. F. Burcharth, B. Zanuttigh, and A. Lamberti. *Environmental design guidelines for low crested coastal structures*. Elsevier, 2010.

- D. Heineke and H. J. Verhagen. On the use of the fictitious wave steepness and related surf-similarity parameter in methods that describe the hydraulic and structural response to waves. In *Coastal Structures 2007: (In 2 Volumes)*, pages 1057–1066. World Scientific, 2009.
- M. A. Hinis. *Cnoidal and sinusoidal wave reflection from a laboratory sand beach*. Drexel University, 2003.
- L. H. Holthuijsen. *Waves in oceanic and coastal waters*. Cambridge university press, 2010.
- H. L. Hunt and R. E. Scheibling. Predicting wave dislodgment of mussels: variation in attachment strength with body size, habitat, and season. *Marine Ecology Progress Series*, 213: 157–164, 2001.
- D.-S. Hur, K.-H. Lee, and D.-S. Choi. Effect of the slope gradient of submerged breakwaters on wave energy dissipation. *Engineering Applications of Computational Fluid Mechanics*, 5(1):83–98, 2011.
- Z. Jiang, Z. Liang, L. Zhu, Z. Guo, and Y. Tang. Effect of hole diameter of rotary-shaped artificial reef on flow field. *Ocean Engineering*, 197:106917, 2020.
- R. Jonker. Homogeneous detached composite breakwater: Cfd study of the design sensitivities in the 2d geometrical layout using a detached homogeneous low-crested structure to reduce sea wall overtopping. 2020.
- L. K. Jordan, D. S. Gilliam, and R. E. Spieler. Reef fish assemblage structure affected by small-scale spacing and size variations of artificial patch reefs. *Journal of experimental marine biology and ecology*, 326(2):170–186, 2005.
- S. Kawamata. Effect of wave-induced oscillatory flow on grazing by a subtidal sea urchin *strongylocentrotus nudus* (a. agassiz). *Journal of Experimental Marine Biology and Ecology*, 224 (1):31–48, 1998. ISSN 0022-0981. doi: [https://doi.org/10.1016/S0022-0981\(97\)00165-2](https://doi.org/10.1016/S0022-0981(97)00165-2). URL <https://www.sciencedirect.com/science/article/pii/S0022098197001652>.
- D. Kim, J. Woo, H.-S. Yoon, and W.-B. Na. Efficiency, tranquillity and stability indices to evaluate performance in the artificial reef wake region. *Ocean Engineering*, 122:253–261, 2016.
- G. Klopman and J. W. van der Meer. Random wave measurements in front of reflective structures. *Journal of waterway, port, coastal, and ocean engineering*, 125(1):39–45, 1999.
- C. Kontaxi and C. Memos. Submerged breakwaters as artificial habitats. In *Proc. 31st IAHR Congress, Seoul*, pages 3967–3975, 2005.
- V. E. Kostylev, J. Erlandsson, M. Y. Ming, and G. A. Williams. The relative importance of habitat complexity and surface area in assessing biodiversity: fractal application on rocky shores. *Ecological Complexity*, 2(3):272–286, 2005.
- B. Le Méhauté. *An introduction to hydrodynamics and water waves*. Springer Science & Business Media, 1976.
- N. K. Li and M. W. Denny. Limits to phenotypic plasticity: flow effects on barnacle feeding appendages. *The Biological Bulletin*, 206(3):121–124, 2004.

- B. Liang, G. Wu, F. Liu, H. Fan, and H. Li. Numerical study of wave transmission over double submerged breakwaters using non-hydrostatic wave model. *Oceanologia*, 57(4):308–317, 2015.
- Lokesh, S. Sannasiraj, and V. Sundar. Hydrodynamic characteristics of a submerged trapezoidal artificial reef unit. *Proceedings of the Institution of Mechanical Engineers, Part M: Journal of Engineering for the Maritime Environment*, 233(4):1226–1239, 2019.
- I. Losada, N. Garcia, and J. Lara. Report on turbulent flow velocities in the surface region of lcs. *Delos report D44 (includes Delos report D23)*, 2003.
- A. Mahmoudi, H. Hakimzadeh, M. J. Ketabdari, N. Cartwright, and M. Vaghefi. Experimental study on wave transmission and reflection at impermeable submerged breakwaters. *International Journal of Coastal and Offshore Engineering*, 1(3):19–27, 2017.
- E. P. Mansard and E. Funke. The measurement of incident and reflected spectra using a least squares method. In *Coastal Engineering 1980*, pages 154–172. 1980.
- K. B. Marchinko and A. R. Palmer. Feeding in flow extremes: dependence of cirrus form on wave-exposure in four barnacle species. *Zoology*, 106(2):127–141, 2003.
- E. Mendoza, A. Rios, I. Marino-Tapia, and R. Silva. Modular coral shaped artificial reefs acting as beach protection barriers. *Coastal Structures 2019*, pages 989–997, 2019.
- A. S. Metallinos, E. G. Repousis, and C. D. Memos. Wave propagation over a submerged porous breakwater with steep slopes. *Ocean Engineering*, 111:424–438, 2016.
- S. Miller. Electrically stimulated artificial mussel (*mytilus edulis*) reefs to create shoreline protection and coastal habitat in st. margaret’s bay, nova scotia. 2020.
- P. Moschella, M. Abbiati, P. Aberg, L. Airoidi, J. Anderson, F. Bacchiocchi, F. Bulleri, G. E. Dinesen, M. Frost, E. Gacia, et al. Low-crested coastal defence structures as artificial habitats for marine life: using ecological criteria in design. *Coastal Engineering*, 52(10-11):1053–1071, 2005.
- K. W. Pilarczyk et al. Design of low-crested (submerged) structures: An overview. In *6th COPEDEC (Int. Conf. on Coastal and Port Engng. in Develop. Countries)*, Sri. Citeseer, 2003.
- G. G. Pina and J. V. F. de Alarcón. Experiments on coastal protection submerged breakwaters: a way to look at the results. In *Coastal Engineering 1990*, pages 1592–1605. 1991.
- A. C. Rambabu and J. Mani. Numerical prediction of performance of submerged breakwaters. *Ocean Engineering*, 32(10):1235–1246, 2005.
- R. Ranasinghe and I. L. Turner. Shoreline response to submerged structures: A review. *Coastal Engineering*, 53(1):65–79, 2006. ISSN 0378-3839. doi: <https://doi.org/10.1016/j.coastaleng.2005.08.003>. URL <https://www.sciencedirect.com/science/article/pii/S0378383905001237>.
- R. Ranasinghe, I. L. Turner, and G. Symonds. Shoreline response to multi-functional artificial surfing reefs: A numerical and physical modelling study. *Coastal Engineering*, 53(7):589–611, 2006.
- R. Ranasinghe, M. Larson, and J. Savioli. Shoreline response to a single shore-parallel submerged breakwater. *Coastal Engineering*, 57(11-12):1006–1017, 2010.

- K. Rodgers, E. Cox, and C. Newton. Effects of mechanical fracturing and experimental trampling on hawaiian corals. *Environmental management*, 31(3):0377–0384, 2003.
- A. Saket, W. L. Peirson, M. L. Banner, and M. J. Allis. Wave breaking onset of two-dimensional wave groups in uniform intermediate depth water. *arXiv preprint arXiv:1703.04354*, 2017.
- T. Schoonees, A. G. Mancheño, B. Scheres, T. Bouma, R. Silva, T. Schlurmann, and H. Schüttrumpf. Hard structures for coastal protection, towards greener designs. *Estuaries and Coasts*, 42(7):1709–1729, 2019.
- S. R. Seabrook and K. R. Hall. Wave transmission at submerged rubblemound breakwaters. In *Coastal Engineering 1998*, pages 2000–2013. 1999.
- D. J. Sheehy and S. F. Vik. The role of constructed reefs in non-indigenous species introductions and range expansions. *Ecological Engineering*, 36(1):1–11, 2010.
- S. Shin, I.-R. Bae, and J.-I. Lee. Physical modelling of the wave transmission over a tetrapod armored artificial reef. *Journal of Coastal Research*, 91(SI):126–130, 2019.
- C. E. Siddon and J. D. Witman. Influence of chronic, low-level hydrodynamic forces on subtidal community structure. *Marine Ecology Progress Series*, 261:99–110, 2003.
- B. Sladonja. *Aquaculture and the Environment: A Shared Destiny*. BoD–Books on Demand, 2011.
- E. R. Smith and N. C. Kraus. Laboratory study on macro-features of wave breaking over bars and artificial reefs. Technical report, Coastal Engineering Research Center Vicksburg Ms, 1990.
- R. Soulsby. Calculating bottom orbital velocity beneath waves. *Coastal Engineering*, 11(4):371–380, 1987.
- C. Srisuwan and P. Rattanamanee. Modeling of seadome as artificial reefs for coastal wave attenuation. *Ocean Engineering*, 103:198–210, 2015.
- D. K. Stauble and J. R. Tabar. The use of submerged narrow-crested breakwaters for shoreline erosion control. *Journal of Coastal Research*, pages 684–722, 2003.
- M. Tajziehchi and R. J. Cox. Numerical and experimental modeling of wave evolution over submerged breakwaters. 2008.
- T. Takeuchi. Design of artificial reefs in consideration of environmental characteristics. In *Japan–US Symposium on Artificial Habitats for Fisheries Proceedings*. Edited by M. Nakamura, RS Grove, and CJ Sonu. Southern California Edison Co., Rosemead, CA, USA, pages 195–203, 1991.
- J. Van der Meer and K. Pilarczyk. Stability of low-crested and reef breakwaters, asce. *Proc. 22th ICCE, Delft*, 1990.
- J. Van der Meer, K. d’Agremond, and E. Gerding. Toe structure stability of rubble mound breakwaters, 1996.
- J. W. Van der Meer and I. F. Daemen. Stability and wave transmission at low-crested rubble-mound structures. *Journal of waterway, port, coastal, and ocean engineering*, 120(1):1–19, 1994.

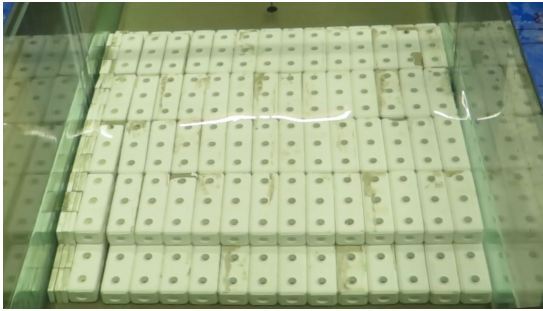
- J. W. Van der Meer, R. Briganti, B. Zanuttigh, and B. Wang. Wave transmission and reflection at low-crested structures: Design formulae, oblique wave attack and spectral change. *Coastal Engineering*, 52(10-11):915–929, 2005.
- R. Van Oosten and J. Peixo Marco. Wave transmission at various types of low-crested structures using neural networks. 2005.
- B. K. van Wesenbeeck, G. Wolters, J. A. Antolínez, S. Kalløe, B. Hofland, W. de Boer, C. Çete, and T. J. Bouma. Woods versus waves: Wave attenuation through non-uniform forests under extreme conditions. 2021.
- K. Vijay, S. Neelamani, C. Nishad, and T. Sahoo. Gravity wave interaction with multiple submerged artificial reefs. *Proceedings of the Institution of Mechanical Engineers, Part M: Journal of Engineering for the Maritime Environment*, 235(2):607–622, 2021.
- M. Villani, J. Bosboom, M. Zijlema, and M. J. Stive. Circulation patterns and shoreline response induced by submerged breakwaters. In *ICCE 2012: Proceedings of the 33rd International Conference on Coastal Engineering, Santander, Spain, 1-6 July 2012*. Coastal Engineering Research Council, 2012.
- T. V. Wamsley and J. P. Ahrens. Computation of wave transmission coefficients at detached breakwaters for shoreline response modeling. In *Coastal structures 2003*, pages 593–605. 2004.
- I. Wenneker and B. Hofland. Optimal wave gauge spacing for separation of incoming and reflected waves. In *Proc., 5th Int. Conf. Coastlab*, volume 14, 2014.
- J. Wright, A. Colling, and D. Park. *Waves, tides and shallow-water processes*, volume 4. Gulf Professional Publishing, 1999.
- B. Zanuttigh and J. W. Van der Meer. Wave reflection from coastal structures in design conditions. *Coastal engineering*, 55(10):771–779, 2008.
- J. Zelt and J. E. Skjelbreia. Estimating incident and reflected wave fields using an arbitrary number of wave gauges. In *Coastal Engineering 1992*, pages 777–789. 1993.

A

PHYSICAL MODEL

A.1 DESIGN CONFIGURATIONS PICTURES AND 3D SKETCHES

Pictures from 2D-structures



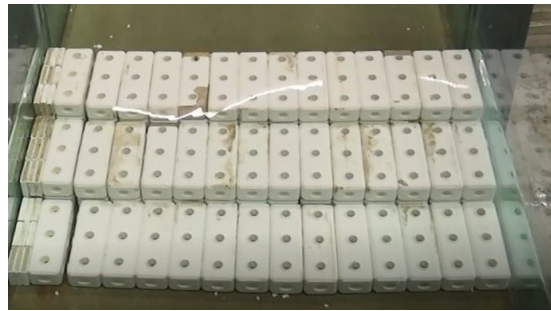
(A) Structure 1



(B) Structure 2



(c) Structure 3



(D) Structure 4



(E) Structure 5



(F) Structure 6



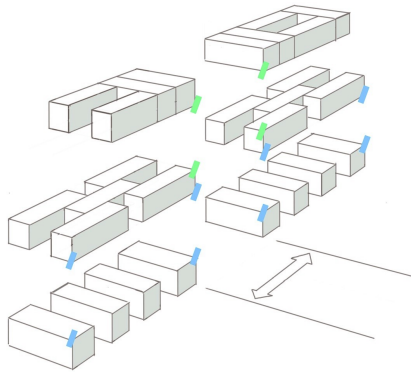
(G) Structure 7



(H) Structure 2 - holes blocked with pipes

FIGURE A.1: Pictures taken from the top sea-side of the 2D structures, except for figure A.1h.

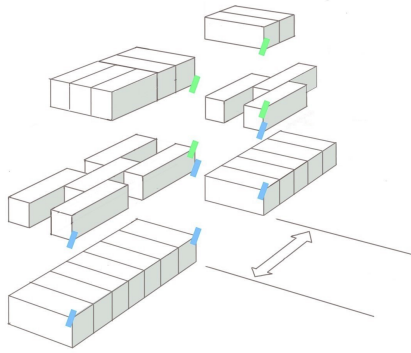
Pictures and sketches from 3D-structures



(A) Structure 8 + picture Structure 8-I



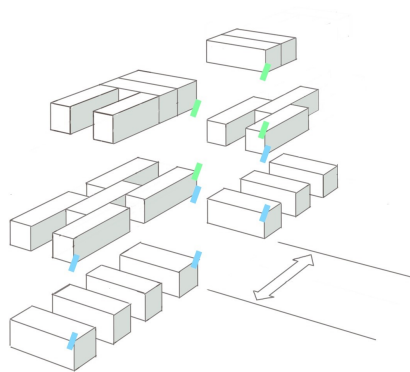
(B) Picture



(c) Structure 9 + picture Structure 9



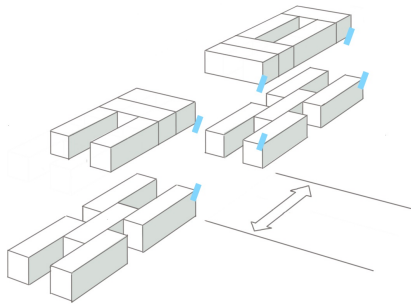
(d) Picture



(e) Structure 10 + picture Structure 10



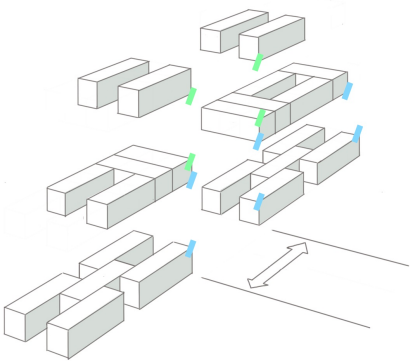
(f) Picture



(g) Structure 11 + picture Structure 11-I



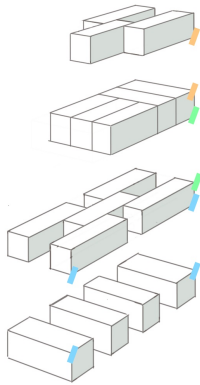
(h) Picture



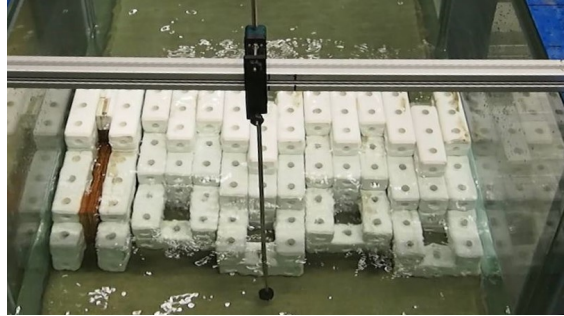
(i) Structure 12 + picture Structure 12-I



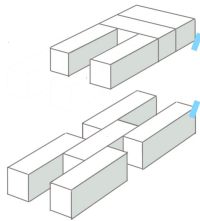
(j) Picture



(κ) Structure 13 + picture Structure 13



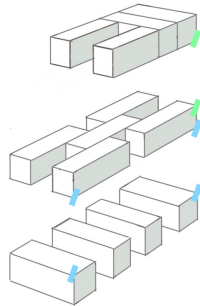
(l) Picture



(μ) Structure 14 + picture Structure 14



(n) Picture



(o) Structure 15 + picture Structure 15

(p) Picture

FIGURE A.2: Sketch + pictures of 3D design configurations. In the sketches, the waves are coming from the left, so the seaward side of structures is visible. The pictures are also taken from the top at the seaward side.

Pictures from structures with corals on top

As can be seen in Figure A.3d, accidentally the Structure 8-I-3D has an extra block on the top of the front structure. Only one test has been performed with this structure, nevertheless, it can not be compared to the other structures as it differs in the amount of blocks as well as in the surface roughness.



(A) Structure 8-I-PVC(38)

(B) Structure 8-I-PVC(69)



(c) Structure 8-I-PVC(169)

(d) Structure 8-I-3D

FIGURE A.3: Pictures of structure 8-I with increased surface roughness. The amount of PVC pipes on top of the structure varies between 38, 69 and 169. The length is constantly 4 cm of each pipe. Also 3D printed corals are tested

Extra pictures



(A) Picture taken in the flume of EVM behind structure 8-I

(B) Picture of ink injection in the channel of structure 12-III

A.2 DEEP WATER DEPTH

A potential pilot project of Reefy was used as guidance for defining the water depth in the wave flume (location confidential). The depth of each condition at the deep water part of the wave flume (d_0) is calculated as a summation of the following aspects:

- Storm surge: three different storm categories and the corresponding storm surge levels were obtained at the off-shore pilot location and transformed to the corresponding values at the near-shore project site. The storm surge during daily conditions is zero, during a yearly occurring storm it is $0.8m$, during a hurricane of category 1-2 it is $1.0m$ and during a hurricane of category 3 it is $1.2m$.
- The tidal range: the tidal range is slightly overestimated as $0.6m$, to get to an integral design.
- Daily clearance: to make sure the structure is always submerged for at least 0.30 meters

- The structural height: two, three and four levels of blocks have been tested during the experiments
- The foreshore: a foreshore of 44 cm has been built for the experiments

The obtained d_0 is converted to the scale of the model and the following water depths are chosen to use during the experiments :0.61m, 0.68m and 0.75m. For each water depth, daily and stormy conditions have been tested.

A.3 OVERVIEW WAVE CONDITIONS + PERFORMED TESTS

In table [A.1](#), an overview can be found of the details from the input values of each wave condition (same as table [3.4](#)) together with the structure numbers that have been tested in this conditions.

For some wave conditions, multiple tests have been performed with the same structure, if for example the EVM switched locations during the experiment. Nevertheless, in this case each structure number is only mentioned one time in the table.

Furthermore, for some wave wave conditions there are no structure numbers written down and the reason behind this are explained below:

For wave condition 9 this is because there has been no reference test (without a structure) performed for this condition, thus it has not been possible to compute the transmission coefficient $K_t(s)$ in which the effect of the foreshore is removed. Therefore, the tests performed in this condition are not evaluated for the hydrodynamic performance.

Wave conditions 21, 27, 33 and 34 have been used during experiments in which the impact of different block characteristics on the stability of a single block have been tested. Examples of different block characteristics which have been tested where: outer surface roughness, rounded/squared corners, weight, coral growth, orientation etc. Due to time shortage, stability has eventually not been further investigated in this thesis. Because it was first the planning to investigate instability as well, these wave conditions were included in the list.

Furthermore, wave conditions 21, 27, 33 and 34 have been used to investigate the performance of a 16th structure. Nevertheless, after the first day of testing no further experiments have been performed with this structure, due to the unstable design. Namely, this 16th was similar to structure 8, but included an extra block on the top layer which had an orthogonal orientation with respect to the wave direction. During the stormy wave conditions, this block started rocking. In Figures [A.5a](#) and [A.5b](#), both designs can be observed.

TABLE A.1: Overview the details from the wave conditions (model scale) and information about which structures are tested in each condition. For irregular wave tests the H stands for H_{m0} and T for T_p of a JONSWAP spectrum. In the 6th column, R stands for Regular and I for Irregular.

Wave condition	$d_0[m]$	$T_{target}[s]$	$H_{target}[m]$	$s[-]$	R/I	Structure #
1	0,61	1,47	0,06	0,02	R	11-I
2	0,61	1,16	0,04	0,02	R	11-I
3	0,61	0,8	0,02	0,02	R	11-I,12-I
4	0,61	0,98	0,06	0,04	R	11-I
5	0,61	1,16	0,04	0,02	I	11-I,11-III,12-I,12-III,14
6	0,68	2,51	0,12	0,02	R	11-I
7	0,68	2,15	0,10	0,02	R	11-I
8	0,68	1,80	0,08	0,02	R	1,2,3,8-I,8-III,8-V,9,10,11-I,15
9	0,68	1,47	0,06	0,02	R	-
10	0,68	1,15	0,04	0,02	R	1,2,3,8-I,8-III,8-V,9,10,15
11	0,68	0,80	0,02	0,02	R	1,2,3,8-I,8-III,8-V,9,10,15
12	0,68	1,47	0,12	0,04	R	11-I
13	0,68	1,31	0,10	0,04	R	11-I
14	0,68	1,15	0,08	0,04	R	1,3,9,10,11-I
15	0,68	0,98	0,06	0,04	R	11-I
16	0,68	1,47	0,06	0,02	I	2,8-0,8-I,8-V,13,15,8-I-PVC(69&169)
17	0,68	0,80	0,02	0,02	I	8-I,15
18	0,68	1,31	0,10	0,04	I	11-I,11-III,12-I,12-III,14
19	0,68	1,15	0,08	0,04	I	8-I,13,8-I-PVC(169)
20	0,68	0,98	0,06	0,04	I	8-0,8-I,8-V,8-I-PVC(169&3D)
21	0,75	3,11	0,16	0,02	R	-
22	0,75	2,76	0,14	0,02	R	2
23	0,75	2,42	0,12	0,02	R	1,2,2-BH,3,4,5
24	0,75	2,09	0,10	0,02	R	1,2,2-BH,3
25	0,75	1,92	0,18	0,04	R	2,15
26	0,75	1,76	0,16	0,04	R	2,4,5,8-I,8-III,8-V,9,10,15
27	0,75	1,60	0,16	0,04	R	-
28	0,75	1,60	0,14	0,04	R	1,2,2-BH,3,4,5,8-I,8-III,8-V,9,10,15
29	0,75	1,45	0,12	0,04	R	1,2,2-BH,3,8-I,8-III,8-V,9,10,15
30	0,75	1,29	0,10	0,04	R	1,2,2-BH,3,8-I,8-III,8-V,9,10,15
31	0,75	1,14	0,08	0,04	R	1,2,2-BH,8-I,8-III,8-V,9,10,15
32	0,75	0,98	0,06	0,04	R	R,8-I,8-III,8-V,9,10,15
33	0,75	0,80	0,04	0,04	R	-
34	0,75	0,40	0,01	0,04	R	-
35	0,75	1,60	0,14	0,04	I	2,2-BH,4,5,6,7,8-I,8-I-PVC(32&69&169)
36	0,75	1,45	0,12	0,04	I	-



(A) Picture Structure "16-I"



(B) Picture Structure 8-I

FIGURE A.5: Comparison design structure 16 and 8. After the first

B | LITERATURE STUDY

B.1 HYDRODYNAMIC PERFORMANCE

B.1.1 Related physical processes

The placement of a Reefy structure induces four main local physical processes related to the hydrodynamic performance:

The first hydrodynamic process is the **dissipation** of the incoming wave energy. For waves near the critical wave height, the reduction in the local water depth above the crest causes the waves to break in deeper water than naturally would occur [Gallerano et al., 2019]. [Bleck and Oumeraci, 2002] described wave breaking observations from visual observations during wave-flume experiments with low crested structures and these are explained in appendix ?? . For non-breaking waves, the fact that the structure forces a flow resistance upon the incoming waves accounts for the largest part in the dissipation process. Furthermore, also a part of the energy is dissipated from friction with the inner- and outer surface area of the structure. [Losada et al., 2003]. This part is higher for artificial reefs with increased porosity compared to conventional rubble mound breakwaters [Cardenas-Rojas et al., 2021]. Lastly, a part is dissipated from turbulence which is formed when travelling through the reef and at the corners of the structure [Kontaxi and Memos, 2005].

The second hydrodynamic effect of a Reefy structure is the **reflection** in seaward direction of a part of the incoming waves. The interference with the incident- and reflected waves creates a partially standing wave field in front of the breakwater [Losada et al., 2003] [Filianoti and Gurnari, 2018]. For regular waves this pattern covers the whole area in front of the breakwater, whereas for random waves it is damped out after approximately two times the spectral peak wave length [Klopman and van der Meer, 1999].

The third hydrodynamic effect of a Reefy structure is the **non linearity**, which occurs as wave travel over the structure mainly from shoaling at the foreshore and/or over the front slope. Non linear effects result in the generation of shorter waves, which are phase-locked with the primary wave. These waves can be released during the breaking phase. Furthermore, above the crest more non-linear interactions occur between different wave phases and some energy can be transferred from the peak frequency to the higher harmonics [Losada et al., 2003]. In the time-domain, this means waves become smaller (lower height) and shorter (lower mean period). This is translated in the frequency domain with a decreasing variance of the energy density spectrum and a part of it shifted to the higher harmonics. Therefore, a broad-banded spectrum is expected to be developed from an incoming narrow-crest spectrum

The fourth hydrodynamic effect is the **variation of the mean water level** at the lee-side of the structure, which is caused by the wave breaking process inducing a mass-flux over the structure [Cáceres et al., 2005]. As this set-up creates nearshore circulation patterns in which sediments

are transported, the shoreline response mode can be predicted from it. Namely, if the ratio of the set-up close behind the structure exceeds the water level at the side of the structure, a divergent current pattern is created which is associated with erosion. And vice versa for accretion. As the current study is based on 2D experiments, predicting empirically and/or modelling the shoreline response mode is not included in this study.

B.1.2 Empirical equations erosion mitigation

The second hydrodynamic function of a Reefy structure is to mitigate the erosion problems of coastal areas. In this chapter the main literature found for this topic is discussed.

In contrast to emergent breakwaters, where accretion in it's lee is expected under all conditions, for submerged structures both accretion and erosion are possible to occur. [Ranasinghe et al., 2006] found that 70 per cent of submerged structures constructed for beach protection had resulted in unexpected net erosion of the shoreline in their lee. The three main processes playing a role in the shoreline response of submerged breakwaters are the transmitted onshore flow over the structure, the long-shore water level gradients and currents along the sides of the structure [Ranasinghe and Turner, 2006].

To predict the shoreline response of submerged breakwaters, 3D numerical model simulations give the most reliable results, including set-up and flow between multiple breakwaters. Better prediction of the 2D-wave transmission and reflection during different weather conditions significantly increases the reliability of such morphodynamic models [Villani et al., 2012]. Therefore, this is the area where this research contributes to the prediction of the shoreline response.

None of the studies have comprehensively tested the impact of structural and environmental variables on the quantitative shoreline response of accretion or erosion. However, there exist some empirical equations predicting the shoreline response to submerged structures. Even though these are not validated, some preliminary design guidance can be obtained from the existing empirical equation [Blacka et al., 2013]. The studies on the morphological response to (submerged) breakwaters are described in Appendix B.1.2 .

Overview equations

Some previous studies conducted research on the shoreline-response mode and came up with prediction formulas. A short description of these studies is given below.

[BLACK AND ANDREWS, 2001] Black & Andrews investigated the beach response to naturally occurring islands and reefs. A relationship between (a) the location and geometry of a structure and (b) the equilibrium shoreline response was formed.

The main disadvantage of these equations in relationship to this research is the fact that they inherently cannot predict shoreline erosion but solely accretion. Furthermore, they do not relate the shoreline response to wave exposure of transmission, which other researcher suggest both have a significant impact [Blacka et al., 2013]. Altogether, the equations of Black &

Andrews are not qualified for design guidance of a Reefy structure and therefore not further discussed.

[PILARCZYK ET AL., 2003] The authors invented a shoreline prediction formula for submerged structures, which includes a transmission term to the formula for emergent breakwaters of Black & Andrews. If the relationship of equation B.1 is met, salient formation is predicted for a single breakwater. The same holds for multiple breakwaters with equation B.2, where G stands for the gap distance between the structures. The rest of the new abbreviations used in equations B.1 and B.2 are explained in Figure B.1

$$\frac{L}{S} < \frac{1}{1 - K_t} \quad (\text{B.1})$$

$$\frac{G * S}{L^2} > 0.5 * (1 - K_t) \quad (\text{B.2})$$

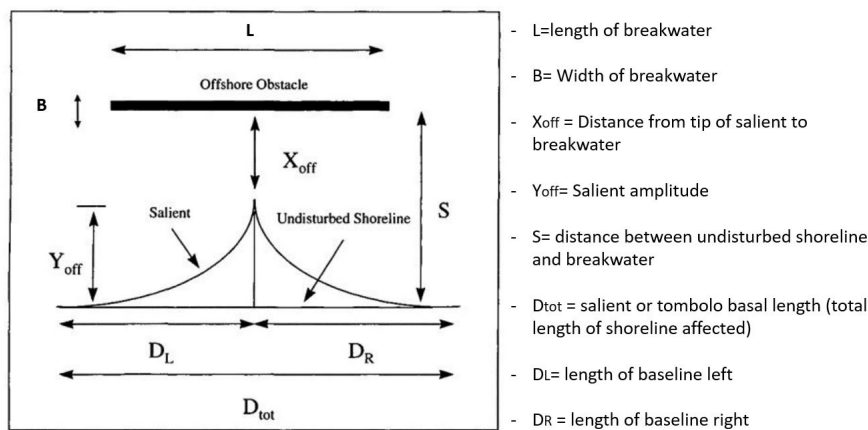


FIGURE B.1: Geometry Definition for Offshore Features by Black & Andrews

[RANASINGHE ET AL., 2006] In this study, a numerical model is used to predict the shoreline response to a submerged breakwater and came up with some preliminary calculations. Namely, if the ratio of the offshore distance S to the width of the natural surf zone S_{ZW} is smaller than 1, then erosion is likely to occur. If the ratio is above 1.5, then accretion is likely to occur. Moreover, accretion is likely to peak if S is twice the width of the natural surf zone .

Nonetheless, it should be noted that the morphodynamic response has never been validated or calibrated. However, the used hydrodynamics have been qualitatively validated with physical experiments [Blacka et al., 2013].

[RANASINGHE ET AL., 2010] For this research, a two-dimensional depth averaged numerical model in Mike21 has been finished to simulate the shoreline response to a single shore-parallel breakwater. This study concluded that two non-dimensional parameters can be used to express whether accretion or erosion occurs, these can be found in the axis of Figure B.2 . The abbreviation A stands for a shape parameter governed by D_{50} of the sediment at the shore.

The conclusion of this study is that accretion is more likely to occur for shallower structures that are located further offshore, together with an increased crest width. Tidal influence appeared to have a minimal impact on the response mode. Nevertheless, these study results are not validated with real cases of physical models [Blacka et al., 2013].

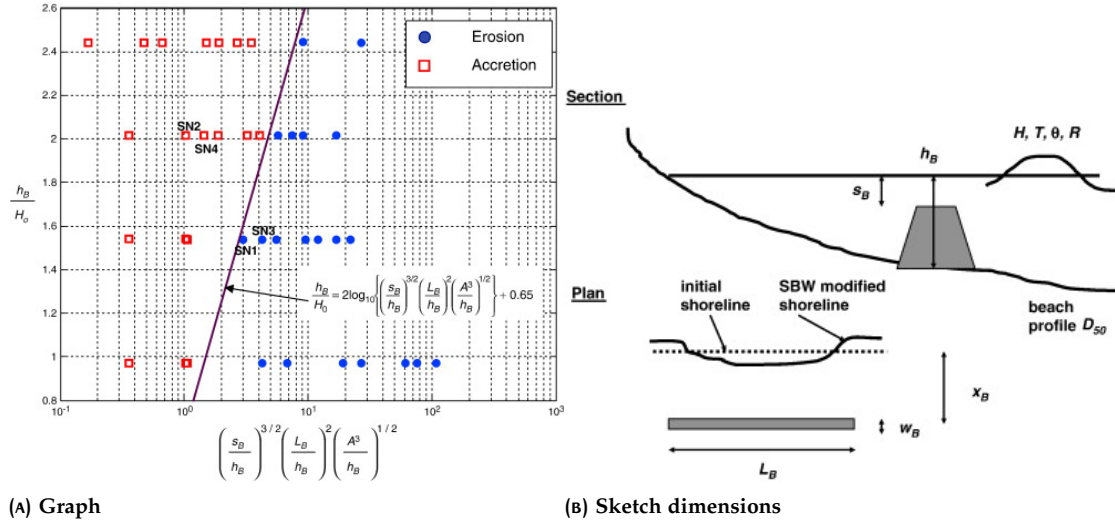


FIGURE B.2: Mode of Shoreline Response to Submerged Breakwaters according to [Ranasinghe et al., 2010].

[VILLANI ET AL., 2012] In 2012, the authors of this study came up with a simple analytical criterion to qualitatively predict the first response mode of a shoreline in the lee side of a structure. The principle is based on the fact that a 4-cell circulation pattern results in accretion and a 2-cell pattern in erosion, see Figure B.3 for an illustration of these patterns. The model is validated with a numerical model in SWASH and experiments performed by [Haller et al., 2002].

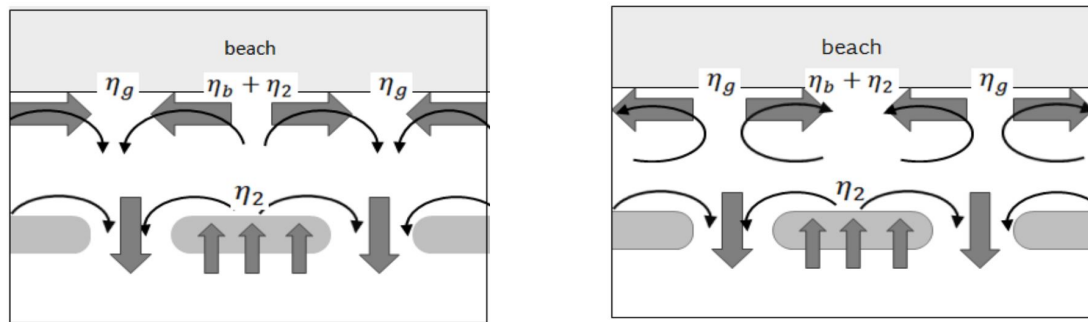


FIGURE B.3: Left: erosive 2-cell circulation pattern. Right: Accretive 4-cell circulation pattern. [Villani et al., 2012]

They propose ratio $r = \frac{\eta_2 + \eta_b}{\eta_g}$ as a criterion, where accretion happens if $r < 1$ and erosion if $r > 1$. This aspect is included the design of the Reefy structure, by increasing the permeability. The reader is referred to the paper of [Villani et al., 2012] to read how the different elevation levels are formulated in terms of incident wave conditions, beach slope and geometrical properties of

the breakwater. The methodology is based on a simplified mass- and momentum balance and assumes that the alongshore variations in set-up is a function of the 1D cross-shore momentum balance.

Summary erosion mitigation

From the results of the studies on the shoreline response mode, a few important design considerations are obtained. These rules are summarized here, nevertheless they not further elaborated in this research.

[Pilarczyk et al., 2003] states that if the transmission coefficient is known, the shoreline response mode can be predicted from the long-shore width of the crest, the distance between the shore and the structure and the transmission coefficient. This rule of thumb is easily applicable after estimating the transmission coefficient, for a fixed location or width. A similar equation is proposed for multiple breakwaters in the long-shore direction.

The study of [Ranasinghe et al., 2006] suggests the breakwater should have a distance to the shore of at least 1.5 times the distance of the natural surf zone, to obtain accretion. Later [Ranasinghe et al., 2010] defined two non-dimensional variables predicting the shoreline response mode. For these variables, the grain size of the shore, incoming waveheight, water depth, freeboard and lateral crest width are needed. Following this rule per location can define boundaries for the desired crest height and/or lateral crest width.

Lastly, [Villani et al., 2012] suggests the flow patterns behind the structure determine the shoreline response mode for multiple structures.

B.1.3 Data bases DELOS

In this section, the newly added databases for the DELOS project are described. The databases are referred to with the abbreviations *UCA*, *UPC*, *GWK* and *M&M* in the main text. Table 2.2 shows the ranges of parameters involved in the tests.

UCA refers to the irregular wave tests performed at University of Cantabria, Spain, in 2001. *UPC* refers to the experiments in the Polytechnic University of Catalonia, Spain. In *UCA* and *UPC* a large range of the relative crest width $B/H_{s,i}$ have been tested. *GWK* refers to the large-scale tests in the Large Wave Channel of the Coastal Research Centre (FZK), in Germany. Finally, experimental data of structures armoured with Coreloc coming from Melito and Melby (*M&M*)(2000) is included [Van Oosten and Peixo Marco, 2005].

Next to the newly done experiments for the DELOS project, [Van der Meer et al., 2005] used the data on aquareefs from Hirose et al. (2002). This structure is protected by aquablocks. A sketch of such structure is shown in Figure B.4.

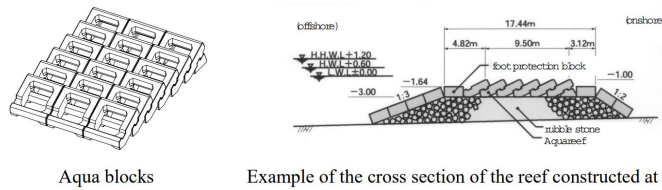


FIGURE B.4: Sketch of the aqua reef design from Japan, obtained from the paper of [Pilarczyk et al., 2003]

B.1.4 Double submerged breakwaters with "Channel"

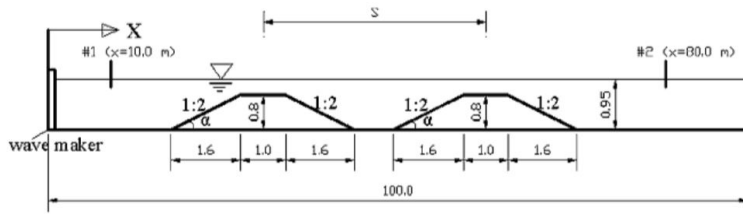
Here, the two existing studies on the spacing between two sub-merged breakwaters are described. The sketches of both studies are shown in Figure B.5. [Liang et al., 2015] used a wave model to find the optimal spacing relative to the incoming wavelength L_0 for wave attenuation. [Rambabu and Mani, 2005] used a numerical model to find the optimum clear spacing relative to the crest-width.

In the study from [Liang et al., 2015], two identical trapezoidal impermeable breakwaters are modelled with a slope of 1 : 2. The optimal spacing between the center of both crests (used abbreviation in this study: S , see Figure B.5a) was found to be 1.11, for a constant breakwater design and a regular wave condition with $R_c/H_i = 1$, $H_i = 0.15$ meters, $T = 2$ seconds and thus $\frac{H_i}{g \cdot T^2} = 0.0038$. This means the total *empty distance*¹ is equal to 2.73 meters. Reformulated this would mean that L_{ch}/L_0 has an optimum at 0.44 and L_{ch}/B has an optimum at 1.37. This study also concluded that the reflection from the second breakwater is dissipated when the wave propagates between the two breakwaters and the spacing has no influence on the reflection.

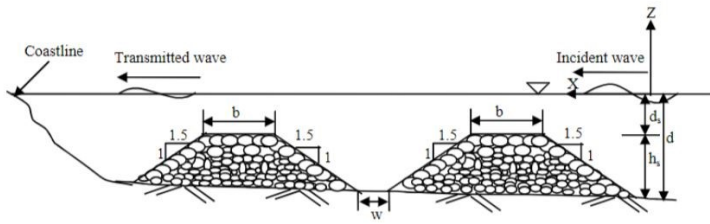
[Rambabu and Mani, 2005] also used a numerical model of two identical trapezoidal impermeable breakwaters with a slope of 1 : 5. The optimum clear spacing between two breakwaters (used abbreviation in this study: w , see Figure B.5b) w/B (or for a Reefy structure L_{ch}/B) has found to be 1.00. This study suggests that clear spacing between breakwaters has a less influence on controlling transmission compared to the study of [Liang et al., 2015], as can be seen in Figure B.7.

[Rambabu and Mani, 2005] is based on a set-up where the crest-width to depth ratio B/d is constantly 0.75, referred to as the optimum crest width for transmission reduction. Whereas, [Liang et al., 2015] used a B/d of 2.11 and thus much wider crests compared to the water depth. Furthermore, the slopes of structure [Liang et al., 2015] is steeper compared to [Rambabu and Mani, 2005]. The wave steepness of [Liang et al., 2015] lies in between the two steepnesses tested by [Rambabu and Mani, 2005].

¹ Empty distance is the length between the back toe of the front structure and the front toe of the back structure



(A) [Liang et al., 2015].



(B) [Rambabu and Mani, 2005].

FIGURE B.5: Details of set-up from numerical experiments on double-submerged breakwaters.

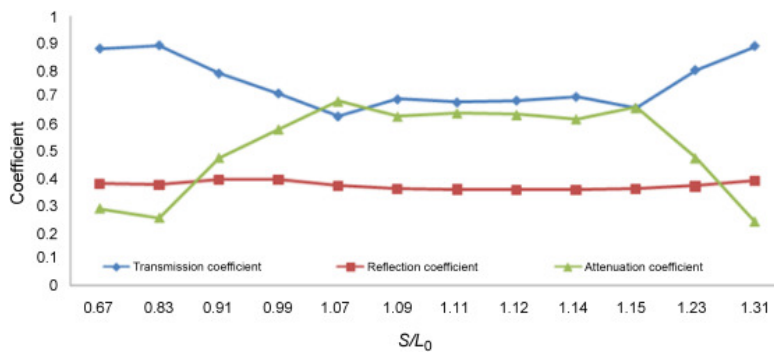


FIGURE B.6: Variation in transmission coefficient K_t , K_r and K_a ($=\sqrt{1 - K_t^2 - K_r^2}$), versus S/L_0 (relative spacing distance) for a regular wave with $\frac{H_i}{g \cdot T^2} = 0.0038$. Result from study of [Liang et al., 2015] on a double submerged breakwater.

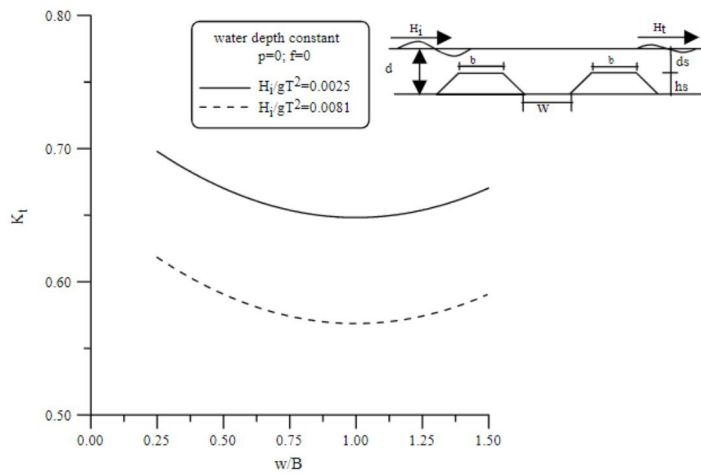


FIGURE B.7: Variation in transmission coefficient K_t versus w/B (relative distance) for a regular waves. Result from study of [Rambabu and Mani, 2005] on a double submerged breakwater. B is calculated as $b + b$.

B.2 ECOLOGICAL PERFORMANCE

B.2.1 Related physical processes

The placement of a Reefy structure is associated with a number of phenomena which can enhance the existing ecosystem and increase the abundance and biodiversity of organisms in the structure:

The high porosity and complexity can create a **sheltered area** in which multiple types of marine flora and fauna can live, increasing the species diversity. Furthermore, as waves travel through and over the structure, turbulence and vortex shedding is created. The nutrients are well distributed within the complex structure due to the **circulation of flow** within and behind the structure. Lastly, an increased porosity allows for the **renewal of coastal water** through the structure and thereby maintain the existing water quality.

The flow blockage of a structure creates **low-flow zones** at the lee-side as well as inside the structure. A low flow zone can be utilized as energy saving zones for fish to congregate and spawn. However, the flow should exceed a certain minimum as this can otherwise result in a deficit of oxygen and siltation. Most literature about structural design guidelines for ecological enhancement are based on the mean flow field around and within the structure, excluding the presence of waves. These methods are good to estimating for example the settlement of larvae and nutrient circulation in periods of critical low flow regimes [Losada et al., 2003].

B.2.2 Limiting conditions aquatic organisms

Here, the information which is summarized in Figure 2.4 is discussed per type of organism.

BARNACLES Barnacles are organisms which live in shallow and intertidal marine environments and do not exist in fresh waters. They are suspension feeders and use feathered like legs (called "cirri") to capture plankton from the water. Barnacles are non-mobile sessile organisms since they attach themselves to a hard substrate.

[Eckman and Duggins, 1993] conducted experiments to investigate amongst others the impact of a constant flow speeds between $0.02 - 0.25\text{m/s}$ on the growth barnacles (6 types)². The study concludes that for the tested species naturally experiencing turbulent conditions, the growth rate is not dependant on the flow field. Whereas the opposite is true for tested species which naturally experience weak flows. However, for this group the type of interdependence differs per species. For some, a decline of growth rates is observed for an increase in flow speed. On the other hand, an increase in flow speed to a maximum speed of 0.08 m/s is associated with an increase in growth rates for the *Balanus crenatus*, after which a decline is observed.

[Marchinko and Palmer, 2003] investigated four intertidal barnacles³. The study concluded that the size and shape of their cirri⁴ changed in response to the local hydrodynamic conditions to which they were exposed. For example, longer cirri are developed in low flow as these create larger feeding areas, whereas shorter ones are less vulnerable to damage and are developed in high energy environments. Nevertheless, [Li and Denny, 2004] concluded that for the *Balanus Glandula*, its capability to adapt their feeding mechanism ceases in wave velocities above $2-4\text{m/s}$. This value is associated with the limit above which barnacles can not feed themselves anymore in general [Geierman, 2007].

MUSSELS Mussels are organisms which live in shallow and intertidal environments, both in fresh- and salt water. They are sessile⁵ and feed themselves from filtering out suspended particles of the water inside their shells. [Hunt and Scheibling, 2001] investigated the dislodgement of two mussel types, named *Mytilus trossulus* and *Mytilus edulis*, in a wave-exposed environment in Canada. The study concluded that these type of mussels start to dislodge from their surface at water velocities higher than 7 m/s . About the growth of mussels, [Hammond and Griffiths, 2004] concluded the growth of mussels increases for an increase in wave forces, until a certain limit is reached after which a decrease is expected again. This study is based on mussel beds in South Africa, with the dominant mussel type of *Mytilus galloprovincialis*.

SEA URCHINS AND SEA STARS Sea urchins and sea stars are both mobile species, which use their tube feet move and attach themselves temporary to the structure. They can be found in intertidal regions as well as in deep in the oceans. [Siddon and Witman, 2003] investigates the dislodgement of a sea urchin type and a sea star type, named urchin *Strongylocentrotus droebachiensis* and *Asterias forbesi* respectively, at a depth of 1 to 4 meters in a wave-exposed coast of the USA. It is concluded from this study that the maximum velocity leading to dislodgement of 95% varies between 7.5 and 9.9 m/s .

² The names of these barnacles are *Balanus glandula*, *Semibalanus Cariosus*, *Pollicipes polymerus*, *Pseudochitinopoma occidentalis*, *Membranipora membranacea* and *Balanus crenatus*. The first three naturally occur in turbulent conditions. The last three naturally occur in weak flow conditions.

³ The names of the four barnacles investigated by [Marchinko and Palmer, 2003] are the *Balanus glandula*, *Chthamalus dalli*, *Semibalanus cariosus* and the *Pollicipes polymerus*.

⁴ The feathered like legs are called "cirri" and are used to capture plankton from the water.

⁵ Sessile means the organism attaches themselves to a hard substratum and do not move.

[Kawamata, 1998] investigated the feeding- and moving limits for another urchin type, named the *Strongylocentrotus nudus*, in a laboratory experiment with waves. From this it is concluded the urchin stops feeding if the maximum velocity exceeds 0.4 m/s and the urchin can not move if the velocity exceeds 0.7 m/s. These velocity limits are based on the mean of $1/3^{th}$ of the peak velocities.

MARINE SNAIL A marine snail is a slow moving species, living in salt water only. This group of species is very large and diverse. [Alfaro and Carpenter, 1999] investigated the dislodgement of a marine snail type, named the *Astraea undosa*. This type naturally occurs in the inter tidal zone as well as in deeper waters. The study is on flow induced hydrodynamic forces and concluded that for all sizes of this snail type, 50% dislodgement occurred at a velocity of 4 m/s and 100% dislodgement occurred at a velocity of 8 m/s.

CORAL LARVAE Corals reproduce themselves during mass spawning events, when all coral species in the area simultaneously release their eggs and sperm. Thereafter, the larvae settle within a few days to weeks. [Hata et al., 2017] investigated the impact of the flow speed on the settlement and distribution of coral larvae. The study concluded that the swimming speeds of coral larval are very low compared to the water flow velocities expected around a reef in an open ocean, even in the low-flow wake region. Therefore, the study concludes that the settlement and distribution is dependent on the turbulence within- and around the structure. To enhance the turbulence and thereby enhance the capture of coral larvae that pass the reef, the authors advise to increase the complexity of the structure. Furthermore, the study shows that waves especially have a negative impact on the settlement of larvae located at the surface on top of the reef. No limiting flow velocities are given.

B.2.3 Modelling tool DELOS

In the book *Environmental Design Guidelines for Low Crested Coastal Structures* different tools for predicting the ecological impact of a low crested structure are explained [Hawkins et al., 2010], as well as on the official website of the DELOS deliverables. One example is highlighted here, developed during the DELOS project and based on a three step approach, namely: predictive modelling, selection of biotopes⁶ and collection of baseline data and analysis of impacts. During the first step, predictive modelling in Delft3D and MIKE 21 simulates amongst others the ecological processes and water quality parameters after building. Next, a marine habitat classification model tool named BioMar, designates for each cell a set of BioMar class values for physical parameters that came out of the numerical model. Next, the biological community which can occur within these set of parameter class values is linked to the cell. Furthermore, in order to calibrate the model and evaluate the impact, baseline data needs to be collected at the site. This method is very useful to predict the impact of an AR system on the biotopes, however it is very site specific and should be done for every case.

⁶ Biotope is the habitat together with its recurring associated community of species, operating together at a particular scale [Aberg et al.].

B.3 WATER WAVES

Every wave has a wave height H , wave length L and wave period T . The steepness can be described as the wave height divided by the length $s = H/L$. Generally, a wave steepness of 0.01 indicates a swell sea environment and a steepness of 0.04 to 0.06 a wind sea environment. In order to describe a propagating wave field, several wave theories exist. Each theory is applicable to a specific range of wave characteristics and water depths. The water depth plays an important role, because once the wave feels the bottom, the particle motion becomes more elliptical, the wave steepens and the wave length decreases. The different wave theories and their ranges of applicability are described in Figure 4.3.

Linear wave theory

The simplest way to describe a wave, propagating along the x -direction is given in equation B.3. This is based on the linear wave theory. In linear wave theory the continuity and momentum balances for a constant density are linearised. The analytical solution of this linearization is a long-crested harmonic wave travelling in the positive x -direction. These sort of waves travel in relatively deep water with no frictional losses. The shape of this progressive two-dimensional gravity wave, in time t and location x , is described by the sine function in equation B.3.

$$\eta(x, t) = a \sin(\omega t + kx) \quad (\text{B.3})$$

Here, the η stands for the surface elevation, a stands for the wave amplitude, ω is the angular velocity and k is the wave number.

For such a wave, the particle velocities, called orbital velocities, are given by equation B.4 and B.5. In deep water, the particle path is in an orbital motion and in shallow water the particles move in ellipses.

$$u_x = \omega a \frac{\cosh[k(d+z)]}{\sinh(kd)} * \sin(\omega t - kx) \quad (\text{B.4})$$

$$u_z = \omega a \frac{\sinh[k(d+z)]}{\sinh(kd)} * \cos(\omega t - kx) \quad (\text{B.5})$$

In the absence of an external force, a wave is subject to only gravitation and called a free wave. For these waves, the relationship between the angular velocity and the wave number can be found in equation B.6. This is called the dispersion relation and shows that the wavelength $L = 2\pi/k$ is depending on the local water depth h and the period $T = 2\pi/\omega$.

$$\omega = \sqrt{gk \tanh(kd_0)} \quad (\text{B.6})$$

The wave length decreases as the wave propagates from deep to shallow water. With $L_0 = gT^2/2\pi$ in deep water and $L = T\sqrt{gh}$ in shallow water. Based on the dispersion relation, the phase speed can be expressed as in B.7 from which it follows that in deep water, longer waves travel faster than shorter waves.

$$c = \frac{gT}{2\pi} \tanh(kd) \quad (\text{B.7})$$

A general property from progressive linear waves is the fact that the kinetic and potential energy densities have an equal contribution to the mean wave energy. The contributions and total wave energy can be estimated with linear wave theory by integrating the energy components over the depth. Adding the kinetic- and potential energy together gives the total energy density, which is proportional to the wave height, as can be seen from equation B.8.

$$E_{tot} = \frac{1}{8} g \rho H^2 \quad (\text{B.8})$$

The wave energy travels in the direction of the wave with the speed of the group velocity, which is related to the phase velocity via equation B.12.

Wave groups

In an irregular wave field, different groups of waves which travel in the same direction and have different frequencies, can interfere with each other. This creates a pattern of nodes and anti-nodes in the surface elevation, where the different frequencies reinforce each others if they are in phase and cancel each other out if they are out of phase. The formation process of wave groups from two harmonic waves, with a different frequency, is presented in Figure B.8. The process can mathematically be described with equation B.9.

$$\eta(x, t) = 2a * \cos\left(\frac{\omega_1 - \omega_2}{2}t - \frac{k_1 - k_2}{2}x\right) * \sin\left(\frac{\omega_1 + \omega_2}{2}t - \frac{k_1 + k_2}{2}x\right), \quad (\text{B.9})$$

with the sinus wave representing the carrier wave and the cosines the envelope wave, which regulates the amplitude of the carrier wave. The phase speed of the carrier wave is equal to:

$$c_{carrier} = \frac{\omega_1}{k_1} \quad (\text{B.10})$$

The phase speed of the envelope, called the group velocity is equal to :

$$c_{envelope/group} = \frac{\Delta\omega}{\Delta k} \quad (\text{B.11})$$

From this it follows that, if the differences between the frequencies, and between the wave numbers is infinitely small, the group velocity follows from:

$$c_g = cn = \frac{1}{2} \left(1 + \frac{2kh}{\sin(2kh)} \right) c \quad (\text{B.12})$$

This means the speed of the individual waves, the phase speed, is always larger or equal to the group velocity.

The length and period of the wave groups are $L_{group} = \frac{2\pi}{\Delta k}$ and $T_{group} = \frac{2\pi}{\Delta \omega}$ respectively.

For narrow spectra, the wave field consists of several wave groups within a small frequency range. This results in many interactions between the groups, which results in a lot of groupiness and wave motion on lower frequencies compared to the wind waves themselves. This is also referred to as an infra-gravity wave, see Figure B.8

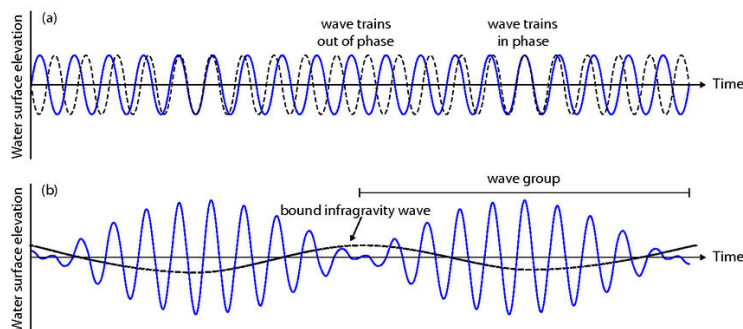


FIGURE B.8: Upper figure: The merging of two wave trains of slightly different wave frequencies, but the same amplitude. Lower figure: The two wave trains form wave groups and induce a long bound wave, called infra gravity wave. [Wright et al., 1999]

Non linear wave theories

The non-linear wave theories are applicable when the sinusoidal shape of the linear wave theory no longer holds. The wave profile changes when a wave becomes too steep in deep water or propagates into shallower water and starts interacting with the bottom (shoaling). Non-linear waves have higher crests than troughs and have frequency and amplitude dispersion. The deformation of the wave profile can continue until a certain limit is reached and the wave breaks. There exist several non-linear wave theories, as described in Figure 4.3.

Shoaling

Shoaling is a consequence harmonic waves interacting with the bottom. As a wave propagates over a gently sloping seabed, with no currents, it retains its frequency, but the water depth decreases. Since the dispersion relation is still valid, the wave length decreases and thus also the phase velocity. Initially, the group velocity increases slightly, but eventually it also decreases.

As the wave propagates into shallower water, the phase speed approaches the group velocity and the phase speed becomes less depended on the frequency (non dispersive). Such variations in group velocity cause variations in the local wave energy, but there is no dissipation of the energy, the amplitude of the wave increases $E_{g,1} * c_{g,1} = E_{g,2} * c_{g,2}$. The energy is proportional to the H^2 , see equation B.8.

The effect of shoaling is initially to decrease, but then to increase the wave amplitude. This phenomena is called energy bunching. As the group velocity approaches zero at the waterline, the amplitude theoretically can grow to infinity. Nevertheless, other processes such as wave breaking prevent this from happening.

Waves interact with the bottom based on their relative depth, so waves with longer wave lengths, become shallow water waves first and interact with the bottom at deeper depths [Anderson et al., 2011]. Therefore, the shoaling effect occurs first for waves at the lower frequency side of the spectrum. Therefore, the mean frequency is slightly shifted towards a lower frequency for irregular waves, which is called a down-shifting.

Set-up

Set-up is the accumulation of water at the lee side of the structure offshore from an impermeable shoreline. The set-up behind the structure is partly caused by a decrease in horizontal momentum-flux (shear stress) after breaking which needs to be compensated by an increase in water level. The other part of set-up is due to the mass-transport of water over the structure. The set-up results in a hydraulic gradient in the water level and therefore creates a seaward flow [Calabrese et al., 2008]. This flow can be cyclic as waves travel over the crest in opposite direction. Different empirical formulae for the prediction of the 2D set-up are discussed by [Jonker, 2020].

For a better understanding of the 3D circulation patterns in the lee-side of an AR, the set-up processes need to be considered. Increased set-up reduces the effectiveness of the freeboard of structures and can cause shoreline erosion [Calabrese et al., 2008].

Wave breaking

Wave breaking can occur both in deep water (white-capping) and shallow water (bottom friction and depth induced). For intermediate and deep water depths, Miche formulated the following steepness breaking limit [Saket et al., 2017]:

$$\frac{H_b}{L_b} = 0.142 \tanh\left(\frac{2\pi d_b}{L_b}\right), \quad (\text{B.13})$$

which becomes equal to 0.142 in deep water. For this study, the wave breaking in shallow water is more relevant.

In shallow coastal areas, the most non-linear process is depth induced breaking, also called surf-breaking. For the depth limited breaking of monochromatic waves, McCowan (1894) formulated a breaker index of 0.78. This means if the ratio between the wave height and the

water depth exceeds 0.78, wave breaking occurs. For an irregular wave field, the breaker index to determine the H_{max} is approximately 0.75, but can vary between 0.5 and 1.5, depending on the bottom slope, wave steepness, wind etc.

For depth-limited breaking, there exist rules to predict the type of breaking if the shore is a flat beach, see Figure B.9. This can be done, using the Iribbaren number ζ , which is the ratio of the steepness of the structure to the relative steepness of the wave, [Holthuijsen, 2010]:

$$\zeta = \frac{\tan\alpha}{\sqrt{H_0/L_0}} \quad (\text{B.14})$$

The following types of breaking are found per Iribbaren number:

- Surging or collapsing $\zeta \geq 3.3$
- Plunging $0.5 < \zeta < 3.3$
- Spilling $\zeta < 0.5$

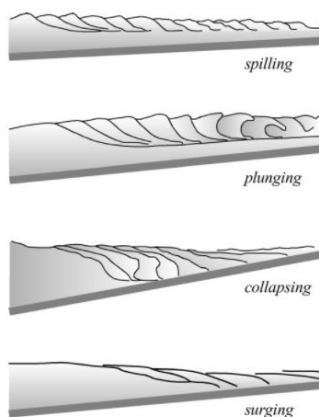


FIGURE B.9: The four main types of depth-breaking waves. [Holthuijsen, 2010]

BREAKING OVER SUBMERGED BREAKWATERS It has been observed by both [Bleck and Oumeraci, 2002] and [Smith and Kraus, 1990], that a return flow over the structure affects the breaking waves. It increases the breaker height index and leads to wave breaking before the incident wave reaches the critical waveheight. From these observations, [Bleck, 2006] formulated three new breaking types, as shown in Figure B.10. As the freeboard decreases, the breaking type tends to move from spilling to drop-type of breaking.

In real cases of coastal areas protected by submerged breakwaters, these phenomena are not observed. Probably because return flow behind the structure behaves different on a 3D scale [Losada et al., 2003]. Furthermore, [Hattori and Sakai, 1995] concluded that the return flow over the crest of the structure reduced if the porosity of the structure increased. As a consequence, less collapsing wave breaking occurs.

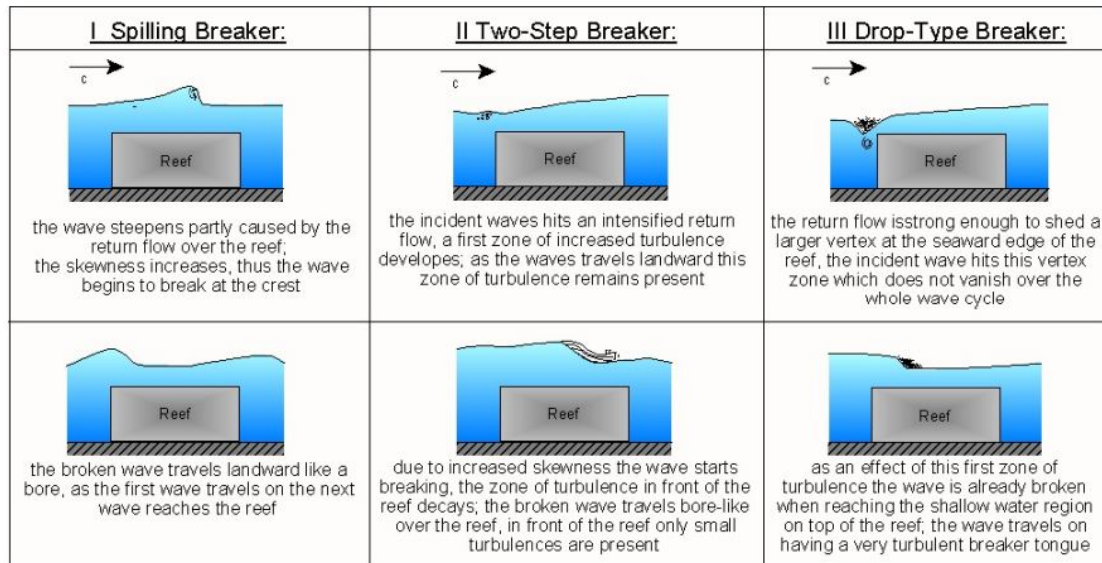


FIGURE B.10: Breaker types at shallow reefs, obtained from visual observations at the laboratory experiments of [Bleck and Oumeraci, 2002]. Spilling, plunging, collapsing and surging breaking types are the globally known categories. See appendix B.3.

Lastly, [Bleck, 2006] compared his observations of non-breaking - and breaking waves travelling over a submerged breakwater in a 2D wave flume. The study concluded that for breaking waves, the seaward vortex changed into a much more turbulent region with mixing of air with water particles and that this turbulence travels further with the wave. On the other hand, the energy losses in the landward vortex became less significant.

Non-linear wave-wave interactions

The resonance condition for three wave components, called triad-resonance, is as follows: for two freely propagating waves, the sum of their frequencies and wave numbers, needs to be equal to the frequency and wave number of a third, freely propagating wave.

$$f_1 + f_2 = f_3 \text{ and } k_1 + k_2 = k_3 \quad (\text{B.15})$$

This condition can only be complied with in very shallow water, where non dispersive waves exist. When the wave components with subscript 1 and 2 are located near the peak frequency of the unimodal incident spectrum, they will transfer energy to the higher and lower frequencies. Namely, to respectively the difference frequency ($f_1 - f_2$) and the sum frequency ($f_1 + f_2$). For a narrow banded spectrum, the difference of the frequencies is small and the generated low-frequency wave that is formed is called a sub-harmonic, or infra-gravity wave. The sum of the frequencies on the other hand generates a super-harmonic, high-frequency peak at twice the peak frequency, and sometimes also peaks at higher multiples of the peak frequency. This added energy is superimposed at the freely propagating energy at this frequency, but it is bound to the primary wave. This distinction between bound and freely propagating waves is not visible from the spectra.

C.1 HYDRODYNAMIC PERFORMANCE

c.1.1 Wave decomposition methods

A wave gauge is a device which has been used to measure the waves during the experiments, a more in-dept explanation is given in chapter 3.2.1. Here, the method for processing the data from these devices is explained.

The total measured signal of a wave gauge consists of an incoming- and reflected wave field. There are three main methods used in hydraulic studies to separate the incoming and reflected wave signal from each other based on linear wave theory in a one-dimensional wave field. These methods are referred to by their authors name, namely [Goda and Suzuki, 1977] (G&S), [Mansard and Funke, 1980] (M&F) and [Zelt and Skjelbreia, 1993] (Z&S). The differences and similarities between these methods are shortly described here.

All three methods are based on the same principle, namely the assumption that the wave elevation is a sum of waves travelling with a different frequency, phase and amplitude ¹. Another assumption which is of importance for these methods, is that these waves travel at their own individual phase velocity, which can be described by the dispersion relation ².

There are also some differences between the methods. The G&S method measures the waves in two points and does not account for any noise from the incoming signal. The M&F on the other hand, uses three points to measure the signal. The information from the third wave gauge is used to minimize the error through a least-square analysis. An innovation over this method is made by Z&S, which can be applied to an arbitrary number of points. It uses a non-uniform weighting coefficient, where the gauges closest to the point of interest are weighted more heavily [Zelt and Skjelbreia, 1993]. For three wave gauges the results of the two last methods are the same. All three methods assume the wave dissipation between the measuring points is negligible.

The method of Z&S is used for the current research. The reader is referred to the open-source paper [Zelt and Skjelbreia, 1993] for more details on their mathematical procedure.

c.1.2 Spectral analysis

From the decomposition of the surface elevation in a reflected- and incoming signal, for each wave gauge a variance density spectrum is created on a Fast Fourier Transform (FFT). From

¹ If regular waves, they are expected to have the same amplitude.

² This assumption has been found to be a good approximation for finite and infinite depths of water [Mansard and Funke, 1980].

this, the amplitude and thus the variance of each frequency is found. Multiplying the variance with the density ρ and the gravitational acceleration g gives the energy density spectra:

$$E_{\text{energy}}(f) = \rho g \lim_{\Delta f \rightarrow 0} \frac{1}{\Delta f} E\left\{\frac{1}{2}\underline{a}^2\right\} \quad (\text{C.1})$$

In equation C.1, the \underline{a} is the amplitude of the harmonic component f and E the expected value of the variance $\frac{1}{2}\underline{a}^2$. The resolution of the raw spectrum equals $\Delta f = 1/D$, with D the duration of the time record. The irregular wave files have a duration of 20-30 minutes and the regular wave files around 3-5 minutes. Nevertheless, to reduce the error the time record is divided into p segments that do not overlap, and each section is Fourier analyzed again. The frequency resolution is not positively impacted from this as it is multiplied with $p \delta f = p * \Delta f$, but the error reduces by a factor of \sqrt{p} : $100\% \frac{1}{\sqrt{p}}$ [Holthuijsen, 2010]. Phasbeen chosen as 40, resulting in a $\delta f = 0.02 - 0.03 \text{ Hz}$ and an error in spectral densities of about 15% for irregular waves. For regular waves the $\delta f = 0.13 - 0.22 \text{ Hz}$ and the same error in spectral densities is achieved. As the spectral density is most important for the determination of H_{m0} , the number of segments p is chosen relatively large.

c.1.3 Foreshore effect based on energy balance

In this section the method to eliminate the foreshore effect via the energy conservation balance is investigated. When the waves travel over the structure, a percentage of the incoming energy (E_i) is dissipated by the structure (E_d). Another percentage is reflected (E_r) and the rest of the energy is transmitted (E_t) through and over the structure into the sheltered area behind the structure. The energy balance of these processes is described in equation 4.1.

$$E_i = E_t + E_r + E_d \quad (\text{C.2})$$

As described in the linear wave theory, the wave energy is proportional to the squared wave height H^2 , see equation B.8. Therefore, for linear waves travelling at the same depth and celerity, equation 4.1 can be written in terms of the waveheight as:

$$H_{m0,i}^2 = H_{m0,t}^2 + H_{m0,r}^2 + H_{m0,d}^2 \quad (\text{C.3})$$

Dividing equation C.3 by $H_{m0,i}^2$ gives the energy balance expressed in structural performance coefficients:

$$\frac{H_{m0,i}^2}{H_{m0,i}^2} = \frac{H_t^2}{H_{m0,i}^2} + \frac{H_{m0,r}^2}{H_{m0,i}^2} + \frac{H_d^2}{H_{m0,i}^2} \rightarrow 1 = K_t^2 + K_r^2 + K_d^2 \quad (\text{C.4})$$

The K_t of equation C.3 is the transmission coefficient, the K_r is the reflection coefficient and K_d is the dissipation coefficient. The three most important structural performance parameters for submerged breakwaters. From equation C.3, the general used expression of the dissipation follows:

$$K_d^2 = 1 - (K_t^2 + K_r^2) \quad (\text{C.5})$$

During the tests with a structure in the flume, equation C.3 can be written for the area between wave gauge 4 and 9 as:

$$1 = K_t(s, f)^2 + K_r(s)^2 + K_d(s)^2 + K_d(f)^2, \quad (\text{C.6})$$

where $K_t(s, f)$ and $K_r(s)^2$ can be calculated from the wave gauge data of the test with a structure. For the $K_d(s)^2$ and $K_d(f)^2$, this is not possible. It is assumed the dissipation over the foreshore is the same in the tests with - and without a structure and the reflection over the foreshore between wave gauges 4 and 9 is negligible³. Therefore, the reference test can be used to calculate $K_d(f)^2$, see equation C.7.

$$1 = K_t(f)^2 + K_r(f)^2 + K_d(f)^2 \rightarrow K_d(f)^2 = 1 - K_t(f)^2, \quad (\text{C.7})$$

The $K_t(f)^2$ from equation C.7 can be calculated from the wave gauge data of the reference test. Adding equation C.7 to equation C.6, gives the following result:

$$1 = K_t(s, f)^2 + K_r(s)^2 + K_d(s)^2 + (1 - K_t(f)^2), \quad (\text{C.8})$$

where the only unknown is $K_d(s)^2$. When equation C.5 is rewritten and only the effects of the structure are considered, equation C.9 is obtained.

$$K_d(s)^2 = 1 - (K_t(s)^2 + K_r(s)^2) \quad (\text{C.9})$$

Combining equation C.9 and C.8 gives the following formulation of $K_t(s)^2$:

$$K_t(s)^2 = 1 + K_t(s, f)^2 - K_t(f)^2, \quad (\text{C.10})$$

which can be solved for every structural test in combination with a reference test of the same wave conditions.

This methodology has been proved to be not applicable for tests where $K_t(f)^2 > 1 + K_t(s, f)^2$, which was the case for partly emerged structures. Therefore, this method is not adopted and the difference between the waveheight at WG789 for the test with- and without a structure is used as the transmission coefficient.

c.1.4 Relative MSE Zelt and Skjelbreia

In Figure C.1 the RMSE for the regular wave tests with different upper frequency limits values are compared. It can be seen that an upper frequency limit at $5 * f_p$ results in the smallest RMSE at WG 456 and 789. Nevertheless, due to the erroneous peak around 3.2Hz, the upper frequency has been set to 3Hz. More details can be found in the main text.

³ It is assumed the wave damper gives minimal reflection outcomes, furthermore it is expected that if there is a reflected wave from the wave damper, it is too small to pass through the structure during a test with a structure in place

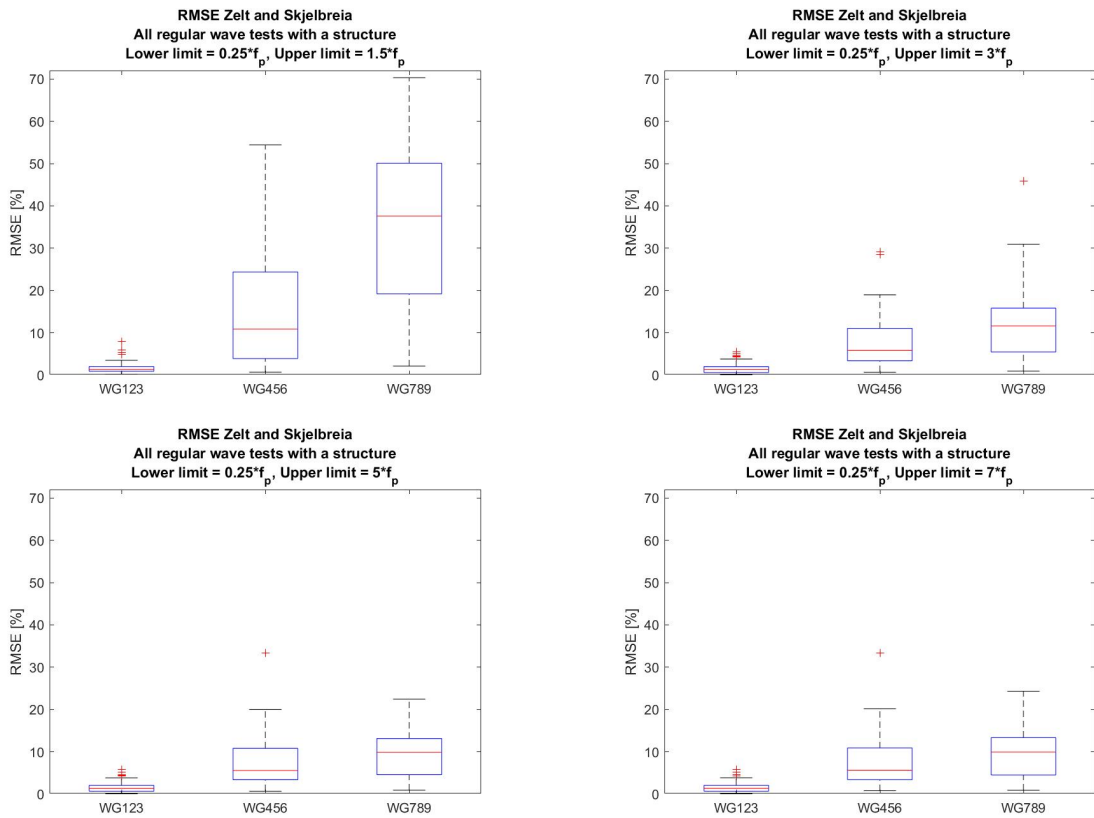


FIGURE C.1: Boxplot of the relative mean square error of Zelt and Skjelbreia method. Between the figures, the upper frequency limit is changed. These are the results for all regular wave tests with a structure.

In Figure C.2 the RMSE for the reference regular wave tests is shown.

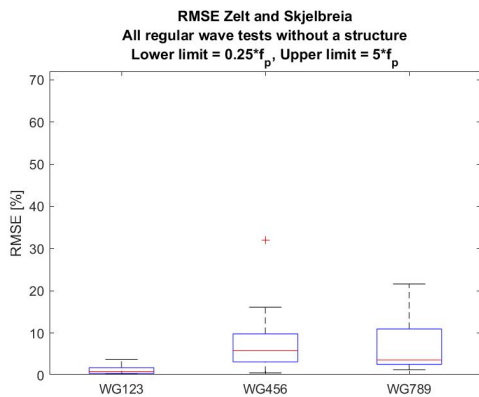
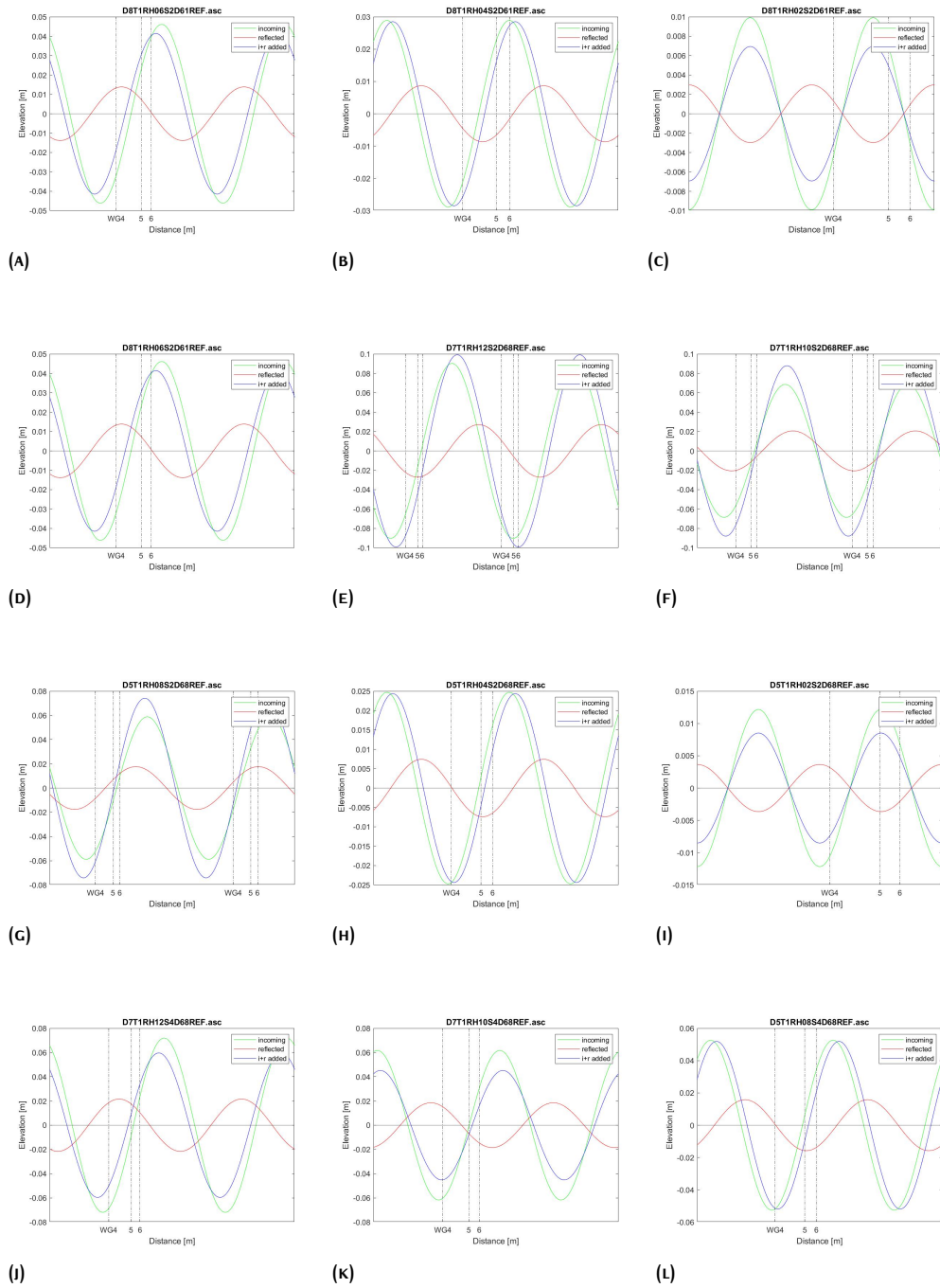
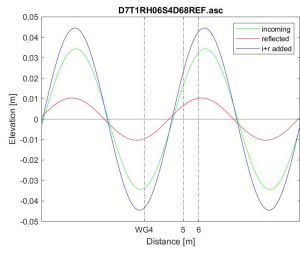


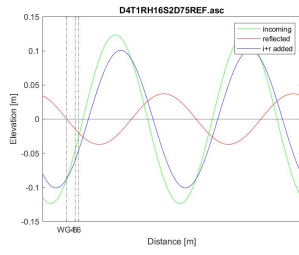
FIGURE C.2: Boxplot of the RMSE of the measured elevation compared to the Z&S calculated elevation for all regular wave tests without a structure.

c.1.5 Relative spacing wave gauges

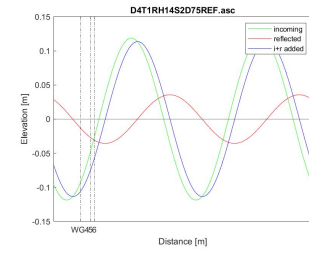




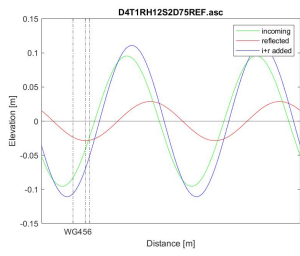
(M)



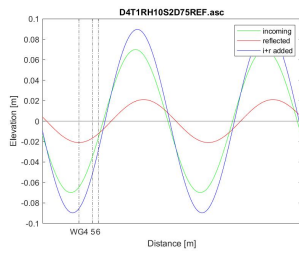
(N)



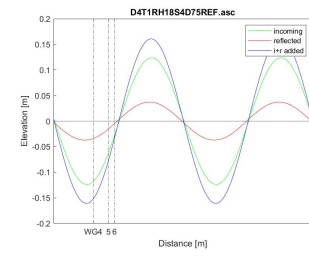
(O)



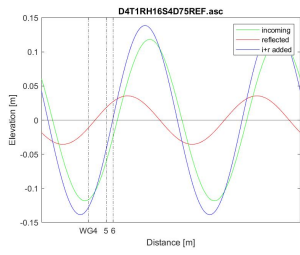
(P)



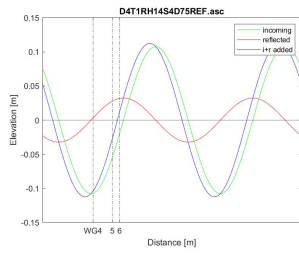
(Q)



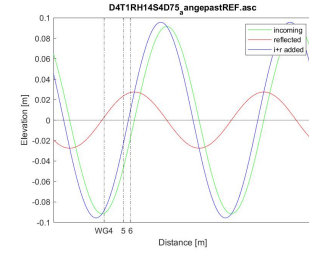
(R)



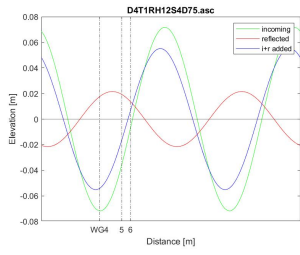
(S)



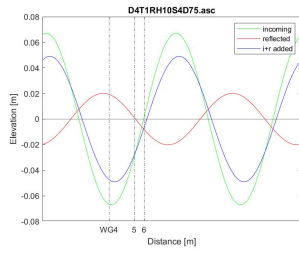
(T)



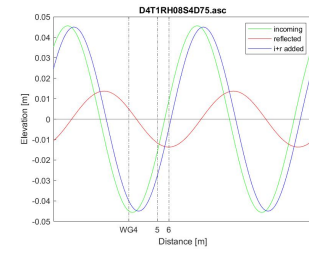
(U)



(V)



(W)



(X)

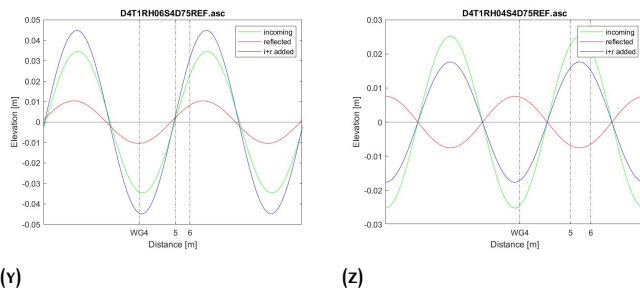


FIGURE C.3: Regular wave conditions converted to perfect sinus wave based on H and L measured at WG456. The distance of the wave gauges with respect to the wave length is visualized in each figure.

C.2 ECOLOGICAL PERFORMANCE

In this section, some extra information from the processing of the EVM data is discussed with the help of figures.

REMOVE MEASUREMENTS BEFORE WAVES OCCURRED In Figure C.4 an example is shown in which the beginning of the EMS-recording had to be removed, because of the absence of waves.

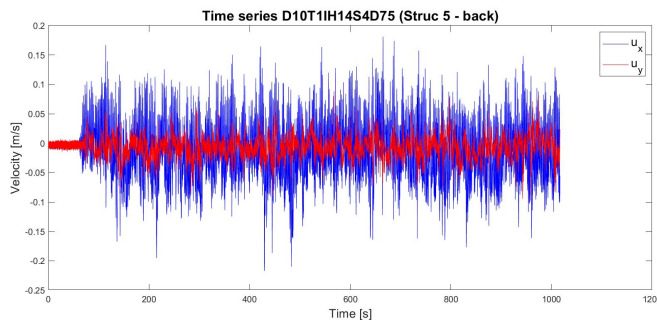


FIGURE C.4: Example of a time-record in which the waves appeared after the start of the velocity measurements. Here, the signal before $x=200$ s is removed.

REMOVE SPIKES In Figure C.5, an example of a time-record is shown in which the EVM was switched from its location during the test. Both time recordings for the comparison of the eCDF are adjusted to the same length.

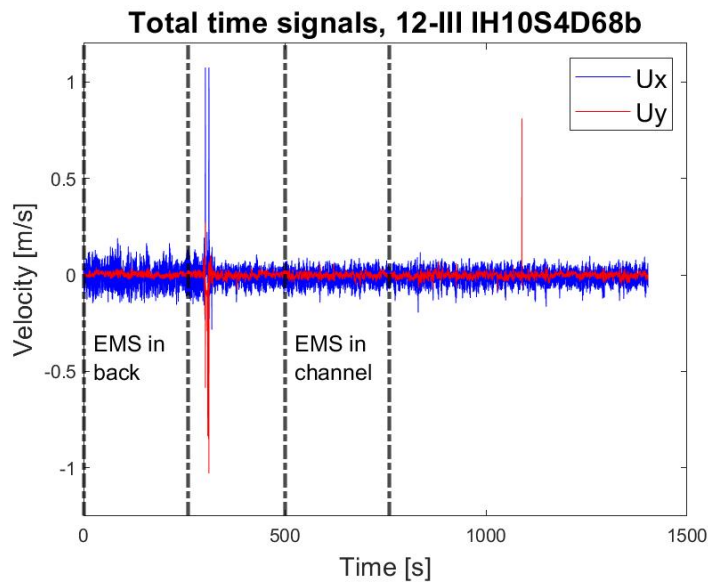


FIGURE C.5: Example of a time-record in which the EVM has been changed from location during the record. Furthermore, a pike is observed at 1090 seconds from the vertical velocity.

INVESTIGATE LOW FREQUENCY VELOCITIES EVM DATA Here, the energy present at the lower frequencies of the horizontal velocity spectra are investigated for all irregular wave conditions which are used in the analysis of the ecological performance. The lower frequency limit for the lowband-pass-filter is set at $0.25 * f_p$ and the resulting time signal is plotted on top of the total time signal. First of all, for the tests without a structure (on left top of Figures C.6, C.7, C.8, C.10 and C.11), the lower frequencies are expected to be part of a bound infra gravity wave, because the trough of the low frequency signal often coincides with the largest velocities from the short wave group. This peak correlation behaviour is less clear, or completely absent, in the back or channel of a structure. The latter is explained from the fact that more turbulent conditions are expected in a wake region. However, a cyclic pattern can sometimes still be observed in the wake region. In this situation, also a return flow from the mass transport over a structure is known to cause these cyclic patterns with the wave groups. All in all, the conditions in the wake are the result of an interplay between many different phenomena, which makes it more difficult to predict the expected observations (infra gravity waves, cyclic return flow due to increased mass transport over the structure, turbulence, undertow).

Secondly, the mean horizontal velocity is also shown in all figures. It can be seen that the velocities have a mean seaward direction, which could show that there is an undertow present. Furthermore, the mean velocity is smaller for the measurements in front of the structure compared to in the wake regions behind the structure. Thus, a part of the undertow is blocked by the structure. Nevertheless, in front the flow still has a net seaward direction, thus a part of the return flow is also able to flow through the structure.

Furthermore, in Figure C.11 it can be seen that the mean seaward flow velocity is highest behind structure 8-0, after which structure 8-I follows and it smallest behind structure 8-V. This

suggests that an increase in channel length decreases the mean seaward flow velocity measured at the back, the same is observed in Figure C.9, in which structure 12-I and 12-III are compared.

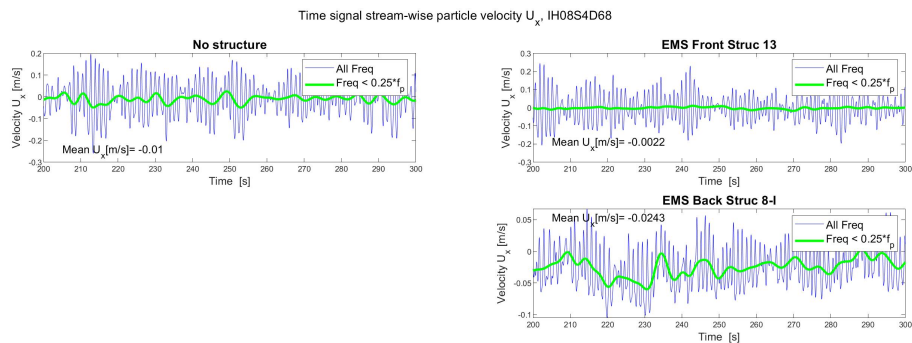


FIGURE C.6: Comparison of the horizontal velocity time-signal from the lower frequencies ($0.25 * f_p = 0.23$ Hz) and the total time-signal, for the filtered signal excluding all frequencies above 3 Hz. Wave condition 19. The time series for the test without a structure is given together with the time series for different locations of the EMS around structure 13 and 8-I.

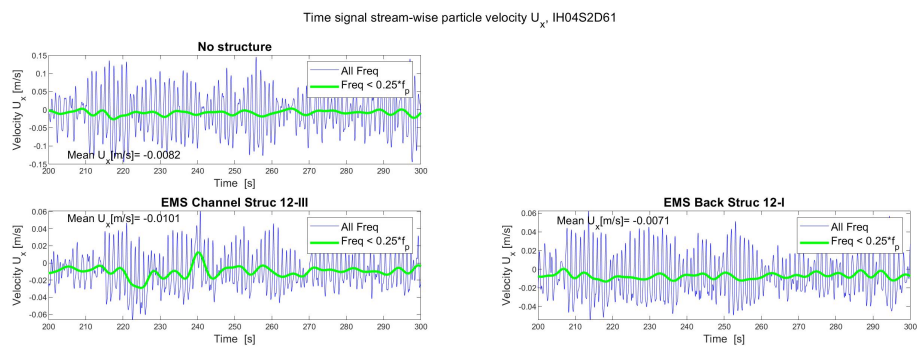


FIGURE C.7: Comparison of the horizontal velocity time-signal from the lower frequencies ($0.25 * f_p = 0.20$ Hz) and the total time-signal, for the filtered signal excluding all frequencies above 3 Hz. Wave condition 5. The time series for the test without a structure is given together with the time series for different locations of the EMS around structure 12-III and 12-I.

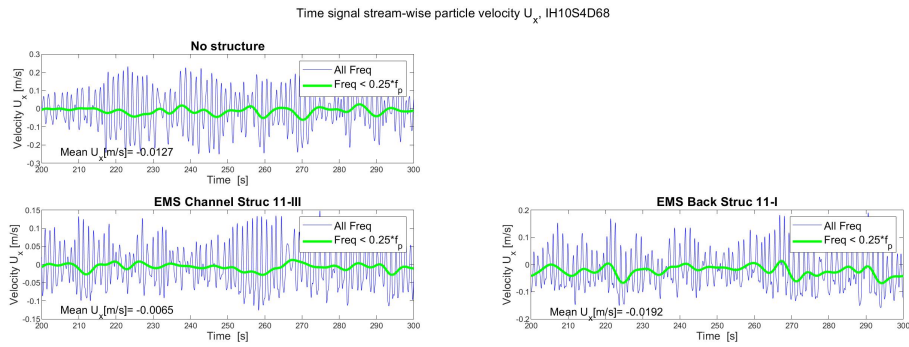


FIGURE C.8: Comparison of the horizontal velocity time-signal from the lower frequencies ($0.25 * f_p = 0.18$ Hz) and the total time-signal, for the filtered signal excluding all frequencies above 3 Hz. Wave condition 18. The time series for the test without a structure is given together with the time series for different locations of the EMS around structure 11-III and 11-I.

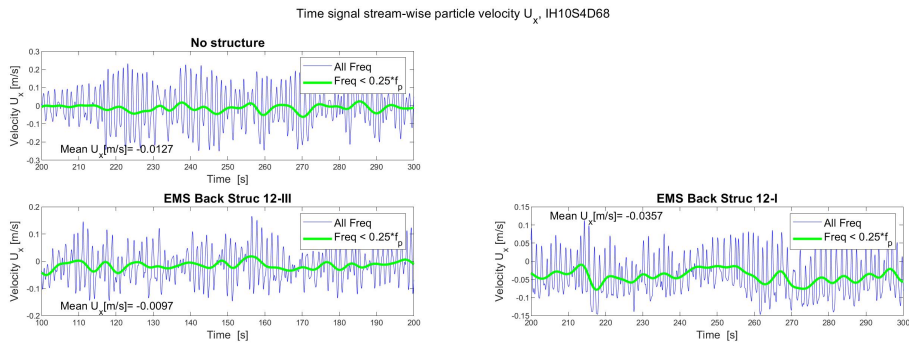


FIGURE C.9: Comparison of the horizontal velocity time-signal from the lower frequencies ($0.25 * f_p = 0.18$ Hz) and the total time-signal, for the filtered signal excluding all frequencies above 3 Hz. Wave condition 18. The time series for the test without a structure is given together with the time series of the EMS at the back of structure 12-I and 12-III.

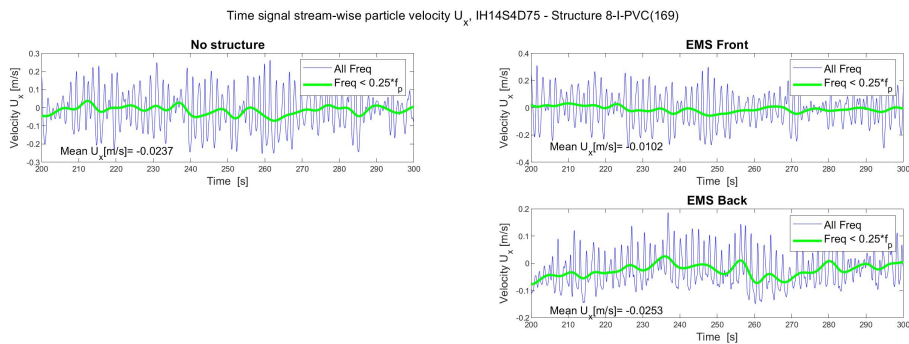


FIGURE C.10: Comparison of the horizontal velocity time-signal from the lower frequencies ($0.25 * f_p = 0.16$ Hz) and the total time-signal, for the filtered signal excluding all frequencies above 3 Hz. Wave condition 35. The time series for the test without a structure is given together with the time series for different locations of the EMS around structure 8-I-PVC(169).

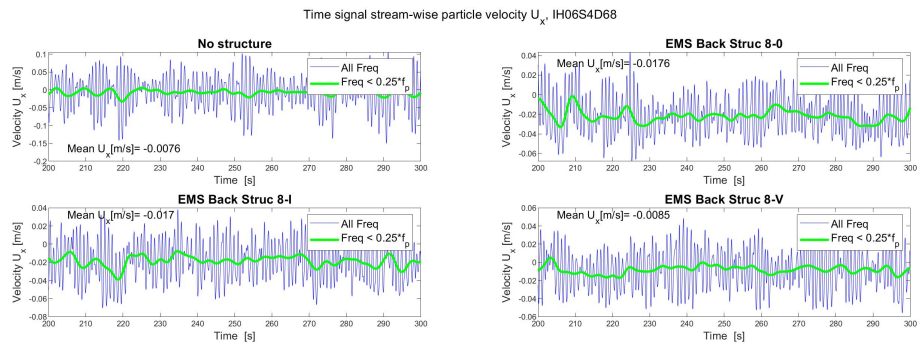


FIGURE C.11: Comparison of the horizontal velocity time-signal from the lower frequencies ($0.25 \cdot f_p = 0.25$ Hz) and the total time-signal, for the filtered signal excluding all frequencies above 3 Hz. Wave condition 20. The time series for the test without a structure is given together with the time series of the EMS at the back of structures 8-0, 8-I and 8-V.

The findings on the lower frequencies can be an interesting field for further research.

D

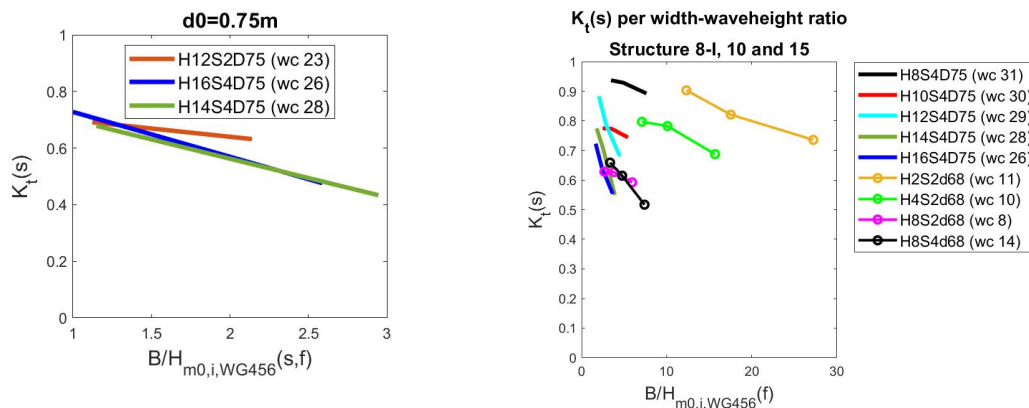
RESULTS HYDRODYNAMIC PERFORMANCE RESULTS

In this section some additional graphs of the results from the experiments and from other studies are represented. These graphs are referred to in the main text and shortly introduced here as well.

D.1 CREST WIDTH

D.1.1 Crest-width relative to incoming waveheight

The crest width has also been investigated for the dimensionless variable of $B/H_{m0,i}$. The results for $k_t(s)$ are plotted in Figure D.1a and D.1b. As can be seen, $K_t(s)$ has a negative correlation with $B/H_{m0,i}$. In general, the gradient increases if $H_{m0,i}$ increases. The same had been observed is the L_0 decreased. This result implies steeper waves are more affected by an increase in crest-width, as these waves are already near the critical steepness and more likely to break over the crest. Breaking increases the wave dissipation and decreases the transmission. The reflection results show no correlation and are therefore not included.



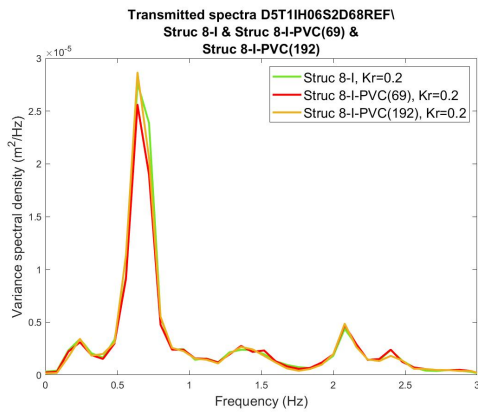
(A) $K_t(s)$ structure 4 and 5.

(B) $K_t(s)$ structure 8-I, 10 and 15.

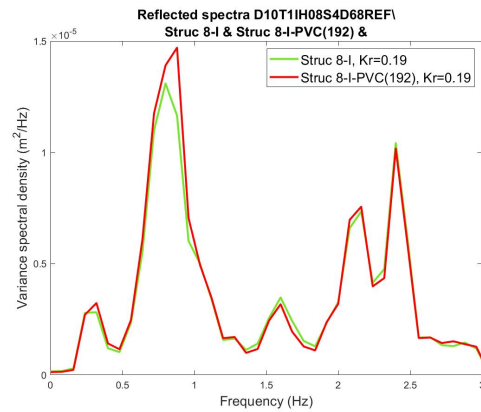
FIGURE D.1: Transmission results per width-waveheight ratio from regular wave tests.

D.2 SURFACE ROUGHNESS

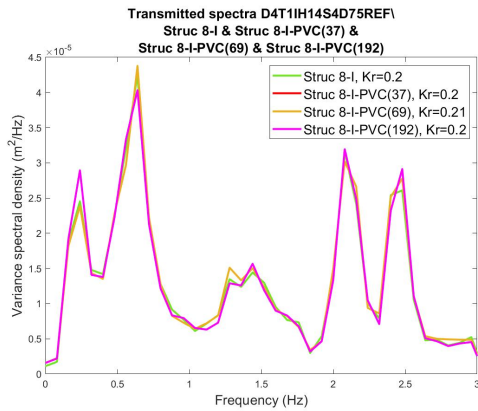
The additional graphs of the reflected spectra for the design variable "surface roughness" are shown here. In the main text, these are not plotted as the impact on the reflection is not consistent and insignificantly small compared to other investigated variables.



(A) WC 16, Structure 8-I, 8-I-PVC(69) and 8-I-PVC(169).



(B) WC 19, Structure 8-I and 8-I-PVC(169).



(C) WC 35, Structure 8-I, 8-I-PVC(38), 8-I-PVC(69) and 8-I-PVC(169).

FIGURE D.2: Reflected energy density spectra measured at WG456 for design variable *surface roughness*. The $K_r(s)$ of each structure can be found in the legends. Structures in figure 5.20e have a relative structure height around 0.27, the others around 0.83

D.3 TYPE OF WAVES

D.3.1 Type of waves and transmission

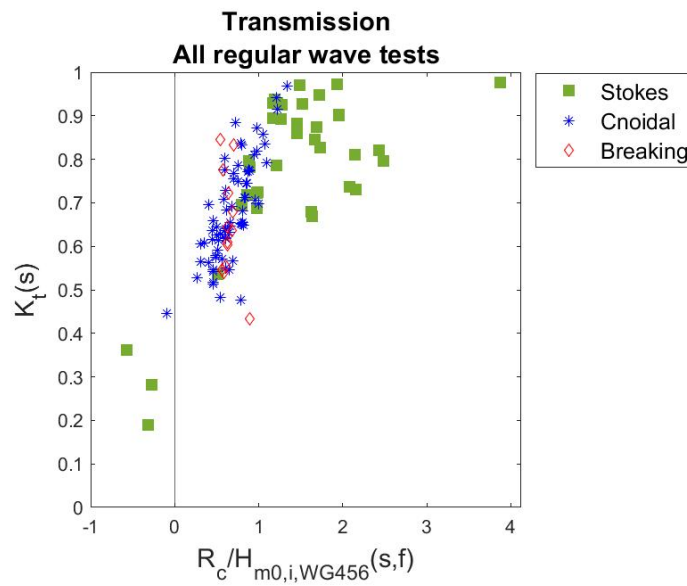
In this section it is investigated whether the $K_t(s)$ over $R_c/H_{m0,i}$ outcomes from the different type of wave tests behave as is expected based on literature ¹. The $R_c/H_{m0,i}$ is chosen, because this is the main variable determining $K_t(s)$ in the empirical equations discussed in chapter 2.1.1. For that matter, the $K_t(s)$ outcomes from all regular wave tests are plotted in Figure D.3a, with the type of waves as an extra variable. The results are evaluated per wave type.

¹ Note: The purpose of this section is **not** to find a relationship between the type of waves and the magnitude of $K_t(s)$.

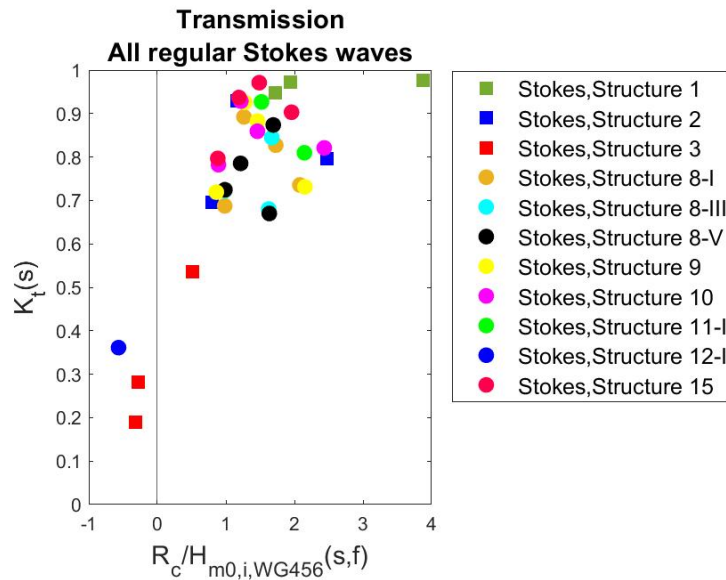
STOKES WAVES Figure D.3b shows the $K_t(s)$ results from only Stokes waves, with the structure number as additional parameter. Roughly interpreted, it can be seen that $K_t(s)$ increases when $R_c/H_{m0,i}$ increases. Still a lot of scatter is observed. The scatter is due to different design variables and wave conditions which are all plotted together and will be further investigated in the next sections of this chapter.

CNOIDAL WAVES Similar as to the Stokes waves, $K_t(s)$ increases for a higher $R_c/H_{m0,i}$. Nevertheless, again the results are scattered.

BREAKING WAVES There is no relation observed between $R_c/H_{m0,i}$ and $K_t(s)$.



(A) Transmission per wave category.



(b) Transmission per Structure number.

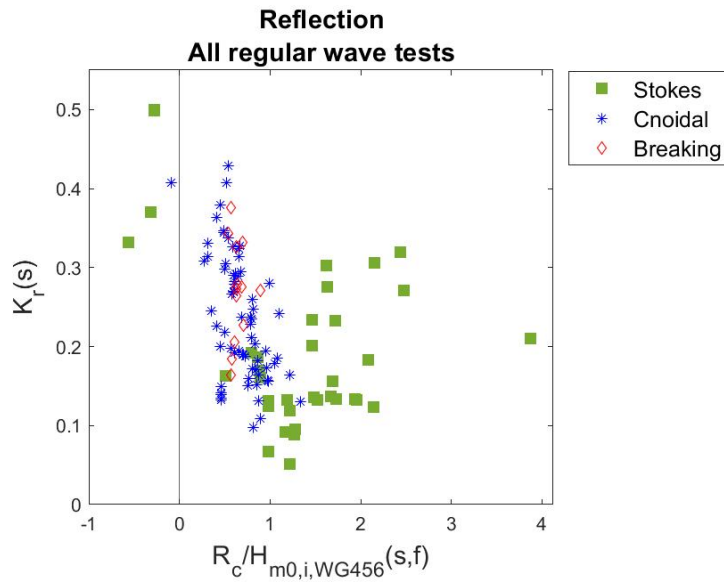
FIGURE D.3: Wave transmission per relative freeboard for regular wave tests.

Normally, the $R_c/H_{m0,i}$ is the main variable used in the empirical equations to predict $K_t(s)$. Namely, if $R_c/H_{m0,i}$ increases, the transmission $K_t(s)$ increases as well. If the $K_t(s)$ shows this expected trend for a specific type of waves, the procedure applied in this research generates reasonable $K_t(s)$ outcomes for this wave type. The tests with breaking waves in front of the structure do not show any relationship between $K_t(s)$ and $R_c/H_{m0,i}$ variables. Therefore, based on the procedure applied in this research, the tests with breaking waves in front of the structure are not suitable to create an empirical equation that predicts the transmission capacity of different designs.

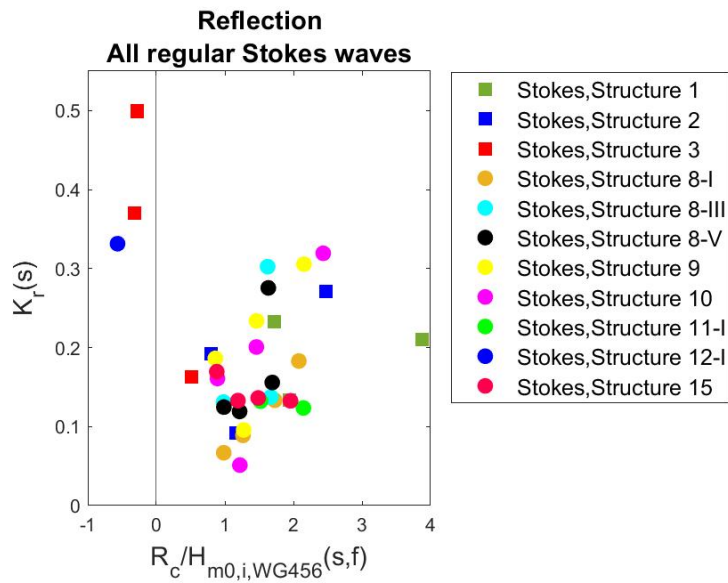
It should be noted that outside the range of $0 < R_c/H_{m0,i} < 1$, there are (almost) no breaking- and cnoidal waves observed. Therefore, the comparison is mostly applicable within this area. All in all, the transmission results from this research are more trustworthy for the cnoidal- and Stoke waves than for the breaking wave tests.

D.3.2 Type of waves and reflection

Similar as for the previous section, here the $K_r(s)$ outcomes for the different type of wave tests are compared, when plotting it against $R_c/H_{m0,i}$. Namely, in the empirical equations discussed in chapter 2.1.3, the $R_c/H_{m0,i}$ is also used to predict the reflection. $K_r(s)$ is plotted for all regular wave tests in Figure D.4a, with the type of waves as an extra variable. In the next paragraphs, the results in Figure D.4a are shortly discussed per type of waves.



(A) Reflection per wave category.



(B) Reflection per Structure number.

FIGURE D.4: Wave reflection per relative freeboard for regular wave tests.

STOKES WAVES There is a lot of variation in the $K_r(s)$ around the same $R_c/H_{m0,i}$ and no consistent trend is visible. However, it can be seen that the highest observed $K_r(s)$ result comes from an emerged structure and the lowest from a submerged structure.

CNOIDAL WAVES In general, the cnoidal waves give more reflection compared to the Stokes waves if the $R_c/H_{m0,i}$ is close to zero. This can be due to the fact that the wavelength of cnoidal waves is long and the water depth is small, both increasing the reflection. Furthermore, a rough trend is visible in which $K_r(s)$ decreases when $R_c/H_{m0,i}$ increases.

BREAKING WAVES For the breaking waves the $K_r(s)$ outcomes are higher and much more scattered than for the Stokes waves at the same $R_c/H_{m0,i}$.

COLOPHON

This document was typeset using \LaTeX . The document layout was generated using the `arsclassica` package by Lorenzo Pantieri, which is an adaption of the original `classicthesis` package from André Miede.